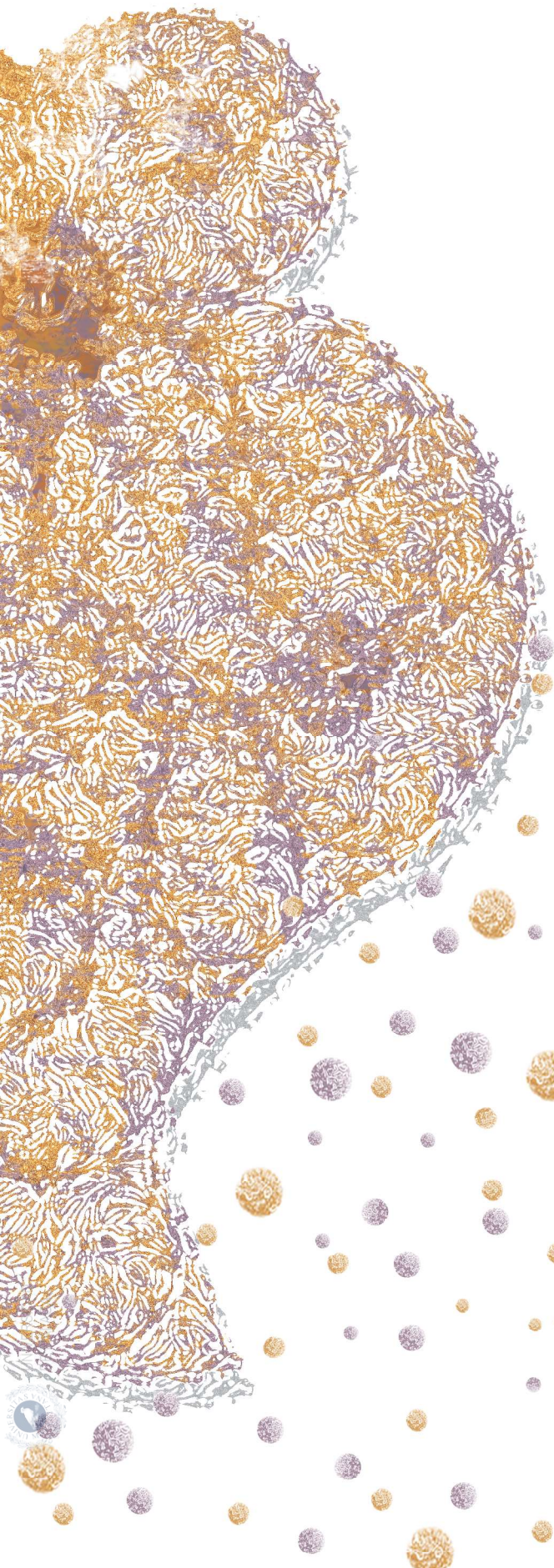




UNIVERSIDAD DE MÁLAGA

# SECRETOME OF EPICARDIAL-DERIVED CELLS

EXTRACELLULAR VESICLES AND MATRIX




Cláudia Oliveira



UNIVERSIDAD  
DE MÁLAGA

AUTOR: Cláudia Patrícia da Costa Oliveira

 <https://orcid.org/0000-0003-1396-0521>

EDITA: Publicaciones y Divulgación Científica. Universidad de Málaga



Esta obra está bajo una licencia de Creative Commons Reconocimiento-NoComercial-SinObraDerivada 4.0 Internacional:

<http://creativecommons.org/licenses/by-nc-nd/4.0/legalcode>

Cualquier parte de esta obra se puede reproducir sin autorización pero con el reconocimiento y atribución de los autores.

No se puede hacer uso comercial de la obra y no se puede alterar, transformar o hacer obras derivadas.

Esta Tesis Doctoral está depositada en el Repositorio Institucional de la Universidad de Málaga (RIUMA): [riuma.uma.es](http://riuma.uma.es)







UNIVERSIDAD  
DE MÁLAGA

## **Tesis doctoral**

EL SECRETOMA DE LAS CÉLULAS DERIVADAS DEL  
EPICARDIO: VESÍCULAS EXTRACELULARES Y MATRIZ

**Cláudia Patrícia da Costa Oliveira**

DEPARTAMENTO DE BIOLOGÍA ANIMAL  
FACULTAD DE CIENCIAS

Dirigida por:

Prof. Dr. José María Pérez Pomares

Dr. Adrián Ruiz Villalba

PROGRAMA DE DOCTORADO  
EN BIOLOGÍA CELULAR Y MOLECULAR

**UNIVERSIDAD DE MÁLAGA**

**2021**





UNIVERSIDAD  
DE MÁLAGA

## **PhD thesis**

SECRETOME OF EPICARDIAL-DERIVED CELLS:

EXTRACELLULAR VESICLES AND MATRIX

**Cláudia Patrícia da Costa Oliveira**

DEPARTMENT OF ANIMAL BIOLOGY  
FACULTY OF SCIENCES

Supervised by:

Prof. Dr. José María Pérez Pomares

Dr. Adrián Ruiz Villalba

CELL AND MOLECULAR BIOLOGY  
PH.D. PROGRAM

**FACULTY OF SCIENCE  
UNIVERSITY OF MÁLAGA**

**2021**





El Prof. José María Pérez Pomares, Catedrático del Departamento de Biología Animal de la Universidad de Málaga, y el Dr. Adrián Ruiz Villalba, Investigador Doctor en el mismo departamento, acreditan que:

Dña. Claudia Oliveira, Graduada en Bioquímica, ha realizado en el Departamento de Biología Animal de la Facultad de Ciencias de la Universidad de Málaga las investigaciones contenidas en la siguiente memoria de Tesis Doctoral, titulada: "Secretome of epicardial-derived cells: extracellular vesicles and matrix".

Como directores de la tesis, consideramos que la presente memoria reúne todos los requisitos para ser sometida a juicio de la Comisión correspondiente, por lo que autorizamos su exposición y defensa pública para la obtención del Grado de Doctor con la mención de Doctor Internacional.

Y para que así conste, en cumplimiento de las disposiciones vigentes, firmamos la presente acreditación en Málaga, a 9 de Agosto de 2021.

PEREZ  
POMARES  
JOSE MARIA

Dr. José María Pérez Pomares

ADRIAN RUIZ VILLALBA

Dr. Adrián Ruiz Villalba







## DECLARACIÓN DE AUTORÍA Y ORIGINALIDAD DE LA TESIS PRESENTADA PARA OBTENER EL TÍTULO DE DOCTOR

D./Dña CLÁUDIA PATRÍCIA DA COSTA OLIVEIRA

Estudiante del programa de doctorado **BIOLOGÍA CELULAR Y MOLECULAR** de la Universidad de Málaga, autor/a de la tesis, presentada para la obtención del título de doctor por la Universidad de Málaga, titulada: **SECRETOME OF EPICARDIAL-DERIVED CELLS: EXTRACELLULAR VESICLES AND MATRIX**


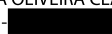

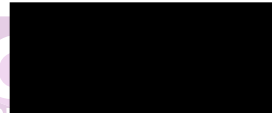

Realizada bajo la tutorización de **PROF. JOSÉ MARÍA PÉREZ-POMARES** y dirección de **PROF. JOSÉ MARÍA PÉREZ-POMARES AND DR. ADRIÁN RUIZ-VILLALBA**. (si tuviera varios directores deberá hacer constar el nombre de todos)

DECLARO QUE:

La tesis presentada es una obra original que no infringe los derechos de propiedad intelectual ni los derechos de propiedad industrial u otros, conforme al ordenamiento jurídico vigente (Real Decreto Legislativo 1/1996, de 12 de abril, por el que se aprueba el texto refundido de la Ley de Propiedad Intelectual, regularizando, aclarando y armonizando las disposiciones legales vigentes sobre la materia), modificado por la Ley 2/2019, de 1 de marzo.

Igualmente asumo, ante a la Universidad de Málaga y ante cualquier otra instancia, la responsabilidad que pudiera derivarse en caso de plagio de contenidos en la tesis presentada, conforme al ordenamiento jurídico vigente.

En Málaga, a 21 de SEPTIEMBRE de 2021

<p>DA COSTA OLIVEIRA CLAUDIA PATRÍCIA - </p> <p>Assinado de forma digital por DA COSTA OLIVEIRA CLAUDIA PATRÍCIA -         Datos: 2021.11.19 10:02:26 +01'00'</p> <p>Fdo.: CLÁUDIA PATRÍCIA DA COSTA OLIVEIRA        Doctorando/a</p>	<p>PEREZ POMARES JOSE MARIA - </p> <p>Date: 2021-11-19 10:21:43        Foxit Reader Version: 9.5.0</p> <p>Fdo.: JOSÉ MARÍA PÉREZ-POMARES        Tutor/a</p>
<p>PEREZ POMARES JOSE MARIA - </p> <p>Date: 2021-11-19 10:22:12        Foxit Reader Version: 9.5.0</p> <p>ADRIAN RUIZ VILLALBA  </p>	





UNIVERSIDAD  
DE MÁLAGA



Escuela de Doctorado

Fdo.: JOSÉ MARÍA PÉREZ-POMARES

ADRIÁN RUIZ-VILLALBA

Director/es de tesis



EFQM AENOR



Edificio Pabellón de Gobierno. Campus El Ejido.

29071

Tel.: 952 13 10 28 / 952 13 14 61 / 952 13 71 10

E-mail: doctorado@uma.es



Este trabajo ha sido realizado en el laboratorio “Desarrollo y Enfermedad Cardiovascular” (DeCA) perteneciente al Departamento de Biología Animal de la Facultad de Ciencias de la Universidad de Málaga, bajo la supervisión del Prof. José María Pérez Pomares y del Dr. Adrián Ruiz Villalba. Parte de dicho trabajo ha sido realizado durante un periodo de corta estancia financiada por las ayudas de estancia internacional de la Universidad de Málaga en *Imperial Centre for Translational and Experimental Medicine* (ICTEM) (Londres, Reino Unido) bajo la supervisión de la Prof. Costanza Emanuelli.

Este trabajo ha sido financiado por los siguientes proyectos de investigación:

“Nicho pericoronario cardíaco: estructura, función y desregulación patológica” (BFU2015-65783R). Ministerio de Economía y Competitividad (MINECO); Plan Nacional de I+D+i.

“Red de Investigación Cooperativa en Terapia Celular” (TERCEL RD2016/0011/0030). Instituto de Salud Carlos III.

“Células mesenquimáticas madre de origen epicárdico en la enfermedad cardiovascular” (RTI2018-095410-B-I00). Ministerio de Ciencia, Innovación y Universidades (MICIU); Plan Estatal de I+D+i.

“Origen embrionario del Síndrome de Canal Auriculoventricular Completo-Tetralogía de Fallot (CAVCToF) y del Defecto de la Comunicación Interauricular (CIA): Mecanismos Celulares y Moleculares” (PIER-0084-2019). Consejería de Salud y Familias 2019 - Proyectos de Investigación en Salud- Junta de Andalucía.

“NanoMedPhD Programme”, European Union’s Horizon 2020 research and innovation programme under the Marie Skłodowska-Curie grant agreement No 713721

Además, parte de los resultados de esta investigación han sido publicados en las siguientes revistas científicas y expuestos en congresos nacionales e internacionales en presentaciones de tipo póster:

*Publicaciones en revistas científicas:*

- Saludas, L.; **Oliveira, C.C.**; Roncal C.; Ruiz-Villalba A.; Prósper F.; Garbayo E.; Blanco-Prieto M. J. Extracellular Vesicle-Based Therapeutics for Heart Repair Nanomaterials. *Nanomaterials* (Basel). 2021. 11(3):570.

*Presentaciones en congresos científicos:*

- Cláudia C. Oliveira, Juan A. Guadix, María I. Castillo, John Pearson, Juan F. López, José M. Pérez-Pomares (2019) Epicardial-derived exosomes in hypoxia and normoxia: a primary characterization. Cardiovascular Development Meeting 2019 - The Official Meeting of the ESC Working Group on Development, Anatomy and Pathology. Málaga, Spain. Poster.
- Cláudia C. Oliveira, Juan A. Guadix, María I. Castillo, John Pearson, Juan F. López, José M. Pérez-Pomares (2019) Epicardial-derived exosomes in hypoxia and normoxia: a primary characterization. NanoMed Europe Conference 2019. Braga, Portugal. Poster.
- Cláudia C. Oliveira, Juan A. Guadix, María I. Castillo, John Pearson, José M. Pérez-Pomares (2019). Exosomes from an epicardial cell line: first steps into cardiovascular messaging. III Congreso Nacional de Jóvenes Investigadores en Biomedicina. Valencia, Spain. Poster.
- Cláudia C. Oliveira, Juan A. Guadix, María I. Castillo, John Pearson, José M. Pérez-Pomares (2018). Exosomes from an epicardial cell line: first steps into cardiovascular messaging. Avances en la investigación biomédica y biotecnológica. Universidad Internacional de Andalucía. Baeza, Spain. Poster.

“Somos o resultado de tanta gente, de tanta história, tão grandes

Sonhos que vão passando de pessoa a pessoa,

Que nunca estaremos sós”

- *O Filho de Mil Homens*, Mia Couto

*To three extraordinary human beings,*

*Martim, Carla & Pai*



## ACKNOWLEDGEMENTS

---





## Acknowledgements

---

I would like to dedicate the first words of gratitude to my supervisor Prof. José María Pérez-Pomares. Thank you very much for having me in your team and for your support throughout this journey. Thank you for always having your door open for me. Despite having more and more responsibilities, you always have a calming attitude and patience that I hope one day to achieve. I'll always remember your warm reception to me in Málaga and your enthusiasm about Portugal. Hopefully one day we can catch up on the Portuguese lessons.

To my co-supervisor, Dr. Adrián Ruiz-Villalba, who put his trust in me and pushed me relentlessly for this day to arrive. We had only started joining forces about a year and a half ago, but a lot has been accomplished in that time thanks to your support and your expertise. I'm grateful to have been your student and to have learned so much from you.

To Dr. Juan António Guadix, thank you for your advice and your interest in my work. Thanks to you, I had the opportunity to be introduced to key researchers at the University of Málaga that helped me to progress further in this thesis.

To my lab colleagues, Silvia, Ana Mari, Ernesto and Chispy, I want to thank you for your companionship, it has been so important to help me fulfil this degree with sanity, and for your helpful tips, hands and brains. I can't wait to see your coming achievements, that I know will be amazing. Thank you for the fun moments at the lab and for persistently improving my Spanish. To Mari, who will never really leave our team, thank you for listening to my thoughts and frustrations. Thank you for always having a kind smile to offer, even back when we couldn't communicate face-to-face with each other. To the newest members of our lab, Pedro and Alejandro, thank you for your contribution to this thesis.

To my previous lab members, Paul, Sara, Clara and Cristina, thank you for teaching me what you know and for patiently training me in many techniques during the time we shared the lab.

To Dr. John Pearson who has been there to help in my research dilemmas and to his ironic sense of humour that I very much appreciate.

## Acknowledgements

To Dr. Fabiana Csukasi and Dr. Gustavo Rico, thank you for sharing your knowledge and tips and for being so kind to me.

Dr. Melissa García and Dr. Beatriz Poveda, thank you for your valuable support and encouragement. Your expertise in cell cultures and metabolic assay has truly helped in improving the quality of this thesis. In special, to Dr. García for persistently aiding with tricky assays, no matter the cost. Your kindness and attention to students are encouraging and inspiring.

To the technicians at SCAI, Auxi, Casimiro, Reme and Goyo, thank you for your endless patience and helpful suggestions. It was a real pleasure to have been taught your subject of expertise by you.

Prof. Costanza Emanuelli, thank you for readily accepting our proposal and having me as a team member. Although it was for a short period, I truly enjoyed working with you and your team. To Francesco, Soumaya and Aran, thank you for training me and for the good company. Juliana, Laura, Walid, your positivity and enthusiasm are contagious. I hope soon we can find time to meet somewhere in São Paulo and have a go at a Brazilian party.

To my COFUND mates, Vladimir, Amene, Jonas, Ashish, Anna, Liliya and Precious, and to whom we consider our grant godmother, Ainhoa. Thank you for your support and for the fun lunches and drinks. In special, I must address a heartfelt thank you to a great colleague, travel companion and friend, Vladimir. I will never stop missing the great time I had with you and the many silly and adventurous stories we have collected. My time in Málaga became much easier when our friendship started.

I am truly grateful to have met and collaborate with great professionals during this journey.

My acknowledgements would be incomplete without thanking the biggest source of my strength, my friends and family.

I have to go first to Isabel. Everyone knows that what a German puts together it will never be set apart. Thank you for being a great friend from the very start of living in Málaga. Thank you for being family and inviting me to your celebrations with our loved ones. Our wild camping will

## Acknowledgements

always be remembered. That and your amazing eggnog. Thank you for being part of my adventures and hopefully one day I can be part of your Montenegro dream in version 1.2.

To my dutch-based family, Novy, Merle, Sahil and Ibra. There will never be enough words to thank you for your immense and valuable friendship. I will always nourish and keep it warm. Yay for more safaris in the cold Netherlands.

To dive further into my personal acknowledgements, I'm going to take some risks and try to write in proper Spanish and also, for my everlasting friends, I will write in my native language, Portuguese.

Silviaaa, que amistad preciosa me llevo. Nunca serán suficiente las palabras de agradecimiento por todas las tardes de confidencias, risas y viajes que hemos compartido. Esa sabiduría gaditana... Gracias por avisar siempre de los 'peligros' de las palabras portuguesas en España. Nunca serán demasiadas las cervezas contigo en Camas, en la Invi o en todas tus (nuestras) terrazas. Gracias por traer a Frida a mis días.

Unzu, Mari Tere and Rebe, no hemos tenido tiempo para crear muchos recuerdos juntos, pero los que tengo son maravillosos. Gracias por vuestras palabras de ánimo, los desayunos imprevistos y las bromas serias. Esa sabiduría universitaria tiene que ser valorada.

A Pepe, el rondeño, qué suerte habernos encontrado en las míticas jornadas. De colegas, a amigos, a colaboradores... gracias por tu entusiasmo, y por acogerme en tu grupo de amigos.

A mi filósofo favorito, gracias José por todas las palabras cargadas de razón y afecto. Siento que soy un óptimo caso de estudio para aplicar tus enseñanzas y teorías. Esperando el momento en que tu portugués mejore.

Abraham, al chico más equivocado y que nunca lleva razón. Gracias por darme la razón y aun así tener tanto respeto y cariño uno por el otro. Deseo con todas mis fuerzas que un día salga la cura para todas tus alergias.

A mí terapeuta de cuatro patas, Zero. Gracias por ignorarme cuando te pido cariño y dármelo cuando ya no lo necesito. No podría ser mejor la bienvenida cada vez que entro en casa. A Lucia, gracias por tu inmensa generosidad y confianza.

## Acknowledgements

A Bea, gracias por la amabilidad y toda la ayuda que me has prestado en estos meses tan caóticos de mi vida. A Violeta y Jimmy, gracias por sacarme de casa y por todos los bailes que bien sabéis que son esenciales para mí.

Agora, a base de tudo isto. O motivo real pelo qual estou aqui hoje vem de Portugal.

Aos amigos universitários e de praxe que ainda hoje estão comigo, Diogo, Lima, e Gusto. Difícil aterrar sem ter já ter o nosso encontro planeado. Diogo, obrigada por me acolheres nas minhas fugas e por fazeres o teu papel de padrinho de forma exemplar. Lima, amiga mais querida, honesta e melhor pasteleira que espero levar sempre ao meu lado. Gusto, mal posso esperar para receber novamente um abraço teu.

Mariana, obrigada pela boa disposição e ternura que sempre trazes contigo. Aury, Toninha e Carlinhos, obrigada pelas parvoíces, viagens, bailaricos e concertos. Sempre indispensáveis.

À Carla, a quem devo a confiança que tenho hoje em mim. Das mulheres mais corajosas que tive a sorte de conhecer. Tens um coração de ouro e és definitivamente um exemplo a seguir. Obrigada pelo amor.

Aos meus pais, obrigada por toda a força que me têm dado desde casa. O esforço e a persistência que põem em tudo o que fazem é uma inspiração. Não chegaria a esta fase sem a vossa ajuda. Ao meu irmão, Ricardo, por me defender, pelos desabafos e pelo *wrestling*, que bem me serviu para o que aí vinha. Tenho muito orgulho na pessoa empática, carinhosa e amável que és.

Às mulheres da minha família, e em especial à Ana, Rosa e Olívia, obrigada por mostrarem que as regras sociais no espaço rural não têm que ser religiosamente seguidas. Por fazerem a melhor comida portuguesa que alguma vez alguém pode comer e sempre terem umas papas de sarrabulho e um pão-de-ló com o meu nome marcado. Sem as minhas tias, voltar a casa não seria o mesmo. À minha prima Leninha, obrigada pelos melhores conselhos e pelo calorzinho suíço, que sempre tens de sobra. Ao Martim, por me ter mostrado que existe um amor e uma força imensa dentro de um ser tão pequenino e frágil. Lembro-me sempre de ti com muita saudade.

A todos os que seguem aqui comigo, um enorme obrigado por ficarem e me apoiarem. É difícil não poder agradecer a todos, mas carrego-vos aqui pertinho.

## List of frequent abbreviations

---

CF	Cardiac fibroblast
CPC	Cardiac-progenitor cell
DLS	Dynamic Light Scattering
ECM	Extracellular matrix
EMT	Epithelial-to-Mesenchymal-Transition
EPDC	Epicardial-derived cells
EPIC	Epicardium-derived interstitial cell line
EPIC IM	EPIC insoluble fraction
EPIC SM	EPIC soluble fraction
ESCRT	Endosomal sorting complex required for transport
EVs	Extracellular vesicles
EVs-H1%	EPIC-derived EVs from 1% O <sub>2</sub> culture
EVs-H5%	EPIC-derived EVs from 5% O <sub>2</sub> culture
EVs-N	EPIC-derived EVs from normoxic culture
EVs-SEC	EPIC-derived EVs enriched via SEC
EVs-UC	EPIC-derived EVs enriched via UC
f-PBS	0,22 µm-filtered PBS
HUVEC	Human umbilical vein endothelial cell
ILV	Intraluminal vesicle
LC-MS/MS	Liquid chromatography with tandem mass spectrometry
MI	Myocardial infarction
MVB	Multivesicular body
NTA	Nanoparticle Tracking Analysis
SEC	Size exclusion chromatography
SEM	Scanning electron microscopy
TEM	Transmission Electron Microscopy
TMT	Tandem mass tags
TMT2plex	TMTtwoplex
TMT6plex	TMTsixplex
UC	Ultracentrifugation
UC-FBS	EVs-depleted FBS



# INDEX

---





Acknowledgements .....	xi
List of frequent abbreviations.....	xi
INTRODUCTION	1
1. Background .....	1
2. Cardiac cell diversity: from embryonic development to adulthood.....	1
3. The cardiac interstitium.....	4
3.1. Cardiac fibroblasts.....	4
3.2. Cardiac extracellular matrix.....	9
4. Cardiac intercellular molecular crosstalk .....	11
4.1. Extracellular Vesicles .....	11
4.2. Technologies to study extracellular vesicles .....	15
4.3. The cardiac extracellular matrix .....	15
5. Cardiac disease .....	17
5.1. Adult responses to myocardial death or malfunction and the origin of cardiac disease .....	18
5.2. Cellular biology of heart conditions .....	18
5.3. Ischemic cardiomyopathy and myocardial infarction.....	19
HYPOTHESIS & OBJECTIVES .....	23
MATERIAL & METHODS.....	27
1. Cell culture .....	27
1.1. EPIC .....	27
1.2. HUVEC.....	27

2.	Extracellular vesicle isolation .....	28
2.1.	Ultracentrifugation.....	29
2.2.	Size Exclusion Chromatography .....	29
3.	Extracellular vesicle physical characterization .....	30
3.1.	Transmission Electron Microscopy.....	30
3.2.	Dynamic Light Scattering.....	30
3.3.	Nanoparticle Tracking Analysis.....	30
4.	Decellularization using ammonium hydroxide.....	31
4.1.	EPIC decellularization .....	31
4.2.	Mice breeding and embryonic hearts decellularization .....	32
5.	Characterization of EPIC-derived ECM.....	33
5.1.	Scanning Electron Microscopy (SEM).....	33
5.2.	Immunocytochemistry .....	34
6.	Protein quantification by bicinchoninic acid .....	34
6.1.	Extracellular vesicles .....	34
6.1.1.	Micro bicinchoninic acid for extracellular vesicles .....	34
6.2.	Extracellular matrix .....	35
6.3.	EPIC lysate .....	35
7.	Proteomic strategy.....	36
7.1.	Tandem Mass Tag multiplexing strategy for extracellular vesicle proteome analysis	36
7.2.	Label-free proteomics for descriptive composition of the extracellular matrix .....	38
7.3.	Liquid chromatography tandem mass spectrometry .....	38
8.	Bioinformatic analysis.....	40
8.1.	Tandem Mass Tags analysis.....	40
8.2.	Label free proteomic analysis.....	41
9.	Western Blot.....	42
9.1.	Extracellular vesicles .....	44
9.2.	EPIC-derived extracellular matrix, E17.5 decellularized heart and Matrigel .....	45
10.	Functional assays of EPIC secretome .....	45
10.1.	Fluorescent labelling of EPIC-derived EVs .....	45

10.2.	Total Internal Reflection Fluorescence imaging of EPIC-derived EVs internalization .	46
10.3.	Cell proliferation assays with EVs .....	47
10.3.1.	EPIC.....	47
10.3.2.	HUVECs .....	47
10.3.3.	5-Ethynyl-2'-deoxyuridine click chemistry reaction .....	47
10.4.	Glycolysis Stress Assay with EVs .....	49
10.5.	HUVEC proliferation assay with ECM .....	52
11.	Statistics.....	52
11.1.	Extracellular vesicle characterization .....	52
11.2.	Functional studies on extracellular vesicles .....	53
11.3.	Analysis and functional studies on extracellular matrix .....	53
RESULTS .....		57
Chapter I – Assessment of isolation strategy and characterization of EPIC-derived extracellular vesicles .....		57
1.1.	Morphological assessment of EPIC-derived extracellular vesicles isolated by size exclusion chromatography and ultracentrifugation .....	57
1.2.	Characterization of EVs-UC and EVs-SEC.....	60
1.2.1.	Physical characterization and quantification.....	60
1.2.2.	Protein concentration and EVs-like protein identification .....	62
1.3.	EVs from EPIC preconditioned to hypoxia and normoxia: morphological assessment...	65
1.4.	Characterization of EVs-N and EVs-H5%.....	67
1.4.1.	Physical characterization and quantification.....	67
1.4.2.	Protein concentration and EVs-like protein identification .....	69
Chapter II– Proteomic characterization of EPIC-derived extracellular vesicles .....		71
2.1.	Comparing multiplexing proteomic strategies: TMT2plex versus TMT6plex quantification .....	71

2.2.	Protein cargo of EPIC-derived EVs .....	74
2.2.1.	Non-differentially enriched surface proteins between extracellular vesicles isolated in normoxia and hypoxia-5% could be considered as potential epicardial-derived EVs markers	74
2.2.2.	Extracellular vesicles isolated from 5% hypoxia are enriched in proteins related to glycolysis .....	77
2.3.	Autocrine signaling of EPIC-derived extracellular vesicles.....	79
2.4.	Paracrine signaling of EPIC-derived EVs.....	84
2.5.	Hypoxia affects the autocrine and paracrine signalling capacity of EPIC-derived extracellular vesicles.....	88
Chapter III– Characterization of EPIC-derived extracellular matrix .....		92
3.1.	EPIC as a source of cardiac extracellular matrix .....	92
3.1.1.	EPIC-derived extracellular matrix structural complexity (i): EPIC cultures .....	92
3.1.2.	EPIC-derived extracellular matrix structural complexity (ii): Decellularization and analysis of the ECM structure.....	92
3.1.3.	Immunocytochemical characterization of EPIC-derived ECM .....	95
3.3.	Epicardial extracellular matrix composition: a proteomic analysis.....	97
3.3.1.	Protein composition differs between different fractions of EPIC-derived extracellular matrix.....	97
3.3.2.	Protein composition of E17.5 decellularized hearts is similar to EPIC-derived extracellular fractions.....	102
3.3.3.	Proteomic comparison between Matrigel and EPIC-derived extracellular matrix ...	106
3.4.	Multicomparison of protein composition between EPIC-derived extracellular matrix, embryonic hearts and Matrigel .....	111
3.5.	EPIC-ECM fractions enhanced the proliferation capacity of endothelial cells .....	115
DISCUSSION .....		123

1.1. Extracellular vesicles isolated by ultracentrifugation are better preserved than by size exclusion chromatography .....	127
1.2. Hypoxia did not affect the physical properties of epicardial-derived extracellular vesicles .....	130
1.3. Extracellular vesicles isolated from epicardial cells submitted to hypoxia are enriched in proteins associated with glycolysis/gluconeogenesis .....	132
1.4. Epicardial-derived cells promote proliferation and a glycolytic metabolism through extracellular vesicles in both autocrine and paracrine manner .....	137
1.5. TMT6 proteomic analysis identifies potential markers for EPIC-derived extracellular vesicles .....	141
1.6. EPIC-derived extracellular matrix is enriched in basement membrane proteins.....	144
1.7. EPIC-derived extracellular matrix is enriched in cardiac ECM proteins .....	147
1.8. Extracellular vesicles and extracellular matrix derived from epicardium and epicardial-derived cells could interact in the cardiac interstitium during cardiac development and in the adult response to damage .....	150
2. Clinical implications .....	153
CONCLUSIONS .....	157
REFERENCES .....	121
RESUMEN .....	179
Introducción .....	179
1. Antecedentes .....	179
1.1. El epicardio embrionario como fuente de células del intersticio cardíaco.....	179
1.2. El epicardio como fuente de componentes cardiacos no celulares .....	180
1.3. El secretoma de las CDEP en la comunicación intercelular del corazón.....	181
1.4. El papel del epicardio en enfermedades cardiovasculares.....	183
2. Hipótesis y objetivos.....	185

3. Resultados .....	186
3.1. Capítulo I: caracterización y comparación de VEs derivadas de epicardio aisladas por dos métodos distintos: ultracentrifugación vs cromatografía de exclusión por tamaño .....	186
3.2. Capítulo II: caracterización proteómica y validación funcional del efecto de la hipoxia en vesículas extracelulares derivadas de epicardio.....	187
3.2.1. La hipoxia afecta al contenido de las vesículas extracelulares derivadas del epicardio .....	188
3.3. Capítulo III: caracterización de matriz extracelular derivada de EPIC .....	190
3.3.1. La matriz extracelular derivada de epicardio muestra más similitudes con la matriz cardiaca que con otras matrices comerciales .....	191
Discusión.....	194
Conclusiones.....	198
APPENDIX: TABLES AND PUBLISHED PAPER .....	201

# INTRODUCTION

---





# Introduction

---

## 1. Background

The mammalian adult heart is a highly complex organ whose proper functioning is crucial to the survival of the individual. Cardiac cells are organized in specialized tissues that coordinate their specific activities to guarantee heart contraction and vascular circulation. Paradoxically, this sophisticated network of interacting cells and tissues forms from a simple cardiac tubular primordium which is primarily constituted of epithelial cells. The progressive increase in the number and diversity of cardiac cells cell types raises the complexity of the molecular mechanisms underlying cell-to-cell interactions and determines the signalling 'architecture' of both the healthy and diseased heart. In my thesis, I have focused in the study of the unexplored part of the secretome of epicardial cells, regarded as a central element of cell communication. This main research objective aims at analysing two relevant aspects of epicardial secreted biological entities: 1) the extracellular vesicles (EVs) involved in intercellular signalling system and 2) molecules of the extracellular matrix (ECM). This introduction will present the necessary information to understand the choice of the topic for this thesis and will provide the necessary information to understand the rationale of my work.

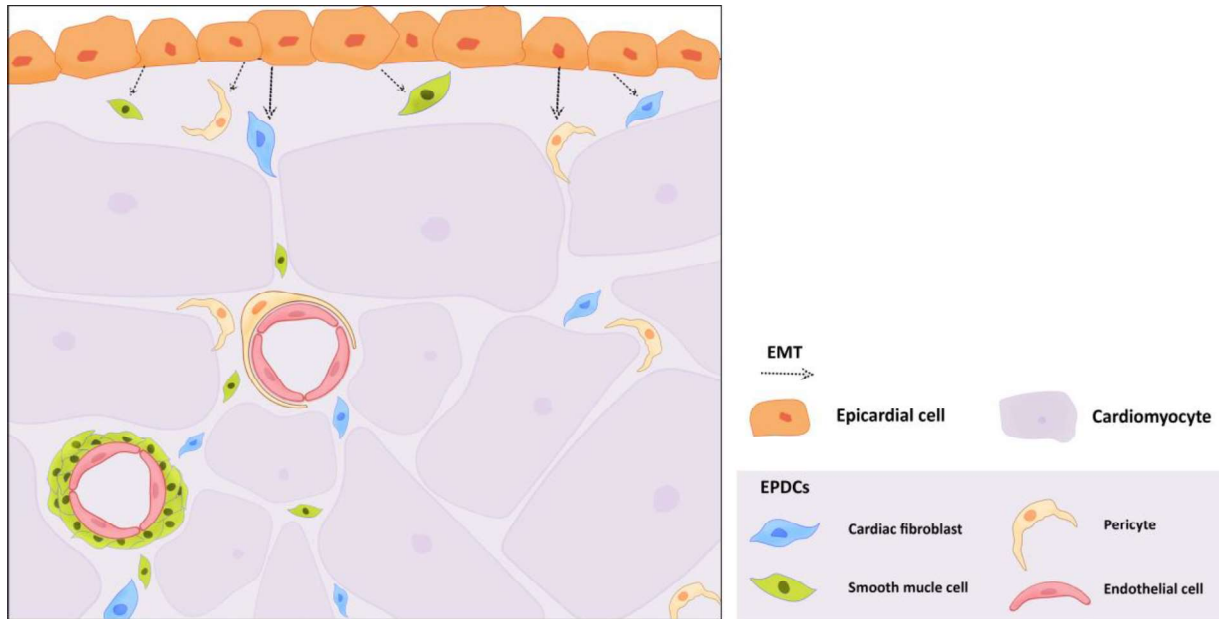
## 2. Cardiac cell diversity: from embryonic development to adulthood

The early embryonic heart has a characteristic tubular shape. Its walls are formed by an outer layer of immature cardiomyocytes (myocardium) and an inner lining of a special vascular endothelium, known as the endocardium, separated by a rich ECM often referred to as the 'cardiac jelly' (Wessels and Pérez-Pomares, 2004). Both, the myocardium and the endocardium, derive from a double pool of mesodermal cardiac progenitors, known as the First Heart Field (FHF) and the Second Heart Field (SHF), that sequentially contribute to the building of the embryonic heart. In addition to the FHF and SHF, other cell populations like the neural crest cell or epicardial lineage cells reach the heart to critically contribute to heart morphogenesis (Markwald *et al.*, 1977; Kirby *et al.*, 1983; Gittenberger-de Groot *et al.*, 1998; Pérez-Pomares *et al.*, 1998; Wessels and Pérez-

Pomares, 2004; Del Monte *et al.*, 2011; De la Pompa and Epstein, 2012). The cells derived from this latter population will be one of the main research subjects of this thesis.

During embryonic development, heart cellular and tissular complexity exponentially increases when the endocardium and the epicardium activate an Epithelial-to-Mesenchymal Transition (EMT) mechanism that allows for the full phenotypical conversion of some endocardial and epicardial cells into mesenchymal cells. EMTs are tightly regulated developmental morphogenetic phenomena in charge of producing new mesenchyme in different defined locations of the embryo (Hay, 2005).

EMT-derived mesenchymal cells are migratory and highly proliferative (Fig. 1). These cells are key players in the building of a great variety of non-myocardial structures, including cardiac interstitium, i.e., the space between cardiac muscular cells. In particular, Epicardial-Derived Mesenchymal Cells (EPDCs) expand all through the cardiac chambers and participate in the formation of the nascent coronary vasculature and various connective tissue cell populations or structures such as the annulus fibrosus or the interstitial mesenchyme (Wessels and Pérez-Pomares, 2004; Cano *et al.*, 2016). As a result of the contribution of cardiac and extracardiac mesenchymal cell populations, the adult cardiac cellulome is established.



**Figure 1 – Epicardium and EPDCs during cardiac development.** EPDCs emerge from the embryonic epicardium through epithelial-to-mesenchymal transition (EMT) and contribute to various cardiac lineages such as cardiac fibroblasts, smooth muscle cells, pericytes and, to a lesser extent, endothelial cells.

### 3. The cardiac interstitium

The adult heart contains large numbers of cells whose origin, diversity and biological roles we are far from understanding (Pinto *et al.*, 2016; Skelly *et al.*, 2018). Remarkably, although cardiomyocytes represent most of the adult cardiac mass, non-myocyte cells are far more abundant than cardiomyocytes in the adult heart. A relatively recent study has quantified the relative proportion of different cardiac cell types and suggested that cardiomyocytes represent, approximately, only 35% of adult heart cells (Pinto *et al.*, 2016). A significant fraction of non-muscle cardiac cells forms part of the cardiac interstitium, i.e., the space between the cardiomyocyte fibres (Fig. 1). Indeed, in addition to cardiomyocytes and endocardial cells, the heart harbours fibroblasts, vascular endothelial and smooth muscle cells (SMC), pericytes, epicardial epithelial cells, lymph endothelial cells, some cardiovascular cell progenitors, neurons and a relevant number of resident blood-borne cells (Pogontke *et al.*, 2019). All these cell types are involved in the primary reparative responses of the heart to stress or changing physiological conditions, but are the main substrate of many cardiac diseases also, most especially of those involving fibrosis (Ruiz-Villalba *et al.*, 2018). In the context of cardiac responses to pathological conditions, the interstitium soon becomes extremely relevant, as it contains cardiac fibroblasts (CFs), the paradigmatic cell type in the diseased heart.

#### 3.1. Cardiac fibroblasts

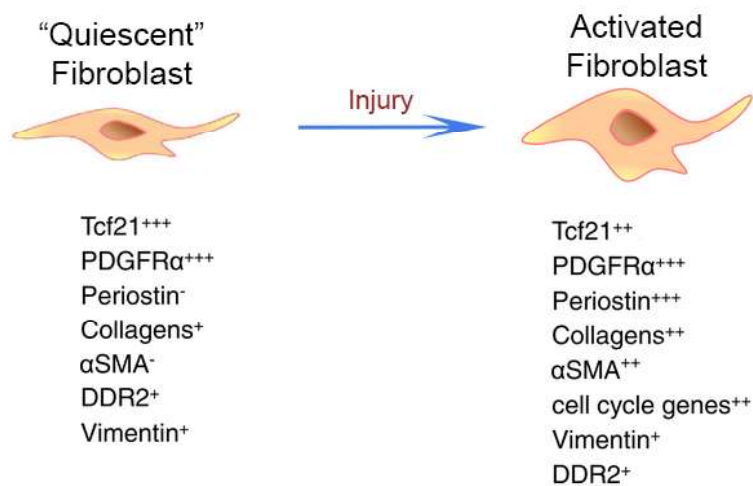
During the last ten years, several laboratories have reported relevant data on the origin, diversity and role of CFs (Ali *et al.*, 2014; Ruiz-Villalba *et al.*, 2020; Aujla and Kassiri, 2021). A general consensus now exists in that the majority of CFs originate from the embryonic epicardium, the monolayered epithelium that covers the heart surface (Smith *et al.*, 2011; Acharya *et al.*, 2012; Ruiz-Villalba *et al.*, 2015).

What do we know about CFs? CFs are a heterogeneous (Fu *et al.*, 2018; Farbehi *et al.*, 2019; Ruiz-Villalba *et al.*, 2020; Hesse, Owenier, *et al.*, 2021), poorly studied cell population that expresses an array of extracellular matrix (ECM) proteins and is inextricably associated to the coronary vasculature. The lack of specific fibroblast markers hampers a clear identification of these cells in homeostatic or fibrotic conditions. Typically, CF identification has relied on a set of proteins that these cells secrete to their

surroundings. “Classic” CFs identification are commonly carried out with collagen I (Col1a1), vimentin (Vim), platelet-derived growth factor receptor  $\alpha$  (Pdgfra), fibroblast-specific protein 1 (Fsp1) and CD90 for “quiescent” CF. Nonetheless, it should be noted that these proteins are also secreted by other cardiac cells. Once activated, CF secrete higher amount of  $\alpha$ -smooth muscle actin ( $\alpha$ SMA) and periostin (Marín-Sedeño *et al.*, 2021) which, if sustained (e.g. in a pathologic context), develops into a stiff extracellular matrix patch and may impair cardiac function (Fig. 2).

State-of-the-art transcriptomics have been covering the search for CFs specific markers. These studies have confirmed an intricate heterogeneity in CFs associated to their location, physiological state and functional properties (Litviňuková *et al.*, 2020; Ruiz-Villalba *et al.*, 2020). Today, it is possible to infer a specific CF function in a given heart area by their protein expression pattern in the homeostatic heart. Between six and ten different CF subpopulations were identified in the healthy heart. Some of these are more represented in the atrium or the ventricle (Farbehi *et al.*, 2019; Litviňuková *et al.*, 2020; Ruiz-Villalba *et al.*, 2020), while other CF subpopulations express genes responsive to TGF $\beta$  signalling (periostin and tenascin) or involved in ECM dynamics (fibulin-2 and procollagen C-endopeptidase enhancer 2 precursors) and arise focally in response to a pathological stimuli (Litviňuková *et al.*, 2020).

In the infarcted heart, different CFs subpopulations have been described as based on their gene expression profile. For instance, 3 days post infarction (dpi) a subset of activated CFs was identified by their ECM gene expression (collagen I, fibronectin, tenascin, CREB-regulated transcription coactivator 1 and periostin) and a prototypical marker was suggested for this specific CF set: cytoskeleton-associated protein 4 (*Ckap4*) (Gladka *et al.*, 2018). In a different study, another CF subset was identified by its expression of Wnt inhibitory factor 1 precursor (*Wif1*) in the same window of time (Farbehi *et al.*, 2019). Furthermore, between 7 and 30 dpi, the collagen triple helix repeat-containing protein 1 (*CTHRC1*) was shown to be highly expressed by a newly described CF subpopulation dubbed reparative CF or RCF (Ruiz-Villalba *et al.*, 2020). Finally, in mature scars of 14 dpi hearts, another set of unique CFs was characterized as quiescent-like fibroblasts (described as matrifibrocytes), displaying low proliferative and secretory activity and expression of ECM and tendon-related genes (Fu *et al.*, 2018).



**Figure 2 – General protein expression in cardiac fibroblasts.** “Quiescent” fibroblasts are localized in the cardiac interstitium where they express matricellular proteins. After injury, fibroblast become activated and rapidly proliferate. At this state, activated fibroblast secrete higher amount of extracellular matrix proteins, stiffening the cardiac muscle and, consequently, impairing its function. Adapted from Tallquist and Molkenin, 2017.

Since a significant amount of activated CFs result from epicardial EMT (Ruiz-Villalba *et al.*, 2015; Kanisicak *et al.*, 2016; Quijada *et al.*, 2020), understanding their parental cell signalling cues may fill an existing gap in understanding the transition of epicardial to activated CFs.

It should be noted that the walls of cardiac (coronary) blood vessels are a reservoir of mature fibroblasts (in the adventitial layer of large coronary arteries), as well as of progenitor-like cells able to differentiate in distinct connective cell types (pericytes, SMC, adipocytes and fibroblasts) (Fioret *et al.*, 2014; Pogontke *et al.*, 2019). The coronary vasculature network is composed of interconnected arteries, arterioles, capillaries, venules and veins in charge of nourishing and oxygenating the working myocardium. Coronary vessels are composed of endothelial cells (ECs), which form the inner vessel layer, and mural cells (pericytes, smooth muscles cells, adventitial fibroblasts and others) which form the vessel walls. Interestingly, recent findings raise the possibility that mural cells, depending on their developmental origin, could differentially contribute to pathological processes such as coronary artery disease or fibrotic scarring (Chen *et al.*, 2016).

Other cardiac interstitial cells that recently showed a growing interest in the cardiovascular fields are the mural cells (Azambuja *et al.*, 2010; Acharya *et al.*, 2012; Volz *et al.*, 2015). These cells stabilize vessels through physical and molecular interactions with adjacent ECs (Daneman *et al.*, 2010; Armulik *et al.*, 2011). Cardiac interstitial cells have been reported to share the expression of chondroitin sulfate proteoglycan 4 (*Cspg4*), platelet-derived growth factor receptor  $\beta$  (*Pdgfrb*), integrin  $\alpha 7$  (*Itga7*), cell surface glycoprotein MUC18 (*CD146*) and regulator of G-protein signalling 5 (*Rgs5*) (Marín-Sedeño *et al.*, 2021). Pericytes are mural cells that express vitronectin (*Vtn*) (Skelly *et al.*, 2018; Farbehi *et al.*, 2019) and enfold blood vessels and regulate their function. These cells were suggested to be intermediaries in epicardial cell differentiation into SMCs, which do not express *Vtn* (Skelly *et al.*, 2018; Farbehi *et al.*, 2019). The signalling effectors for this differentiation was shown to be regulated by Notch3 and Jagged-1 (Volz *et al.*, 2015). SMC differentiation from epicardial cells was also previously demonstrated to be



regulated by retinoic acid and VEGF (Azambuja *et al.*, 2010). In fact, a recent report by Quijada *et al.* demonstrated that EPDCs regulate ECs maturation, specification and location fate during cardiac development (Quijada *et al.*, 2021). Here, it described that epicardial cells undergoing EMT express *Slit2*, while quiescent epicardial cells this trait is silenced. Additionally, *Slit2*<sup>+</sup> CFs and pericytes were shown to be close to subepicardial ECs suggesting a regulatory angiogenic potential and assist in vascular stability (Quijada *et al.*, 2021).

Despite the evident biomedical relevance of coronary vasculature, the cellular diversity of the blood vessels that compose it, and its potential role as a true integrative reactive centre upon cardiac injury has not been studied in detail. Research from the 'Cardiovascular Development and Disease' (DeCA) research team at the University of Málaga has pioneered important discoveries on CFs in a series of papers published over the last two decades (Pérez-Pomares *et al.*, 1998; Pérez-Pomares, Carmona, *et al.*, 2002; Pérez-Pomares, Phelps, *et al.*, 2002; Guadix *et al.*, 2006; Wessels *et al.*, 2012; Ruiz-Villalba *et al.*, 2013; Cano *et al.*, 2016) proving the material contribution of epicardial-derived CFs to important cardiac structures such as coronary blood vessels, cardiac atrioventricular valves and cardiac connective tissue entities like the *annulus fibrosus*. Importantly, these epicardial-derived CFs synthesize significant amounts of collagen and other ECM proteins (Wessels and Pérez-Pomares, 2004; Ruiz-Villalba *et al.*, 2013, 2015, 2018; Pogontke *et al.*, 2019).

In addition to their known embryonic roles, epicardial-derived CFs are an extremely reactive cardiac cell population that responds rapidly to cardiac injury from their interstitial location. It is thus a paradox that CF numbers remain low in the healthy heart to be expanded massively after cardiac injury only. Our research team at the University of Málaga was the first one to prove that the origin of fibroblasts in the adult ischemic heart is the embryonic epicardium and not blood-borne cells (Ruiz-Villalba *et al.*, 2015). This finding has received further support from subsequent reports by other researchers (Yano *et al.*, 2005; Kanisicak *et al.*, 2016; Moore-Morris *et al.*, 2018; Quijada *et al.*, 2019).

### 3.2. Cardiac extracellular matrix

Cardiac ECM is formed by the progressive accumulation of molecules primarily secreted by cardiac cells. Although the cardiac cell-specific ECM secretome has not been characterized in depth, it is evident that cardiac epithelia and their related mesenchymal progenies are major contributors to the embryonic cardiac ECM (Wessels and Pérez-Pomares, 2004). During all these early stages of heart development, not much space between cardiomyocytes exists, and the ECM deposited between contracting cells seems to be scarce and mostly related with the cardiac jelly and the subepicardial matrix (i.e., the extracellular space between the cardiomyocyte surface and the epicardial epithelium).

The main components of cardiac ECM are fibronectin, whose synthesis precedes the arrival of the epicardial cells to the myocardium (Kálmán et al., 1995), and collagens I, IV, V, and VI (Tidball, 1992; Hurlé et al., 1994; Bouchey et al., 1996b; Kim et al., 1999). Other relevant proteins of the cardiac ECM are laminins and diverse proteoglycans (Kálmán et al., 1995), fibrillin-2, elastin, vitronectin (Bouchey et al., 1996a), tenascin-X (Burch et al., 1995), flectin (Tsuda et al., 1998), and fibulin-2 (Tsuda et al., 2001) among other molecules. In addition to the structural scaffold provided by all these proteins, the cardiac ECM also stores growth factors such as basic fibroblast growth factor (FGF2), vascular endothelial growth factor (VEGF) (Tomanek et al., 1998, 1999, 2001, 2002; Zheng et al., 2001), hepatocyte growth factor (HGF) (Rappolee et al., 1996; Song et al., 1999), transforming growth factors (TGF- $\beta$ s) and bone morphogenetic proteins (BMPs) (Yamagishi et al., 1999; Nakajima et al., 2000). Most importantly, the kinetics and action of these instructive signals seems to be partially controlled by the interactions with the ECM (Martino *et al.*, 2014).

Collagen is the main component of the adult cardiac ECM. Continuous renewal of interstitial collagen fibrils, which are in direct contact with the cardiomyocytes, is a clear example of the cell-ECM dynamic that shapes physiological response according to the received stimuli (Spinale, 2007). In fact, distinct mediators, including bioactive molecules and possibly EVs as well, are embedded in the interstitial ECM, supporting a complex signalling cross-talk that affects both cellular state and ECM stability (Visconti and

Markwald, 2006; Spinale, 2007; López et al., 2010). These biomolecules can be growth factors such as TGF- $\beta$ , platelet-derived growth factor (PDGF), VEGF, and FGF2, hormones like endothelin-I, angiotensin-II, atrial natriuretic peptide (ANP) or the B-type natriuretic peptide (BNP), and proinflammatory cytokines like Interleukin-6 (IL-6) and Tumour Necrosis Factor- $\beta$  (TNF- $\beta$ ) that interact with this signalling network and modifying the cell microenvironment (Pogontke *et al.*, 2019).

Cardiomyocyte death triggers extensive modification in cardiac ECM, locally or even remotely, as it happens in the infarcted heart. One of the main triggers of this response involves the activation of CFs by the altered mechanical and structural microenvironment, so that CFs migrate to the injured area and mainly secrete collagen in an attempt to contain the damage and secure structural support. Such response leads to the accumulation of matricellular proteins, culminating in a condition known as fibrosis. In the other hand, cardiac damage repair also involves an interplay between leukocytes, SMC and fibroblasts. Their participation in ECM dynamics is also linked to a matrix degradation signalling via matrix metalloproteinases (MMP), including A disintegrin, metalloproteinase domain-containing protein (ADAM), and ADAM with thrombospondin motifs (ADAMTS) all of which participate in the continuous remodelling of the injured area (Rog-Zielinska *et al.*, 2016; Spinale *et al.*, 2016). Molecules such as tenascin-C, osteopontin, basement-membrane protein 40 (SPARC), periostin, fibronectin ED-A domain, fibronectin or osteoglycin also accumulate in the damaged area. These molecules are able to induce changes in inflammatory, fibrotic and vasculogenic responses (Frangogiannis, 2017a). Just recently, human cardiac ECM was evaluated in non-transplantable hearts and hearts with dilated cardiomyopathy (DCM) and ischemic heart disease (IHD), and compared with murine models of acute and chronic myocardial infarction (MI) (Perestrelo *et al.*, 2021). Increased deposition of collagen fibres and fibronectin was clearly visible in diseased hearts, whereas connexin 43 (highly expressed in cardiomyocytes) was substantially decreased, especially in IHD patients and murine chronic MI. The highly compacted ECM in chronic MI shows a composition that is different to that of ECM derived from non-damaged hearts, becoming evident that the CF secretory profile has transformed into a fibrotic-like one (Perestrelo *et al.*, 2021).

In summary, the cardiac ECM is not only necessary to the physical integrity of cardiac muscular walls, but it also is the environment in which the intercellular signals that determine cardiac homeostasis and the responses of the organ to pathologic stimuli are articulated.

#### 4. Cardiac intercellular molecular crosstalk

The full description of the molecular signalling systems involved in cardiac homeostasis and diseases is beyond the scope of this thesis. It is, however, important to take into account several aspects associated to epicardial-related signalling in the heart. The first one is that epicardial cells have for long been known to secrete molecules that promote the proliferation of the adjacent myocardium (Guadix *et al.*, 2011). The full composition of this secretome, which is known to be dependent on activated retinoic acid in the embryonic epicardium (Chen *et al.*, 2002; Stuckmann *et al.*, 2003), is still to be deciphered. Nevertheless, it is assumed that FGFs (FGF1 and 2, mainly), hedgehog signalling agents, and members of the TFG- $\beta$  superfamily (Morabito *et al.*, 2001; Pennisi and Mikawa, 2005; Lavine and Ornitz, 2008) stimulate epicardial-cardiac cells crosstalk. To the best of our knowledge, only a very recent study (del Campo *et al.*, 2021) has considered and studied the relevance of the supramolecular epicardial secretome represented by EVs. One of the essential goals of this thesis is to further characterize this fraction of the epicardial secretome. A second major relevant, but often overlooked aspect of epicardial-related molecular signalling, is the multiple roles of the ECM as key transducer of signals between the cells and their extracellular milieu, as mediator of those other signals based on secreted, diffusible molecules, and as a dynamically responsive element to the cellular environmental conditions. In accordance with these findings, the second part of this PhD thesis will focus on the analysis of the protein content of epicardial-derived EVs.

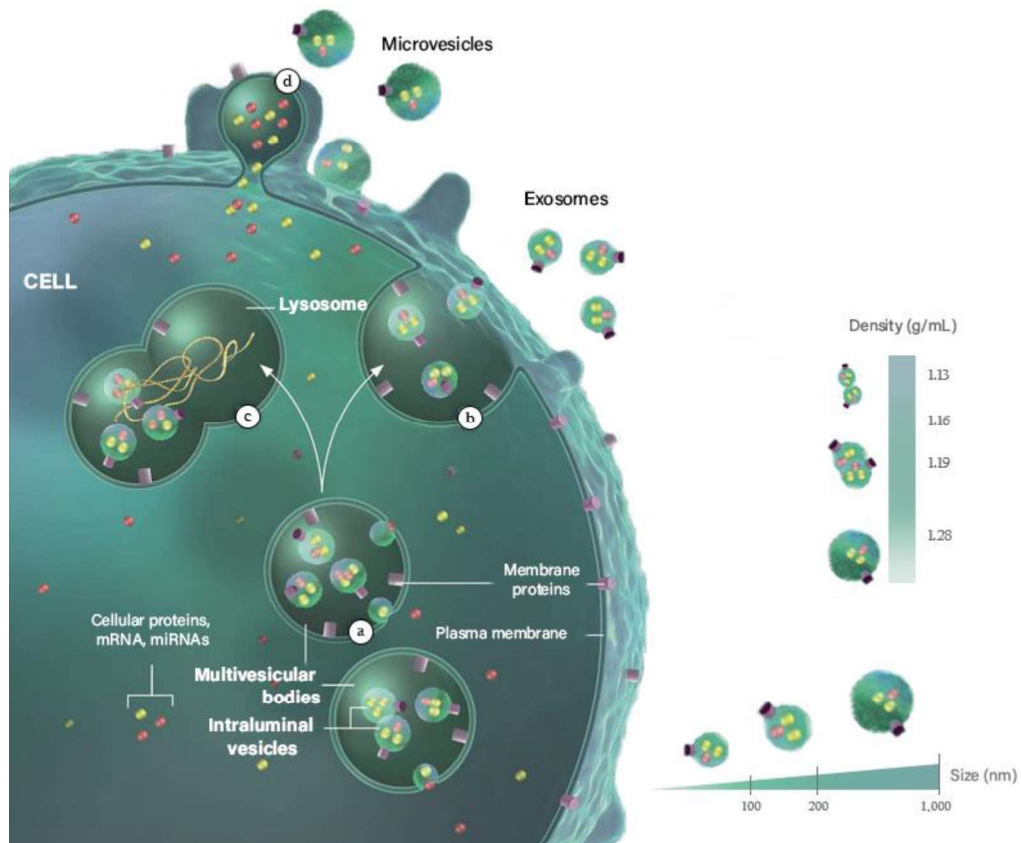
##### 4.1. Extracellular Vesicles

The term EVs is used to refer to any type of secreted vesicles, which are virtually released by all cells. These vesicles are quite heterogeneous, reason why vesicle characterization and function studies are still an ambitious task in this field.

These vesicles are known to carry cellular-derived components (nucleic acids, proteins and lipids) that act in cell-to-cell signalling and regulate cellular homeostasis. EVs are categorized into exosomes, microvesicles, and apoptotic bodies, being their biogenesis pathway what biologically distinguishes each EV type. Herein, however, we will be focusing in the description of two of the most studied EVs: exosomes, generally considered to present a size range of 30 to 150 nm, and microvesicles, with a broader size range of 50 to 1,000 nm (Van Niel *et al.*, 2018).

Exosome formation is dependent on the assembly of early endosomes named multivesicular bodies (MVBs; Fig. 3a). MVB membrane is then internalized and form intraluminal vesicles (ILVs) under endosomal sorting complex required for transport (ESCRT)-dependent or independent mechanism that induces vesicle bending and budding. During MVB biogenesis, determined molecules are selectively loaded into these structures. However, the formation and loading mechanism of these large vesicles may target them for endosomal-lysosomal degradation pathway or for ILV release to the extracellular space (Fig. 3b and c). Once ILVs are release to the extracellular space by fusion of MVBs with the plasma membrane (Fig. 3b), these vesicles are called exosomes. Nevertheless, particle recruiting mechanism and vesicle fate decision has not yet been completely understood (Peng *et al.*, 2020).

Microvesicles, in the other hand, are formed by outward budding and fission of the plasma membrane (Fig. 3d). Changes in membrane protein and lipid composition as well as  $\text{Ca}^{2+}$  drive plasma membrane rearrangement, causing membrane bending and actin cytoskeleton rearrangement. Here, cargo selection appears to be related to their affinity to lipid rafts encountered close to microvesicle budding sites. As such, exosome release is controlled by additional regulatory checkpoints as compared to microvesicles, which may also be regulated as well by the cellular physiological state (Van Niel *et al.*, 2018).



**Figure 3 – Extracellular vesicles biogenesis and physical properties.** Exosomes and microvesicles are the most studied EVs. During exosome formation (a) cytoplasmic components are enclosed in early endosomes named multivesicular bodies (MVB). MVBs membrane bud inwards to form intraluminal vesicles (ILVs). Once the MVB membrane fuses with the plasma membrane, ILVs are released to the extracellular space and called exosomes (b). Alternatively, MVBs may fuse with lysosomes that will degrade MVBs content (c). Microvesicles originate from direct budding of the plasma membrane (d). Since it is not yet possible to confidently characterize the EVs subtypes based on their biogenesis, EVs characterization relies on a nomenclature where, for instance, sizes and densities of EVs are considered. Figure adapted from Théry, 2011.

Current EV characterization relies heavily of their size. This feature, however, hampers the obtention of purified EV subtypes and specific exosomal or microvesicle-like proteins are used to assess EV population enrichment. Nevertheless, conclusive EV population enrichment are not yet achievable and a consensual nomenclature has been implemented based on EV size, densities and protein composition (Théry *et al.*, 2018).

Due to discrepancies in EVs reports and terminology, the International Society of Extracellular Vesicles (ISEV) has stipulated a standardized set of conditions for EVs characterization (Théry *et al.*, 2018). Currently, EVs are described as small (< 100 nm), medium (100 – 200 nm) and large (200 – 1,000 nm) secreted structures limited by a biological lipidic membrane similar to the cytoplasmic one. EVs can also be classified by their low (1.13-1.19 g/mL), medium (1.16 – 1.28 g/mL) or high (> 1.28 g/mL) density (Fig. 3) (Théry *et al.*, 2018). The best studied of all these vesicles are exosomes. Additionally, while presence of transmembrane and cytosolic-related proteins in isolated EVs should be shown, the level of purity of an EV sample against serum-associated proteins ought to be presented. All lipoproteins, apolipoproteins, albumin, ribosomal proteins, histones, cytochrome c, calnexin, Golgin subfamily A member 2 (GM130), Actinin1/4, cytokeratin 18 among other molecules related to the endoplasmic reticulum, Golgi apparatus, as well as proteins associated to other intracellular compartments are currently advised to be assessed for purity control used as non-EV co-isolated proteins (Théry *et al.*, 2018).

The EV content is considered to significantly differ from cell to cell. EV membrane carries a significant number of proteins; other proteins and important molecules such as miRNAs are to be found as cargo inside the EVs (Saludas *et al.*, 2021). Although the ability of EVs to impact the biology of cells has been shown both *in vitro* and *in vivo* (Feng *et al.*, 2014; Adamiak *et al.*, 2018; J. Zhu *et al.*, 2018; Wu *et al.*, 2020; del Campo *et al.*, 2021), it still remains largely unknown which ones are the specific set of EV-bound molecules responsible for such specific responses.

EVs have been proposed as a substrate for advanced therapies to cure the diseased heart.

Several pre-clinical studies have shown improved cardiac function, reduced scar size and inflammation in animals (mice, rats and pigs) inflicted with cardiac injury and

then treated with EVs isolated from different cells types (Saludas *et al.*, 2021). In fact, there are currently 86 clinical trials registered within the study object “extracellular vesicles” and 235 within “exosomes”, according to the database [www.ClinicalTrials.gov](http://www.ClinicalTrials.gov). Of them, 9 of these studies are focused on cardiac conditions. In this context, understanding the molecular mechanisms underlying these positive effects of EVs in a pathologic context is mandatory to progress in the treatment of many complex, prevalent diseases.

#### 4.2. Technologies to study extracellular vesicles

EVs, as many other extracellular and secreted agents, such as virus, lipoproteins and microparticles, have a small size (Kreimer *et al.*, 2015). Consequently, tools such as Dynamic Light Scattering (DLS), Nanoparticle Tracking Analysis (NTA) and Transmission Electron Microscopy (TEM) are the most used to assess their size, particle concentration, polydispersity and vesicle structure (Théry *et al.*, 2018). TEM is the most direct approach to the characterization of EV size and form, whereas NTA, based on light dispersion and particle Brownian movements, can provide a precise information on particle concentration (Filipe *et al.*, 2010; van der Pol *et al.*, 2014). Sources of variability for NTA estimation of EV samples are, unfortunately, many (type of camera, laser wavelength, cleanliness of the microfluidic device, duration of measurement, operator proficiency, refractive index, among others) so all these factors have to be taken into consideration as they can affect reading standardization (Filipe *et al.*, 2010; Gardiner *et al.*, 2013).

#### 4.3. The cardiac extracellular matrix

As previously discussed, the ECM is a fundamental element in cell signalling, both as the supporting environment for the transportation of extracellular signals and as a triggering element of specific cell responses to a variety of environmental cues, including changes in cell shape or migration.

Cardiac ECM consists of molecules secreted by many different cell types. Therefore, if sufficient cardiac tissue is available, the bulk composition of cardiac ECM can be studied using various methods, of which proteomics is the most complete and more precise one. The risks of working with large *in vivo* tissue samples, however, are multiple.



The most relevant one is the necessity of establishing a decellularization protocol and a subsequent elution routine able to wash out extracellular proteins. In addition, using this approach, we may lose the option to study the specific contribution of each different cardiac cell type to ECM composition.

In the heart, mesenchymal cells are major contributors to the cardiac ECM. Due to their relevance, in this thesis we will focus on the study of EPDC-derived ECM. From an ontogenetic perspective, the ECM plays a crucial role in the development of EPDCs, which as indicated, appear through the activation of epicardial epithelium EMT. It is still not fully understood how EMT is triggered, but the ECM is a necessary element in the completion and, most probably, the activation of epicardial EMT. A recent transcriptomic study in developing chick hearts suggests that the ECM components regulate epicardial cell migration, such as fibronectin, periostin and agrin (Mantri *et al.*, 2021). Agrin was also recently shown to be necessary for epicardial cells to undergo EMT during cardiac development (Sun *et al.*, 2021). These reports suggest that epicardial differentiation is affected by the ECM secreted by epicardial cells and its derivatives during cardiac development. Moreover, since EPDCs are the first cardiac cells to invade the nascent cardiac interstitium and considering what it is known regarding their paracrine influence in the cardiac microenvironment, these cells are crucial for ECM synthesis and structure during cardiac development and ECM maintenance in adult hearts.

As it can be inferred from previous sections of this thesis introduction, epicardial-derived CFs are especially important players in ECM remodelling (Bax *et al.*, 2019; Silva *et al.*, 2021). During cardiac development, embryonic CFs support cardiac growth by forming a fibrous scaffold of matricellular proteins that adult CFs are not fully able to reproduce (Ieda *et al.*, 2009). It was then hypothesized that components secreted by embryonic CFs may retain a proliferative capacity for cardiomyocytes that adult CFs fail to deliver, leading to an hypertrophic cardiomyocyte phenotype (Lajiness and Conway, 2012). Detailed embryonic EPDC-derived ECM studies may result in novel insights into cardiac cells response to their surroundings, and could be potentially used in favour of cardiac recovery after homeostatic alterations.

To analyse EPDC-derived ECM large numbers of cells are required. Epicardial primary *in vitro* cultures are difficult to set up and their average life is short. Thus, epicardial-derived EV and ECM analysis largely rely on the use of continuous epicardial cell lines for the isolation of significant amounts of EVs and ECM proteins. The number of immortalized cell lines of embryonic epicardium available is very restricted; in this work we have used EPIC, immortalized cells from E11.5 epicardium (Ruiz-Villalba *et al.*, 2013). As EPIC were shown to be a suitable epicardial-derived cell model, its continuous cell culture allows the harvesting of larger quantities of its secreted nanostructures while minimizing animal sacrifice for primary culture of epicardial cells. Although it is evident that EPIC derived ECM could represent a fraction of the total, native cardiac ECM composition only, data available in the literature on the highly secretory nature of epicardial cells suggests that epicardial-secreted ECM is very likely to represent a most significant part of it. For this reason, we have favoured a strategy based on the use of EPIC, an epicardial-derived cell line, to study cardiac ECM. Our choice will also allow us to obtain important amounts of ECM minimizing the contamination of intracellular proteins in our samples.

## 5. Cardiac disease

Cardiovascular disease is the leading cause of death among developed countries (the EU estimate for healthcare costs related to cardiovascular diseases is 111.000 million €/year) (Wilkins *et al.*, 2017). There are multiple social and environmental determinants that have a significant impact on the continuous increase of cardiovascular conditions in Western populations. These include smoking, alcohol consumption, unbalanced food intake, sedentary lifestyle, stress and multiple psychosocial factors (Saban *et al.*, 2014).

Although it is widely accepted that early diagnosis and treatment of disease are key to reduce the burden of cardiovascular conditions, our limited knowledge of the pathophysiology of many of these ailments hampers progress in the development of new, effective therapies to treat them. Accordingly, current treatments for many severe cardiovascular diseases still rely on the common use of poorly specific drugs like beta-blockers, anticoagulants or anti-arrhythmic compounds. Therefore, further systematic research is needed to identify novel molecular therapeutic targets that can transform

generic pharmacological approaches into highly accurate, cell-targeted ones. In this context, extensive preclinical research on animal models is required to dissect the responses of different cardiovascular cells/tissues to a variety of pathological stimuli, allowing for the identification of potential pharmacological targets to minimize or cure cardiovascular diseases.

### **5.1. Adult responses to myocardial death or malfunction and the origin of cardiac disease**

Unlike embryonic tissues, adult organs frequently respond to a significant loss of functional cells by activating a reparative mechanism based on the substitution of the parenchymal tissue by a fibrous one. This phenomenon is known as fibrosis, and, although some common triggering signals and cellular effectors can be found in different fibrotic events, significant differences have been recorded for many of them (Wynn and Ramalingam, 2012). The specific pattern of activation and the phenotypic alterations exhibited by CFs depend on the type and severity of the myocardial injury. Cardiac fibrosis can be primarily local, massive and fast, as in ischemic cardiomyopathy/acute MI. In this particular disease, local inflammation is a relevant factor that involves CFs not only as targets of pro-fibrotic signals, but also as modulators of the inflammatory process. In other conditions, like those associated with pressure overload (e.g. hypertension and aortic stenosis), CFs undergo chronic activation, secreting small amounts of ECM during an extended period of time, giving rise to a diffuse reactive interstitial fibrosis that mostly contributes to diastolic dysfunction (Ruiz-Villalba *et al.*, 2018; Frangogiannis and Kovacic, 2020; Oatmen *et al.*, 2020). In arrhythmogenic cardiomyopathy, other characteristic human cardiac disease, primary cardiomyocyte desmosomal anomalies activate the progressive substitution of cardiomyocytes by fibroblasts and adipocytes (Asimaki *et al.*, 2016). Each one of these ailments shows a particular histopathological profile characterized by a unique set of cell-to-cell interactions and seems to involve differential responses from CF-like cells.

### **5.2. Cellular biology of heart conditions**

Cardiomyocyte death is the central pathophysiological feature of most cardiac diseases, but may not be the responsible agent of the long-term impact of many of these

ailments. Indeed, cardiomyocyte death evokes multiple dynamic responses from non-muscle cardiac cells living between cardiac muscle fibres (the cardiac interstitial space or cardiac interstitium), that deeply transforms the histo-architecture of the ventricular wall (ventricular remodelling, VR). This severe histological transformation ultimately impairs cardiac performance and drives to heart failure. For all these reasons, some authors have proposed the term interstitial diseases to refer to some adult cardiovascular conditions (Schelbert *et al.*, 2014). The cellular interstitial community, however, is complex and diverse and therefore responds differently to pathological stimuli in a well-defined characteristic manner. Unfortunately, true CFs are too often taken for the only relevant cell population of the cardiac interstitium, so that the terms ‘cardiac fibroblasts’ and ‘cardiac interstitial cells’ are frequently used as synonyms (Pogontke *et al.*, 2019). In this section we will detail the interstitial-specific features of ischemic cardiomyopathy, the most prevalent cardiac condition in the World.

### 5.3. Ischemic cardiomyopathy and myocardial infarction

Cardiac ischemic disease is a prevalent condition in the Western world. A direct consequence of cardiac ischemia is MI, which is a complex condition determined by the primary myocardial death, the post-mitotic nature of the adult myocardium and the massive inflammatory response that follows necrosis of the cardiac muscle. Dead cardiomyocytes are substituted by fibroblasts, which proliferate, secrete large amounts of ECM proteins, and extend to form an akinetic post-MI scar. This process, which is known as ventricular remodelling, severely impairs cardiac function, leading to heart failure. Relatively few laboratories have focused on the study of methods to minimize post-MI cardiac fibrosis and scarring.

CFs, which are the cells responsible for cardiac fibrosis and scarring after MI, have been recently shown to display a variable transcriptional profile, both in the context of the ischemic heart (Fu *et al.*, 2018) and in the postnatal transition to cardiac tissue maturation (Sampaio-Pinto *et al.*, 2018). This suggests that the CF population holds an intrinsic heterogeneity (Ruiz-Villalba *et al.*, 2020). While many laboratories have attempted, unsuccessfully, to develop cell-based strategies to generate new, functional cardiomyocytes in the infarcted heart (Lian *et al.*, 2012; Zhang *et al.*, 2012; Isomi *et al.*, 2019), relatively few laboratories have focused in the study of methods to minimize post-

MI cardiac fibrosis and scarring (Hughey *et al.*, 2012; Leask, 2015; Thavapalachandran *et al.*, 2020). Indeed, halting or reducing cardiac scarring is a very relevant clinical objective to hamper the progression of VR and prevent heart failure (HF) (Leask, 2015). Since current pharmacological tools to minimize cardiac fibrosis are far from being effective (Gourdie *et al.*, 2016), it is mandatory to develop novel approaches to identify specific cellular targets for advanced pharmacological treatment of cardiac fibrosis.

To properly tackle the objective of developing novel successful therapies to handle VR after MI, our understanding of the pathophysiological basis of cardiac fibrosis need to improve significantly. So far, experimental attempts to reduce cardiac fibrosis after MI have relied on the use of different chemical agents to disrupt signals responsible for triggering and promoting cardiac fibrosis, including inflammatory ones (Sun *et al.*, 2000; Westermann *et al.*, 2006; Leask, 2015; Fan and Guan, 2016), but further, systematic research is needed to translate this knowledge into new, effective therapies to treat this disease.

# HYPOTHESIS & OBJECTIVES

---



## Hypothesis & Objectives

---

Extracellular vesicles (EVs) are widely studied for their potential use in disease discovery and therapeutical approaches. EV content includes bioactive molecules that undergo a selection process to be secreted in enclosed vesicles. Besides that, EV components can also be used to identify its cellular origin as well as its physiological state. A single study on the content of epicardial-derived EV is present in the literature (del Campo *et al.*, 2021). In this thesis we report a detailed protein composition of epicardial-derived EVs isolated from different environmental conditions (hypoxia and normoxia) and study their effect in autocrine and paracrine communication.

As for epicardial-derived ECM, the specific contribution of epicardial-derived cells (EPDCs) to the embryonic myocardial walls has not yet been assessed. Moreover, as activated CFs are responsible for the accumulative ECM tissue in damaged areas of the heart, studying the matricellular composition of their known progenitor cells might help understand the fibrotic response mediated by cell-ECM interactions. Herein, we took advantage of proteomic tools to assessed different fractions of epicardium-derived interstitial cell line (EPIC)-derived ECM and compare it with the embryonic heart and a commercially available basement membrane.

In accordance with the previously discussed topics, the general hypothesis of this thesis is that epicardial-derived ECM and EVs are important elements of cardiac cell-to-cell communication. Accordingly, the main objective of this thesis is to define the composition and function of the secretome (EVs and ECM) of EPIC.

The specific scientific objectives of this thesis are:

**OBJECTIVE 1:** To establish an EV enrichment method at our laboratory to allow for epicardial-derived EV physical and molecular characterization.



OBJECTIVE 2: To characterize the protein content of epicardial-derived EVs in samples isolated from normoxic and hypoxic EPIC cultures and to assess their role in paracrine and autocrine signalling.

OBJECTIVE 3: To describe epicardial-derived ECM and its role in endothelial cell behaviour.

Results corresponding to the different objectives are presented in separate chapters as follows:

In chapter I, the enrichment quality of EPIC-derived EVs is studied. EVs obtained from two distinct methods –ultracentrifugation (UC) and size exclusion chromatography (SEC)– were studied using physical and molecular analysis, being the selected method employed to characterize normoxic and hypoxic-derived EVs.

In chapter II, a specific signalling pathway involved in EV secreted by EPIC preconditioned to normoxia and hypoxia is studied. First, protein composition of EPIC-derived EVs was assessed and *in silico* analysis employed to study possible EPIC-derived EV markers as well as its differential cargo assessment in EVs from both conditions. Then, after targeting a potential bioactive role of EPIC-derived EVs, its functional activity was studied considering two modes of cell signalling: autocrine and paracrine.

In chapter III, EPIC-derived ECM is detailed and compared with embryonic cardiac ECM and Matrigel, a widely used mouse tumour-derived ECM. We have researched the proliferative potential of epicardial-derived ECM in human endothelial cells based on the bioinformatic analysis provided by EPIC-matricellular composition.

# MATERIAL & METHODS

---



# Material & Methods

---

## 1. Cell culture

### 1.1. EPIC

EPIC is a cell line developed in our laboratory in 2013 at the University of Málaga (Ruiz-Villalba *et al.*, 2013). Epicardial explants from mouse embryos at embryonic day 11.5 (E11.5) were cultured until spontaneously immortalized, and the phenotype of this heterogeneous cell population was confirmed to resemble that of epicardial-derived cells (EPDCs) (Ruiz-Villalba *et al.*, 2013). Complete media for EPIC cell culture is composed of Dulbecco's Modified Eagle's Medium (DMEM, Gibco) supplemented with 10% Fetal Bovine Serum (FBS, Gibco), 100 U/mL penicillin (Sigma), 100 µg/mL streptomycin (Sigma), and 2mM L-Glutamine (Sigma).

For EPIC passage, cells were detached from culture flasks using a final concentration of 0.05% Trypsin-Ethylenediamine tetraacetic acid (EDTA) (Gibco) diluted in Hanks' Balanced Salt Solution without calcium and magnesium and containing phenol red (HBSS<sup>-</sup>; Gibco), and incubated at 37 °C. Trypsinization was discontinued with the addition of EPIC culture medium (including FBS) and centrifugated (Heraeus Labofuge 400, Thermo Fisher) at 300 g for 5 minutes to remove traces of trypsin. The EPIC pellet was then resuspended in EPIC culture media, and cell density was quantified by diluting the working cell suspension 1:1 with trypan blue (Sigma) and counting cells in a Neubauer chamber. EPICs were plated in T182 flasks at 2.7 and 3.8x10<sup>3</sup> cells/cm<sup>2</sup> density or stored at -80 °C. For cell cryopreservation, up to 1x10<sup>6</sup> EPIC were resuspended in 950 µL of complete EPIC media and 50 µL of Dimethyl Sulfoxide (DMSO; Sigma) and frozen at -80°C in an isopropanol-filled container to be transferred to nitrogen cell tank for long term storage.

### 1.2. HUVEC

Human umbilical vein endothelial cells (HUVECs) are primary, non-immortalized cells isolated from the vein of the umbilical cord, first isolated in the 1970s (Jaffe *et al.*,

1973). This primary cell culture is commonly used as experimental system for vascular biology, especially for the implementation of proliferation and angiogenic assays.

HUVECs are cultured in Endothelial Growth Media (EGM, Lonza). EGM is composed of Endothelial Cell Growth Basal Medium-2 (EBM-2, BulletKit™, Lonza) supplemented with 2% FBS, 0,1% heparin, 0,1% VEGF, 0,1% Ascorbic acid, 0.1% Gentamicin sulfate-Amphotericin (GA-1000), 0.1% R<sup>3</sup>-insulin-like growth factor-1 (R<sup>3</sup>-IGF-1), 0.1% recombinant human Epidermal Growth Factor (rhEGF) and 0.04% hydrocortisone, 0.4% recombinant human Fibroblast Growth Factor-β (rhFGF-β) (all culture supplements from Lonza) and 100 U/mL penicillin (Sigma), 100 µg/mL streptomycin (Sigma).

Nunc EasyFlask T25 cell culture flasks (Thermo Fisher) were coated with 1% gelatine in PBS by covering the bottom with the gelatine solution and incubating at 37 °C for a minimum of 10 minutes. The solution was then removed completely to ensure the cell growing surface had no excess of gelatine. A density of 6.25-7x10<sup>3</sup> cells/cm<sup>2</sup> HUVECs at passage 6 to 8 (kindly donated by Dr. Beatriz Poveda) were cultured in gelatine-coated Nunc EasyFlask T25 flask and incubated at 37 °C and 5% CO<sub>2</sub>. At approximately 80% confluency, HUVECs were washed twice with PBS and incubated with 0.05% Trypsin-EDTA (Gibco) diluted in HBSS<sup>-</sup> (Gibco) for 5 minutes at 5% CO<sub>2</sub> and 37 °C. Trypsinization was interrupted by the addition of EGM, which contains FBS, and the cell suspension was centrifuged at 300 g for 5 minutes. HUVECs pellet was then resuspended in EGM-2 and cells were counted in a Neubauer chamber for plating 6.25-7x10<sup>3</sup> cells/cm<sup>2</sup> HUVECs per gelatine-coated T25 flask, Nunc™ 24 well-cell culture plates (Thermo Fisher) or V7-PS cell culture microplate (Agilent).

## 2. Extracellular vesicle isolation

Between 2.7 and 3.8x10<sup>3</sup> EPIC/cm<sup>2</sup> were cultured in T182 flasks (VWR) at 37 °C and 5% CO<sub>2</sub>. At approximately 80% confluency, EPIC were washed twice with warm phosphate-buffered saline (PBS) solution and incubated with EV-depleted medium at 37 °C, and in 5% CO<sub>2</sub>/20% O<sub>2</sub> atmosphere, (“normoxic condition”), or either at 1% or 5% O<sub>2</sub>

("hypoxic conditions"). Complete culture medium was replaced by EV-depleted one, in which 10% FBS is replaced with 10% ultracentrifuged FBS (from here onwards UC-FBS) for the purpose of specifically studying EV derived from EPIC. Briefly, standard FBS is ultracentrifuged (Sorvall Discovery 90SE) at 100,000 g in fixed angle rotor F40L-8x100 (Thermo Fisher) for 5 hours and 30 minutes at 4 °C, the supernatant is filtered with a 0.2 µm-pore filter (SARSTEDT) and stored at -20 °C until further use. Conditioned media from EPIC between passage 7 and 9 were harvested every 24h for two days and kept at 4 °C until being used (please, check subchapters 2.1. and 2.2. below).

### 2.1. Ultracentrifugation

EV isolation by ultracentrifugation (UC) was adapted from a previously described protocol (Lobb *et al.*, 2015). Conditioned media containing EPIC EVs was centrifuged at 10,000 g for 50 minutes at 4 °C in a floor-model ultracentrifuge (Sorvall Discovery 90SE). The pellet was discarded and the supernatant ultracentrifuged at 100,000 g for 70 minutes at 4 °C in a fixed angle rotor F40L-8x100 (Thermo Fisher). The supernatant was discarded and the pellet was resuspended in 1 mL of 0.22 µm-filtered PBS (f-PBS) and 30 mL of f-PBS was added to wash the EVs at 100,000 g for 70 minutes at 4 °C. EVs isolated by UC (EVs-UC) was resuspended in 100 µL of f-PBS and stored at -80 °C.

### 2.2. Size Exclusion Chromatography

EVs isolated by SEC were obtained at Imperial College London during a short stay at the laboratory of Prof. Costanza Emanuelli. Briefly, conditioned media containing EPIC EVs from normoxic cultures were centrifuged (Hettich Universal 320R) at 300 g in Hettich swing-out rotor for 10 minutes at room temperature, followed by another centrifugation of the resulting supernatant at 2,000 g for 20 minutes at 4°C. The supernatant was filtered using a 0.22 µm pore-sized PES membrane filter (Millipore). Then, a concentration step was performed using 100 kDa filters in centrifugal units (Amicon Ultra-15, Millipore) at 3,600 g and 4 °C, according to manufacturer's protocol, until a final volume of 500 µL was reached. EVs were isolated using qEVoriginal/35 nm (IZON) SEC columns according to manufacturer's protocol. Fractions 7 to 10 were collected, resulting in 2 mL of EVs-enriched samples. The isolated fractions were concentrated using 10 kDa filters in centrifugal units (Amicon Ultra-4, Millipore), by centrifugation at 3,600 g at 4 °C until a

final volume between 150 and 250  $\mu\text{L}$  was reached. EPIC EVs enriched via SEC (EVs-SEC) were then stored at  $-80\text{ }^{\circ}\text{C}$  until further use.

### 3. Extracellular vesicle physical characterization

#### 3.1. Transmission Electron Microscopy

To analyse the structure of EPIC EVs from UC and SEC isolations, and normoxic and hypoxic conditions, 5  $\mu\text{L}$  of EVs suspension were loaded onto glow-discharged Formvar/Carbon-coated 200-mesh copper grids for 15 minutes at room temperature. Excessive fluid was slightly drained with filter paper, grids rapidly washed with 3 drops of Milli-Q water and then the adsorbed nanoparticles were negatively stained with 1% uranyl acetate for 30 seconds. Finally, the air-dried grids were observed using a transmission electron microscope (TEM; Thermo Fisher Scientific Tecnai G2 20 Twin) operating at 120 kV.

#### 3.2. Dynamic Light Scattering

Dynamic Light Scattering (DLS) was pursued to analyse particle size distribution in isolated EVs. Isolated EVs were diluted to 1/10 in 300  $\mu\text{L}$  of f-PBS and measured in a plastic cuvette. DLS measurements were performed with Zetasizer Nano ZS90 (Malvern Instruments). Intensity and number distribution data for each sample were collected on a continuous basis for ninety seconds in sets of ten. At least three technical measurements were performed for the analysis. Data were presented as average size  $\pm$  standard deviation.

#### 3.3. Nanoparticle Tracking Analysis

Nanoparticle Tracking Analysis (NTA) allows for particle visualization and analysis of particles size, concentration, and size distribution. EVs size distribution curves and concentration measurements were carried out by NTA using Nanosight NS300 (Malvern Instruments, UK) with NTA software version 3.2 (Malvern Instruments). EVs were diluted at 1:1,000 and 1:2,000 in sterile water and injected into the flow cell of NanoSight NS300. Once loaded, the sample was passed through the system using a syringe pump at a rate of 50 arbitrary units (a.u.). Camera level was set at 14 and an analysis detection threshold of 9. To confirm cleanliness of the flow cell, measurements were performed with sterile

water (Fresenius Kabi, UK), which revealed the absence of particles. Four consecutive videos were recorded for each exosome preparation at 25 °C. The videos had a duration of 30 seconds with frame rates of 25 frames/second.

## 4. Decellularization using ammonium hydroxide

### 4.1. EPIC decellularization

In order to obtain EPIC-derived ECM, chemical decellularization was pursued using ammonium hydroxide. The decellularization protocol used in this thesis was adapted from Harris et al., 2018. Briefly,  $5.3 \times 10^3$  cells/cm<sup>2</sup> were seeded in 4-well plates (SARSTEDT) containing glass coverslips, 100 mm dishes (Corning) or T182 (VWR) flasks containing 24 mm-diameter sterile glass coverslips (Thermo Fisher) depending on the experimental design. To stimulate ECM deposition, EPIC culture media was refreshed daily from 70% cell confluency until decellularization takes place. EPIC were kept in culture three days after 100% confluency was reached to obtain an enriched content on ECM proteins. Culture media was then removed, and cells were gently washed three times with PBS warmed at 37 °C. Decellularization was carried out by carefully pipetting 10 mL of 20 mM of Ammonium Hydroxide (Honeywell) diluted in de-ionized water while avoiding abrupt shakes of the cell container. This reagent induces hypotonic stress to EPIC cells, which become round and eventually burst, leaving behind a network of ECM proteins attached to the surface (Zhou *et al.*, 2016). Cells were incubated for 5 minutes at room temperature carefully tilting the container to ensure lysis of all cells and allowing for the detachment of cellular and soluble extracellular components.

The recovered solution of ammonium hydroxide containing cellular and extracellular components, from here onwards called EPIC soluble matrix (EPIC SM), was collected and washed twice in deionized sterile water by centrifugation. EPIC SM samples were centrifuged at 9,000 g for 20 minutes at 4 °C and the washing solution discarded. After washing EPIC SM twice in deionized water, the pellet was washed three times in PBS using centrifugation at 9,000 g for 20 minutes at 4 °C. The fraction attached to the bottom of the culture plate, from here onwards named EPIC insoluble matrix (EPIC IM), was carefully washed in cold and sterile deionized water for five times, in the flask.



For LC-MS/MS, both fractions of ECM were homogenised in Laemmli buffer (LB) (6% (v/v) glycerol, 2% (m/v) SDS, 100 mM dithiothreitol (DTT) and 0.05 M Tris-HCl pH 6.8). Because of its insoluble nature, a high concentration of DTT was applied to improve the efficiency of the extraction of EPIC-derived ECM. EPIC IM was thoroughly scraped in LB with 100 mM DTT using cell scrapers and boiled at 95 °C for 5 minutes. For EPIC SM homogenisation samples were boiled at 95 °C in LB with 100 mM DTT for 15 minutes and intermittently vortexed every 2 minutes. Posteriorly, EPIC SM samples were sonicated in an ultrasonic bath for 5 minutes and centrifuged at 14,000 g for 5 minutes. The supernatant was used for mass spectrometry analysis. LB-homogenized EPIC IM and SM were stored at -80 °C.

For further functional assays (please, check subchapter 10.6), each T182 flask containing EPIC IM was incubated with 8 mL of 2 M of urea dissolved in cold sterile PBS and filtered using 0.22 µm filter, after being carefully washed with sterile deionized water. Flasks of EPIC IM containing 2 M urea were scraped using cell scrapers and over ice. Flasks were incubated at 4 °C for 72 hours in a rocking shaker. EPIC IM was then scraped again using cell scrapers and collected to Amicon Ultra centrifugal filter units of 3 kDa cutoff (Amicon) and cold sterile PBS was added until the centrifugal unit was at maximum capacity. Samples were centrifuged at 9,000 g for 20 minutes at 4 °C. The content in the filtrate collection falcon was discarded and sterile PBS was added to the concentrate collection tube until maximum capacity was reached and samples were centrifuged at 9,000 g for 20 minutes at 4 °C (this process was repeated for a minimum of 4 times). At the last washing step, EPIC IM was concentrated in sterile PBS until a maximum of 250 µL volume is left in the concentrate collection tube. Regarding EPIC SM, previously washed pellets were homogenized in a maximum of 5 mL of sterile PBS.

#### **4.2. Mice breeding and embryonic hearts decellularization**

All animals used in this study were handled in compliance with institutional and European Union guidelines for animal care and welfare under a specific experimental procedure approved by the Ethics Committee of the University of Málaga.

Mouse embryos were staged considering the presence of the vaginal plug as embryonic day (ED) 0. CD1 pregnant females were sacrificed by cervical dislocation, and embryos isolated from the uterus and washed in PBS. Six embryonic hearts at stage E17.5 were excised, washed three times in PBS and incubated at room temperature for 4 hours and 30 minutes in 20 mM NH<sub>4</sub>OH. The resulting embryonic cardiac mesh was then washed four times in MiliQ water and homogenized in SDS-PAGE buffer as previously described. Samples were stored at -80 °C until LC-MS/MS analysis was carried out.

## 5. Characterization of EPIC-derived ECM

### 5.1. Scanning Electron Microscopy (SEM)

Scanning Electron Microscopy (SEM) was pursued to provides information on the EPIC and EPIC IM surface conformation and topology. A total of 7-8 x10<sup>5</sup>/cm<sup>2</sup> EPIC were seeded in 100 mm dishes containing four 24 mm coverslips (Thermo Fisher). At 100% confluency, EPIC were decellularized as describe in subchapter 4.1 and the EPIC IM fraction was washed in PBS and fixed in 2% (v/v) glutaraldehyde (Sigma) diluted in PBS for 1 hour at room temperature. Confluent dishes containing EPIC cells were fixed in 2% glutaraldehyde and imaged as the EPIC IM cellular counterpart. After fixation, cellular and ECM samples were washed again in PBS and incubated with increasing concentrations of ethanol for sample dehydration. Samples were incubated for periods of 15 minutes in 30% ethanol, followed by 50%, 70%, 80%, 90%, 96% and 100% ethanol and then kept at 4 °C in 100% ethanol until being processed for SEM imaging. Dehydrated samples were air dried and deposited in an aluminium drum with a conductive double-sided adhesive tape and sputter-coated with a thin layer of gold (300 Å) in a Sputtering QOURUM Q 150R (QOURUM). Samples were observed with JEOL JSM6490LV SEM (JEOL) operating at 15 kV and a working distance of 10 mm.

The analysis of fibre diameter in the sample were done using ImageJ 1.53i software. By using image size bar, number of pixel/nm was assessed, and diameters were measured using the “Measure” tool in Analysis toolbar. From SEM images of EPIC IM, seventeen fibre measurements were taken per photo, from a total of six photos, while from EPIC cells images, five to eight measurements per photo were taken from four photos.

## 5.2. Immunocytochemistry

Coverslips containing EPIC-IM were fixed with 4% paraformaldehyde (PFA, Sigma) for 10 minutes at room temperature whereas wells containing EPIC cells were fixed with 4% PFA for 20 minutes at room temperature. Extracted EPIC-SM was fixed in 4% PFA for 30 minutes after washes by centrifugation in PBS. Fixed ECM fractions were then washed three times in PBS followed with blockage with SBT (10% horse serum, 1.5% BSA and 0.5% Triton X-100 in TPBS) for 1 hour at room temperature (RT). Coverslips were washed again three times with PBS and incubated overnight at 4 °C with primary antibody (either 1:100 rabbit polyclonal anti-fibronectin (Sigma) or 1:200 monoclonal anti-Laminin subunit  $\alpha$ 1 (Sigma) both diluted in SBT) or SBT as negative control. Coverslips were washed three times in PBS and then incubated with 4',6-diamidino-2-phenylindole (DAPI) (1:2,000 in PBS) and anti-rabbit AF647 (1:200 in PBS; Jackson Immuno Research) for 1 hour at RT. Finally, coverslips were washed three times in PBS. For F-actin staining, EPIC and EPIC ECM were incubated with 0.6  $\mu$ M of Phalloidin Atto 488 (Thermo Fisher) and 1:2,500 DAPI for 20 minutes in a rocking shaker at room temperature in dark. Coverslips were mounted in microscope glass slides with PBS:Glycerol (1:1). All samples were analysed using Leica SP5 HyD Confocal Microscope. Images were processed using *ImageJ 1.53i* software in which max intensity from stacked images were applied from "Z Project" tool.

## 6. Protein quantification by bicinchoninic acid

### 6.1. Extracellular vesicles

For EVs protein quantification, 10  $\mu$ L EVs were lysed in 6  $\mu$ L of lysis buffer composed of 1% Triton-X100 (Sigma) and 0.1% sodium dodecyl sulfate (SDS; Sigma) in H<sub>2</sub>O for 30 minutes on ice. A volume of 44  $\mu$ L of distilled water was added for a final dilution EVs of 6X. Standard curve for colorimetric assay was prepared using BSA (Sigma) at 2 mg/mL in distilled water to quantify and serial dilutions from 2 to 0.016 mg/mL.

#### 6.1.1. Micro bicinchoninic acid for extracellular vesicles

During a research visit at Imperial College London the method used for EVs protein quantification was Micro BCA™ Protein Assay Kit (Thermo Fisher). Briefly, standard curve from 0 to 40  $\mu$ g/mL of BSA was prepared from a stock solution of 2 mg/mL BSA (Sigma) diluted in PBS. To lyse EVs and avoid protein degradation, a lysis solution was

prepared containing 1% of protease inhibitor cocktail (Sigma) in RIPA buffer (Sigma). EVs or plasma alone (positive control) were mixed with lysis solution in a 4:1 proportion and homogenised by pipetting and incubated on ice for 15 min. The resulting solution was then centrifuged at 17,000 g for 20 minutes at 4 °C and diluted in PBS to obtain 100 times diluted working samples. A total of 150 µL of BSA solutions and samples were added to each well in transparent 96-well plates (SARSTEDT). MicroBCA reagents were mixed in 25:24:1 proportion (Reagent A:Reagent B:Reagent C) and 150 µL of MicroBCA working reagent was added to each well. Plates were incubated for 2 hours at 37 °C. Absorbances were measured at 562 nm in a plate reader Dynex Opsys MR Microplate Photometer (Aspect Scientific) within 10 minutes. The blank corresponded to PBS.

### 6.2. Extracellular matrix

For protein quantification of EPIC-derived ECM, EPIC IM obtained after urea solubilization, washes in PBS and concentrated as described in subchapter 4.1 was diluted in PBS 1:3 proportion), and EPIC SM diluted at 1:10 proportion in PBS.

### 6.3. EPIC lysate

For protein quantification of cell lysates, EPIC cell pellets were washed three times in PBS and incubated with radioimmunoprecipitation assay (RIPA) buffer (5 mM of Trizma (Sigma), 15 mM NaCl (Sigma), 0.1% Triton X-100 (Sigma), 0.1 mM EDTA (Sigma) and 0.6 mM of sodium deoxycholate (Sigma) in distilled water). The pH was adjusted to 7.4 with 3 N of HCl (Sigma)] containing 1% of protease inhibitor cocktail (Sigma) on ice for 5 minutes. Cell lysate was homogenised and centrifuged at 12,000 g for 10 minutes at 4 °C, and the supernatant was collected for protein quantification by bicinchoninic acid (BCA) assay and further proteomic assays.

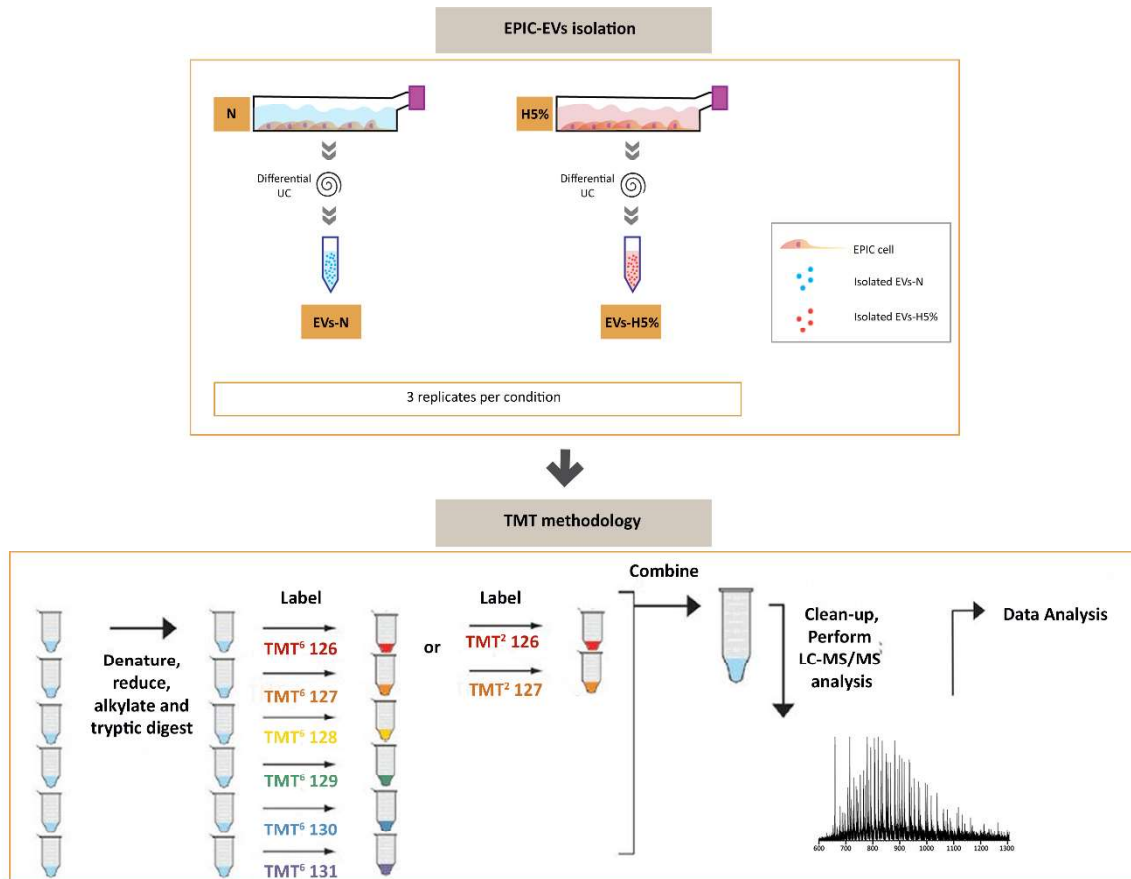
Standard curve for colorimetric assay was prepared using Bovine Serum Albumin (BSA, Sigma) at 2 mg/mL and using 2 to 0.031 mg/mL serial dilutions in RIPA buffer (for cell lysate solutions), distilled water (for EVs) or PBS (for ECM). To implement BCA reaction, 25 µL of BSA solution or cell lysate diluted in PBS 1X was pipetted into each well followed by 200 µL of working reagent composed of 50 parts of solution A and 1 part of solution B from Pierce™ BCA Protein Assay Kit (Thermo Fisher) in a 96 well-plate (SARSTEDT). Blank corresponded to RIPA buffer only for EPIC lysate, distilled water for

EVs and PBS for ECM. The plate was incubated at 60 °C for 2 hours and absorbances were read in Asys Expert Plus plate reader (Biochrom) with 550 nm filter within 10 minutes. The plate was incubated at 37 °C for 1 hour and absorbances were read in Asys Expert Plus plate reader (Biochrom) with a 550 nm filter within 10 minutes. For the estimation of protein concentration in samples of cell lysate and EV solutions, absorbance value attributed to blank was subtracted to all absorbances measures and standard curves equations were calculated with a correlation ( $R^2$ ) higher than 0.98.

## 7. Proteomic strategy

### 7.1. Tandem Mass Tag multiplexing strategy for extracellular vesicle proteome analysis

Tandem Mass Tags (TMT) were employed to allow the analysis of multiple samples in the same assay and diminishing the technical error variability (Fig. 4). Three normoxic and three hypoxic representative samples were selected to perform TMT sixplex (TMT6plex) and twoplex (TMT2plex) isobaric label for liquid chromatography with tandem mass spectrometry (LC-MS/MS) analysis. Each sample was adjusted to a final concentration of 1  $\mu\text{g}/\mu\text{L}$  of protein. Five microliters of 200 mM *tris* (2-carboxyethyl)phosphine (TCEP) was added to each sample and incubated at 55 °C for 1 hour. Then 60 mM of iodoacetamide with tetraethylammonium bromide buffer (TEAB) was added and samples were incubated in the dark for 30 min. Proteins were precipitated in six volumes of acetone at  $-20$  °C for 4 hours, followed by a centrifugation step at 8,000 *g* for 10 minutes at 4 °C, after which the supernatants were removed and discarded. Pellets were resuspended in 100  $\mu\text{L}$  of TEAB (50 mM, pH 8.5). Trypsin was added to the samples in a proportion of 1:50 (trypsin: protein, w/w) and incubated overnight at 37 °C. Each sample was tagged with a Thermo Scientific TMTsixplex Isobaric Mass Tagging Kit (Thermo Fisher Scientific, Rockford, IL) according to the manufacturer's instructions. Briefly, 500  $\mu\text{g}$  of each sample ( $n=3$  per condition) were marked with TMT 126, 127, 128, 129, 130 and 131 Da. The reaction was stopped using 8  $\mu\text{L}$  of 5% hydroxylamin and incubated at room temperature for 15 min. The chemically tagged samples were combined into one tube and dried using SpeedVac. Purified samples were resuspended with 0.1% of formic acid (FA) and analysed by liquid chromatography tandem mass spectrometry (LC-MS/MS; please, see subchapter 7.3).



**Figure 4 – Tandem mass tag methodology for extracellular vesicle proteome studies.** EVs-N and EVs-H5% were harvested and isolated by ultracentrifugation. In order to allow the analysis of multiple samples in a single liquid chromatography tandem mass spectrometry (LC-MS/MS) assay, triplicates of EVs-N and EVs-H5% were digested and then labelled with isobaric tags. After probing each sample, all conditions are mixed. TMT2plex was performed in triplicate while TMT6plex was a single assay.

## 7.2. Label-free proteomics for descriptive composition of the extracellular matrix

Bottom-up label-free proteomics were pursued for qualitative information on ECM composition. EPIC IM (n=3), EPIC SM (n=3) and decellularized E17.5 hearts (n=6) solubilized in SDS-PAGE buffer and Matrigel (Corning) (n=3), were denatured at 95 °C for 15 minutes and vortexed intermittently every 2 minutes. Samples were then sonicated for 5 minutes and centrifuged at 14,000 g for 5 minutes. To eliminate incompatible components of LC-MS, supernatants were run in a gel-assisted proteolysis by mixing 45 µL of sample with 14 µL of 40% acrylamide. Then 2.5 µL of 10% ammonium persulfate and 1 µL TEMED were quickly added and incubated for 20 minutes. Gels were cut in 1-2 mm cubes and treated with 50% acetonitrile (ACN)/25 mM ammonium bicarbonate. Samples were dehydrated and dried with ACN and then reduced with 10 mM DTT in 50 mM ammonium bicarbonate for 30 minutes at 56 °C. Cysteine residues were carbamidomethylated with 55 mM iodoacetamide in 50 mM of ammonium bicarbonate for 20 minutes at room temperature in the dark. Gel fractions were dehydrated, and proteins digested by rehydrating gel fractions in 10 ng/µL trypsin (Promega) overnight at 30 °C. Peptides were extracted with 0.1% ACN/formic acid (FA) for 30 minutes at room temperature. Samples were dried using SpeedVac to eliminate residual ACN and ammonium bicarbonate and dissolved in 0.1% FA and treated with ultrasound for 3 minutes and centrifuged at 13,000 g for 5 minutes. Samples were then purified and concentrated using C18 ZipTip (Merck) according to manufacturer's instructions. Purified samples were then analysed by LC-MS/MS (please, see subchapter 7.3).

## 7.3. Liquid chromatography tandem mass spectrometry

For LC-MS/MS analysis, purified samples were injected in an Easy nLC 1200 UHPLC coupled to Q Exactive HF-X Hybrid Quadrupole-Orbitrap mass spectrometer (ThermoFisher Scientific). Mobile phases of HPLC were the following: solvent A consisted of 0.1% FA (in water) and solvent B of FA/acetonitrile (ACN) (0.1%/80%). Using a thermostated automatic injector, 1 µL (correspondent to 100 ng) of the peptide samples was loaded in a pre-column Acclaim PepMap 100, 75 µm x 2 cm, C18, 3 µm, 100 A (ThermoFisher Scientific) at a flow of 20 µL/min and eluted in a 50 cm analytical column (PepMap RSLC C18, 2 µm, 100 A, 75 µm x 50 cm; Thermo Fisher Scientific).

ECM-derived peptides were eluted from the analytical column with a 120 minute gradient from 5% to 20% of solvent B in solvent A, followed by a 5 minute gradient from 20% to 32%, and finally to a 95% for 10 minutes before rebalancing with 5% of solvent B in solvent A. EVs peptides tagged with TMT were eluted with a gradient of 2 to 20% of solvent B in solvent A for 4 hours. This step was followed by a 20 to 35% gradient of solvent B elution for 30 minutes and finally a gradient of 95% of solvent B elution for 15 minutes before rebalancing the column with 2% of solvent B. For both ECM and EV peptides, the elution was performed with a constant flow of 300 nL/min. Calibration solution LTQ Velos ESI Positive Ion Calibration Solution (Pierce, IL, USA) was used to externally calibrate the instrument prior to sample analysis and internal calibration was performed with polysiloxane ion signal at  $m/z$  445.120024 from ambient air.

For ECM peptides, MS scans were performed in the  $m/z$  375-1,600 range at a resolution of 120,000  $m/z$ . Using a data dependent acquisition mode, the 15 strongest precursor ions were isolated from all precursor ions with a charge of +2 to +5 within a 1.2  $m/z$  window and fragmented to obtain the corresponding MS<sup>2</sup> spectra. Fragmentation ions were generated in a high energy collisional dissociation cell (HCD) with a fixed first mass at 110  $m/z$  and detected on an orbitrap mass analyzer at a resolution of 30,000. The dynamic exclusion for the selected ions was 30 s. The maximum allowed ion accumulation time in MS and MS<sup>2</sup> mode was 50 ms and 70 ms, respectively. Automatic gain control was used to prevent overfilling of the ion trap and was set to  $3 \times 10^6$  ions and  $2 \times 10^5$  ions for a full MS and MS<sup>2</sup> scan, respectively.

For EVs tagged with TMT, the resolution of MS survey scans was set to 120,000  $m/z$ . while for MS/MS the resolution was set to 30,000. The ion pulverization voltage was set to 2.2 kV with an  $m/z$  window from 350 to 1500, an isolation window of 0.7  $m/z$  and dynamic exclusion of 20 s.

Software versions used for data acquisition and manipulation were *Tune 2.9* and *Xcalibur4.1.31.9*.



## 8. Bioinformatic analysis

Searches of the MS/MS<sup>2</sup> spectra were performed against the SwissProt *Mus musculus* version 2017.10.25 protein database (25,097 sequences). The raw data acquired was analyzed on the Proteome Discoverer 2.2 platform (Thermo Fisher Scientific) with the Sequest HT search engine.

### 8.1. Tandem Mass Tags analysis

The search parameters in Sequest HT search engine for EVs tagged with TMT include 10 ppm peptide precursor mass tolerance and 0.6 Da fragments mass tolerance. The search space also included two sites of tryptic excision. The rate of false positives was determined with the *Percolator* software, which uses a reversed protein database as signal. The estimated false positive rate was kept at 1% at the protein level. The data was filtered to accept only proteins with at least two peptide sequences. It is important to highlight that detected peptides may match one unique protein or a group of proteins that share a determined peptide. Tandem mass tagging efficiency corresponded to 83-84%. Protein identifications related to sample contaminants, DECOY peptides, and proteins base on only one identified peptide were eliminated. For both TMT2plex and TMT6plex analysis, proteins that were not identified in, at least, two lists of both conditions, would not be considered for analysis. Protein abundancies were transformed using Log<sub>2</sub> and normalized by quantile normalization. Statistical analysis between EVs-N and EVs-H5% can only be performed using TMT6plex data since TMT2plex shows low statistical power between the absence/presence of identified peptides in replicated assays. For statistical analysis, a paired t-test was employed in which proteins with a p-value < 0.05 were considered statistically different and used for differential expression analysis recurring to the normalized data. Protein abundancies were based on the intensity on precursor ions and used to calculate EVs-H5%/EVs-N ratio.

The proteins shown to be enriched in EVs-N and EVs-H5% were analysed in *STRING* (<https://string-db.org/>) set for a minimum interaction score of 0.70 of confidence. Protein lists, analysed against KEGG pathways database, were organized from the lowest false discovery rate (FDR) to the highest FDR.

## 8.2. Label free proteomic analysis

Sequest HT search engine (ECM peptides) was set for mass tolerances of 10 ppm and 0.02 Da for the precursor ions and fragment ions, respectively. Two lost tryptic cleft sites were allowed. Oxidation of methionine and N-terminal acetylation were established as variable modifications, while carbamidomethylation of cysteine residues were established as fixed modification. Exploratory protein identification was pursued by identifying protein presence or absence in two or more biological samples with three replicates for EPIC IM, EPIC SM and Matrigel and six replicates for E17.5 decellularized hearts. Proteins were considered part of an experimental condition if they were present in at least two replicates. The FDR for consecutive protein and peptide assignments was determined using the *Percolator* software package, that it is based on a target-decoy approach that uses an inverted protein database as a decoy, imposing a strict limit of 1% of FDR. The results were filtered to accept only those proteins with at least two peptide sequences. Relative abundances of sample replicates were prepared by calculating the abundance of a protein relative to total abundance per condition. In detail, and to obtain a percentage for the relative abundance of each protein, relative abundances were calculated per protein as follows:

$$\frac{\text{Average of protein abundance}}{\text{Total proteins abundance}} \times 100$$

Total abundance was calculated from the sum of abundances per replicate, and then an average of replicate total abundance was performed to obtain the total abundance per condition. A list of proteins and respective abundances were then filtered in “cellular component” tab for “extracellular” term. For ECM analysis, only extracellular proteins were considered.

Proteins found on different experimental conditions were compared at qualitative level (presence or absence). Lists of proteins were enriched in Gene Ontology (GO) terms using *clusters\_to\_enrichments.R* script from *ExpHunterSuite* (González Gayte *et al.*, 2017). This script uses over-representation analysis (ORA). This method takes a group of significant proteins and performs a Fisher’s exact test for each GO term. Fisher’s exact

test P-value were corrected with Benjamini-Hochberg procedure. GO terms with adjusted P value lower than 0.05 were discarded.

## 9. Western Blot

Western Blot (WB) was pursued to confirm the presence or absence of EPIC secretome-related proteins. The separator polyacrylamide gel was prepared with a percentage of acrylamide that better diffuses the protein of interest in the gel. For longer denatured proteins, 8% of acrylamide was used, while for smaller proteins a 12% acrylamide content was employed. Separator gels were prepared following the order described below:

Components	Final concentration of bis-acrylamide		
	8%	10%	12%
MiliQ water	4.6	4	3.3
Acrylamide 30% (BIO-RAD)	2.67	3.33	4
Tris pH 8.8 (separator)		2.5	
SDS 10% (Sigma)		0.1	
APS 10% (Sigma)		0.1	
TEMED (Sigma)		0.004	
Final volume (2 gels)		10	

Separator gel is poured in 10 x 8 cm cast size of 0.75 mm glass plates and a layer of distilled water was added on top to obtain a homogeneous surface devoid of air bubbles. Once separator gel was polymerized, concentrator gel was prepared following the order described:

Components	Volume (mL)
MiliQ water	2.1
Acrylamide 30% (BIO-RAD)	0.5
Tris pH 6.8 (concentrator)	0.38
SDS 10% (Sigma)	0.03
APS 10% (Sigma)	0.03
TEMED (Sigma)	0.003
Final volume (2 gels)	3

Concentrator gel was then added to the gel cast and a comb of 10 wells was placed between the glass plates.

Before loading the samples, casted gels were run at a 100 V for 10 min. Gels were run in Mini-PROTEAN Tetra Vertical electrophoresis cell coupled to PowerPac HC High-Current Power Supply (BIO-RAD) and cold electrophoresis buffer (3% (m/v) Trizma (Sigma), 14.4% Glycine (Sigma) and 1% SDS in distilled water). Precision Plus Protein Dual Color Standard (BIO-RAD) with a range of 10 to 250 kDa were used to localize the desired proteins. For WB of EVs proteins, 16 µg of EPIC lysate, EVs-UC, EVs-SEC, EPIC-derived EVs from normoxic condition culture (EVs-N) and EPIC-derived EVs from 5% O<sub>2</sub> culture (EVs-H5%) samples were prepared in LB 2X concentrated. For ECM peptides, 10 µg of EPIC lysate, EPIC IM, EPIC SM, Matrigel and E17.5 decellularized heart samples were prepared in LB 2X concentrated. LB is composed of 0.03 M Tris-HCl pH 6.8, 1% SDS, 2.5% (v/v) β-mercaptoethanol, 0.025% (v/v) bromophenol blue and 10% (v/v) glycerol.

After boiling protein samples at 95 °C for 5 minutes, the samples and ladder were loaded and run at 100 V for 10 minutes to allow the solutions to enter in the gel homogeneously. Proteins were then separated in SDS-polyacrylamide gel with concentrations of bis-acrylamide between 8 and 12% at 200 V for an average of 90 minutes. Polyacrylamide pore sizes were selected according to the size of proteins of interest, thus the bigger the protein, the lower percentage of bis-acrylamide was added. For instance, for large proteins such as fibronectin (220 kDa) 8% bis-acrylamide gels

would be used, as for Alix (90 kDa) electrophoresis gels of 10% bis-acrylamide would be employed.

Separated proteins were transferred onto nitrocellulose membranes (Protan, 0.45  $\mu\text{m}$ ) using Mini Trans-Blot Cell system coupled to PowerPac HC High-Current Power Supply (BIO-RAD) in transfer buffer (3% (m/v) Trizma, 14.4% Glycine and 20% (v/v) Methanol (Sigma) in distilled water). Transfer was ran at 350 A for 3 hours at 4 °C.

After transference, membranes were washed in Tris-buffered saline with Tween20 detergent (TBST; 4% (m/v) NaCl, 0.1% KCl, 12.5% (v/v) 1 M Tris HCl pH 7.5 and 0.01% Tween 20 (Sigma) in distilled water) for 10 minutes to eliminate traces of Laemmli transfer buffer. To confirm protein transference to nitrocellulose membrane, a Ponceau staining (5% (m/v) Ponceau in 0.1% (v/v) acetic acid) was performed. Membranes were submerged in the Ponceau staining for 2 minutes and washed twice in tap water. Membranes were stained with Ponceau to be able to visually compare that loaded protein quantities were similar in each lane since housekeeping proteins cannot be used to compare the protein cargo of EVs. An image is captured to verify of protein distribution and quantities between samples. Membranes were washed in TBST to eliminate traces of ponceau staining. Then, membranes were blocked in blocking buffer (5% (m/v) non-fat dry milk in TBST buffer) for 1 hour at room temperature in a rocking shaker.

### 9.1. Extracellular vesicles

For EVs protein presence and enrichment, TSG101 and ALIX were used. Nitrocellulose membranes with transferred EVs proteins were washed three times for 10 minutes in TBST and incubated with primary mouse anti-TSG101 (1:100; Santa Cruz Biotechnology) or anti-ALIX (1:100, Santa Cruz Biotechnology) in blocking buffer overnight at 4 °C in a rocking shaker. Following incubation, membranes were washed three times for 10 minutes in TBST and incubated with an anti-mouse IgG secondary antibody in blocking solution (1:4,000; Sigma) for 1 hour. Membranes were then washed three times for 10 minutes in TBST and incubated for 5 minutes in the dark with SuperSignal® West Pico PLUS Chemiluminescent Substrate reagent (ThermoFisher) according to manufacturer's instructions. The signal was revealed using Chemidoc XRS+ (BIO-RAD) and images processed using Image Lab software (BIO-RAD).

## 9.2. EPIC-derived extracellular matrix, E17.5 decellularized heart and Matrigel

For WB of ECM samples and EPIC lysate, ECM-related proteins laminin  $\alpha 1$  and fibronectin were used. Nitrocellulose membranes with transferred proteins were washed three times for 10 minutes in TBST and incubated with primary monoclonal anti-Laminin subunit  $\alpha 1$  (1:1,000; Sigma) or polyclonal anti-fibronectin (1:1,000; Sigma) in blocking buffer overnight at 4 °C in a rocking shaker. Following incubation, the membranes were washed three times for 10 minutes in TBST and incubated with an anti-rabbit secondary antibody in TBST (1:10,000; Sigma) for 1 hour at room temperature. Membranes were finally washed three times for 10 minutes in TBST and incubated for 5 minutes in the dark with SuperSignal® West Pico PLUS Chemiluminescent Substrate reagent (ThermoFisher) according to manufacturer's instructions and signal developed using ultra-violet imaging from Chemidoc XRS+ (BIO-RAD). Images processed using *Image Lab* software (BIO-RAD).

## 10. Functional assays of EPIC secretome

### 10.1. Fluorescent labelling of EPIC-derived EVs

EPIC-derived EVs were probed with fluorescent dyes to confirm that EVs are internalized in EPIC and HUVECs. For probing EVs with CellTracker™ CM-Dil (Invitrogen), EVs were isolated as described in subchapter 2.1. After washing EVs-enriched pellet in f-PBS, the washed pellet was resuspended in 0.8  $\mu\text{M}$  of CellTracker™ CM-Dil (Invitrogen), diluted in f-PBS and ultracentrifuged at 20,300 g for 70 minutes at 4 °C. Supernatant was discarded and Dil-probed EVs were resuspended in f-PBS and stored at -80 °C. The negative control for this procedure corresponds to 0.8  $\mu\text{M}$  of CellTracker™ CM-Dil alone diluted in f-PBS and ultracentrifuged at 20,300 g for 70 minutes at 4 °C to, finally, be resuspended in f-PBS and stored at -80 °C.

EVs probing with PKH26 Red Fluorescent Cell Linker Kit (Sigma) was performed with 1  $\mu\text{L}$  of PKH26 diluted in Diluent C (1/10 dilution) to be then homogenized in 3  $\mu\text{g}$  of EPIC-derived EVs. As negative control, 1  $\mu\text{L}$  of PKH26 diluted in Diluent C was added to 4  $\mu\text{L}$  of f-PBS (same volume as in EVs). Then, 95  $\mu\text{L}$  of Diluent C was added to both samples and incubated for 5 minutes at room temperature. Next, 100  $\mu\text{L}$  of f-PBS was added and samples were incubated again for 5 minutes at room temperature. Finally, samples were

centrifuged at 10,000 g for 60 minutes at 25 °C, the supernatant was collected to a new tube and centrifuged at 16,000 g for 30 minutes (25 °C). All samples were stored at -80°C.

## 10.2. Total Internal Reflection Fluorescence imaging of EPIC-derived EVs internalization

To minimize the appearance of artifacts and optimize EVs attachment to a glass surface, 24 mm diameter coverslips (Thermo) were first cleaned and sonicated in a water bath (Sonorex Bandelin) for 30 minutes in a 50 mL falcon containing 1% MicroSon (Fisher Scientific) in distilled warm water. Coverslips were rinsed 10 times with distilled water and sonicated for 15 minutes twice. Coverslips were then rinsed 3 times in 70% and then 3 times in 100% ethanol, being sonicated for 15 minutes after each washing step with the rinsing media. Finally, coverslips were rinsed once with 100% ethanol and stored in 100% ethanol. Before adding the EVs solution of negative control, the coverslips to be used were collected and let to dry in a Petri dish. Twenty  $\mu\text{L}$  of Dil-probed EVs or Dil-containing PBS were added to treated coverslips and incubated at room temperature for 20 minute to allow exosome to sink and attach to the surface of the coverslip. Samples in coverslip were then washed three times in f-PBS.

In order to study EPIC-derived EVs internalization *in vitro*,  $8 \times 10^3$  EPIC / $\text{cm}^2$  were seeded in  $\mu$ -Slide 8 well chamber slides (Ibidi). When 70 to 80% confluency was reached, a volume of 30  $\mu\text{L}$  from either a 1/100 diluted Dil-probed EVs solution, PBS containing Dil or PBS alone, was diluted in EV-depleted medium to a final volume of 400  $\mu\text{L}$  and incubated with EPIC for 4 hours at 37 °C and 5%  $\text{CO}_2$ . Then, to assess EPIC-derived EVs internalization in HUVECs, cells were seeded in  $\mu$ -Slide 8 well chamber slides (Ibidi) at a density of  $7 \times 10^3$  cells/ $\text{cm}^2$  and incubated at 37 °C until a confluency of 70 to 80% was reached. A quantity of 40  $\mu\text{g}$  of PKH26-dyed EVs, PBS containing PKH26 or only PBS was added to each well, diluted in EBM-2 for a final volume of 400  $\mu\text{L}$  and incubated at 37 °C and 5%  $\text{CO}_2$  for 4 hours. For both cell types, Hoechst 33342 dye (Thermo Fisher) was added at a final concentration of 1,5  $\mu\text{g}/\text{mL}$  for 30 minutes, and, before image acquisition, a final concentration of 50 nM of LysoTracker® Green DND-26 (Thermo Fisher) was added to stain acidic compartments in live cells (e.g. lysosomes). In about two minutes under continuous excitation, LysoTracker is photobleached which limits the tracking period.

Samples were imaged using Eclipse Ti TIRF Microscope (Nikon) and images were collected by iXon3 897 EM-CCD camera (Andor). Acquired data were processed using ImageJ 1.53i software.

### **10.3. Cell proliferation assays with EVs**

#### **10.3.1. EPIC**

To infer if EPIC-derived EVs have a proliferative effect on their parental cells,  $6.25 \times 10^3$  EPIC/cm<sup>2</sup> (passages 9 to 11) were plated in Nunc™ 24 well-cell culture plates (Thermo Fisher) with EPIC complete media and incubated at 37 °C and 5% CO<sub>2</sub>. At 70% confluency, cells were washed twice in PBS and starved overnight at 37 °C and 5% CO<sub>2</sub> with DMEM, 100 U/mL penicillin and 100 µg/mL streptomycin (0% FBS media). The following day, EPIC-derived EVs were directly added to the well. EVs-N and EVs-H5% were added at a concentration of 20 or 50 µg/mL of EVs proteins and incubated for 24 hours. Complete EPIC media and 0% FBS media were used as positive and negative controls, respectively. Additionally, EVs derived from EPIC incubated at 1% O<sub>2</sub> (EVs-H1%) were also used for functional studies.

#### **10.3.2. HUVECs**

To infer if EPIC-derived EVs have a proliferative effect in a paracrine manner, Nunc™ 24 well-cell culture plates (Thermo Fisher) were coated with 1% gelatine and incubated for 10 minutes at 37 °C. Then,  $6.25 \times 10^3$  cells/cm<sup>2</sup> HUVECs (passages 7 or 8) were plated in the gelatine-coated plates with EGM-2 and incubated at 37 °C and 5% CO<sub>2</sub>. At 70% confluency, cells were carefully washed twice with PBS and starved overnight at 37 °C and 5% CO<sub>2</sub> in 1% FBS media (EBM-2, 100 U/mL penicillin, 100 µg/mL streptomycin and 1% of UC-FBS). The following day, EVs-N, EVs-H5% and EVs-H1% were added to the cell culture at 20 and 50 µg/mL of EVs proteins and incubated for 24 hours. EGM-2 and 1% FBS media were used as positive and negative controls, respectively.

#### **10.3.3. 5-Ethynyl-2'-deoxyuridine click chemistry reaction**

Proliferation assays were evaluated according to their activity on DNA synthesis phase (S phase) by the level of incorporation of a thymidine analogue, 5-Ethynyl-2'-deoxyuridine (EdU). To carry out cell proliferation quantification, cells were incubated



during 15 minutes at 37 °C with 10  $\mu$ M of EdU. EPIC and HUVECs were then washed twice with PBS, fixed with 4% PFA for 20 minutes at room temperature, and washed three times in PBS. Fluorescent labelling of proliferating cells is assured by a click chemistry reaction. The reagents are an azide-conjugated fluorochrome, and copper (I), this latter acting as the catalyzer of the click reaction. Due to EdU smaller size than antibody-based detection, it presents a higher diffusion rate and cell/tissue penetration (Salic and Mitchison, 2008). Cells were permeabilised with 0.5% of Triton X-100 for 20 minutes at room temperature and washed again in DPBS for two times. DPBS buffer is composed of 0.01% (w/v)  $\text{CaCl}_2$  and  $\text{MgCl}_2(\text{H}_2\text{O})_6$ , 0.8% (w/v) NaCl and 0.22% (w/v)  $\text{Na}_2\text{HPO}_4$  dilute in distilled water (all reagents from Sigma). DPBS pH is corrected to 7.4 using 3 N HCl. The reagents were mixed in the precise order indicated in the following table to induce the click reaction:

Component (stock concentration)	Final concentration
PBS 4:DMSO 1	88,8% (v/v)
200 mM $\text{CuSO}_4$ (Sigma)	2 mM
4 mM Alexa-fluor 545 (Sigma)	8 $\mu$ M
200 mg/mL ascorbic acid (Sigma)	20 mg/mL

The alkyne handler of EdU can ligate to azide-containing molecules through a click chemistry reaction allowing detection of proliferative cells by fluorescent microscopy. Thus, cells were incubated with the click reaction mix for 15 minutes in the dark at room temperature, and washed with PBS twice. To quantify the final number of cells, plates were incubated with 1:4,000 DAPI in PBS for 15 minutes in the dark and then washed again with PBS for three times.

Culture plates were analysed in an Operetta High Content Screening system (Perkin Elmer) using the Harmony 4.8 software. In each well, images were taken using confocal imaging with 10x objective (59 fields). The objective was set at 4.5  $\mu$ m height from the plate, with laser exposure for 50 ms for DAPI and 180 ms exposure for Alexa Fluor 545 data collection. For image analysis, method C algorithm to identify cell nuclei was used assuming a roundness > 0.8 and nucleus area between 68 and 700  $\mu\text{m}^2$ . Proliferative cells were established by indicating Alexa-Fluor 545 minimum intensity to be

considered to score a proliferative cell. Minimal positive intensity was selected according to differential basal intensity of Alexa-fluor 545. DAPI and Alexa labelled nuclei were counted and a percentage of EdU positive cells per well was calculated using the following formula:

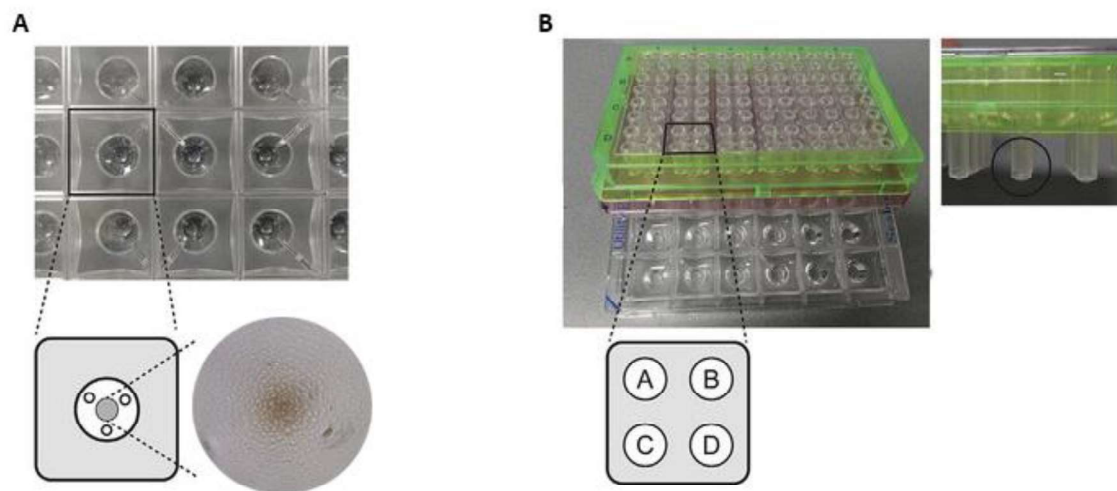
$$\frac{\text{Number of EdU positive nucleus}}{\text{Number of DAPI – labelled nucleus}} \times 100$$

#### 10.4. Glycolysis Stress Assay with EVs

A glycolysis stress assay was used to measure glycolytic parameters in cultured cells by adding D-glucose (Sigma), Complex V inhibitor oligomycin (Agilent), and hexokinase inhibitor 2-Deoxy-D-glucose (2-DG; Sigma). EPIC or HUVECs were plated in Seahorse XF24 cell culture plates (Agilent) at 28,000 cells/well ( $1 \times 10^5$  cells/cm<sup>2</sup>), leaving four wells empty for blank reading. For HUVECs, wells were previously coated with 1% gelatine. After 48 hours, cells were washed in warm PBS and incubated in starving media overnight. The following day, starving media was replaced with 20 or 50 µg/mL of EVs-N, EVs-H5% or EVs-H1%. For EPIC, complete medium, containing 10% FBS, was used as positive control and 0% FBS media as negative control. For HUVECs, EGM-2 was used as positive control and 1% FBS, in EBM-2 medium, as negative control. Cells were incubated for 12 hours at 37 °C and 5% CO<sub>2</sub>. The sensor cartridge, which harbours fluorophores associated to O<sub>2</sub> and H<sup>+</sup> for each well, was hydrated with XF Calybrant at 37 °C in a non-CO<sub>2</sub> incubator overnight. The following day, cells were incubated for 1 hour at 37 °C in a non-CO<sub>2</sub> incubator in pyruvate-free glycolytic assay medium composed of XF base media (Agilent) with 2 mM glutamine (Sigma) and pH corrected to 7.4.

In the sensor cartridge (Agilent; Fig. 5), 59 µL of 100 mM D-glucose (Sigma) solution was pipetted in all Ports A, 62 µL of 10 µM Oligomycin A (Agilent) was pipetted in ports B, 69 µL of 500 mM 2-deoxy-D-Glucose (2-DG; Sigma) was pipetted in ports C, and finally 75 µL of XF base media with 2 mM L-glutamine was loaded in ports D of the sensor cartridge. All reagents were homogenized in XF base media with 2 mM L-glutamine. After injection of reagents in each port, final concentrations per well were 10 mM of D-glucose, 1 µM of Oligomycin A and 50 mM of 2-DG, respectively. The cell plate was loaded together with the sensor cartridge in Seahorse XFe24 Analyzer (Agilent). After

three baseline measurements, glycolytic parameters were calculated using 10 mM of D-glucose, 1  $\mu$ M of Oligomycin A and 50 mM of 2-DG (2-deoxy-D-glucose), three cycles of measurements after each injection. Values were normalized to protein quantity measured by BCA quantification assay and data analysed with *Wave 2.6.1* software (Agilent) and *GraphPad 8.0.2*.



**Figure 5 – Agilent Seahorse plates and cartridges and their structure.** A) Seahorse utility plate where cells are plated. Cells must be homogeneously spread and at about 80-90% confluency for metabolic analysis to be reliable. EPIC brightfield picture taken before cell starvation is shown in circular image; B) Sensor cartridge contains four injection ports (A, B, C and D) for each well in the utility plate. Sensor is marked with a circle in transversal view of the sensor cartridge plate. For the glycolysis stress assay, D-glucose, oligomycin A and 2-deoxy-D-glucose were pipetted into ports A, B and C, respectively. Adapted from Ludikhuize *et al.*, 2021.

## 10.5. HUVEC proliferation assay with ECM

To evaluate the effect of the different EPIC-derived ECM fractions on cell proliferation, a density of  $1.3\text{-}1.4 \times 10^4$  cells/cm<sup>2</sup> of HUVECs (passage 6 to 8) were plated in duplicate over matrix-coated Nunc™ 24 well-cell culture plates (Thermo Fisher) with EGM-2 and incubated at 37 °C for 3 or 5 days. The matrix coating used were i) 1% gelatine (negative control), ii) 1% gelatine containing 100 µg EPIC IM, iii) 1% gelatine containing 100 µg EPIC SM, iv) 1% gelatine containing 100 µg Matrigel (Corning), v) 1% gelatine containing 100 µg EPIC IM plus 100 µg Matrigel, and vi) 1% gelatine containing 100 µg EPIC IM plus 100 µg EPIC SM plus 100 µg Matrigel. Coated plates were incubated for 2 hours at 37 °C in the coating solution. Then, excess solution was aspirated, and wells were let to dry. A density of  $1.3\text{-}1.4 \times 10^4$  cells/cm<sup>2</sup> of HUVECs were added and after 3 or 5 days of incubation at 37 °C and 5% CO<sub>2</sub>, EdU was added to the samples at a final concentration of 10 µM (15 minutes incubation at 37 °C and 5% CO<sub>2</sub>). HUVECs were washed in PBS, fixed in 4% PFA for 20 minutes at room temperature and washed again in PBS for three times. The click chemistry reaction was performed as previously described (subchapter 10.4.3).

## 11. Statistics

In order to perform the appropriate statistical analysis, the distribution of all the data was inspected using normality tests. The normality methods used were Shapiro-Wilk and Kolmogorov-Smirnov tests with a significance level of 0.05.

### 11.1. Extracellular vesicle characterization

EVs modal sizes datasets between EVs-UC and EVs-SEC followed a normal distribution. Because of that, statistical significance was assessed using an unpaired t-test. In contrast, EVs modal size for EV-N and EVs-H5% showed a non-normal distribution and the statistical analysis was performed with Mann-Whitney test. Datasets for the comparisons of modal sizes and particle concentration between DLS and NTA from EVs-UC and EVs-SEC followed a normal distribution. Statistical significance for the comparisons of modal sizes were assessed using Two-way analysis of variance (ANOVA) with Tukey corrections. For particle concentration per size analysis, two-way ANOVA with Bonferroni's correction was employed.

Particle concentration per million of cells, protein concentration and particle concentration per size datasets followed a normal distribution. Because of that, statistical significance was assessed using an unpaired t-test, as well as protein concentration per particle in EVs-SEC versus EVs-UC. In contrast, statistical significance of protein concentration per particle in EVs-N versus EVs-H5% was assessed with Mann-Whitney test because the lack of normality in the distribution of the data.

### **11.2. Functional studies on extracellular vesicles**

Datasets of proliferative rates and glycolytic activity of EPIC and HUVECs incubated with EPIC EVs were non-normally distributed. Proliferation data of EPIC and HUVECs incubated with EVs were assessed using nonparametric Kruskal-Wallis test. Three biological replicates were assessed per condition. In each biological replicate three technical replicates were included. For statistical analysis of glycolysis stress assay parameters in both EPIC and HUVECs incubated with EVs, Two-way ANOVA with Tukey corrections were employed. Three biological replicates were assessed for each condition. In each biological replicate two technical replicates were included.

### **11.3. Analysis and functional studies on extracellular matrix**

Fibre diameter distribution and proliferative rate of HUVECs incubated with EPIC ECM did not follow a normal distribution. Because of that, the analysis of fibre diameters taken from SEM images was performed using the Mann-Whitney test. Accordingly, statistical significance of the proliferation rate of HUVECs grown in EPIC IM, EPIC SM, Matrigel and gelatine was performed using nonparametric Kruskal-Wallis test. Three biological replicates per time point (3 and 5 days) and condition were studied. For each biological replicate four technical replicates were included.



## RESULTS

---





## Results

---

### Chapter I – Assessment of isolation strategy and characterization of EPIC-derived extracellular vesicles

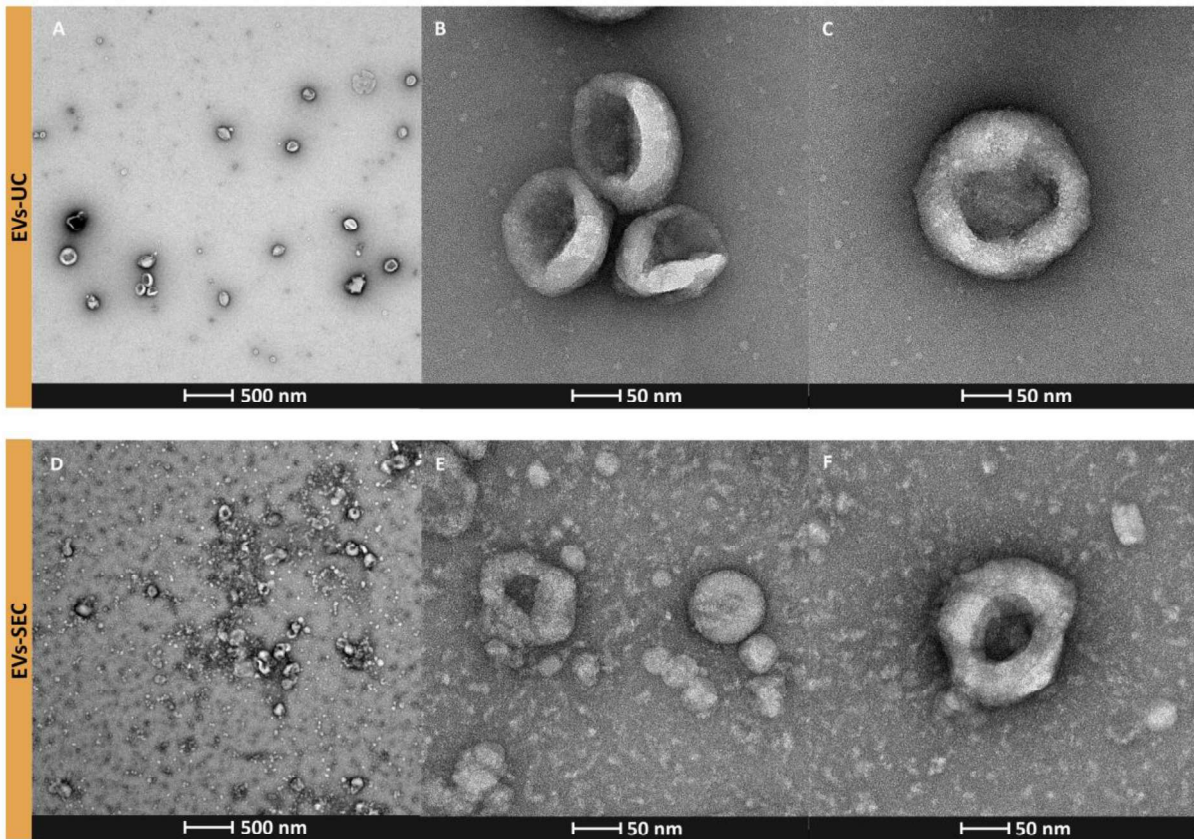
#### 1.1. Morphological assessment of EPIC-derived extracellular vesicles isolated by size exclusion chromatography and ultracentrifugation

Diverse extracellular vesicles (EVs) enrichment methods are currently used for downstream studies of their function and characterization. Different methods will impact resulting EVs enrichment fractions, purity and stability (Royo *et al.*, 2016). The most used ones are ultracentrifugation (UC) and size exclusion chromatography (SEC) (Saludas *et al.*, 2021). Because of that, both methods were used to isolate EPIC-derived EVs and EVs obtained were assessed by physical and molecular characterization following the recommendations of the International Society of Extracellular Vesicles (ISEV) (Théry *et al.*, 2018).

First, and in order to evaluate and compare the morphology of EPIC-EVs isolated using both SEC and UC methods, Transmission Electronic Microscopy (TEM) was used to characterize EVs. Both UC and SEC-isolated EPIC-EVs (from here onwards EVs-UC and EVs-SEC, respectively) show similar form and size (Fig. 6), presenting what is commonly described as “cup-shaped” morphology. This EV conformation has been suggested to derive from the sample dehydration procedures employed for TEM imaging.

In EVs-UC, the sample background is clear and it shows few structural artefacts (Fig. 6A, B and C). In EVs-SEC, however, a characteristic background patterning is observed that results from particles and deformed EVs (Fig. 6D, E and F). We interpret that this background may derive from the method of isolation: while in UC the EVs pellet was recovered using filtered PBS (f-PBS), for EVs-SEC isolation, a non-filtered sterile PBS was employed to elute and wash the fractions containing small EVs. Moreover, centrifugal filter units were employed to concentrate the resulting EVs-SEC fractions, so that this approach might contribute to concentrate not only EVs, but also nanoparticles

larger than 10k MWCO, thus contributing to deform or break EVs (Konoshenko *et al.*, 2018). In addition, these EVs, which were isolated in London, were stored frozen for a long period during the pandemic, what may have also provoked some vesicular damage (Muller *et al.*, 2014).



**Figure 6 - TEM images of EPIC-EVs from UC and SEC isolation methods.** A) EVs-UC captured at 50,000x magnification (scale bar 500 nm) showing nanovesicles dispersed in a clear background; B and C) EVs-UC captured at 240,000x magnification (scale bar 50 nm) showing the concave topology of different vesicles; D) EVs-SEC captured at 50,000x magnification (scale bar 500 nm) showing aggregates containing nanovesicles in a spotted background; E and F) EVs-SEC captured at 240,000x magnification (scale bar 50 nm) showing the concave topology of distinct vesicles as well as round-shaped vesicles smaller than 50 nm and other artefacts.

## 1.2. Characterization of EVs-UC and EVs-SEC

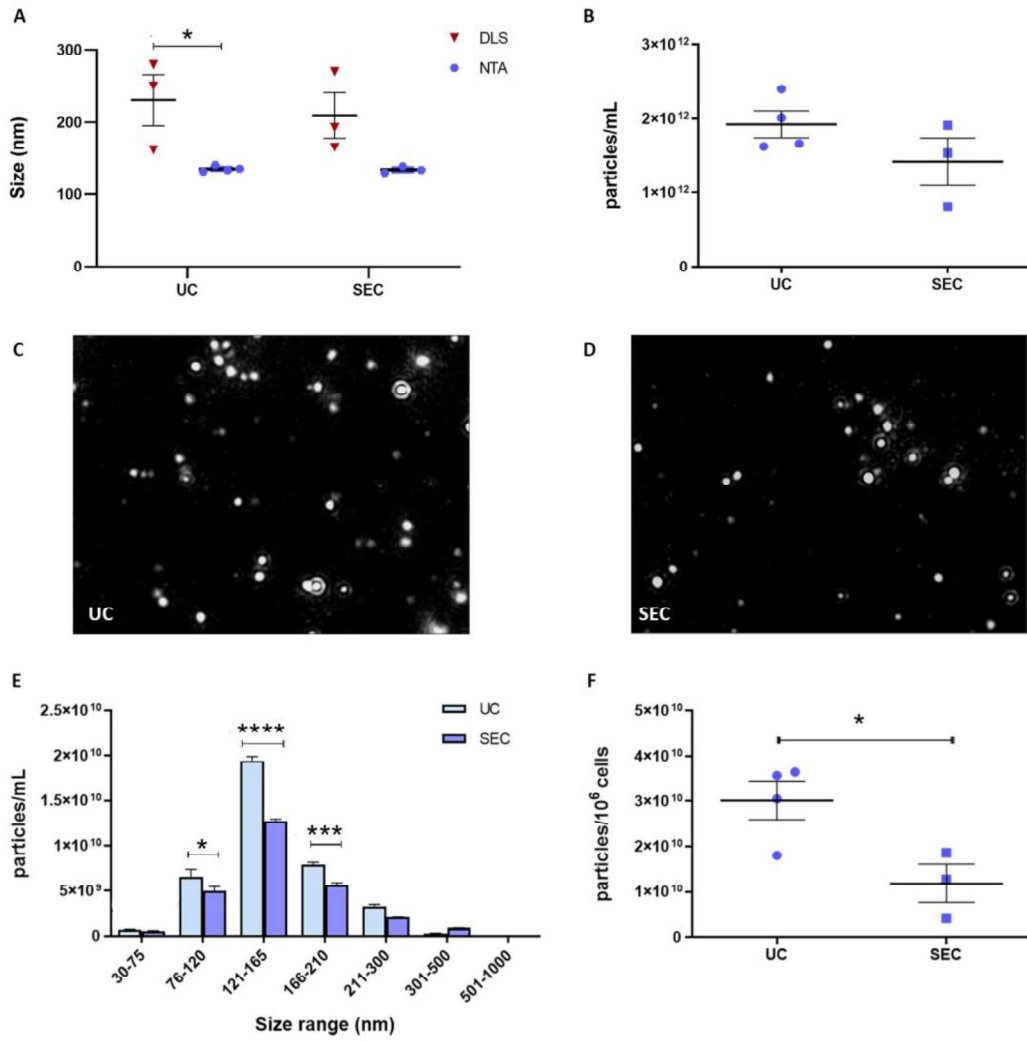
### 1.2.1. Physical characterization and quantification

Next, and in order to determine the size distribution of EPIC-EVs, Dynamic Light Scattering (DLS) and Nanoparticle Tracking Analysis (NTA) were performed (Fig. 7). Both technologies infer particle hydrodynamic size from Brownian motion using the Stokes–Einstein assumption. The EV size measurement that results from DLS analysis of samples isolated from both UC ( $230.32 \pm 35<.58$  nm) and SEC ( $209.10 \pm 31.48$  nm) indicates larger diameters and higher vesicle variability than in NTA analysis ( $135.18 \pm 1.92$  nm for EVs-UC and  $134.03 \pm 2.60$  nm for EVs-SEC) (Fig. 7A). These results are in accordance with what could be expected for DLS, as peak resolution is not reliable for a polydisperse solution, such as the one including our EVs. This fact can account for an increased average of particle sizes. Size discrepancy of EVs-UC reached a significant difference of 95.14 nm average size when measured by DLS versus NTA, while in EVs-SEC the difference (75.07 nm) was not significant. Independently of the technical differences found between these two methods, we observe that EVs-UC and EVs-SEC appear to have similar sizes (Fig. 7A). Thus, DLS measurements are shown to be more unreliable than NTA for EV size characterization, and therefore NTA was chosen as the standard method to evaluate the EVs studied in this thesis.

EVs-UC samples present a mean of  $1.92 \pm 0.18 \times 10^{12}$  particles/mL, while the EVs-SEC mean concentration is  $1.42 \pm 0.32 \times 10^{12}$  particles/mL, i.e., it is 26% less concentrated than EVs-UC (Fig. 7B). These data suggest that resulting EVs-UC tend to be slightly larger or clustered in solution than EVs-SEC (Fig. 7C and 7D, respectively).

Next, we sought to describe particle concentration grouped by size range (Fig. 7E and 7G). This representation shows that EVs-UC display higher concentration of particles than EVs-SEC, ranging from 76 to 210 nm. Thus, UC seems to collect higher quantity of particles than SEC isolation, especially in the size range that corresponds to exosomes (Van Niel *et al.*, 2018).

In order to characterize particle enrichment in relation with the number of parental cells, particle concentration from EVs-UC or EVs-SEC obtained over 48 hours of culture was associated to the total number of cultured EPIC. The data show a significant difference in particle concentration per million of cells between EVs-UC and EVs-SEC ( $3.01 \pm 0.42 \times 10^{10}$  and  $1.18 \pm 0.42 \times 10^{10}$  particles/ $10^6$  EPIC, respectively; Fig. 7F).



**G**

Size range (nm)	EVs-UC (particles/mL)	EVs-SEC (particles/mL)	P-value
30-75	6,98 ± 0,66 x10 <sup>8</sup>	5,28 ± 0,70 x10 <sup>8</sup>	>0,9999
76-120	6,59 ± 0,79 x10 <sup>9</sup>	4,97 ± 0,49 x10 <sup>9</sup>	0,0119
121-165	1,94 ± 0,05 x10 <sup>10</sup>	1,27 ± 0,02 x10 <sup>10</sup>	<0,0001
166-210	7,94 ± 0,21 x10 <sup>9</sup>	5,61 ± 0,32 x10 <sup>9</sup>	0,0002
211-300	3,29 ± 0,20 x10 <sup>9</sup>	2,06 ± 0,02 x10 <sup>9</sup>	0,1030
301-500	3,06 ± 0,17 x10 <sup>8</sup>	8,88 ± 0,27 x10 <sup>8</sup>	>0,9999
501-1000	6,97 ± 0,68 x10 <sup>6</sup>	1,53 ± 0,16 x10 <sup>7</sup>	>0,9999

**Figure 7— Size distribution and protein concentration of EPIC-derived EVs isolated by UC and SEC.** A) DLS average sizes and NTA modal sizes distribution from UC ( $230.32 \pm 35.58$  nm from DLS,  $n=3$ , and  $135.18 \pm 1.92$  nm from NTA,  $n=4$ ) and SEC ( $209.10 \pm 31.48$  nm from DLS and  $134.03 \pm 2.60$  nm from NTA,  $n=3$ ) isolated EVs; B) Particle concentration of UC ( $1.92 \pm 0.18 \times 10^{12}$  particles/mL,  $n=4$ ) and SEC ( $1.42 \pm 0.32 \times 10^{12}$  particles/mL,  $n=3$ ) isolated EVs, obtained from NTA analysis; C) Representative image from a NTA video frame of UC isolated EVs; D) Representative image from a NTA video frame of SEC isolated EVs; E) Concentration of particles grouped by specific size ranges, obtained from NTA analysis in UC and SEC isolated EVs; F) Graphical representation of particle concentration per million of cells from UC isolation ( $3.01 \pm 0.42 \times 10^{10}$  particles/ $10^6$  EPIC,  $n=4$ ) and SEC ( $1.18 \pm 0.42 \times 10^{10}$  particles/ $10^6$  EPIC,  $n=3$ ); G) Particle concentration for each size range analysed from EVs-UC and EVs-SEC in sizes ranging from 30 nm to 1,000 nm. \* $p < 0.05$ , \*\*\* $p < 0.001$ , \*\*\*\* $p < 0.0001$ .

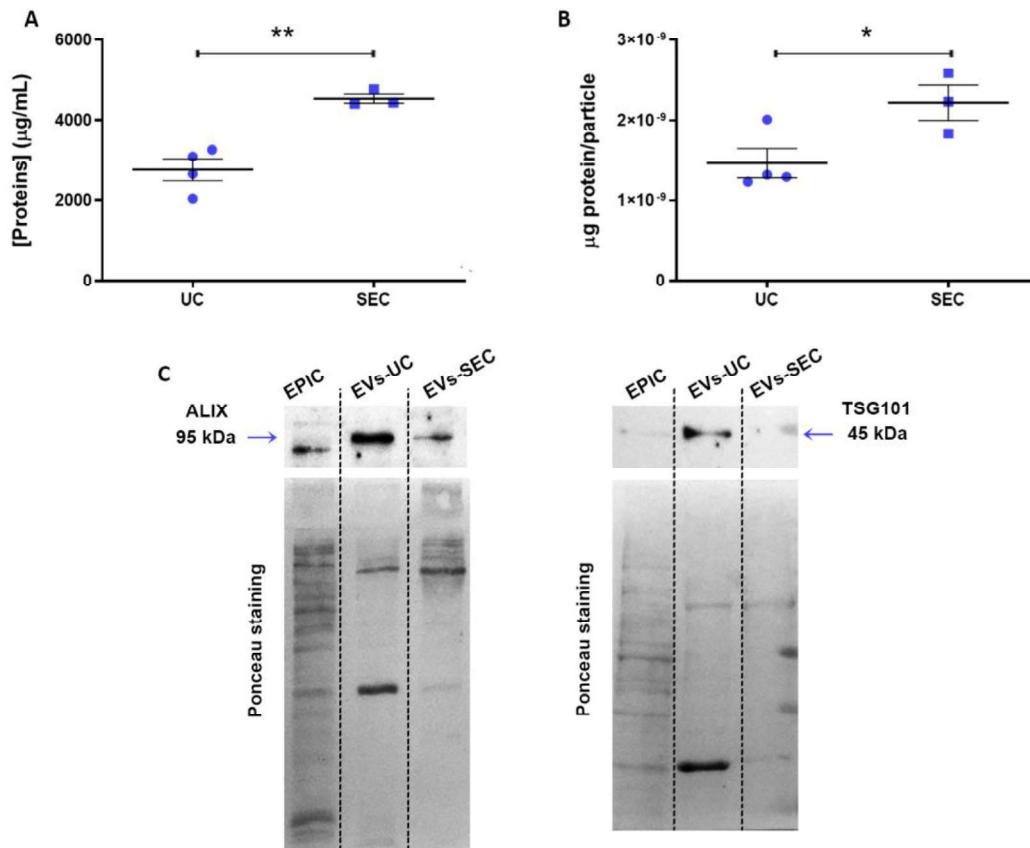
### 1.2.2. Protein concentration and EVs-like protein identification

Finally, we completed the characterization of EVs using western blot analysis of proteins that are enriched in EVs, such as ALIX and TSG101. First, protein concentration of EVs-UC and EVs-SEC was quantified using Micro BCA assay (Beltrami *et al.*, 2017). Interestingly, protein concentration is significantly lower in EVs-UC than in EVs-SEC ( $2,763 \pm 273.3$   $\mu\text{g/mL}$  versus  $4,536 \pm 117.3$   $\mu\text{g/mL}$ , respectively; Fig. 8A). To infer the quantity of protein per particle, protein concentration was normalized to the total number of particles. EVs-SEC show a statistically higher quantity of protein per particle than EVs-UC ( $2.22 \pm 0.22 \times 10^{-9}$  and  $1.46 \pm 0.18 \times 10^{-9}$   $\mu\text{g}$  of protein/particle, respectively). This could be related to co-isolated protein particles or proteins released from disrupted EVs-SE (Fig. 8B).

Based on those calculations, 16  $\mu\text{g}$  of EVs each sample were loaded into polyacrylamide gels. ALIX antibodies revealed a clear and strong band for EVs-UC (Fig. 8C, right membrane, lane EVs-UC) at the 95 kDa region, while for EVs-SEC samples (Fig. 8C, right membrane, lane EVs-SEC) it is visible a fainter band also at the 95 kDa region. EPIC lysate (Fig. 8C, right membrane, lane EPIC) was used as positive technical control. Here, a faint band at a lower molecular weight was identified, possibly due to the presence in the cell of potential protein isoforms. Regarding the TSG101 antibody, EVs-UC sample (Fig. 8C, left membrane, lane EVs-UC) presented a strong signal at 45 kDa band, while no band from EVs-SEC (Fig. 8C, left membrane, lane EVs-SEC) could be identified at a similar molecular weight reference. It is important to highlight that housekeeping proteins used in semi-quantitative Western Blots are not commonly enclosed in EVs, or they can be

present at different levels in other cellular fractions (Yoshioka *et al.*, 2013). Because of that, we decided to use the general staining Ponceau Red as reference in our Western Blots. Indeed, EVs-UC and EVs-SEC presented different protein profiles throughout the lanes, making it difficult to properly compare EVs proteins enrichment from SEC and UC isolations (Fig. 8C). It is noted that EVs-UC present a stronger band in a lower section of the membrane than EVs-SEC in the same area, while in the upper section of the membrane, EVs-SEC tend to have stronger bands than EVs-UC (Fig. 8C).





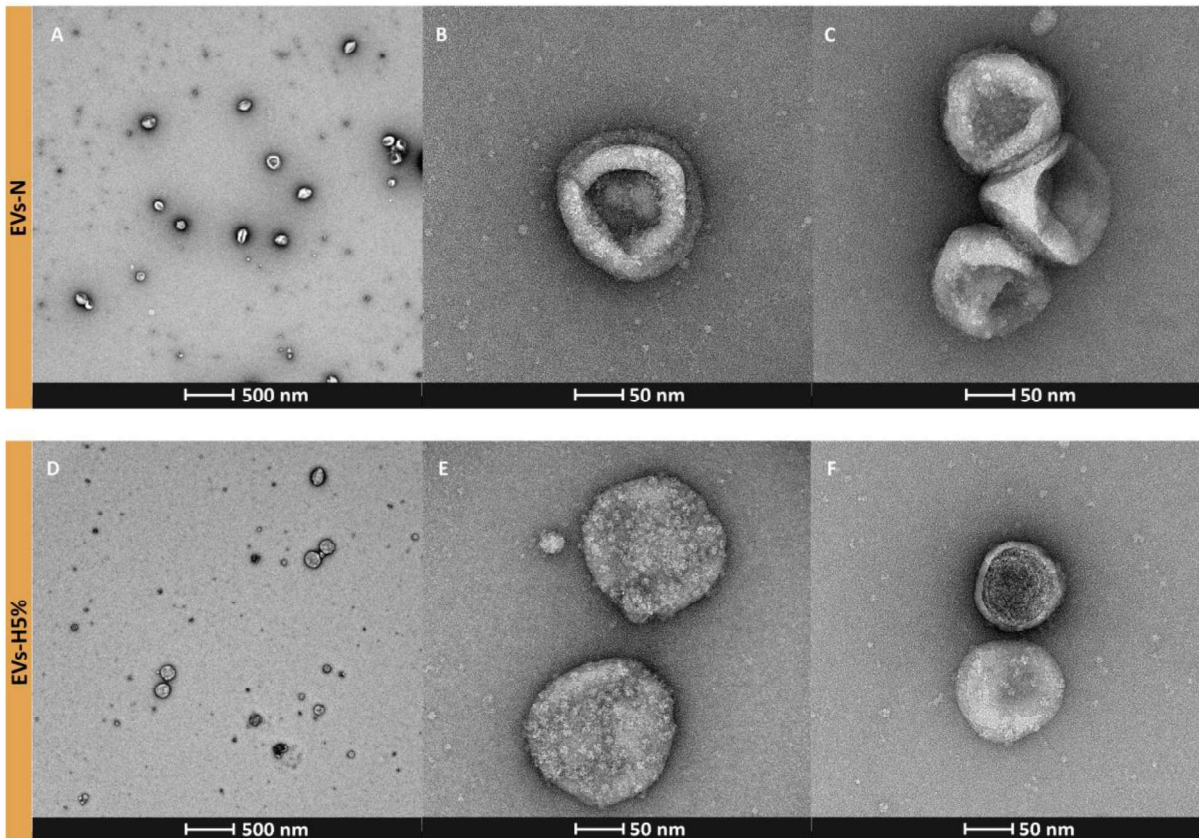
**Figure 8 – Protein characterization of EPIC-derived EVs enriched from UC and SEC isolation methods.** A) Protein concentration of UC ( $2,763 \pm 273.3 \mu\text{g/mL}$ ,  $n=4$ ) and SEC ( $4,536 \pm 117.3 \mu\text{g/mL}$ ,  $n=3$ ) isolated EVs, representing mean  $\pm$  SEM; B) Estimation of protein quantity per particle in UC ( $1.46 \pm 0.18 \times 10^{-9} \mu\text{g}$  of protein/particle,  $n=4$ ) and SEC ( $2.22 \pm 0.22 \times 10^{-9} \mu\text{g}$  of protein/particle,  $n=3$ ) isolated EVs, representing mean  $\pm$  SEM; C) Western Blot against small-size EVs positive markers ALIX (95 kDa) and TSG101 (45 kDa) on 16  $\mu\text{g}$  EPIC lysate, EVs-UC or EVs-SEC. Ponceau staining was used as reference for sample loading quantity. \* $p < 0.05$ , \*\* $p < 0.01$ .

Taken together, these data suggest that the previously described UC protocol allows for the isolation of a clean sample enriched in small/medium EVs ranging in size from 76 to 210 nm (Fig 6A, B and C and R1.2.1E). Moreover, TEM images from EVs-SEC show particles that could not be analyzed in detail (Fig. 6D, E and F), and non-vesicular protein aggregates co-isolated with the EVs. Accordingly, a significant higher quantity of protein yield was detected in EVs-SEC (Fig. 8A and B). This may affect the analysis of EPIC vesicles secretory profile. Additionally, EVs disruption into smaller vesicles after several filtration steps may have resulted in particles not being detected by NTA (van der Pol *et al.*, 2014).

Considering all the results from this section, we believe that the UC methodology is a more reliable characterization method for our nanovesicles. Also, being a faster and cheaper method than SEC, downstream assays on EPIC-derived EVs in this thesis are resorting to EVs isolated by UC only.

### **1.3. EVs from EPIC preconditioned to hypoxia and normoxia: morphological assessment**

One of the most attractive properties of EVs is that they are sensitive to changes in their parental cells, and this has fostered their use as biomarkers or cell-to-cell messengers (de Jong *et al.*, 2012; Ribeiro-Rodrigues *et al.*, 2017; Ontoria-Oviedo *et al.*, 2018; Walbrecq, Lecha, *et al.*, 2020). In order to evaluate potential modifications in EVs derived from parental cells submitted to different stimuli, the morphology of EVs isolated from EPIC cultured under different oxygen levels were compared (Fig. 9). For that, EVs were harvested and isolated by UC from normoxic (21% oxygen; EVs-N) and hypoxic (5% O<sub>2</sub>; EVs-H5%) EPIC cultures. Wide field images from TEM analysis of EVs-N (Fig. 9A, 9B and 9C) and EVs-H5%; (Fig. 9D, 9E and 9F) show that vesicles are homogeneously dispersed in the sampling solution. In close-up images, EVs-N and EVs-H5% present similar sizes and tend to equally collapse as described for typical dehydrated EVs (van der Pol *et al.*, 2014). Hence, oxygen conditions do not seem to affect the morphology of EPIC-derived EVs.



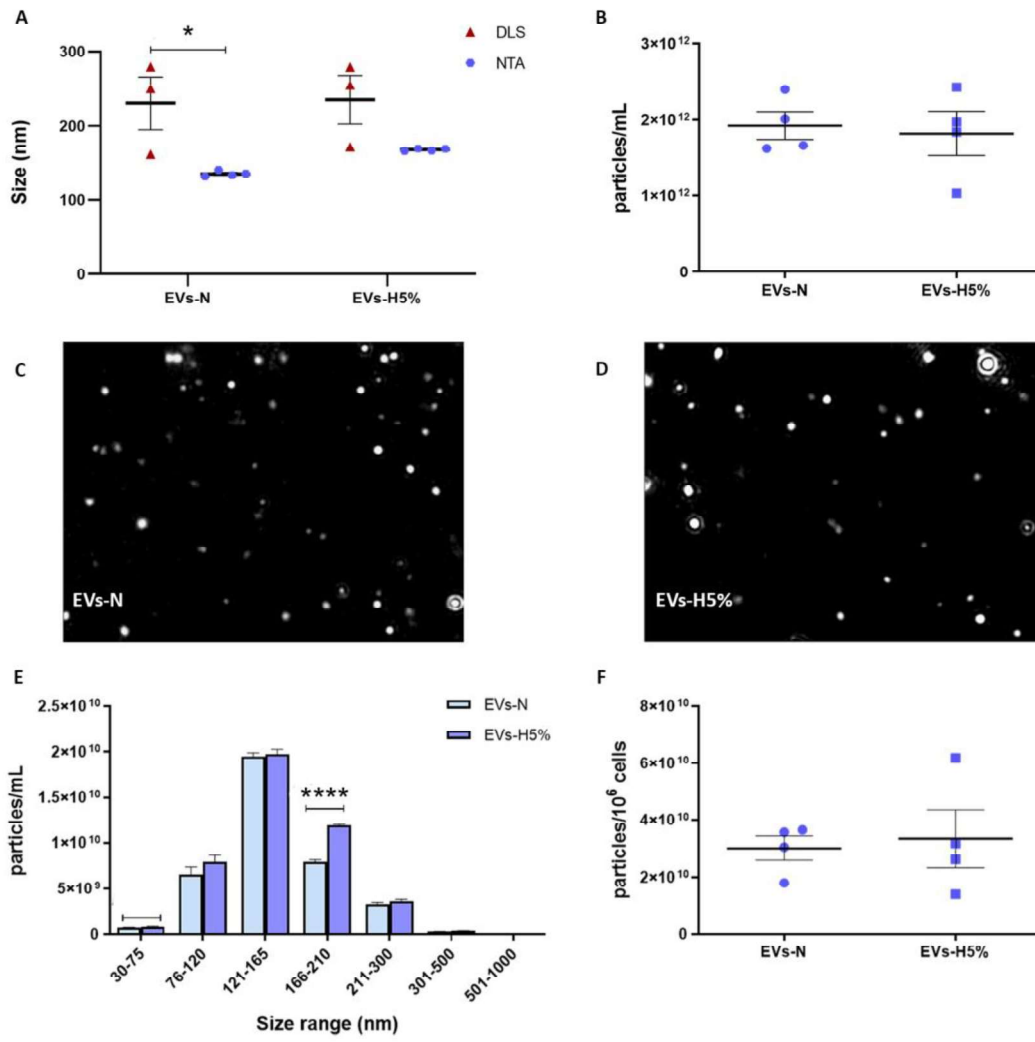
**Figure 9 - TEM images of EVs-N and EVs-H5% isolated by UC.** A) EVs-N captured at 50,000x magnification (scale bar 500 nm) showing nanovesicles dispersed in a clear background; B and C) EVs-N captured at 240,000x magnification (scale bar 50 nm) showing a concave topology in different vesicles; D) EVs-H5% captured at 50,000x magnification (scale bar 500 nm) also presenting spherical and biconcave topologies; E and F) EVs-H5% captured at 240,000x magnification (scale bar 50 nm) showing round-shaped vesicles larger than 50 nm in diameter.

## 1.4. Characterization of EVs-N and EVs-H5%

### 1.4.1. Physical characterization and quantification

After EVs-UC and SEC comparison, EVs-N and EVs-H5% were estimated to be larger in size when analysed by DLS than when studied using NTA (Fig. 10A). In detail, EVs-N show a mean diameter of  $230.32 \pm 35.58$  nm by DLS and a modal size of  $135.18 \pm 1.92$  nm by NTA. EVs-H5% displayed  $235.17 \pm 32.71$  nm of mean diameter by DLS analysis and  $167.33 \pm 0.86$  nm diameter as studied by NTA. Size discrepancy of EVs-N reached a significant difference of 95.14 nm average diameter size when measured by DLS versus NTA, while in EVs-H5% the difference did not reach a statistical significance (67.84 nm).

Regarding particle concentration, EVs-N and EVs-H5% did not show significant differences ( $1.92 \pm 0.18 \times 10^{12}$  particles/mL and  $1.82 \pm 0.29 \times 10^{12}$  particles/mL, respectively) (Fig. 10B). In terms of size distribution, NTA frames show EVs-N fraction containing more small particles than EVs-H5% (please, compare Fig. 10C with Fig. 10D). However, EVs-H5% revealed a significant enrichment of particles within 166 and 210 nm size range in comparison with EVs-N (Fig. 10E and 10G). When considering the number of particles per million of cells (Fig. 10F), it resulted in a similar quantity of particles in EVs-N and EVs-H5%, of  $3.01 \pm 0.42 \times 10^{10}$  particles and  $3.34 \pm 1.01 \times 10^{10}$  particles/ $10^6$  EPIC, respectively.



**G**

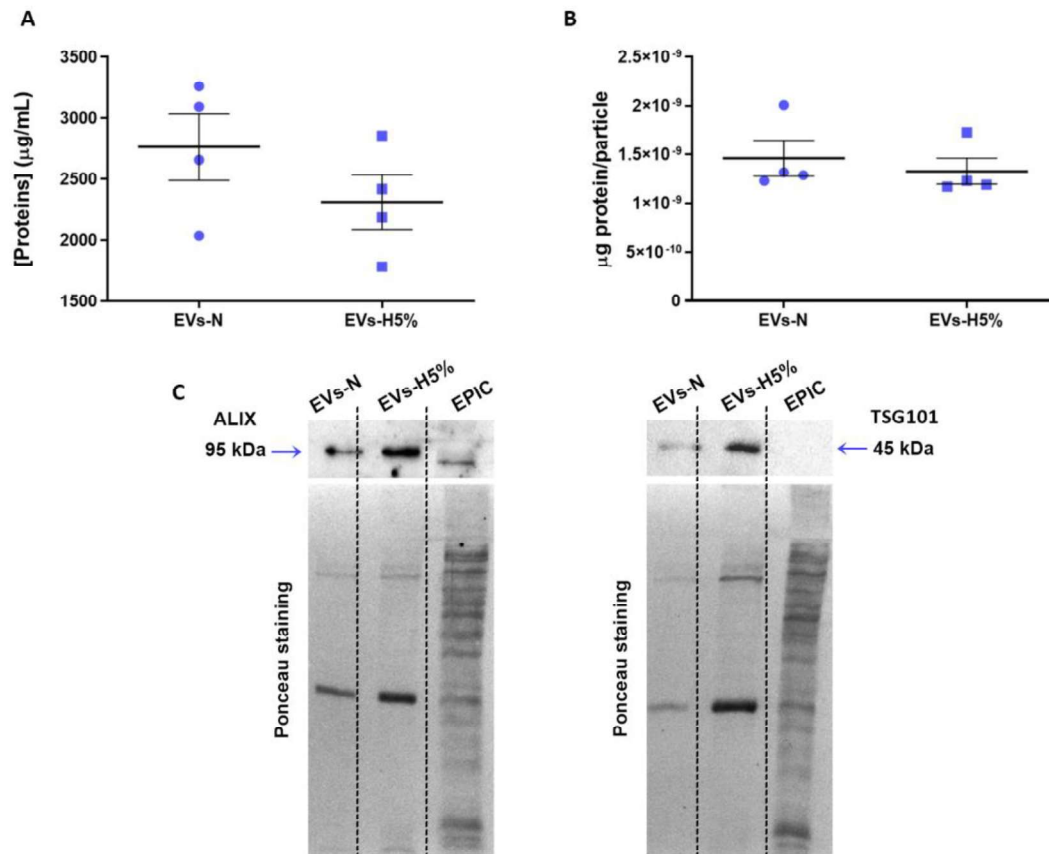
Size range (nm)	EVs-N (particles/mL)	EVs-H5% (particles/mL)	P-value
30-75	6,98 ± 0,66 x10 <sup>8</sup>	8,25 ± 0,82 x10 <sup>8</sup>	>0,9999
76-120	6,59 ± 0,79 x10 <sup>9</sup>	7,89 ± 0,74 x10 <sup>9</sup>	0,1125
121-165	1,94 ± 0,05 x10 <sup>10</sup>	1,97 ± 0,06 x10 <sup>10</sup>	>0,9999
166-210	7,94 ± 0,21 x10 <sup>9</sup>	1,19 ± 0,02 x10 <sup>10</sup>	<0,0001
211-300	3,29 ± 0,20 x10 <sup>9</sup>	3,61 ± 0,22 x10 <sup>9</sup>	>0,9999
301-500	3,06 ± 0,17 x10 <sup>8</sup>	3,86 ± 0,22 x10 <sup>8</sup>	>0,9999
501-1000	6,97 ± 0,68 x10 <sup>6</sup>	7,70 ± 0,45 x10 <sup>6</sup>	>0,9999

**Figure 10 – Size distribution measurements of EVs-N and EVs-H5%.** A) DLS average sizes and NTA modal distribution of sizes from EVs-N ( $230.32 \pm 35.58$  nm from DLS,  $n=3$ , and  $135.18 \pm 1.92$  nm from NTA,  $n=4$ ) and EVs-H5% ( $235.17 \pm 32.71$  nm from DLS,  $n=3$ , and  $167.33 \pm 0.86$  nm from NTA,  $n=4$ ); B) Particle concentration of EVs-N ( $1.92 \pm 0.18 \times 10^{12}$  particles/mL,  $n=4$ ) and EVs-H5% ( $1.82 \pm 0.29 \times 10^{12}$  particles/mL,  $n=4$ ), obtained from NTA analysis; C) Representative image from a NTA video frame of EVs-N; D) Representative image from a NTA video frame EVs-H5%; E) Concentration of particles grouped by specific size ranges, obtained from NTA analysis in EVs-N and EVs-H5% isolated EVs ( $n=4$ ). Data are plotted as mean  $\pm$  SEM; F) Graphical representation of the particle concentration per million of cells at the final EVs harvesting in EVs-N ( $3.01 \pm 0.42 \times 10^{10}$  particles/ $10^6$  EPIC,  $n=4$ ) and EVs-H5% ( $3.34 \pm 1.01 \times 10^{10}$  particles/ $10^6$  EPIC,  $n=4$ ) isolated EVs; G. Particle concentration for each size range analysed from EVs-N and EVs-H5% (sizes ranging from 30 nm to 1,000 nm). \* $p < 0.05$ , \*\*\*\* $p < 0.0001$ .

#### 1.4.2. Protein concentration and EVs-like protein identification

Protein concentration of EVs-N and EVs-H5% was also assessed using a Micro BCA assay. EVs-N and EVs-H5% show similar quantities, although it comes associated with high variability. In EVs-N, protein concentration was of  $2,763 \pm 273.3$   $\mu\text{g/mL}$  and from EVs-H5% their average concentration was of  $2,311 \pm 223.8$   $\mu\text{g/mL}$  (Fig. 11A). When analysing the quantity of proteins per particle, EVs-N and EVs-H5% showed similar values, ( $1.46 \pm 0.18 \times 10^{-9}$   $\mu\text{g protein/particle}$  and  $1.33 \pm 0.13 \times 10^{-9}$   $\mu\text{g protein/particle}$ , respectively) (Fig. 11B).

Western Blot analysis was performed to evaluate the enrichment of EVs-N and EVs-H5% in ALIX and TSG101 proteins (Fig. 11C). First, both EVs fractions are enriched in small EVs as compared to EPIC lysate. However, ALIX appears to be more enriched in EVs-H5%, while TSG101 protein contents seem to be similar between the groups, especially when considering the loaded protein enrichment stained with Ponceau red. Nevertheless, EVs-H5% shows a stronger band for both proteins than in EVs-N, as verified by the loaded sample after Ponceau staining. In the EPIC lysate lane, TSG101 was not detected, probably because the relative abundance of these proteins in total cell lysate was low.



**Figure 11 – Protein characterization and proteins-associated to EVs of EVs-N and EVs-H5%.** A) Protein concentration of EVs-N ( $2,763 \pm 273.3 \mu\text{g/mL}$ ,  $n=4$ ) and EVs-H5% ( $2,311 \pm 223.8 \mu\text{g/mL}$ ,  $n=4$ ). Data plotted as mean  $\pm$  SEM; B). Estimation of protein quantity per particle ( $\mu\text{g}$  protein/particle) in EVs-N and EVs-H5% of  $1.46 \pm 0.18 \times 10^{-9} \mu\text{g}$  of protein/particle and  $1.33 \pm 0.13 \times 10^{-9} \mu\text{g}$  of protein/particle, respectively. Data plotted as mean  $\pm$  SEM; C) Western Blot against small-size EV markers ALIX (95 kDa) and TSG101 (45 kDa) on 16  $\mu\text{g}$  EVs-N, EVs-H5% and EPIC lysate. Ponceau staining was used as reference for sample loading quantity.

## Chapter II– Proteomic characterization of EPIC-derived extracellular vesicles

### 2.1. Comparing multiplexing proteomic strategies: TMT2plex versus TMT6plex quantification

As mentioned above, the cargo of EVs is generally related to their cellular origin, their extracellular environment, and their function. Since EVs have been recognized as multi-molecular messengers in a different pool of cells, understanding EPIC-derived EVs content and evaluating the potential impact of these vesicles in autocrine and paracrine cell signaling may provide new insights on cell-to-cell communication in physiological and diseased states.

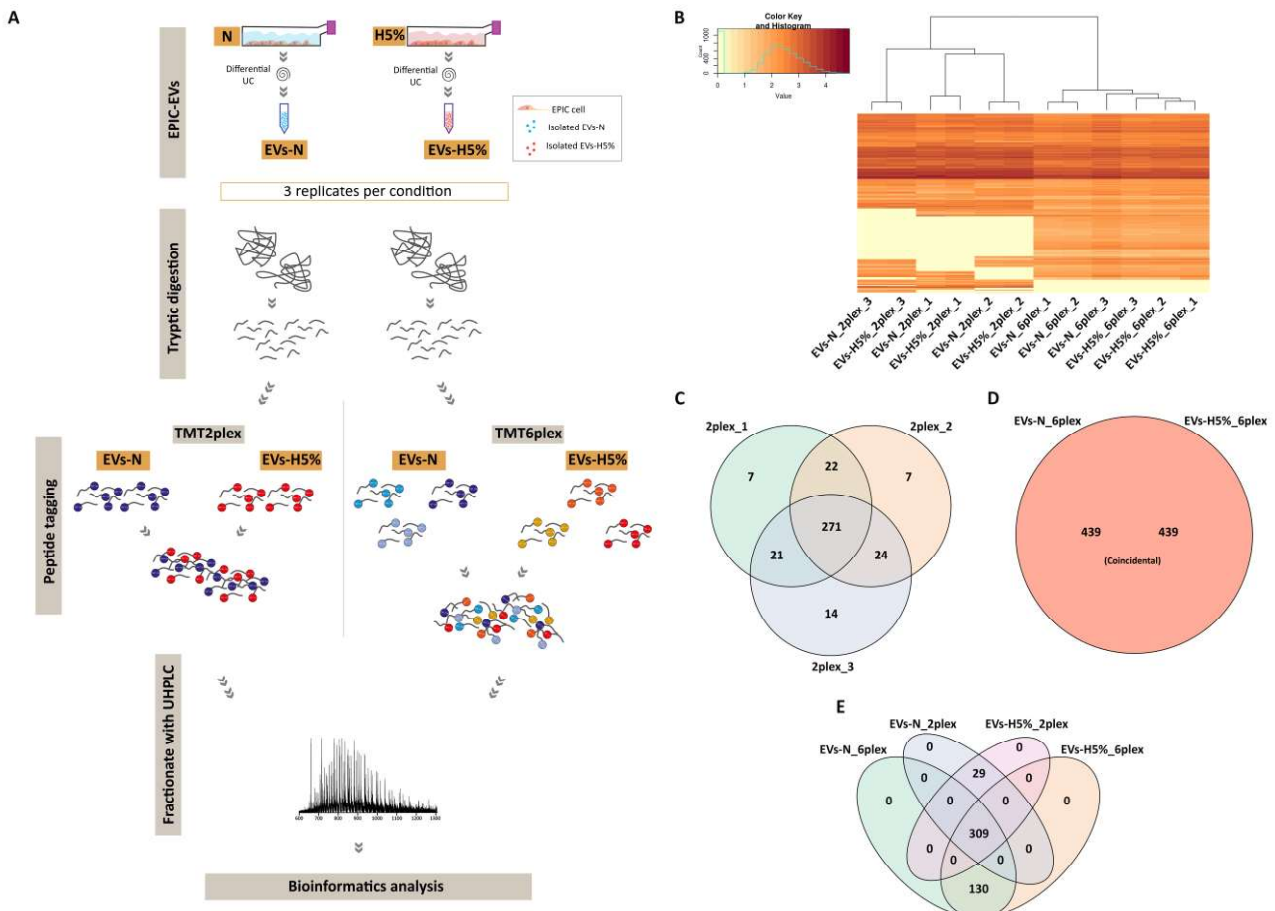
In order to characterize and quantify the proteomic cargo of the EVs isolated from hypoxic and normoxic EPIC conditions, we performed TMT2plex and TMT6plex techniques. Briefly, in this technique, individual samples are tagged with isobaric markers allowing for sample multiplexing (Fig. 12A) (please, see Materials & methods, section 7.1, for more details). Then, the bioinformatic analysis allowed us to select the identified peptides that were present in at least two of the three biological replicates and associate them with specific proteins.

A first explorative approach showed that TMT2plex dataset contained less proteins than the TMT6plex one (Fig. 12B). Additionally, some discrepancies appeared between biological replicates coming from the TMT2plex analysis. In detail, the assays 2plex\_1, 2plex\_2 and 2plex\_3 have identified 321, 324 and 330 proteins, respectively. Both 2plex\_1 and 2plex\_2 have 7 unique proteins in each replicate and share 22 proteins, while 2plex\_3 presents 14 unique proteins, and 21 and 24 proteins in common with 2plex\_1 and 2plex\_2, respectively (Fig. 12C). In the three assays, 271 proteins were identified as present in EPIC-derived EVs. However, TMT6plex analysis showed that identified proteins are present in the all conditions (Fig. 12B-D). In this dataset, 439 proteins were identified in all the three biological replicates for both EVs-N and EVs-H5%samples (Fig. 12D).



When TMT2plex and TMT6plex datasets were compared, 309 common proteins were detected. Interestingly, 130 of the proteins found in TMT6plex were not identified in at least two of the TMT2plex assays. On the other hand, 29 proteins listed in, at least, two TMT2plex assays were not detected in the TMT6plex assay (Fig. 12E and Table A1 in the Appendix chapter).

These results suggest that TMT2plex is an unreliable method for quantitative comparisons between EVs-N and EV-s-H5%. As such, and as TMT6plex offered higher sensitivity, reproducibility, and allows for the analysis of differentially displayed proteins in EVs-N and EVs-H5% than in TMT2plex, downstream bioinformatic analysis were pursued for proteins identified by the TMT6plex approach one.



**Figure 12- Comparative study of two tagging strategies for EVs-derived protein quantification: TMT2plex and TMT6plex.** A) Summarised concept of TMT2plex and TMT6plex isobaric procedures; B) Heatmap comparing TMT2plex (EVs-N\_2plex\_1, EVs-N\_2plex\_2, EVs-N\_2plex\_3, EVs-H5%\_2plex\_1, EVs-H5%\_2plex\_2, EVs-H5%\_2plex\_3) and TMT6plex results (EVs-N\_6plex\_1, EVs-N\_6plex\_2, EVs-N\_6plex\_3, EVs-H5%\_6plex\_1, EVs-H5%\_6plex\_2, EVs-H5%\_6plex\_3) with 3 biological replicates per treatment for each approach; C) Venn diagram comparing identified protein from three TMT2plex assays; D) Venn diagram comparing proteins identified in the TMT6plex assay; E) Venn diagram comparison between proteins identified in TMT6plex and, at least, two TMT2plex assays.

## 2.2. Protein cargo of EPIC-derived EVs

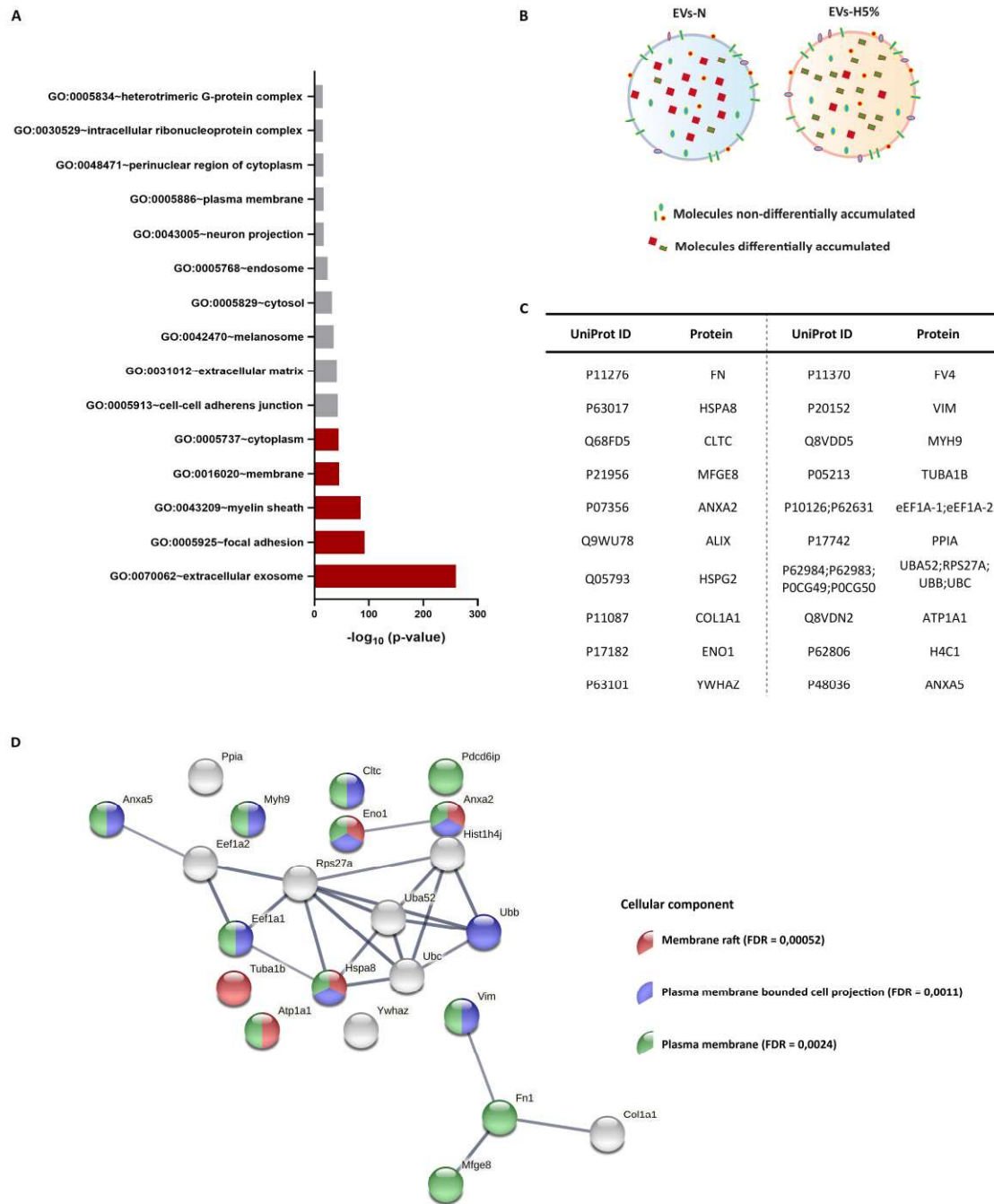
### 2.2.1. Non-differentially enriched surface proteins between extracellular vesicles isolated in normoxia and hypoxia-5% could be considered as potential epicardial-derived EVs markers

In order to search for a general perspective about the kind of proteins that are found in the cargo of EPIC-derived EVs, an unsupervised gene ontology (GO) analysis for cellular component was performed (Fig. 13A). As expected, this preliminary analysis shows that most of the identified EVs proteins are enriched in the GO term named “extracellular exosomes” (GO:0070062). Interestingly, the other enriched proteins are related to cellular communication processes, such as “focal adhesion” (GO:0005925), “myelin sheath” (GO:0043209), “membrane” (GO:0016020) and “cytoplasm” (GO:0005737).

Next, abundancies of each identified protein were compared between EVs-N and EVs-H5% to determine which ones were differentially up or down regulated per condition. First, we focused on the ones that showed no statistical differences because they were considered as significantly common between both EVs populations (Fig. 13B). Of those, we highlighted the first 20 proteins with the highest intensities. However, some identified peptides could not be assigned to a single protein, so that our final list included 24 proteins (Fig. 13C). As the proteins are recognized based on the identified peptide sequences, and due to database limitations such as redundancies, post-translational modifications or even absences, some peptides could not be assigned to a single protein (Duncan *et al.*, 2010). This increases the number of putative enriched proteins from 20 to 24.

Some of these proteins are normally used to identify enriched small-size EVs fractions, such as CD9, CD63, CD81 and TSG101. Other proteins are related to ECM interactions (collagen  $\alpha$ 1 type 1, fibronectin and integrins, such as integrin  $\alpha$ 3 and integrin  $\beta$ 1). Looking for potential surface markers for EPIC-derived EVs, a supervised GO term analysis that restricted the search on surface proteins was applied (please, see Materials & Methods -section 8.1 -for details) (Fig. 13D). The GO term with the lowest false discovery rate (FDR; FDR of 0.00052) was “membrane raft” (GO:0045121) that contains proteins as ANXA2, ENO1, TUBA1B, HSPA8 and ATP1A1. Other significant GO terms detected in this analysis were “plasma membrane bounded cell projection”

(GO:0120025), including VIM, UBB, CLTC, MYH9, ANXA5, eEF1A-1 and HSPA8; and “plasma membrane” (GO:0005886) cellular component, containing ALIX, FN1 and MFGE8.



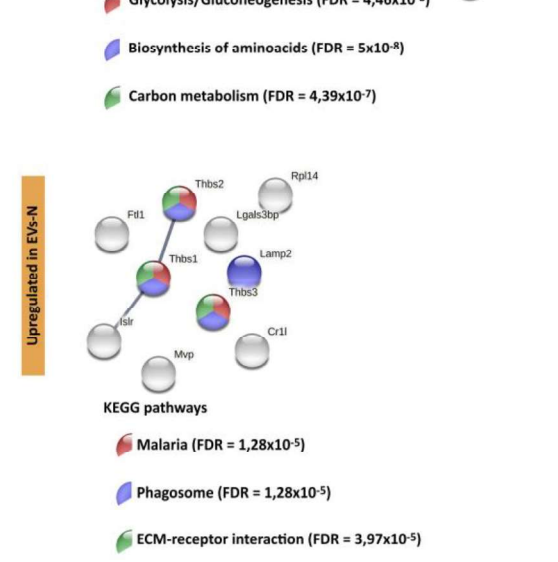
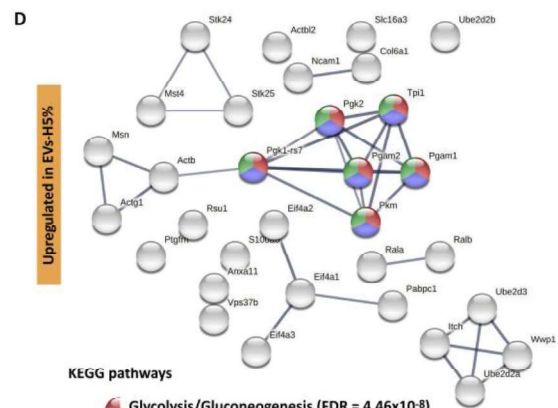
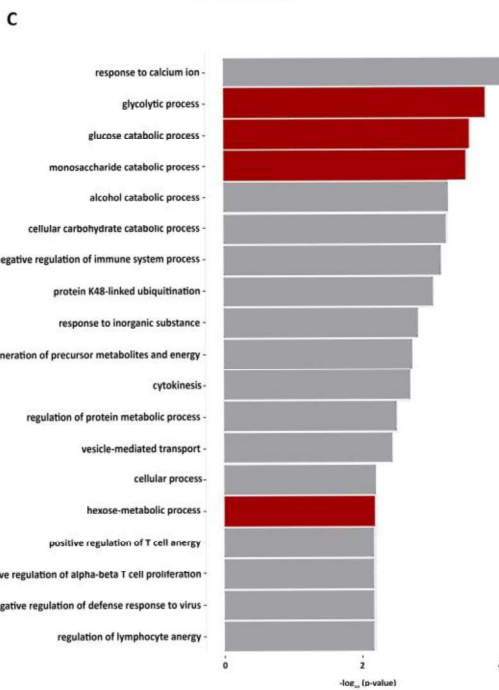
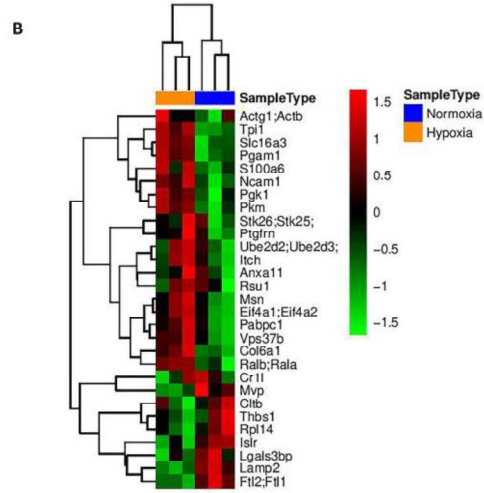
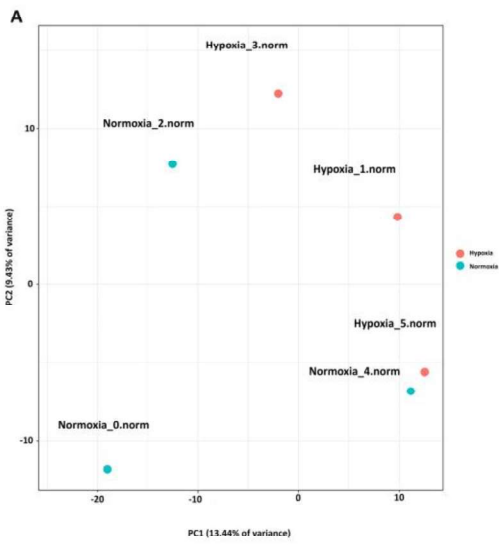
**Figure 13 – Bioinformatic analysis of TMT6plex data.** A) Cellular components (gene ontology analysis). The graph represents the top 15 gene ontology cellular components organized based from highest (bottom) to lowest (top)  $-\log_{10}(p\text{-value})$ ; B) EV representation of molecules differentially and non-differentially accumulated in EPIC-EVs from different conditions; C) UniProt protein IDs and respective gene names of 24 of the non-differentially expressed proteins with highest normalized intensities in EVs-N and EVs-H5%; D) STRING analysis of the 24 most abundant and non-differentially accumulated proteins identified in EVs-N and EVs-H5%, representing the three cellular component GO annotations related to cell membrane with the lowest FDR values.

### 2.2.2. Extracellular vesicles isolated from 5% hypoxia are enriched in proteins related to glycolysis

To explore the behaviour of the different biological datasets, the samples were submitted to a Principal Components Analysis (PCA; Fig. 14A). PC1 component explains a variance of 13.44% and PC2 a variance of 9.43%. Although the PCA does not represent a clear distinction between some of the replicates, a statistical significance difference between the abundance of proteins in EVs-N versus EVs-H5% (Fig. 14B) was found. In EVs-H5%, proteins such as Actin (ACTG1; ACTB), triosephosphate isomerase 1 (TPI1), monocarboxylate transporter 4 (SLC16A3/MCT4), phosphoglycerate mutase 1 (PGAM1), protein S100-A6, phosphoglycerate kinase 1 (PGK1) or pyruvate kinase (PKM), are found to be more enriched than in EVs-N, while 9 proteins were found to be more enriched in EVs-N than in EVs-H5%, such as clathrin light chain B (CLTB) or thrombospondin-1 (THBS1).

In order to compare the enriched biological processes identified between cell culture conditions, GO analysis was performed (Fig. 14C). Some of the most important biological processes enriched in the set of differentially expressed proteins included “glycolytic process” (GO:0006096), “glucose catabolic process” (GO:0006007), “monosaccharide catabolic process” (GO:0046365) and “hexose-metabolic process” (GO:0019318; Fig. 14C). In parallel, STRING DB was employed to determine the KEGG pathways that are more representative for the enriched proteins in EVs-H5% and EVs-N (Fig. 14D). Regarding the proteins upregulated in EVs-H5%, 6 out of 32 proteins were correlated with “Glycolysis/Gluconeogenesis” (mmu00010), “Biosynthesis of aminoacids” (mmu01230) and “Carbon metabolism” (mmu01200) KEGG pathways (FDR of  $4.46 \times 10^{-8}$ ,  $5.00 \times 10^{-8}$  and  $4.39 \times 10^{-7}$ , respectively). In the case of upregulated proteins found in EVs-N, 3 out of 10 proteins were correlated to “ECM-receptor interaction” and 4 proteins were related to “Phagosome”, with FDR of  $3.97 \times 10^{-5}$  and  $1.28 \times 10^{-5}$ , respectively (Fig. 14D).

From both bioinformatic approaches, we concluded that proteins contained into EVs-H5% are associated to glycolysis, suggesting a potential effect of these EVs on the glycolytic function of the receiving cell. To validate this hypothesis, we performed a set of experiments in two different cell types, EPIC and HUVECs, allowing us to discern at the same time between potential autocrine and paracrine effects of EPIC-EVs.



**Figure 14 – Bioinformatic analysis of differentially expressed proteins between EVs-N and EVs-H5% from TMT6plex data.** A) PCA of identified proteins from EVs-N, represented as “Normoxia\_0.norm”, “Normoxia\_2.norm” and “Normoxia\_4.norm”, and EVs-H5%, represented as “Hypoxia\_1.norm”, “Hypoxia\_3.norm” and “Hypoxia\_5.norm”; B) Heatmap representation of statistically significant proteins of EVs-N versus EVs-H5% (p-value < 0.05). Scale represent  $\log_2$  of protein expression; C) Graphical representation of the top 19 gene ontology biologic processes, based on the statistical significance of the FDR. Glycolysis-related terms are highlighted in red; D) STRING analysis of upregulated proteins in EVs-H5% and EVs-N, representing the three KEGG pathways that present the lowest FDR values.

### 2.3. Autocrine signaling of EPIC-derived extracellular vesicles

To evaluate the potential effect of EPIC-EVs in host EPIC, we first tracked EPIC-derived EVs and verified their internalization into host EPIC. In order to tackle this objective, EPIC-EVs were stained with CellTracker™ CM-Dil (EVs-Dil) and observed using TIRF microscopy. Different fluorescent dots were identified in EVs-Dil sample but not in the control one (PBS-Dil) (Fig. 15A and B, respectively). Then, EPIC were cocultured with EVs-Dil. The internalization of EVs-Dil (red in Fig. 15C i, iii and iv) was corroborated with the counterstaining LysoTracker, a selective dye for acidic organelles, such as lysosomes (green in Fig. 15C ii, iii and iv).

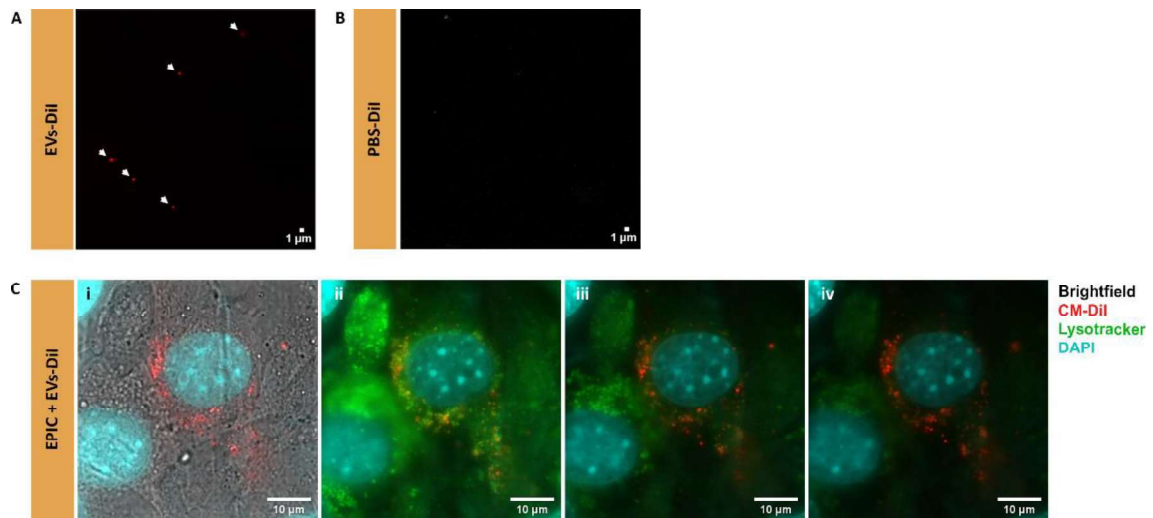
Once EVs internalization in EPIC was assessed, we aimed at identifying whether these vesicles carried modulators of cell metabolism. In accordance with the known relevance of glycolytic metabolism in hypoxic environments we decided to evaluate the capacity of EPIC-derived EVs to induce a glycolytic response in host cells in an autocrine manner, also assessing the proliferation rate of EPIC cultured with different sets of EPIC-derived EVs (EVs-N or EVs-H5%) after 24 hours of coculture. EPIC incubated with 10% FBS or 0% FBS, but without EVs, were included in the experimental design as positive and negative controls, respectively (Fig. 16). EPIC cultured with EVs-N (both at 20 and 50  $\mu\text{g}/\text{mL}$ ), together with the negative control, displayed significant differences in comparison with the positive control (Fig. 16A and 16B). However, EPIC incubated with 20  $\mu\text{g}/\text{mL}$  of EVs-H5% showed a trend to increase their proliferation in comparison with the basal condition (0% FBS) and showed less differences with the positive control than these samples, from a statistical point of view. Accordingly, EPIC incubated with 50  $\mu\text{g}/\text{mL}$  of EVs-H5% yield the result that was closest to the positive control (Fig. 16A and 16B).



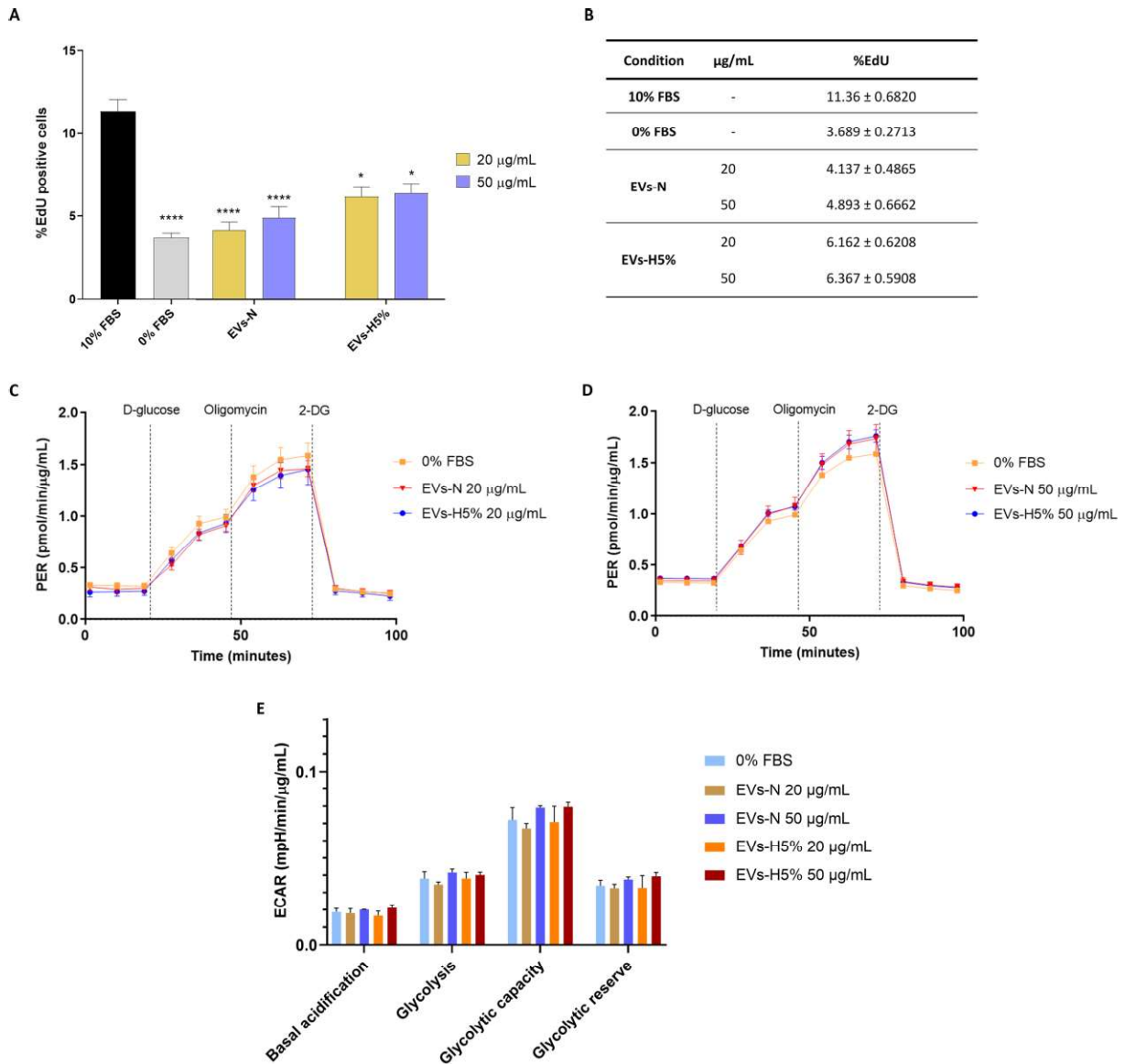
These results indicate that the cargo of EVs isolated from hypoxic EPIC, as compared to EVs isolated from normoxic EPIC, is able to foster cell proliferation in an autocrine manner.

The effect of EVs on cell proliferation, together with our results on glycolysis-related proteins accumulation in EVs-H5% proteomic profiling (please, see chapter 2.2.2), prompted us to study the effects of EPIC-derived EVs on the glycolytic pathway. In order to assess this point, we performed a Seahorse Glycolysis Stress Test in EPIC incubated with different concentration of EVs-N and EVs-H5% (Fig. 16C and 16E). This test analyses the glycolytic metabolism of the cells based on changes in the pH of the cell conditioned media through the proton efflux rate (PER). PER reflects the number of protons extruded over time (Fig. 16C and 16D), that is measured from the extracellular acidification rate (ECAR), that is recorded (Fig. 16E).

EPIC treated with 20  $\mu\text{g}/\text{mL}$  of EVs-N and EVs-H5% tend to exhibit a decrease in PER as compared to 0% FBS treatment throughout the experiment (Fig. 16C), whereas EPIC tend to release more protons when incubated with 50  $\mu\text{g}/\text{mL}$  of EPIC-EVs (Fig. 16D). The analysis of the resulting glycolytic parameters such as basal acidification, glycolysis, glycolytic capacity and glycolytic reserve, did not reveal any statistical significance between experimental conditions and controls for any of these parameter (Fig. 16E and Table 1). Taken together, these results show that the addition of both EVs-N and EVs-H5% up to 50  $\mu\text{g}/\text{mL}$  did not affect their parental cells glycolytic response.



**Figure 15 – EPIC-EVs are internalized by in vitro cultured EPIC.** A) EPIC-EVs probed with 0.8  $\mu\text{M}$  Dil and washed with f-PBS by UC. Scale bar represents 1  $\mu\text{m}$ ; B) Dil diluted in PBS to 0.8  $\mu\text{M}$  and ultracentrifuged. Scale bar represents 1  $\mu\text{m}$ ; C) EPIC after incubation for 1 hour with EVs-Dil. Nucleus stained with DAPI; i) Representative image of EPIC incubated with EVs-Dil. Bright field, DAPI and Dil channels merged; ii), iii) and iv) Frames of time lapse of EPIC incubated with EVs-Dil and acidic vesicles stained with Lysotracker at time 0 seconds, 72 seconds and 154 seconds, respectively. Scale bars represent 10  $\mu\text{m}$ .



**Figure 16 - Autocrine effect of EPIC-derived EVs.** A) Percentage of EdU incorporation in EPIC incubated for 24 hours with 10% FBS (black bar), starving media (0% FBS, grey bar), 20 µg/mL (yellow bars) or 50 µg/mL (blue bars) of EVs-N or EVs-H5%. \* $p < 0.05$ , \*\*\*\* $p < 0.0001$  against 10% FBS condition; B) Proliferation rate of EPIC incubated with 10% FBS, starving media (0% FBS), 20 µg/mL or 50 µg/mL of EVs-N or EVs-H5%. Data represents mean  $\pm$  SEM ( $n=3$ ); C) Glycolysis stress assay was used to measure bioenergetics parameters, by adding glucose, oligomycin, and 2-DG ( $n=3$ ). Metabolic flux plots of EPIC incubated for 10 hours with 0% FBS (orange line) or 20 µg/mL of EVs-N (red line) or EVs-H5% (blue line), where PER was measured as a function of time; D) Metabolic flux plots of EPIC incubated for 10 hours with 0% FBS (orange line), or 50 µg/mL of EVs-N (red line) or EVs-H5% (blue line), where PER was measured as a function of time; E) Glycolysis stress test parameters (basal acidification, glycolysis, glycolytic capacity, and glycolytic reserve) were calculated for EPIC in each experimental condition. Metabolic-related graphs show data normalized to the concentration of proteins at the end of the assay.

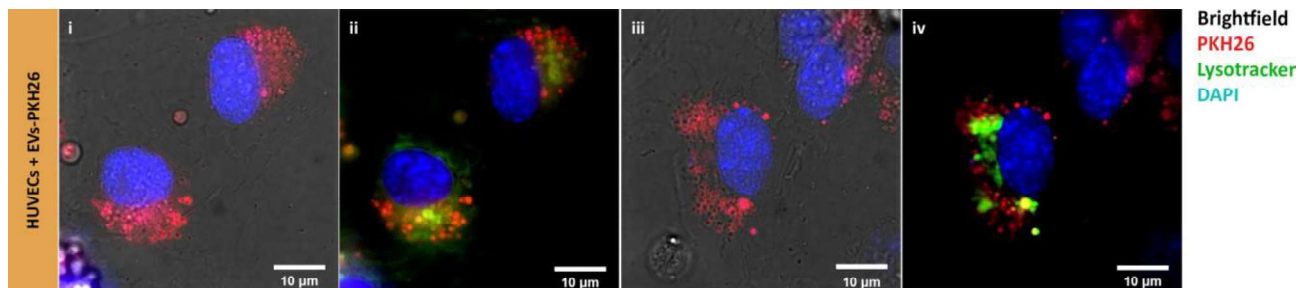
**Table 1 – ECAR measurement parameters of EPIC treated with 0% FBS, EVs-N or EVs-H5% at 20 or 50  $\mu\text{g}/\text{mL}$ .** Basal acidification, glycolysis, glycolytic capacity and glycolytic reserve are calculated according to ECAR measurements over time before and after the addition of glucose, oligomycin and 2-DG. Data represent mean  $\pm$  SEM (n=3).

Condition	$\mu\text{g}/\text{mL}$	Basal acidification	Glycolysis	Glycolytic capacity	Glycolytic reserve
		(mpH/min/ $\mu\text{g}/\text{mL}$ )			
0% FBS	-	0.019 $\pm$ 0.002	0.038 $\pm$ 0.004	0.072 $\pm$ 0.007	0.034 $\pm$ 0.003
EVs-N	20	0.018 $\pm$ 0.003	0.035 $\pm$ 0.001	0.067 $\pm$ 0.003	0.033 $\pm$ 0.002
	50	0.020 $\pm$ 0.000	0.042 $\pm$ 0.002	0.079 $\pm$ 0.001	0.038 $\pm$ 0.001
EVs-H5%	20	0.017 $\pm$ 0.003	0.038 $\pm$ 0.004	0.071 $\pm$ 0.009	0.033 $\pm$ 0.007
	50	0.021 $\pm$ 0.002	0.040 $\pm$ 0.002	0.080 $\pm$ 0.003	0.039 $\pm$ 0.002

## 2.4. Paracrine signaling of EPIC-derived EVs

It was previously shown that EPDCs provide signalling cues that support angiogenesis in the context of cardiac development (Guadix *et al.*, 2006; Cano *et al.*, 2016) and ischemic injury (Dubé *et al.*, 2017). Accordingly, we used human umbilical vein endothelial cells (HUVECs) to study the potential paracrine effect of EPIC-EVs. First, the EPIC-EVs internalization capacity was also pursued in HUVECs. EPIC-EVs were internalized in HUVECs and, similarly to what occurs in EPIC, also found surrounding the nucleus and co-localized with LysoTracker stained organelles (Fig. 17).

Similar to the *in vitro* analysis carried out on EPIC, proliferation analysis was also pursued to evaluate how would EPIC-derived EVs affect endothelial cells. To implement this task, HUVECs were incubated for 24 hours in different conditions including complete endothelial growth medium (EGM), starving medium (1% of FBS), and EVs-N or EVs-H5% diluted in starving medium. In this experiment, there is a tendency to increase the proliferation rate of HUVECS correlate with an increase in the concentration of EPIC-EVs (Fig. 18A and 18B). The tested conditions presented significantly lower proliferation rates as compared to HUVECs treated with EGM, except for HUVECs incubated with 50 µg/mL of EVs-H5%. These results indicate that EVs-H5% may encourage endothelial cell proliferation.



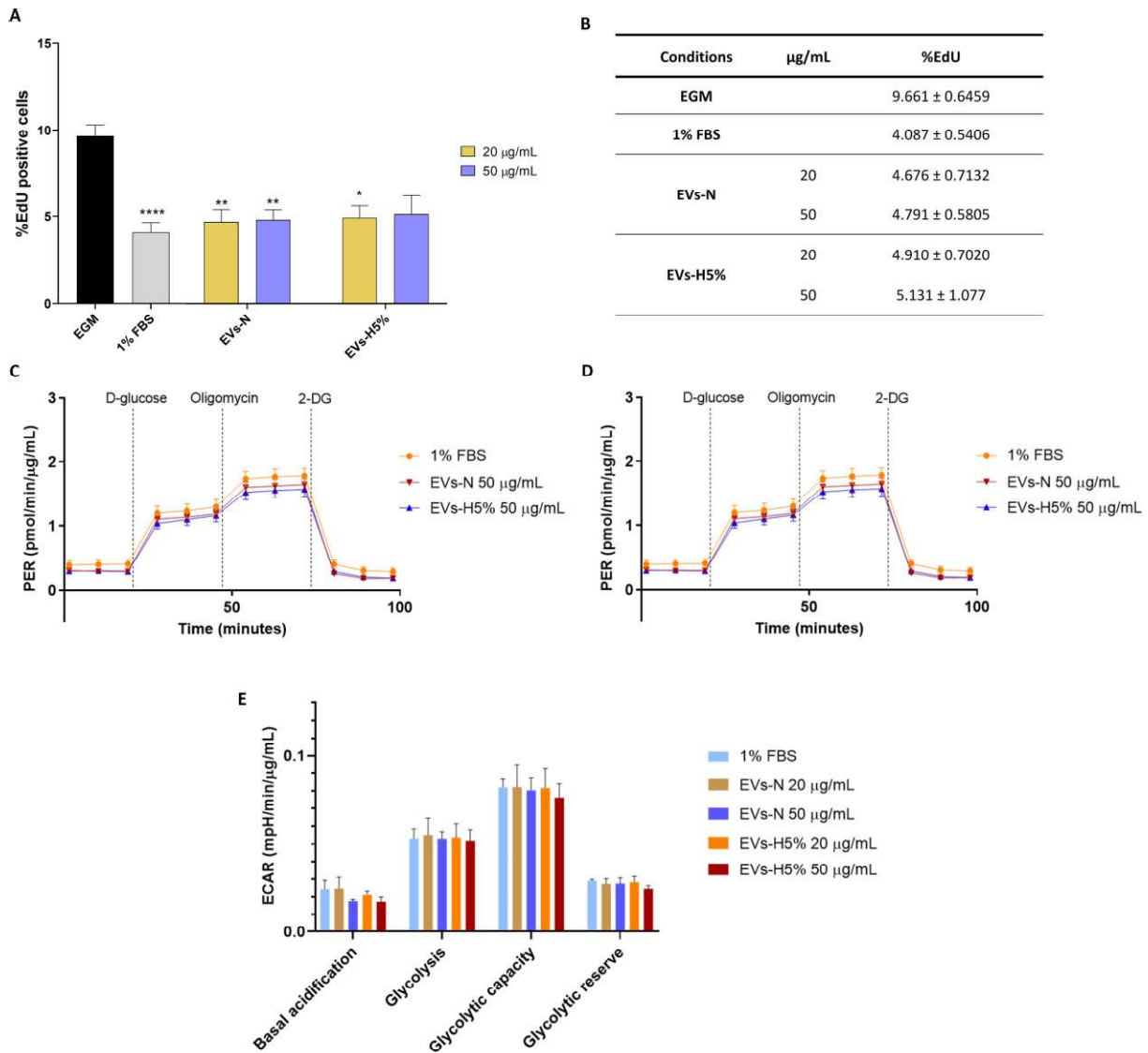
**Figure 17 –EPIC-EVs internalization in HUVEC cultures.** HUVECs after 1 hour incubation with EVs-PKH26. Cell nuclei were stained with DAPI and acidic organelles counterstained with Lysotracker. i), iii) Bright field, DAPI and PKH26 channels merged; ii), iv) Lysotracker, DAPI and Dil channels merged. Scale bar represents 10  $\mu\text{m}$ .

As with EPIC, the glycolytic rate of HUVECs cultured with different quantities of EPIC-EVs was measured. HUVECs treated with 20  $\mu\text{g}/\text{mL}$  of EVs-N and EVs-H5% behaved similarly to HUVECs incubated with EGM and 1% FBS (Fig. 18D). At a concentration of 50  $\mu\text{g}/\text{mL}$ , both EVs-N and EVs-H5% underperformed as compared to experimental controls (Fig. 18E). These observations are sustained by glycolysis stress assay parameters (Fig. 18E and Table 2) where it was observed a tendency for 20  $\mu\text{g}/\text{mL}$  of EVs to behave similarly to experimental controls. However, no statistically significant difference was recorded between EVs and experimental conditions, indicating that EPIC-EVs did not induce any kind of detectable effect on the metabolism of HUVECs at these concentrations.

**Table 2 – ECAR measurement parameters of HUVECs treated with 1% FBS, EVs-N or EVs-H5% at 20 or 50  $\mu\text{g}/\text{mL}$ .** Basal acidification, glycolysis, glycolytic capacity and glycolytic reserve are calculated according to ECAR measurements over time before and after the addition of glucose, oligomycin and 2-DG. Data represent mean  $\pm$  SEM (n=3).

Condition	$\mu\text{g}/\text{mL}$	Basal acidification	Glycolysis	Glycolytic capacity	Glycolytic reserve
		(mpH/min/ $\mu\text{g}/\text{mL}$ )			
1% FBS	-	0.024 $\pm$ 0.005	0.053 $\pm$ 0.005	0.082 $\pm$ 0.005	0.029 $\pm$ 0.001
EVs-N	20	0.025 $\pm$ 0.006	0.055 $\pm$ 0.009	0.082 $\pm$ 0.012	0.027 $\pm$ 0.003
	50	0.018 $\pm$ 0.001	0.053 $\pm$ 0.004	0.080 $\pm$ 0.007	0.027 $\pm$ 0.003
EVs-H5%	20	0.021 $\pm$ 0.002	0.054 $\pm$ 0.011	0.082 $\pm$ 0.008	0.028 $\pm$ 0.003
	50	0.017 $\pm$ 0.003	0.052 $\pm$ 0.006	0.076 $\pm$ 0.008	0.024 $\pm$ 0.002

In summary, no significant effects were found in the glycolysis stress tests when incubating HUVECs with 20 or 50  $\mu\text{g}/\text{mL}$  of EVs-N or EVs-H5%. However, the higher concentration of EVs-H5% revealed an improvement in the proliferation of HUVECs. Accordingly, a tendency for augmenting proliferation in their parental cells is observed in comparison with EVs-N. All these results indicate an effect associated to hypoxic-derived EVs. For this reason, and in order to unravel a potential effect of hypoxia in the properties of EVs, a new set of experiments were performed using EPIC-EVs isolated from EPIC cultured in 1% oxygen (EVs-H1%).



**Figure 18 – Paracrine effect of EPIC-EVs in HUVECs.** A) Percentage of EdU incorporation in HUVECs incubated for 24 hours with EGM (black bar), starving media (1% FBS, grey bar), 20 µg/mL (yellow bars) or 50 µg/mL (blue bars) of EVs-N or EVs-H5%. \* $p < 0.05$ , \*\* $p < 0.01$ , \*\*\*\* $p < 0.0001$  against EGM condition; B) Proliferation rate of HUVECs incubated with EGM, starving media (1% FBS), 20 µg/mL or 50 µg/mL of EVs-N or EVs-H5%. Data represents mean  $\pm$  SEM ( $n=3$ ); C) Glycolysis stress assay was used to measure bioenergetics parameters, by adding glucose, oligomycin, and 2-DG ( $n=3$ ). Metabolic flux plots of HUVECs incubated for 10 hours with 1% FBS (orange line) or 20 µg/mL of EVs-N (red line) or EVs-H5% (blue line), where PER was measured as a function of time; D) Metabolic flux plots of HUVECs incubated for 10 hours with 1% FBS (orange line), or 50 µg/mL of EVs-N (red line) or EVs-H5% (blue line), where PER was measured as a function of time; E) Glycolysis stress test parameters (basal acidification, glycolysis, glycolytic capacity, and glycolytic reserve) were calculated for HUVECs in each experimental condition. Metabolic-related graphs show data normalized to the concentration of proteins at the end of the assay.



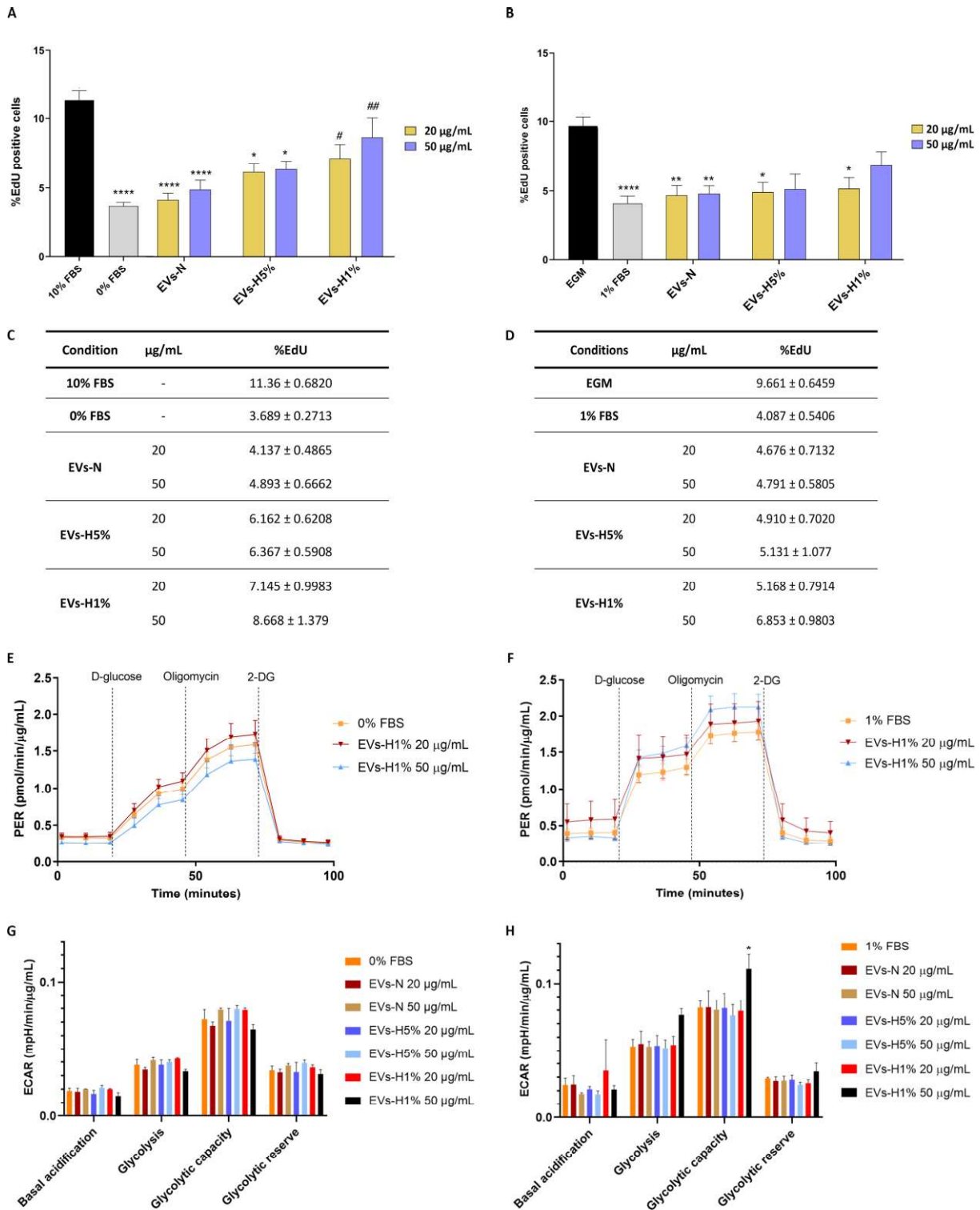
## 2.5. Hypoxia affects the autocrine and paracrine signalling capacity of EPIC-derived extracellular vesicles

To evaluate the effect in EV cargo resulting from oxygen level reduction in culture of parental cells, EPIC were incubated under 1% oxygen to obtain EPIC-derived EVs from this specific condition (EVs-H1%) and study their properties.

Once isolated and characterized, and similarly to previous experimental conditions, EPIC and HUVECs were incubated with 20 or 50  $\mu\text{g}/\text{mL}$  of EVs-H1% for 24 hours (Fig- 19A-D). Regarding EPIC, the proliferation rate of EV-treated cells showed a significant increase in both 20 and 50  $\mu\text{g}/\text{mL}$  EVs-H1% conditions in comparison with the basal media ( $7.15 \pm 0.99$  and  $8.67 \pm 1.38\%$  vs  $3.69 \pm 0.27\%$ , respectively) (Fig.1 19A and 19C). From the perspective of the paracrine effect of the treatments, it was noted that EGM condition (positive control) did yield significantly different results from those collected from basal medium (1% FBS), EVs-N (p-values  $< 0.0001$ ), EVs-H5% (p-values of 0.0001 for 20  $\mu\text{g}/\text{mL}$  and 0.0013 for 50  $\mu\text{g}/\text{mL}$ ) and 20  $\mu\text{g}/\text{mL}$  of EVs-H1% (p-value of 0.0204) assays. However, HUVECs incubated with 50  $\mu\text{g}/\text{mL}$  of EVs-H1%, did not reach a statistical difference in their proliferation rates as compared to the positive controls (Fig. 19B and 19D); these results were similar to those from experiments using 50  $\mu\text{g}/\text{mL}$  of EVs-H5% (Fig. 18A and 18B).

Regarding the assessment of metabolic behaviour, no significant differences were found when incubating EPIC with EVs-H1% (Fig. 19E and 19G, Tables 3 and 4). Nonetheless, HUVECs incubated with 50  $\mu\text{g}/\text{mL}$  of EVs-H1% showed an increase in proton efflux in comparison with the basal medium (1% FBS) (Fig. 19F). Moreover, the glycolytic capacity of HUVECs treated with 50  $\mu\text{g}/\text{mL}$  of EVs-H1% was found to be higher to that induced by 50  $\mu\text{g}/\text{mL}$  of EVs-H5% (Fig. 19H). Interestingly, when comparing the glycolytic behaviour of EPIC and HUVECs, it was noted that HUVECs were immediately affected by D-glucose, oligomycin and 2-DG, while EPIC took more time to build their response after each injection (Fig. 19E and 19F).

Taken together, these data indicate that the reduction of oxygen levels in the parental cells reflected a changed in both autocrine and paracrine signalling capacities of EPIC-EVs.



**Figure 19 – Functional assays of EPIC and HUVECs treated with EVs-H1%.** A) Percentage of EdU incorporation in EPIC (\*p < 0.05, \*\*\*\*p < 0.0001 against 10% FBS condition, and #p < 0.05 and ##p < 0.01 against 0% FBS condition) and B) HUVECs (\*p < 0.05, \*\*p < 0.01 \*\*\*\*p < 0.0001 against EGM condition) incubated for 24 hours with 10% FBS (black bar) or 0% FBS (grey bar) in EPIC cultures, or EGM (black bar) or 1% FBS (grey bar) in HUVECs culture, 20 µg/mL (yellow bars) or 50 µg/mL (blue bars) of EVs-N, EVs-H5% or EVs-H1%; C) Proliferation rate of EPIC incubated with EVs-N, EVs-H5% or EVs-H1% at 20 or 50 µg/mL, 0% FBS or 10% FBS. Data represents mean ± SEM (n=3); D) Proliferation rate of HUVECs incubated with EVs-N,

EVs-H5% or EVs-H1% at 20 or 50  $\mu\text{g}/\text{mL}$ , 1% FBS. Data represents mean  $\pm$  SEM (n=3); E) Metabolic flux plots of EPIC incubated with 0% FBS (orange line), 20  $\mu\text{g}/\text{mL}$  (red line) or 50  $\mu\text{g}/\text{mL}$  (blue line) of EVs-H1% for 10 hours, where PER was measured as a function of time; F) HUVECs incubated with 1% FBS (orange line), 20  $\mu\text{g}/\text{mL}$  (red line) or 50  $\mu\text{g}/\text{mL}$  (blue line) of EVs-H1% for 10 hours, where PER was measured as a function of time; G) Glycolysis stress test parameters (basal acidification, glycolysis, glycolytic capacity, and glycolytic reserve) were calculated for EPIC and H) HUVECs in each experimental condition (n=3). Metabolic-related graphs show data normalized to concentration of proteins at the end of assay.

**Table 3 – ECAR measurement parameters of EPIC treated with 0% FBS, EVs-N, EVs-H5% or EVs-H1% at 20 or 50  $\mu\text{g/mL}$ .** Basal acidification, glycolysis, glycolytic capacity and glycolytic reserve are calculated according to ECAR measurements over time before and after the addition of glucose, oligomycin and 2-DG. Data represent mean  $\pm$  SEM (n=3).

Condition	$\mu\text{g/mL}$	Basal acidification	Glycolysis	Glycolytic capacity	Glycolytic reserve
		(mpH/min/ $\mu\text{g/mL}$ )			
0% FBS	-	0.019 $\pm$ 0.002	0.038 $\pm$ 0.004	0.072 $\pm$ 0.007	0.034 $\pm$ 0.003
EVs-N	20	0.018 $\pm$ 0.003	0.035 $\pm$ 0.001	0.067 $\pm$ 0.003	0.033 $\pm$ 0.002
	50	0.020 $\pm$ 0.000	0.042 $\pm$ 0.002	0.079 $\pm$ 0.001	0.038 $\pm$ 0.001
EVs-H5%	20	0.017 $\pm$ 0.003	0.038 $\pm$ 0.004	0.071 $\pm$ 0.009	0.033 $\pm$ 0.007
	50	0.021 $\pm$ 0.002	0.040 $\pm$ 0.002	0.080 $\pm$ 0.003	0.039 $\pm$ 0.002
EVs-H1%	20	0.020 $\pm$ 0.000	0.043 $\pm$ 0.000	0.079 $\pm$ 0.001	0.036 $\pm$ 0.002
	50	0.015 $\pm$ 0.002	0.033 $\pm$ 0.001	0.065 $\pm$ 0.004	0.031 $\pm$ 0.003

**Table 4 – ECAR measurement parameters of HUVECs treated with 1% FBS, EVs-N, EVs-H5% or EVs-H1% at 20 or 50  $\mu\text{g/mL}$ .** Basal acidification, glycolysis, glycolytic capacity and glycolytic reserve are calculated according to ECAR measurements over time before and after the addition of glucose, oligomycin and 2-DG. Data represent mean  $\pm$  SEM (n=3).

Condition	$\mu\text{g/mL}$	Basal acidification	Glycolysis	Glycolytic capacity	Glycolytic reserve
		(mpH/min/ $\mu\text{g/mL}$ )			
1% FBS	-	0.024 $\pm$ 0.005	0.053 $\pm$ 0.005	0.082 $\pm$ 0.005	0.029 $\pm$ 0.001
EVs-N	20	0.025 $\pm$ 0.006	0.055 $\pm$ 0.009	0.082 $\pm$ 0.012	0.027 $\pm$ 0.003
	50	0.018 $\pm$ 0.001	0.053 $\pm$ 0.004	0.080 $\pm$ 0.007	0.027 $\pm$ 0.003
EVs-H5%	20	0.021 $\pm$ 0.002	0.054 $\pm$ 0.011	0.082 $\pm$ 0.008	0.028 $\pm$ 0.003
	50	0.017 $\pm$ 0.003	0.052 $\pm$ 0.006	0.076 $\pm$ 0.008	0.024 $\pm$ 0.002
EVs-H1%	20	0.035 $\pm$ 0.023	0.054 $\pm$ 0.006	0.080 $\pm$ 0.008	0.026 $\pm$ 0.003
	50	0.021 $\pm$ 0.003	0.077 $\pm$ 0.005	0.111 $\pm$ 0.011	0.034 $\pm$ 0.006

## Chapter III– Characterization of EPIC-derived extracellular matrix

### 3.1. EPIC as a source of cardiac extracellular matrix

Epicardial and epicardial-derived cells (EPDCs) originally contribute to the formation of the subepicardial space, an extracellular matrix (ECM)-rich environment that separates the epicardium from the myocardium (Wessels and Pérez-Pomares, 2004). Then, EPDCs will progressively invade the cardiac chamber interstitium, where they also participate in the deposit of ECM molecules (Pogontke *et al.*, 2019). The epicardial-derived ECM therefore is a key element to understand both cell behaviour and cell responses to changes in their microenvironment (Silva *et al.*, 2021). In this chapter of the Results section, we will characterize the ECM of EPIC to determine the contribution of the epicardial-derived component to the cardiac ECM.

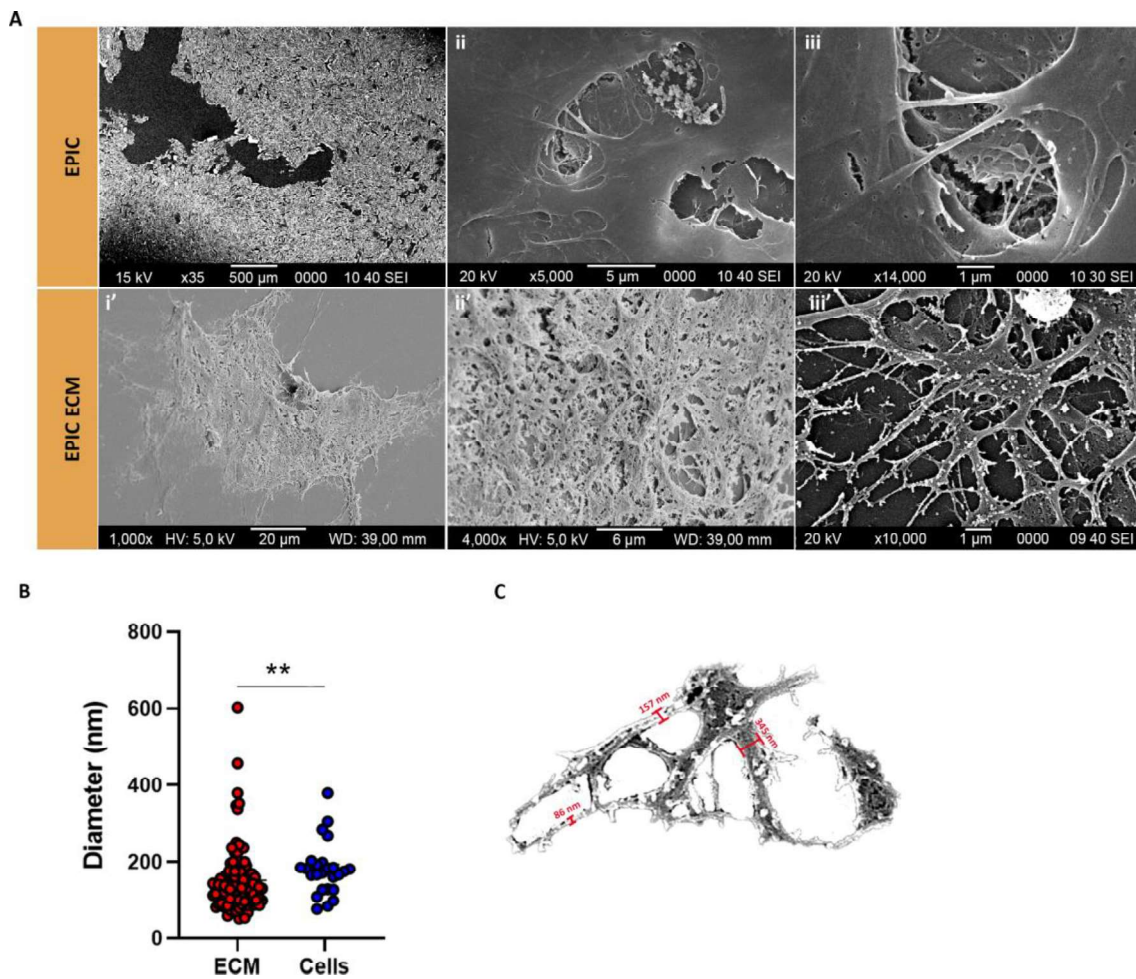
#### 3.1.1. EPIC-derived extracellular matrix structural complexity (i): EPIC cultures

In order to study the structural complexity of EPIC-derived ECM, we first cultured EPIC over glass coverslips placed in plastic dishes until confluency (7 days of culture) to be analysed using scanning electron microscopy (SEM). EPIC grew normally, displaying a characteristic flattened, mesenchymal phenotype, with the cells showing multiple filopodia and lamellipodia (Fig. 20A). Due to cell culture confluency, some EPIC were found to grow in stacks, forming a multi-layered cell culture. In close-up SEM images (Fig. 20A ii and iii), at least three layers could be distinguished. The ECM fibrillar networks are occasionally observed between the cells.

#### 3.1.2. EPIC-derived extracellular matrix structural complexity (ii): Decellularization and analysis of the ECM structure

After 7 days of culture, EPIC were submitted to a decellularization process to expose the EPIC-secreted ECM (see chapter III section Material & Methods). The resulting EPIC-ECM remained attached to the glass coverslip displaying a rough surface and a typical irregular pattern. Fibres were assembled forming a mesh-like organization (Fig. 20B). ECM tubular-like projections are morphologically distinct from EPIC cell membrane

projections as they are thinner and non-flattened (Fig. 20A). Moreover, the diameter of both fibres was measured in the middle of its longitudinal length recurring to SEM images and ImageJ. The diameter of the ECM fibres ( $151 \pm 8.5$  nm) showed a significant difference with the diameter of EPIC protrusions ( $179.9 \pm 13.91$  nm) (Fig. 20C).



**Figure 20– Microscopic characterization of EPIC-ECM.** A) SEM images of EPIC at 35x (i), 5,000x (ii) and 14,000x (iii) magnification, and EPIC-derived ECM at 1,000x (i'), 4,000x (ii') and 10,000x (iii') magnification; B) Representative visual image of fibre diameters in EPIC-ECM and EPIC protrusions measured via ImageJ using SEM images. \*\* $p < 0.01$ ; C) Data from 6 biological replicates and 17 technical measurements each one for ECM samples, and 4 biological replicates with between 5 and 8 measurements each one for EPIC.

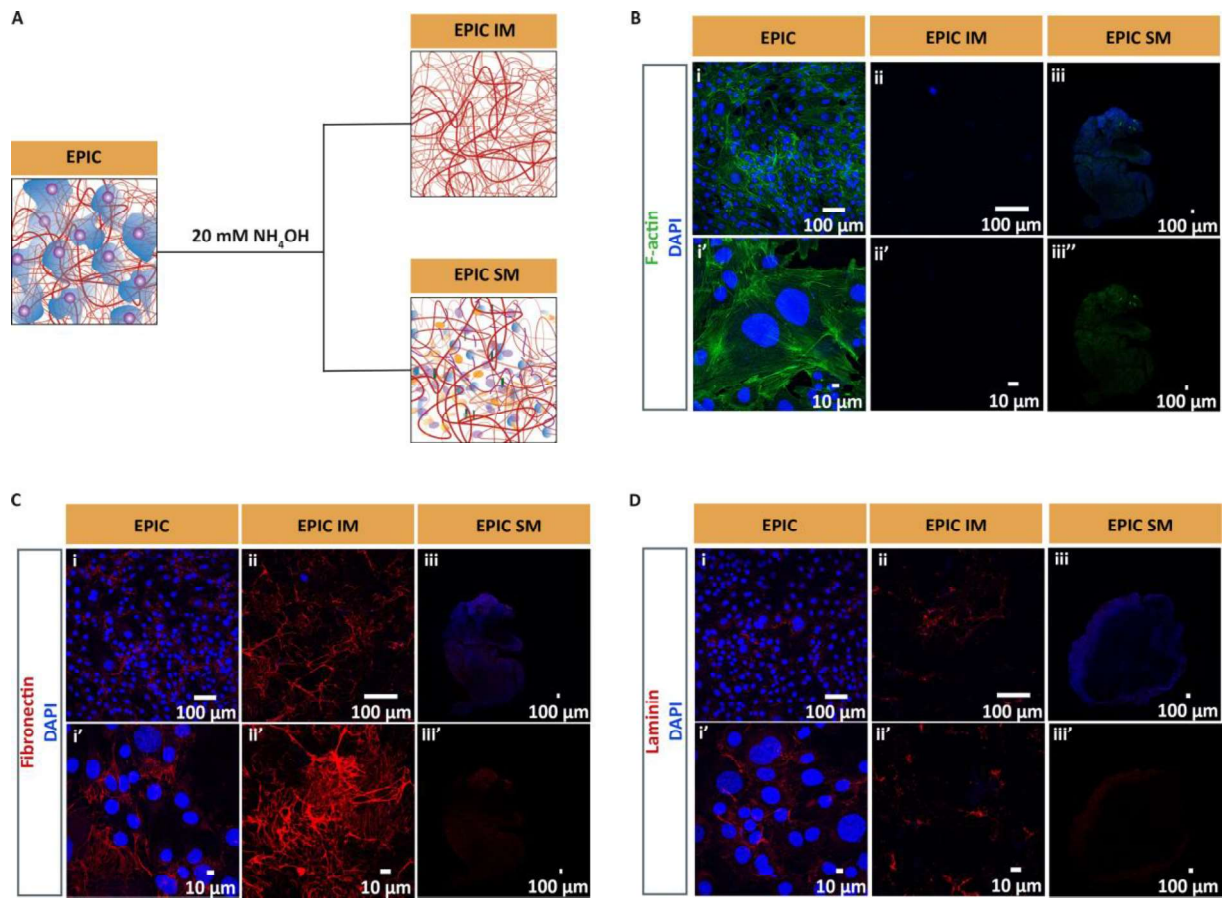
### 3.1.3. Immunocytochemical characterization of EPIC-derived ECM

In order to confirm the presence of ECM-related proteins after the decellularization process, samples were analysed by immunocytochemistry (ICC). During EPIC-derived ECM isolation, ECM was divided in two fractions: EPIC insoluble matrix (EPIC IM) and soluble matrix (EPIC SM). EPIC IM phase corresponds to the insoluble fraction that remains attached to the surface of the dish, while EPIC SM is related to the components that are present in the solution when the matrix is isolated after cellular disruption (Fig. 21A).

For a first exploratory approach, and to evaluate the decellularization process, phalloidin, a toxin that stabilizes F-actin polymers and labels the cellular cytoskeleton, and DAPI, a DNA intercalating agent that allowed us to identify DNA contamination, were used in all samples (Fig. 21B). As expected, EPIC presented a high actin filament density in the cell cortex (Fig. 21B v and vi), while in EPIC IM, no F-actin is detected (Fig. 21B ii and ii'). However, in EPIC SM F-actin staining spreading in the soluble protein mass sample was observed (Fig. 21B iii and iii'), indicating a potential intracellular protein contamination in this fraction. Accordingly, EPIC SM presents high amount of DNA contamination (Fig. 21B-D iii). However, it is noteworthy that ammonium hydroxide decellularization method results in low amount of DNA contamination in the insoluble fraction without recurring to DNase treatment.

Second, to confirm the extracellular nature of the samples, an ICC for fibronectin and laminin, two of the main components of basement membrane matrices (Silva *et al.*, 2021), was performed. EPIC showed expression of fibronectin in their surroundings, reaching neighbouring cells (Fig. 21C i and i'). After decellularization, it was evident that fibronectin remained attached to the surface in EPIC IM samples (Fig. 21C ii and ii'). Regarding EPIC SM, traces of fibronectin were also observed throughout the sample (Fig. 21C iii and iii'). Regarding laminin  $\alpha$ 1 deposition, this seemed to be reduced as compared to that of fibronectin (Fig. 21D i and i'). However, similar to fibronectin, laminin is found enclosing EPIC (Fig. 21D i and i'). A similar pattern is also found in EPIC IM, however scarcely distributed if compared to fibronectin immunostaining (Fig. 21D ii and ii'). Traces of laminin  $\alpha$ 1 were also observed to be sparsely distributed in EPIC SM samples (Fig. 21B iii and iii').





**Figure 21 – Immunocytochemistry characterization of EPIC, EPIC IM and EPIC SM.** A) Schematic representation of resulting ECM phases from EPIC decellularization with ammonium hydroxide. B) ICC analysis of F-actin, C) fibronectin in fibronectin and D) laminin subunit  $\alpha$ 1 in EPIC (i and i'), EPIC IM (ii and ii') and EPIC SM (iii to iii'), respectively.

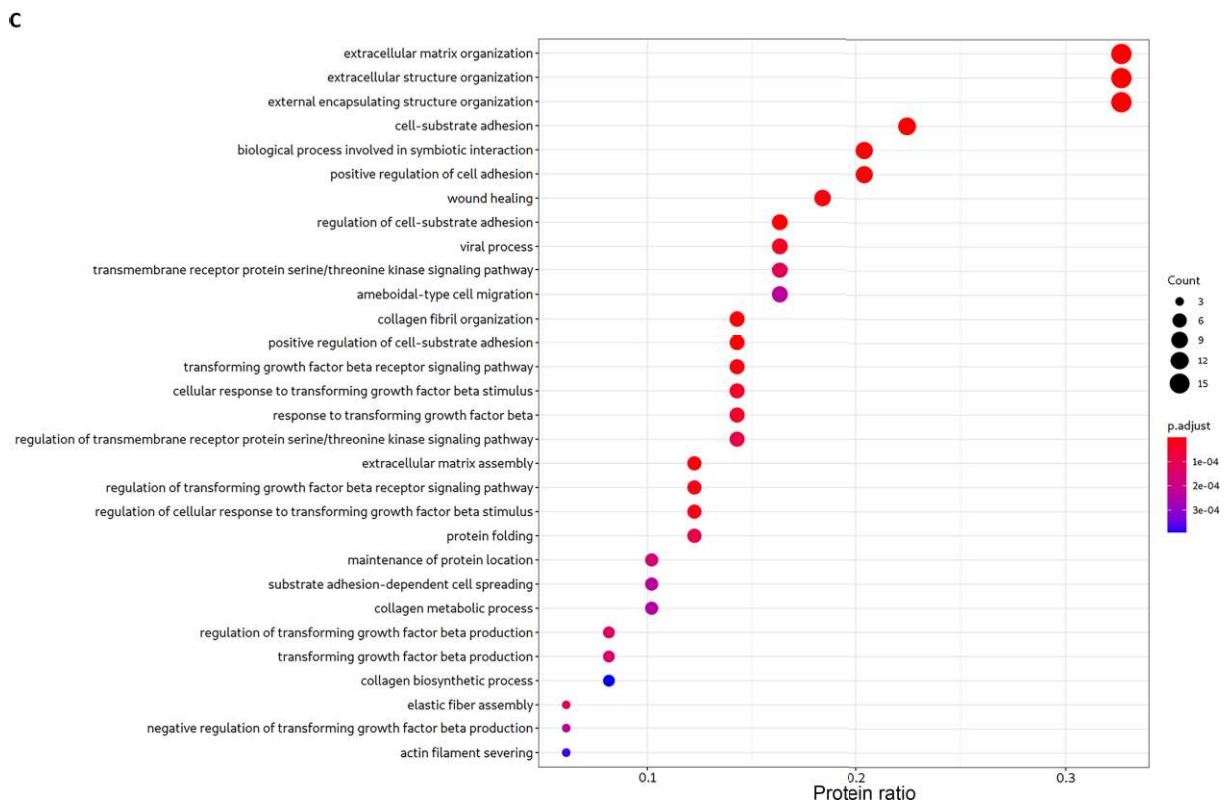
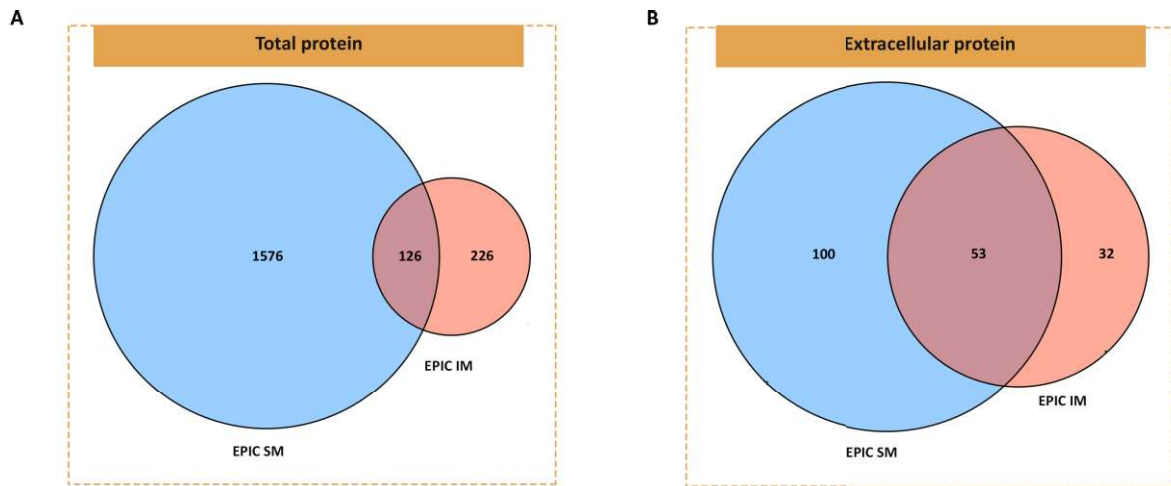
### 3.3. Epicardial extracellular matrix composition: a proteomic analysis

#### 3.3.1. Protein composition differs between different fractions of EPIC-derived extracellular matrix

After the initial exploratory analysis of EPIC-derived ECM fractions, shotgun proteomics was pursued for a detailed composition study in EPIC IM and EPIC SM. Contemporary shotgun proteomics allows separation of peptides into smaller subsets, thus decreasing ion competition and increasing detection sensitivity. This way, current mass spectrometry experiments can resolve peptides from more than 10,000 proteins, allowing their identification and quantification (Lam *et al.*, 2016).

Lists of extracellular proteins from EPIC IM were compared with those identified from EPIC SM to analyse differences in protein content between both fractions. Our results indicate that EPIC SM fraction has more proteins than EPIC IM (1,702 versus 352, respectively, in at least two of the three replicates; Fig. 22). Secondly, and due to our interest in ECM proteins, an “extracellular protein” filter was applied. After applying this filter, 153 extracellular proteins identified in EPIC SM and 85 in EPIC IM were considered for further analysis (Fig. 22A and Table A7 in Appendix). Of them, 53 extracellular proteins were shared between both fractions (Fig. 22B and Table A8 in Appendix).

The common proteins identified in EPIC IM and EPIC SM are associated to GO terms related to extracellular functions, such as “extracellular matrix organization” (GO:0030198, p.adjust value =  $4.09 \times 10^{-10}$ ), “extracellular structure organization” (GO:0043062, p.adjust value =  $4.09 \times 10^{-10}$ ), and “external encapsulating structure organization” (GO:0045229, p.adjust value =  $4.09 \times 10^{-10}$ ) (Fig. 22C). Additionally, biological processes related to wound healing and TGF- $\beta$  signalling pathway were identified in EPIC ECM fractions, as “wound healing” (GO:0042060, p.adjust value =  $4 \times 10^{-4}$ ), “transforming growth factor beta receptor signalling pathway” (GO:0007179, p.adjust value =  $1.37 \times 10^{-5}$ ) and “cellular response to transforming growth factor beta stimulus” (GO:0071560, p.adjust value =  $4.08 \times 10^{-5}$ ) (Fig. 22C).



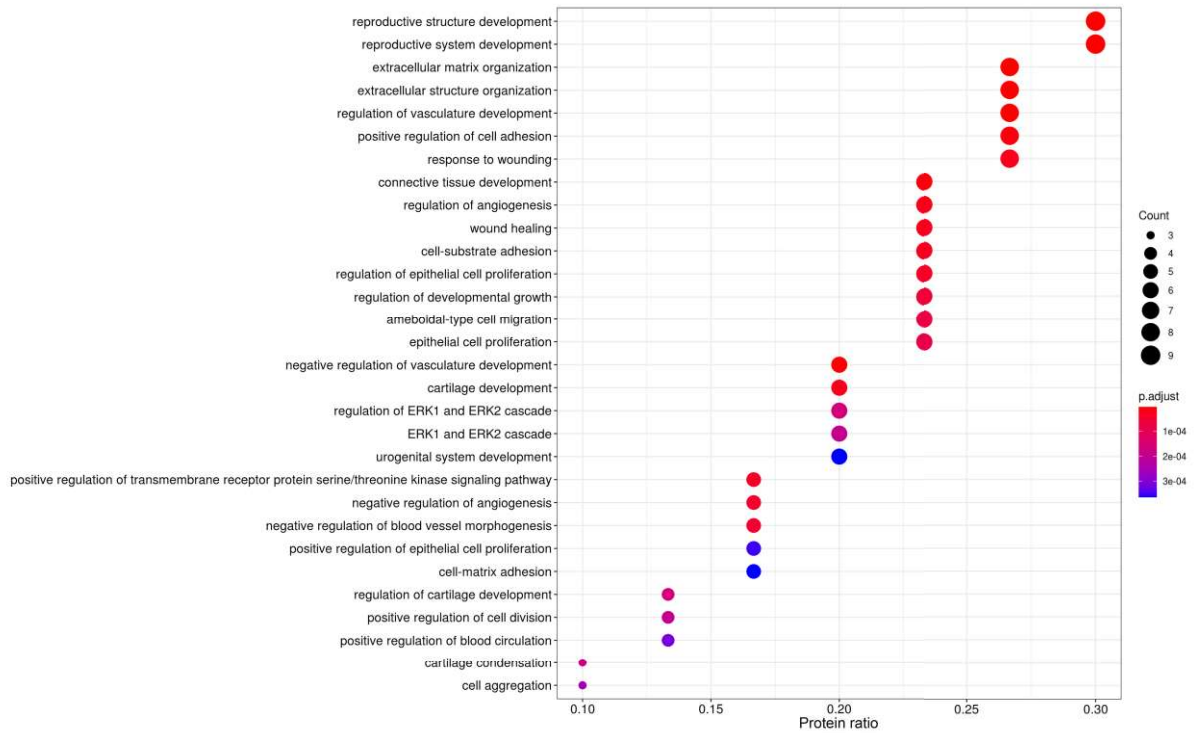
**Figure 22 – Qualitative comparison of identified proteins in label-free proteomics from EPIC IM and EPIC SM.** A) Venn diagram representation of total proteins identified in EPIC IM and EPIC SM indicating the number of unique proteins identified in, at least, two biological replicates of EPIC IM (226 proteins) and EPIC SM (1,576 proteins), as well as proteins found to be common to both fractions (126 proteins); B) Venn diagram representation of extracellular proteins identified in EPIC IM and EPIC SM indicating the number of unique proteins found in, at least, two biological replicates of EPIC IM (32 proteins) and EPIC SM (100 proteins), and proteins in common in both fractions (53 proteins). C) Biological processes (gene ontology analysis) of extracellular proteins in common between EPIC IM and EPIC SM represented in a dot plot graph. The most highly significant categories in descending order in categories of protein ratio, defined as the proportion of significant genes that are found in the functional category. The x-axis represents the protein ratio and the dot size the number of genes associated with the functional category and the dot colour corresponds to the p.adjust value.

Then, a GO term analysis was performed to characterize each fraction based on unique proteins in each condition (Fig. 23A). For the EPIC IM extracellular proteins, “extracellular matrix organization” (GO:0030198) and “extracellular structure organization” (GO:0043062) appear between the first the top 5 biological processes (p.adjust value =  $2.35 \times 10^{-6}$ ) followed by “regulation of vascular development” (GO:1901342) (p.adjust =  $3.67 \times 10^{-6}$ ), “positive regulation of cell adhesion” (GO:0045785) (p.adjust =  $1.08 \times 10^{-5}$ ) and “response to wounding” (GO:0009611) (p.adjust =  $2.22 \times 10^{-5}$ ) (protein ratio = 0.267). It is important to emphasize that the same protein can be included in different GO annotations and, because of that, other biological terms can be enhanced (such as “GO:0048608 - reproductive structure development” and “GO:0061458 - reproductive system development”). Proliferation and developmental-related GO terms are also represented with high p-adjust values, such as “regulation of angiogenesis” (GO:0045765) (p.adjust =  $2.22 \times 10^{-5}$ ), “regulation of epithelial cell proliferation” (GO:0050678) (p.adjust =  $3.79 \times 10^{-5}$ ), among others, with a protein ratio of 0.2.

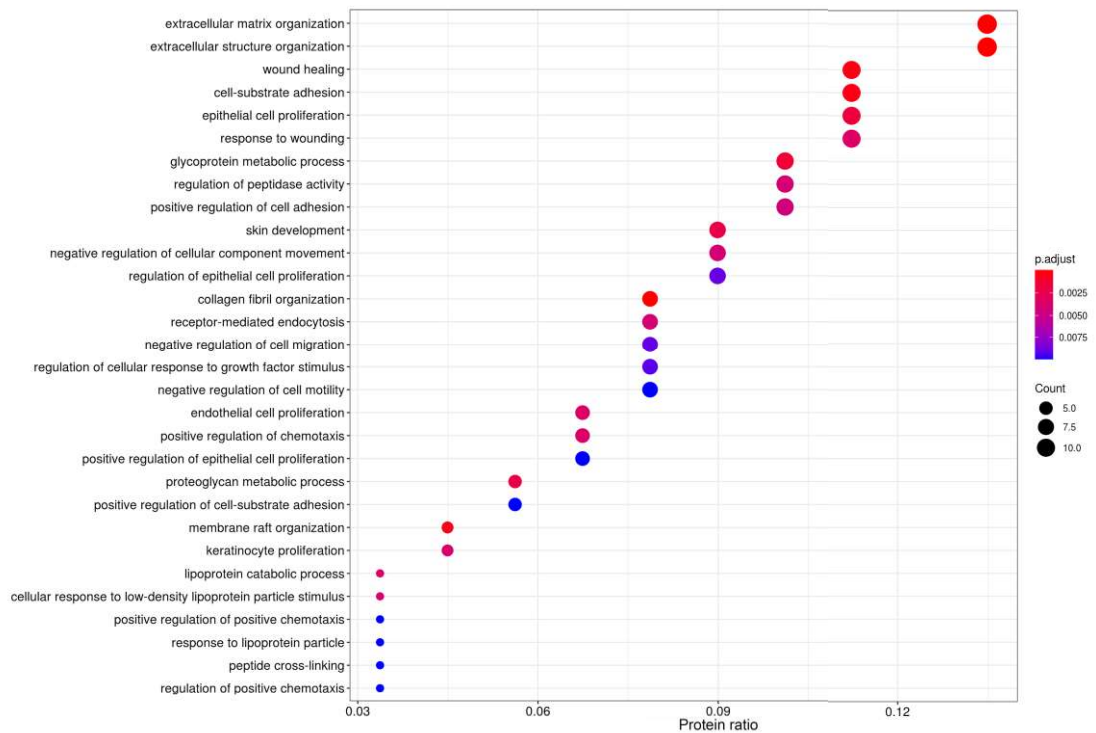
In what concerns EPIC SM unique extracellular proteins, the top GO terms related to biological processes were “extracellular matrix organization” (GO:0030198) and “extracellular structure organization” (GO:0043062) (p.adjust of  $1.28 \times 10^{-6}$ ) with a protein ratio of 0.134 (Fig. 23B). In comparison with protein ratio associated to the EPIC IM extracellular proteins, EPIC SM fraction contains less extracellular matrix-associated proteins. In accordance to these findings, GO terms related to extracellular, wounding,

angiogenic and vascular development are highly represented in EPIC IM versus EPIC SM. Such analysis suggests a potential matrix support and reparative role from EPIC IM in comparison with EPIC SM.

A



B



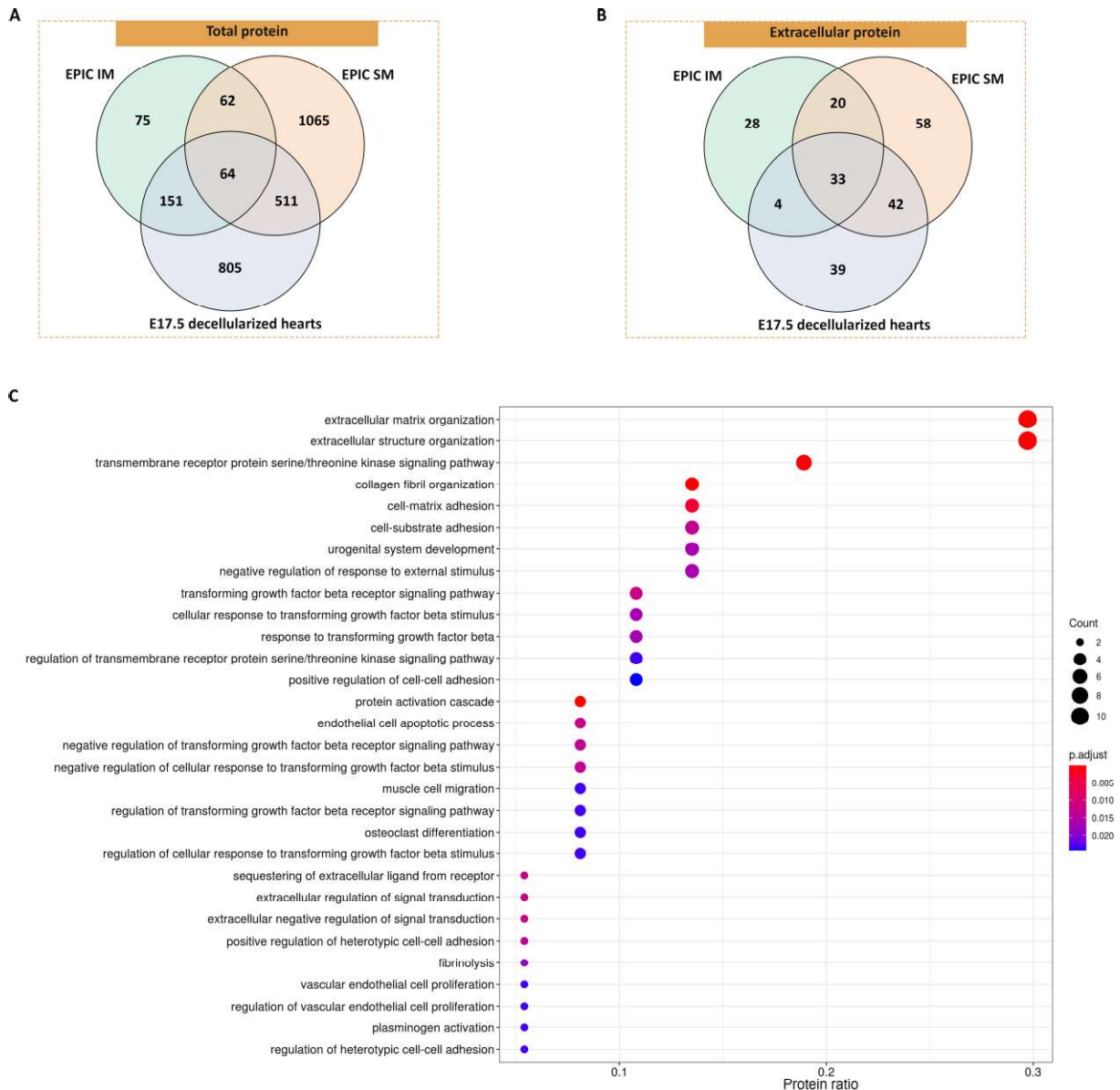
**Figure 23 – Functional enrichment analysis of EPIC IM and EPIC SM extracellular proteins.** A) Biological processes (gene ontology analysis) of EPIC IM extracellular proteins represented in a dot plot graph; B) Biological processes (gene ontology analysis) of EPIC SM extracellular proteins represented in a dot plot graph. The x-axis represents the protein ratio, the dot size the number of genes associated with the functional category and the colour corresponds to the p.adjust value.

### 3.3.2. Protein composition of E17.5 decellularized hearts is similar to EPIC-derived extracellular fractions

The next step was to evaluate the similarities between EPIC-derived ECM and proteins isolated from murine embryonic hearts at day 17.5 (Fig. 24). For that, decellularized E17.5 hearts were prepared for shotgun proteomics and analysed in the same way than EPIC-ECM.

In murine decellularized hearts, 1,563 proteins were identified, being 1,531 found in, at least, two biological replicates. On one hand, EPIC IM and E17.5 hearts shared 215 proteins, from which 151 were uniquely found in these samples (Fig. 24A). On the other hand, EPIC SM and E17.5 hearts shared 575 proteins, from which 511 were found in at least two biological replicates of each condition. Finally, EPIC IM, EPIC SM and E17.5 hearts shared 64 proteins in total.

After selecting the extracellular-related proteins, 118 proteins were identified in E17.5 hearts. Of them, 39 proteins were found to be unique in this dataset (Fig. 24B). These proteins were mainly associated with extracellular matrix-related terms (GO:0030198 – “extracellular matrix organization” and GO:0043062 – “extracellular structure organization”, with  $p.adjust = 4.30 \times 10^{-10}$  and protein ratio of 0.297; Fig. 24B), and with other terms related with the biology of the matrix (e.g. GO:0007178 – “transmembrane receptor protein serine/threonine kinase signalling pathway” and GO:0007160 – “cell-matrix adhesion”). Finally, at least three GO terms related to TGF- $\beta$  signalling were also found: “transforming growth factor beta receptor signalling pathway” (GO:0007179,  $p.adjust$  of 0.012 and protein ratio ratio of 0.108) and “negative regulation of transforming growth factor beta receptor signaling pathway” (GO:0030512,  $p.adjust$  of 0.013) and “negative regulation of cellular response to transforming growth factor beta stimulus” (GO:1903845,  $p.adjust$  of 0.013), with protein ratios of 0.081 (Fig. 24B).

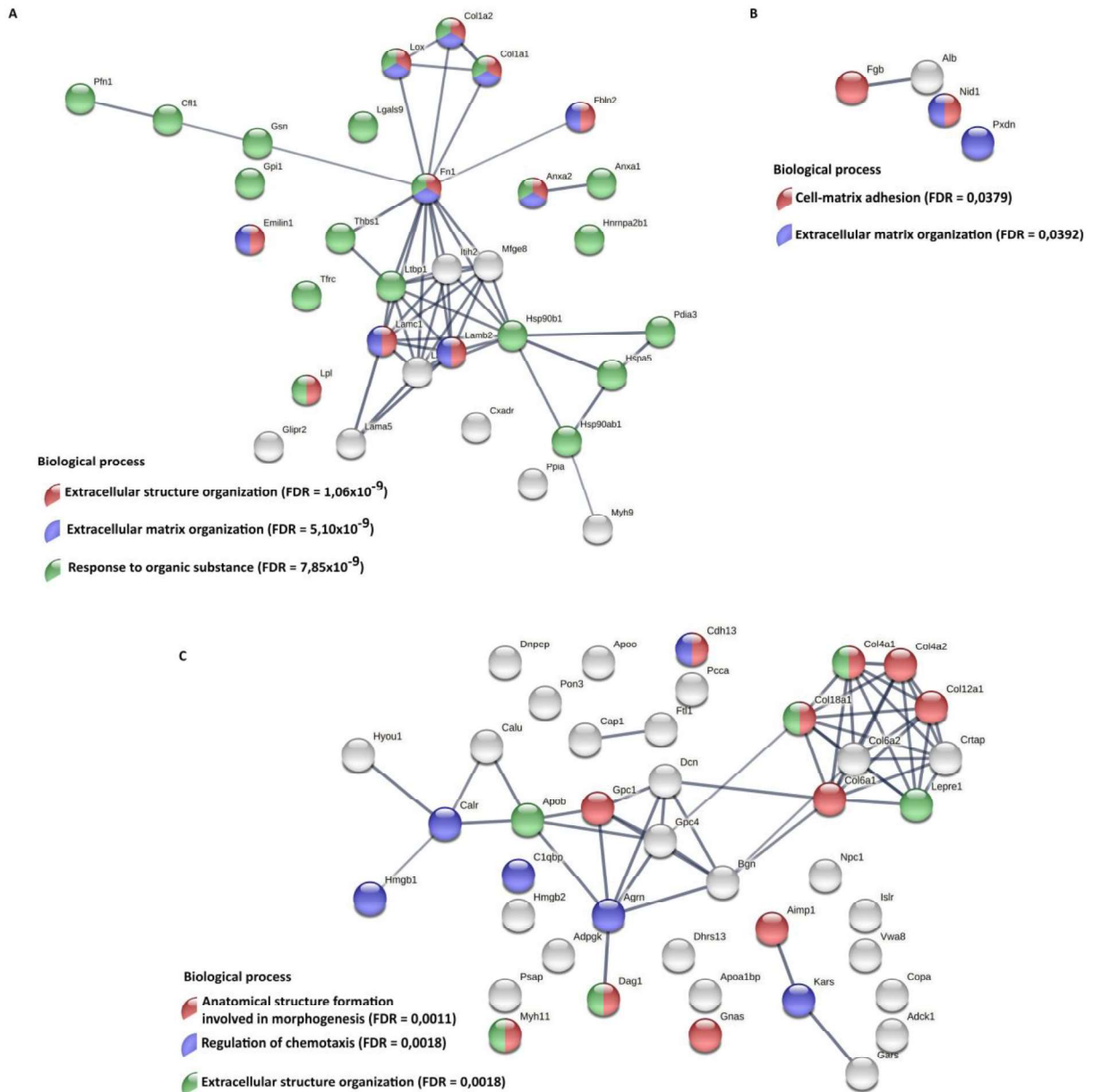


**Figure 24 – Qualitative comparison of identified proteins in label-free proteomics from EPIC IM, EPIC SM and E17.5 decellularized hearts.** A) Venn diagram representation of total proteins in EPIC IM, EPIC SM and E17.5 hearts. EPIC IM, EPIC SM and E17.5 hearts contain 75, 1,065 and 805 unique proteins, respectively. EPIC IM shares 151 proteins with E17.5 hearts, and EPIC SM shares 511 proteins with embryonic hearts. Sixty-four proteins are found to be in common between all samples; B) Venn diagram representation of extracellular proteins in EPIC IM, EPIC SM and E17.5 hearts. EPIC IM, EPIC SM and E17.5 hearts contain 28, 58 and 39 unique proteins, respectively. EPIC IM shares 4 proteins with E17.5 hearts, and EPIC SM shares 42 proteins with embryonic hearts. Thirty-three proteins are found to be in common between all samples; C) Biological processes (gene ontology analysis) of extracellular proteins from E17.5 decellularized hearts represented in a dot plot graph. The most highly significant categories in descending order in categories of protein ratio, defined as the proportion of significant genes that are found in the functional category. The x-axis represents the protein ratio and the dot size the number of genes associated with the functional category and the dot colour corresponds to the p.adjust value.



Next, we explored the similarities between E17.5 cardiac ECM and EPIC-ECM. To do that, the protein-protein interactions among the shared proteins between embryonic hearts and EPIC-ECM fractions were studied using STRING DB (Fig. 25). It should be considered that this tool also returns a GO functional enrichment against a universal *Mus musculus* database. This allows us to explore the biological significance of the identified proteins in the animal model from which EPIC derive. First, embryonic hearts, EPIC IM and EPIC SM were found to share 33 extracellular proteins that are associated to biological processes such as “extracellular structure organization” (GO:0043062) (FDR of  $1.06 \times 10^{-9}$ ), or “extracellular matrix organization” (GO:0030198) (FDR of  $5.10 \times 10^{-9}$ ). Second, only 4 proteins were found in common with EPIC IM (Fig. 25A and Table A9 in Appendix). Finally, 42 proteins were shared between embryonic hearts and EPIC SM (Fig. 25A and Table A9 in Appendix). The GO annotations found to be more enriched in biological process for these proteins are “anatomical structure formation involved in morphogenesis” (GO:0048646; FDR of 0.0011), “regulation of chemotaxis” (GO:0050920; FDR of 0.0018) and “extracellular structure organization” (GO:0043062; FDR of 0.0018) (Fig. 2.5C).

In summary, our results reveal that the EPIC-ECM fractions contain a similar profile of extracellular proteins as in the decellularized embryonic hearts, suggesting an important contribution of epicardial-derived ECM into the development of the cardiac ECM.

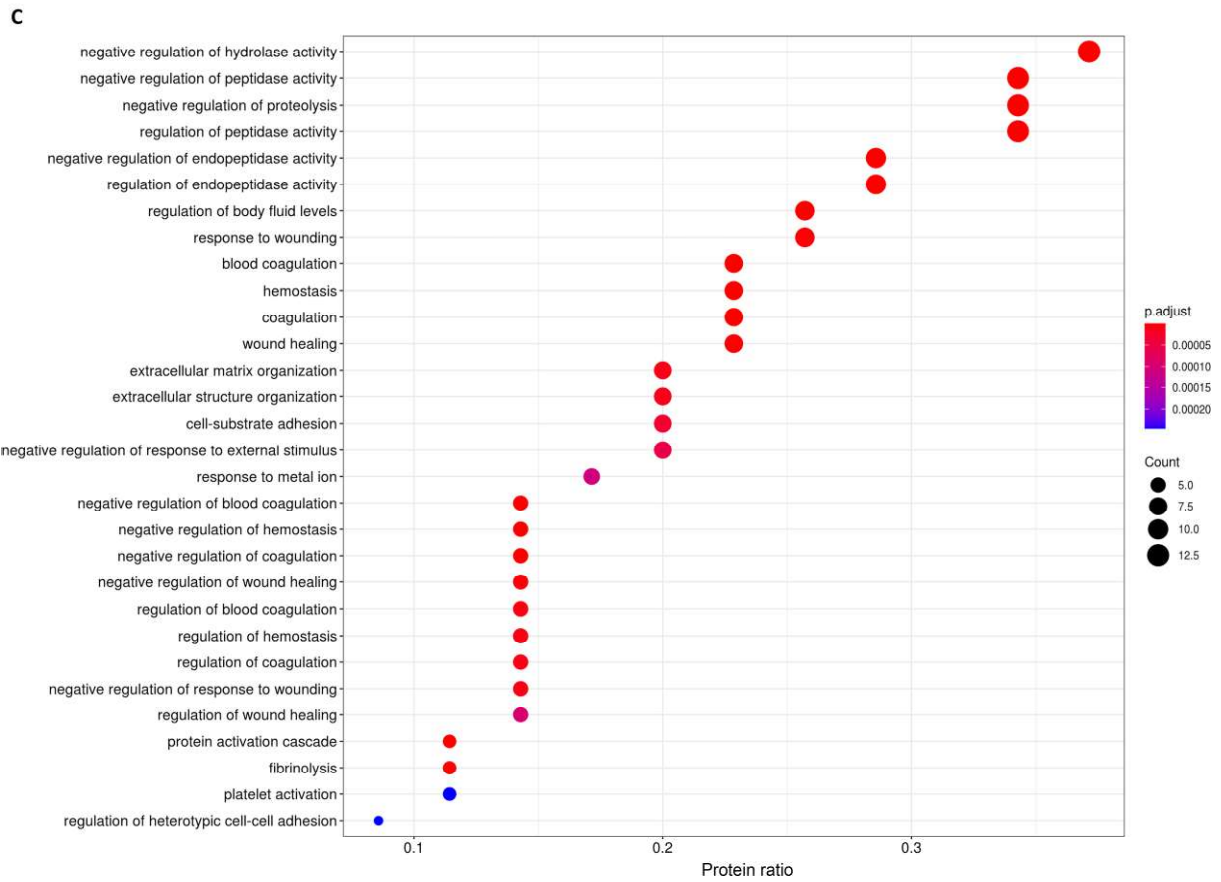
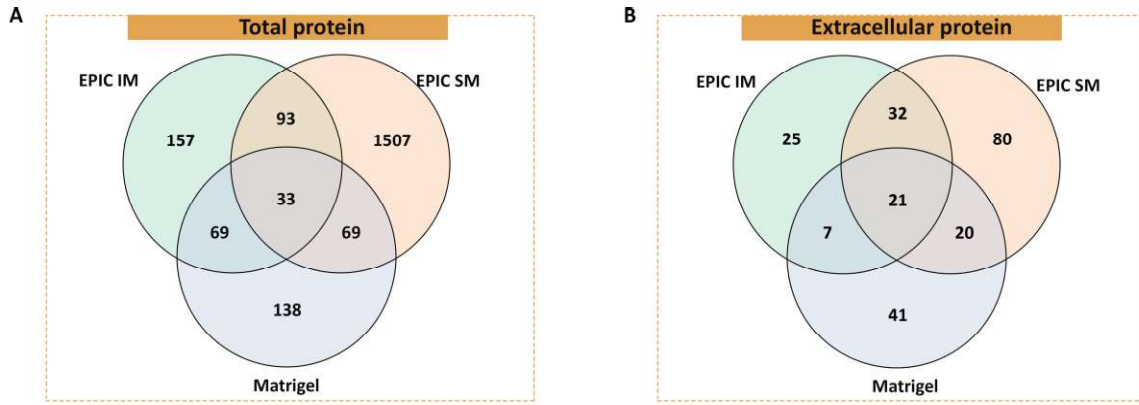


**Figure 25 - *In silico* network analysis of extracellular proteins shared between EPIC IM, EPIC SM and embryonic decellularized hearts.** A) STRING analysis of proteins shared between EPIC IM, EPIC SM and E17.5 hearts, here representing the three terms for biological processes that show the lowest FDR values; B) STRING analysis of proteins shared between EPIC IM and E17.5 hearts, here representing the two biological process terms that show the lowest FDR values; C) STRING analysis of proteins shared between EPIC SM and E17.5 hearts, here representing the three biological process terms that show the lowest FDR values.

### 3.3.3. Proteomic comparison between Matrigel and EPIC-derived extracellular matrix

In order to understand how similar may EPIC-derived ECM content be in relation to a commercially available ECM, Matrigel was analysed by label-free LC-MS/MS. Matrigel, one of the most widely used matrices for *in vitro* and *in vivo* studies, is a solubilized basement membrane extracted from murine Engelbreth-Holm-Swarm tumor (EHS). Matrigel is frequently used for cell migration, proliferation and angiogenic *in vitro* assays (Benton *et al.*, 2014).

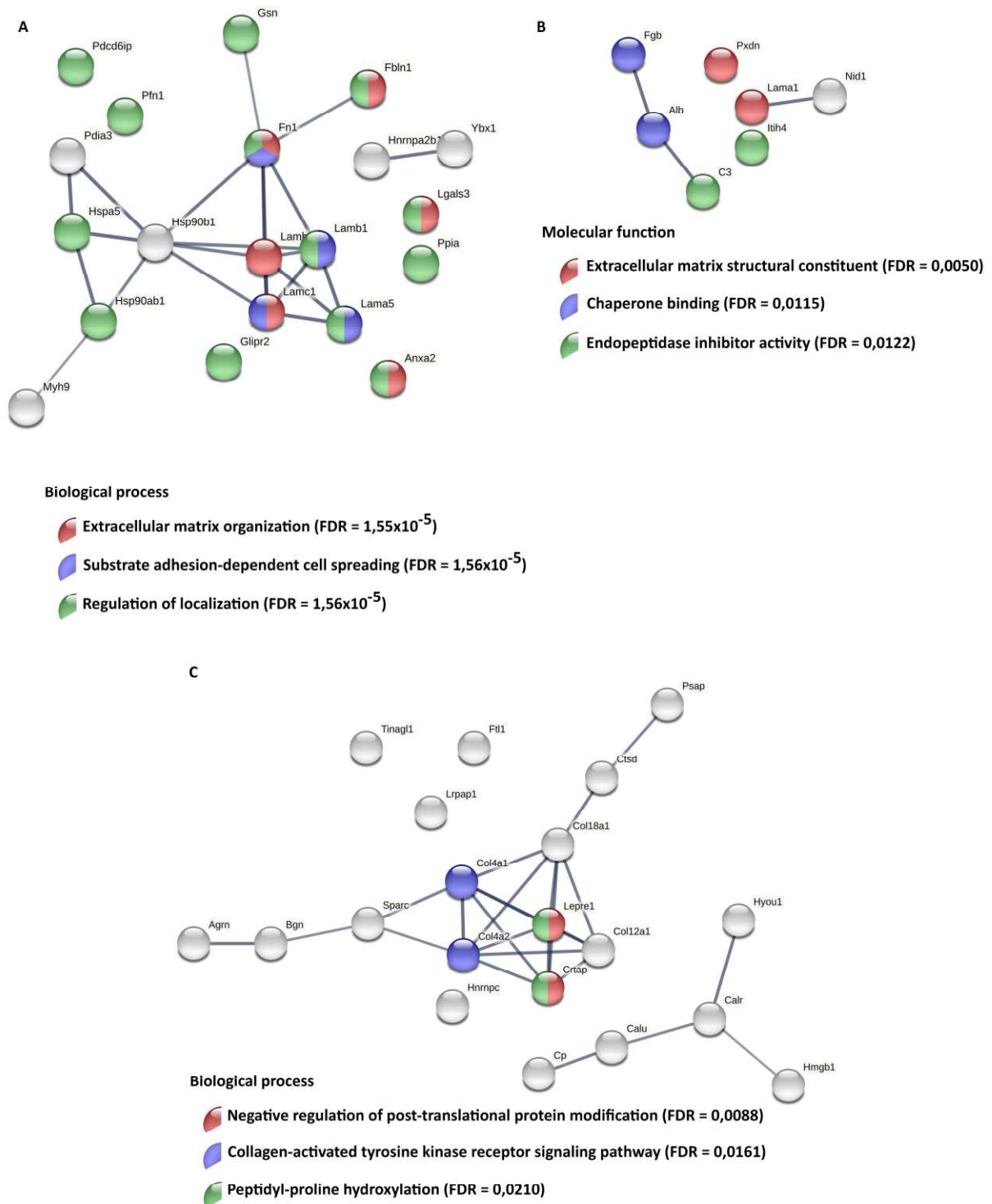
In our analysis, 314 proteins were identified in Matrigel, being 309 found in, at least, two replicates. Of them, a group of 69 proteins were found to be shared with the EPIC IM fraction, while a distinct group also containing 69 proteins were shared between Matrigel and EPIC SM. EPIC IM, SM and Matrigel had 33 proteins in common (Fig. 26A). After selecting the proteins annotated as “extracellular”, 89 proteins were found to be present in two out of the three replicates of Matrigel (Fig. 26B). Of them, 41 were unique for Matrigel, and, unexpectedly, associated to GO terms for biological processes mostly related to the negative regulation of enzymatic activity such as “negative regulation of hydrolase activity” (GO:0051346; p.adjust =  $5.74 \times 10^{-12}$  and protein ratio of 0.371), and “negative regulation of peptidase activity” (GO:0010466; p.adjust =  $9.95 \times 10^{-13}$ ) or “negative regulation of proteolysis” (GO:0045861; p.adjust =  $2.25 \times 10^{-11}$ ; Fig. 26C).



**Figure 26 – Qualitative comparison of identified proteins in label-free proteomics from EPIC IM, EPIC SM and Matrigel.** A) Venn diagram representation of total proteins in EPIC IM, EPIC SM and Matrigel. EPIC IM, EPIC SM and Matrigel contain 157, 1,507 and 138 unique proteins, respectively. EPIC IM shares 69 proteins with Matrigel, and EPIC SM shares 69 proteins with Matrigel. Thirty-three proteins are found to be in common between all samples; B) Venn diagram representation of extracellular proteins identified in EPIC IM, EPIC SM and Matrigel. EPIC IM, EPIC SM and Matrigel contain 25, 80 and 41 extracellular proteins, respectively. EPIC IM shares 7 extracellular proteins with Matrigel, and EPIC SM shares 20 extracellular proteins with Matrigel. Twenty-one proteins are shared between all samples; C) Biological processes (gene ontology analysis) of extracellular proteins from Matrigel represented in a dot plot graph. The x-axis represents the protein ratio and the dot size the number of genes associated with the functional category and the colour corresponds to the p.adjust value.

It is important to emphasize that 21 of these 89 extracellular proteins are shared between the three samples (Fig. 26B and tables A10 and A11 in the Appendix). These proteins are associated to GO terms related to extracellular functions, such as “GO:0030198 - extracellular matrix organization” (FDR of  $1.55 \times 10^{-5}$ ), “GO:0034446 - substrate adhesion-dependent cell spreading” (FDR of  $1.56 \times 10^{-5}$ ), and “GO:0032879 - regulation of localization” (FDR of  $1.56 \times 10^{-5}$ ) (Fig. 27A). In the list of proteins shared between EPIC IM and Matrigel, no biological process were assigned due to the small number of proteins uniquely found in these two conditions (only 7 proteins listed in tables A10 and A11 in the Appendix) (Fig. 27B). Finally, 20 proteins were shared between EPIC SM and Matrigel (Fig. 26B, Tables A10 and A11 in the Appendix), but these proteins showed a poor protein-protein interactions between them (Fig. 27C). Furthermore, as observed when comparing EPIC SM with E17.5 decellularized hearts, EPIC SM proteins were uniquely shared with Matrigel are not directly related to ECM-associated processes.

Taken together our results indicate that EPIC-ECM fractions present a significantly different protein composition than Matrigel.

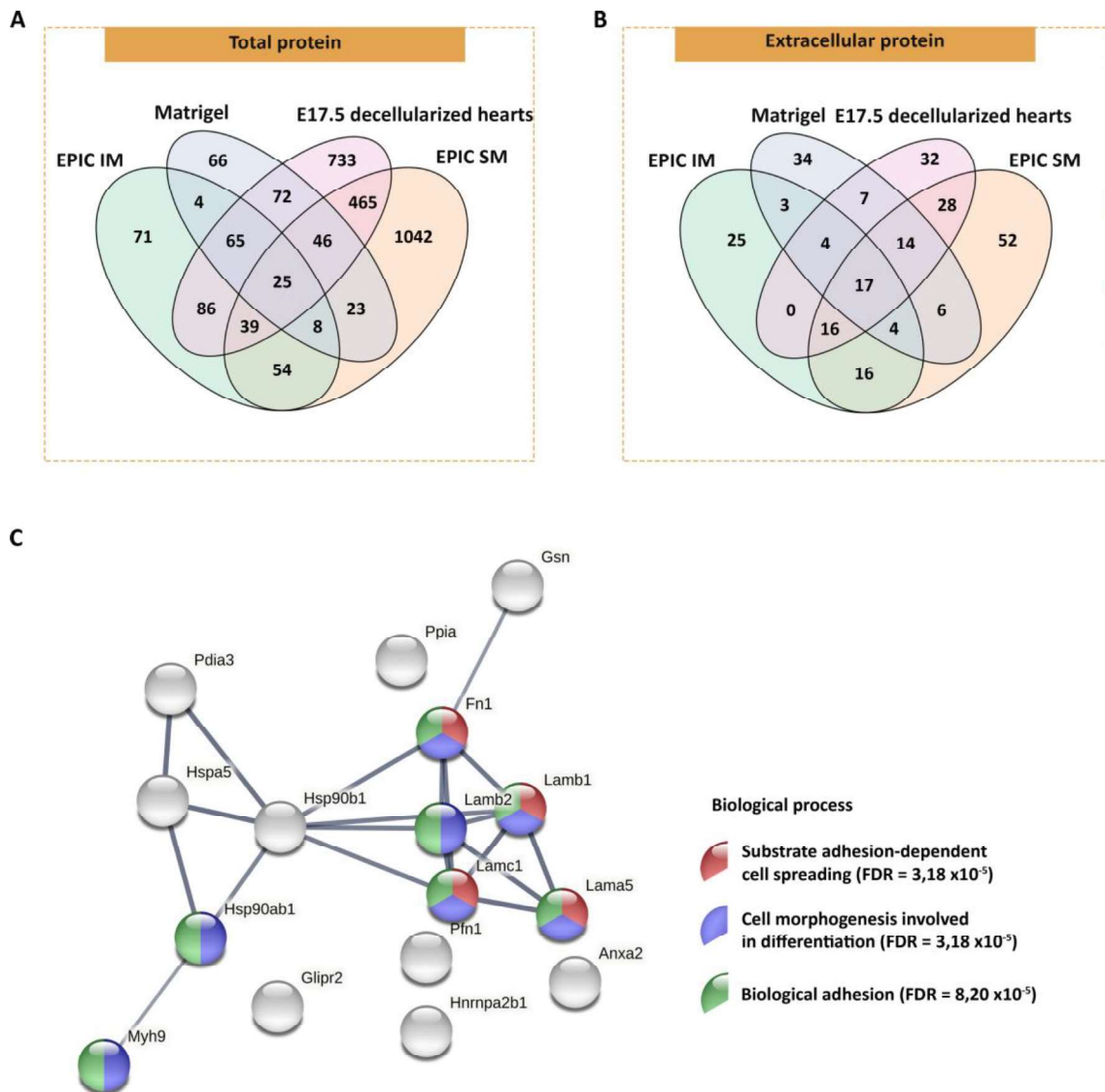


**Figure 27 - *In silico* network analysis of extracellular proteins shared between EPIC IM, EPIC SM and Matrigel.** A) STRING analysis of extracellular proteins shared between EPIC IM, EPIC SM and Matrigel, and the three biological process terms that show the lowest FDR values; B) STRING analysis of extracellular proteins shared between EPIC IM and Matrigel, and the three molecular function terms that show the lowest FDR values; C) STRING analysis of extracellular proteins shared between EPIC SM and Matrigel, and the three biological process terms that show the lowest FDR values.

### 3.4. Multicomparison of protein composition between EPIC-derived extracellular matrix, embryonic hearts and Matrigel

In order to evaluate the specificity of EPIC IM and SM fractions, a general comparison between all the datasets previously studied was performed: EPIC IM, EPIC SM, E17.5 decellularized hearts and Matrigel (Fig. 28). By analysing all groups of samples together, it was observed that E17.5 decellularized hearts shared 99 proteins with both EPIC-ECM fractions. Both fractions, however, only shared 45 proteins with Matrigel. The four studied datasets shared only 25 total proteins, of which 17 were extracellular proteins (Fig. 28A and 28B). From these, the most significant biological processes identified by our GO analysis were not directly associated to ECM-related functions but to cell attachment, flattening and differentiation, such as “substrate adhesion-dependent cell spreading” (GO:0034446; FDR of  $3.18 \times 10^{-5}$ ), “cell morphogenesis involved in differentiation” (GO:0000904; FDR of  $3.18 \times 10^{-5}$ ) and “biological adhesion” (GO:0022610; FDR of  $8.20 \times 10^{-5}$ ) (Fig. 28C).





**Figure 28 – Qualitative comparison of identified proteins in label-free proteomics from EPIC IM, EPIC SM, E17.5 decellularized hearts and Matrigel.** A) Venn diagram representation of total proteins in EPIC IM, EPIC SM E17.5 decellularized hearts and Matrigel. EPIC IM, EPIC SM, E17.5 hearts and Matrigel contain 71, 1,042, 733 and 66 unique proteins, respectively. Twenty-five proteins are found to be in common between all samples; B) Venn diagram representation of total proteins in EPIC IM, EPIC SM E17.5 decellularized hearts and Matrigel. EPIC IM, EPIC SM, E17.5 hearts and Matrigel contain 25, 52, 32 and 34 unique proteins, respectively. Seventeen proteins are found to be in common between all samples; C) STRING analysis of proteins shared between EPIC IM, EPIC SM, E17.5 hearts and Matrigel, and the three biological process terms that show the most significant FDR values.

In order to unravel the composition of each dataset, relative abundances of extracellular proteins in the total protein pool were calculated per condition (Fig. 29A). In EPIC IM, serine protease HTRA1 (HTRA1) represented 15.21% of the total abundance, followed by 5.26% of stromal cell-derived factor 1 (CXCL12), 3.36% of fibronectin (FN1), 3.01% of EMILIN-1 and 2.76% of Laminin subunit  $\alpha$ -1 (LAMA1) (Fig. 29A). On the other hand, EPIC SM was highly enriched in fibronectin, showing an abundance reaching 40.43% of the total proteins identified, followed by myosin-9 (MYH9) with 19.76%, endoplasmic reticulum chaperone protein (HSP90B1) with 2.92%, annexin A2 (ANXA2) showing 2.55% of abundance, and, finally, 78 kDa glucose-regulated protein (HSPA5) with 1.94% of abundance (Fig. 29A). For Matrigel, widely acknowledged to be a laminin-enriched ECM, three laminins are found to be on the top of protein abundances. LAMA1 presents an abundance of 33.09%, followed by laminin subunit  $\beta$ -1 (LAMB1) with 22.30% and laminin subunit  $\gamma$ -1 (LAMC1) with 19.43%. In addition, Nidogen-1 (NID1) and basement membrane-specific heparan sulfate proteoglycan core protein (HSPG2) present abundances of 14.55% and 1.62%, respectively (Fig. 29A). Regarding decellularized embryonic hearts, FN1 was the most enriched extracellular protein in the total proteins identified with 0.82%, followed by 0.61% of HSPG2, 0.28% of HSPA5, 0.27% of collagen  $\alpha$ -2(I) chain (COL1A2) and 0.23% of MYH9 (Fig. 31A). Here, it is noted that the most enriched extracellular proteins in decellularized embryonic hearts were similar to the ones described in EPIC SM, although they were found at a lower concentration.

To validate the previous results, a Western Blot for both fibronectin (220 and 94 kDa bands) and laminin (460 kDa) was performed (Fig. 29B, left). EPIC SM fraction presents the strongest band than other samples, while from E17.5 heart and Matrigel the band is visible but clearly fainter. In EPIC IM fraction, a thin band was also visible at the top of the membrane. In the case of laminin, Matrigel detained the strongest signal. EPIC SM also showed signal at the top of the membrane. In EPIC IM, EPIC lysate and E17.5 embryonic hearts, no bands were detected (Fig. 29B, right).

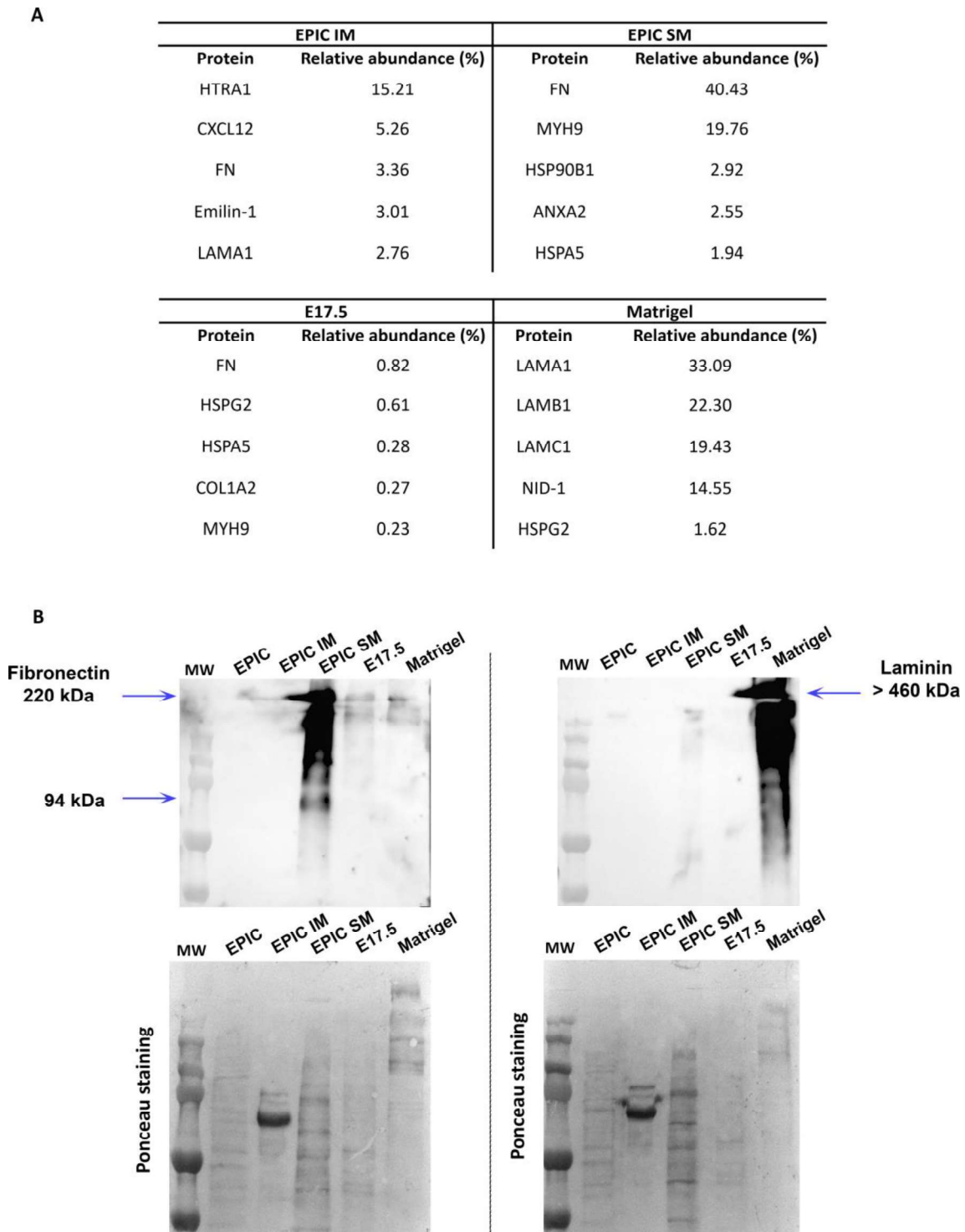


Figure 29 – Extracellular protein abundancies in EPIC IM, EPIC SM, Matrigel and E17.5 embryonic hearts.

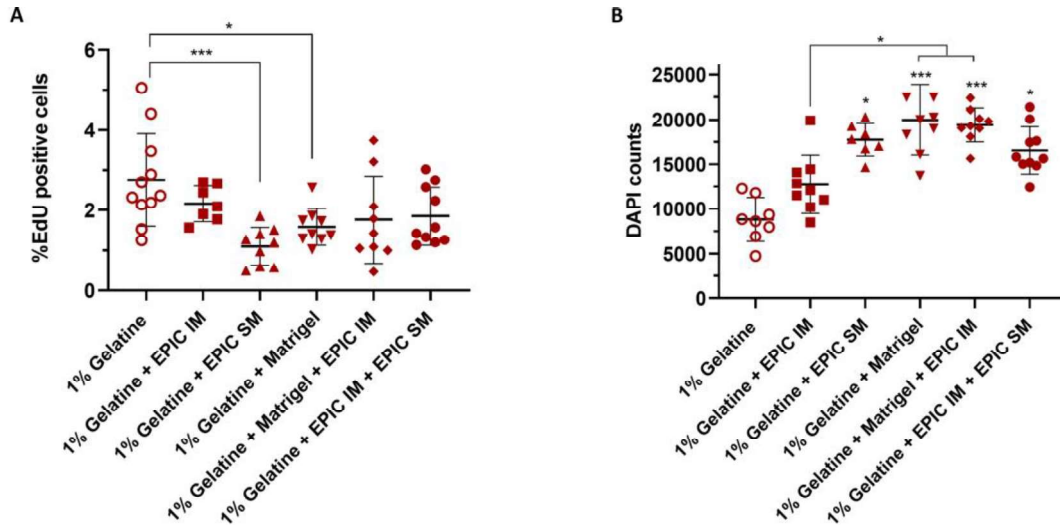
A) Relative abundances (percentages) of the top 5 extracellular proteins in the total pool of proteins identified per condition analysed; B) Western Blot of EPIC lysates, EPIC IM, EPIC SM, E17.5 hearts and Matrigel against fibronectin and laminin subunit  $\alpha 1$  and corresponding Ponceau staining to confirm presence of proteins.

### 3.5. EPIC-ECM fractions enhanced the proliferation capacity of endothelial cells

Along the proteomic study, our *in silico* data suggest that EPIC-ECM fractions have a potential role in different biological processes associated to expected functions of the extracellular matrix, such as “extracellular matrix organization” (GO:0030198) and “extracellular structure organization” (GO:0043062), together with other biological processes associated to cardiac development [“regulation of vascular development” (GO:1901342), “positive regulation of cell adhesion” (GO:0045785), “response to wounding” (GO:0009611), or “regulation of angiogenesis” (GO:0045765)] (Figure 23). Accordingly, EPIC-ECM fractions are really similar to the cardiac ECM in perinatal stages (E17.5) (Figures R3.3.2 and 3.3.2') and to the biological processes associated to the proteomic composition of the Matrigel (Figures 26 to 29). However, the analysis also showed significant differences with the Matrigel, the gold standard commercial extracellular matrix for different *in vitro* assays (Benton *et al.*, 2014).

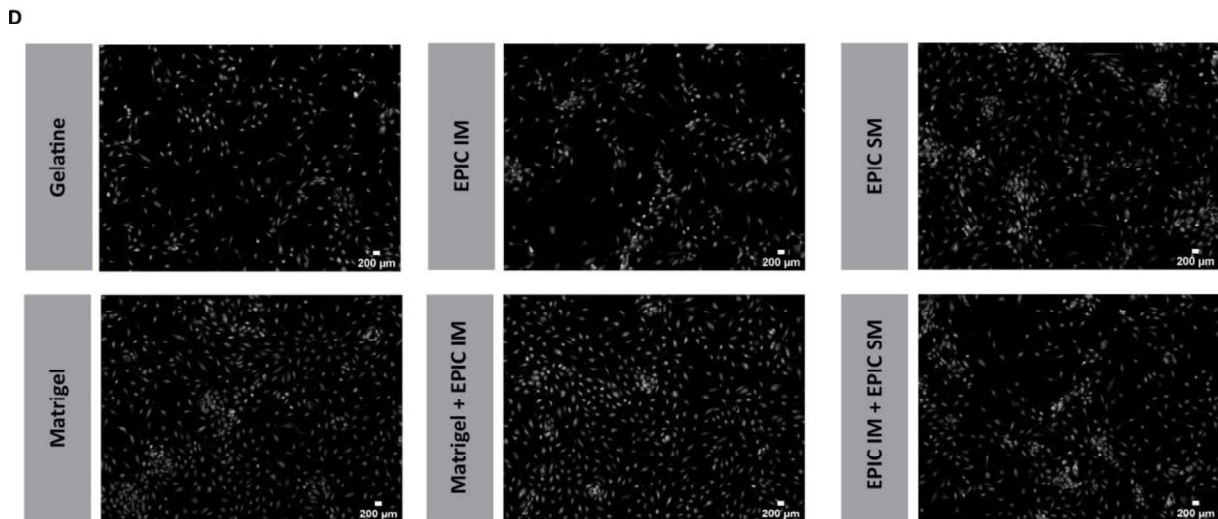
In order to experimentally confirm these differences, we performed an *in vitro* proliferation assay culturing HUVECs on wells coated with 0,1% of gelatine alone or with (1) 100 µg/mL of EPIC IM; (2) 100 µg/mL of EPIC SM; (3) 100 µg/mL of Matrigel; (4) 100 µg/mL of Matrigel plus 100 µg/mL of EPIC IM; or (5) 100 µg/mL of EPIC IM plus 100 µg/mL of EPIC SM. The cell proliferation rate, based on EdU incorporation, and the total number of cells, based on DAPI staining quantification, were measured after three (Figure 30) or five days (Figure R3.5') in culture.

After three days of incubation, proliferation rate of HUVECs cultured over gelatine only was significantly higher than in wells coated with EPIC SM or Matrigel ( $2.76 \pm 0.35\%$  vs  $1.10 \pm 0.16\%$  and  $1.59 \pm 0.15\%$ , respectively; Fig. 30A and 30C). When considering the number of nuclei, all conditions revealed a statistical increase in comparison with the control (1% gelatine) (Fig. 30A and 30C). However, the treatments that contained Matrigel showed a lower p.value. Interestingly, no statistical differences were found between conditions containing EPIC SM and the ones with Matrigel (Fig. 30A and 30C). These differences are confirmed by immunostaining (Fig. 30D).



**C**

Condition	%EdU ( $\pm$ SEM)	DAPI counts ( $\pm$ SEM)
1% Gelatine	2.76 $\pm$ 0.35	1.26 $\pm$ 0.17 $\times 10^4$
1% Gelatine + EPIC IM	2.16 $\pm$ 0.17	1.27 $\pm$ 0.11 $\times 10^4$
1% Gelatine + EPIC SM	1.10 $\pm$ 0.16	1.78 $\pm$ 0.07 $\times 10^4$
1% Gelatine + Matrigel	1.59 $\pm$ 0.15	2.00 $\pm$ 0.13 $\times 10^4$
1% Gelatine + Matrigel + EPIC IM	1.76 $\pm$ 0.36	1.94 $\pm$ 0.06 $\times 10^4$
1% Gelatine + EPIC IM + EPIC SM	1.85 $\pm$ 0.23	1.66 $\pm$ 0.08 $\times 10^4$

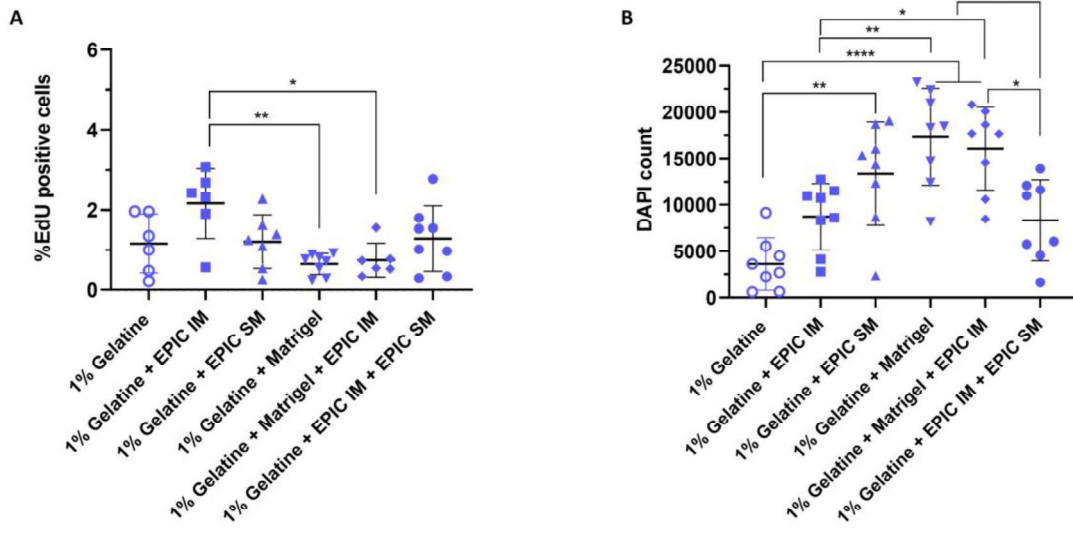


**Figure 30 – Proliferation assay of HUVECs on EPIC-derived ECM and Matrigel coated surfaces after three days incubation.** A) Percentage of EdU incorporation in HUVECs incubated for three days with 1% gelatine, 1% gelatine + 100 µg/ml of EPIC IM, 1% gelatine + 100 µg/ml of EPIC SM, 1% gelatine + 100 µg/ml Matrigel, 1% gelatine + 100 µg/ml Matrigel + 100 µg/ml of EPIC IM, or 1% gelatine + 100 µg/ml of EPIC IM + 100 µg/ml of EPIC SM (\*p < 0.05, \*\*\*p < 0.001); B) HUVECs nuclei count obtained from HUVECs incubated for three days with 1% gelatine, 1% gelatine + 100 µg/ml of EPIC IM, 1% gelatine + 100 µg/ml of EPIC SM, 1% gelatine + 100 µg/ml of Matrigel, 1% gelatine + 100 µg/ml of Matrigel + 100 µg/ml of EPIC IM, or 1% gelatine + 100 µg/ml of EPIC IM + 100 µg/ml of EPIC SM (\*p < 0.05); C) Proliferation rates and DAPI counts of HUVECs on 1% gelatine and 1% gelatine + EPIC IM + EPIC SM + Matrigel, Matrigel + EPIC IM or EPIC IM + EPIC SM coated surfaces after three days of incubation; D) Phase contrast images of HUVECs plated on surfaces coated with gelatine, gelatine with EPIC IM, gelatine + EPIC SM, gelatine + Matrigel, gelatine + EPIC IM + Matrigel, or gelatine + EPIC IM + EPIC SM, after three days incubation.

As expected, Matrigel promoted cell proliferation within the first 72 hours of culture. Interestingly, EPIC SM fraction revealed a similar capacity to stimulate the proliferation of HUVECs.

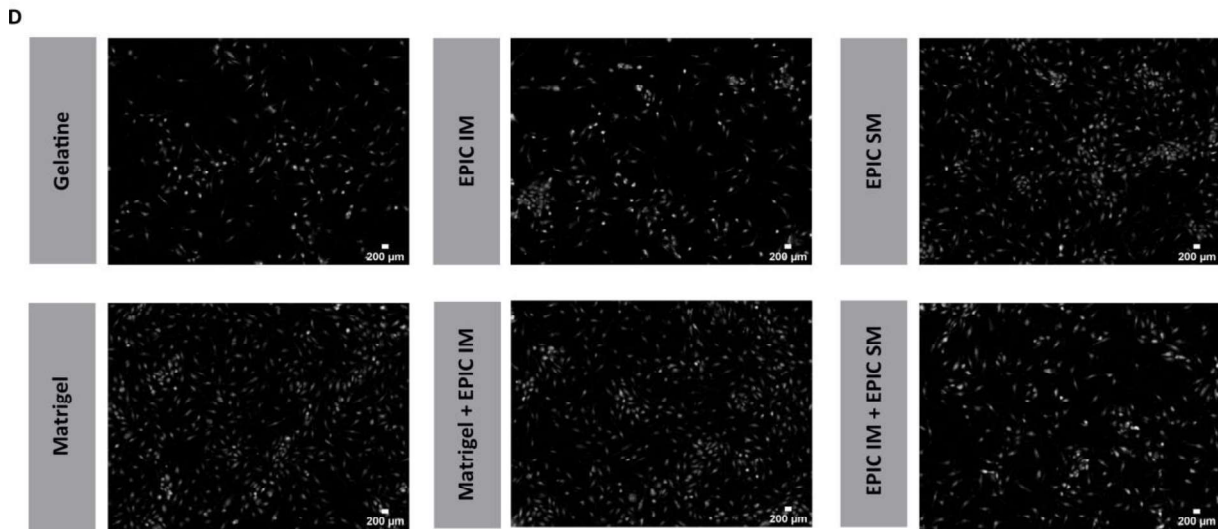
Then, the same measurements were performed after five days of incubation (Fig. 31). Both conditions in which HUVECs were plated with Matrigel ( $0.65 \pm 0.09\%$  for Matrigel and  $0.75 \pm 0.17\%$  for Matrigel together with EPIC IM) showed a lower rate of proliferation than those cultured in EPIC IM fraction ( $2.16 \pm 0.16\%$ ) (Fig. 31A). Regarding cell nuclei quantification, HUVECs cultured in 1% gelatine, EPIC IM or EPIC IM + EPIC SM showed the lowest number of cells after 5 days of culture ( $0.36 \pm 0.10 \times 10^4$ ,  $0.87 \pm 0.13 \times 10^4$  and  $0.83 \pm 0.15 \times 10^4$  HUVECs, respectively) (Fig. 31B). Again, HUVECs cultured in coated plates with Matrigel, Matrigel plus EPIC IM and EPIC SM alone revealed the major rates of proliferation also five days of incubation (Fig. 31B and 31C).

Taken together, these results described a differential role of EPIC-ECM fractions in proliferation and, potentially, in angiogenesis, confirming our *in silico* approach.



**C**

Condition	%EdU ( $\pm$ SEM)	DAPI counts ( $\pm$ SEM)
1% Gelatine	1.16 $\pm$ 0.30	0.36 $\pm$ 0.10 $\times 10^4$
1% Gelatine + EPIC IM	2.16 $\pm$ 0.36	0.87 $\pm$ 0.13 $\times 10^4$
1% Gelatine + EPIC SM	1.21 $\pm$ 0.25	1.34 $\pm$ 0.20 $\times 10^4$
1% Gelatine + Matrigel	0.65 $\pm$ 0.09	1.73 $\pm$ 0.18 $\times 10^4$
1% Gelatine + Matrigel + EPIC IM	0.75 $\pm$ 0.17	1.61 $\pm$ 0.16 $\times 10^4$
1% Gelatine + EPIC IM + EPIC SM	1.28 $\pm$ 0.29	0.83 $\pm$ 0.15 $\times 10^4$



**Figure 31 - Proliferation assay of HUVECs on EPIC-derived ECM and Matrigel coated surfaces after five days incubation.** A) Percentage of EdU incorporation in HUVECs incubated for five days with 1% gelatine, 1% gelatine + 100 µg/mL of EPIC IM, 1% gelatine + 100 µg/mL of EPIC SM, 1% gelatine + 100 µg/mL Matrigel, 1% gelatine + 100 µg/mL Matrigel + 100 µg/mL of EPIC IM, or 1% gelatine + 100 µg/mL of EPIC IM + 100 µg/mL of EPIC SM (\*p < 0.05, \*\*p < 0.01); B) HUVECs nuclei count obtained from HUVECs incubated for five days with 1% gelatine, 1% gelatine + 100 µg/mL of EPIC IM, 1% gelatine + 100 µg/mL of EPIC SM, 1% gelatine + 100 µg/mL of Matrigel, 1% gelatine + 100 µg/mL of Matrigel + 100 µg/mL of EPIC IM, or 1% gelatine + 100 µg/mL of EPIC IM + 100 µg/mL of EPIC SM (\*p < 0.05, \*\*p < 0.01, \*\*\*\*p < 0.0001); C) Proliferation rates and DAPI counts of HUVECs on 1% gelatine and 1% gelatine + EPIC IM + EPIC SM + Matrigel, Matrigel + EPIC IM or EPIC IM + EPIC SM coated surfaces after five days of incubation; D) Phase contrast images of HUVECs plated on surfaces coated with gelatine, gelatine with EPIC IM, gelatine + EPIC SM, gelatine + Matrigel, gelatine + EPIC IM + Matrigel, or gelatine + EPIC IM + EPIC SM, after five days incubation.





## DISCUSSION

---



## Discussion

---

The epicardium is the monolayered epithelium that covers the heart. This tissue has for long been regarded as a passive component of both the embryonic and adult heart whose only function was to protect the myocardial surface. However, almost three decades of discoveries in the cardiovascular developmental field have unambiguously shown that the epicardium crucially participates in heart development. At around 11.5 days of murine development, epicardial cells undergo an epithelial-to-mesenchymal transition (EMT) that transforms some epicardial epithelial cells into a group of mesenchymal cells known as epicardial-derived cells (EPDCs). These EPDCs materially contribute to the formation of various cardiac tissues and structures such as the coronary vascular system and pioneer the colonization of the cardiac interstitium, i.e. the space between the forming cardiomyocyte fibres (Ruiz-Villalba *et al.*, 2015). Several reports have demonstrated the importance of the epicardium and EPDCs in the growth and maturation of the ventricular wall. One of them includes the fate of the EPDCs, as these give origin to mural perivascular, endothelial cells and cardiac fibroblasts (CFs) (Morabito *et al.*, 2001; Pérez-Pomares, Phelps, *et al.*, 2002; Ruiz-Villalba *et al.*, 2013, 2015; Volz *et al.*, 2015; Palmquist-Gomes *et al.*, 2018; Farbehi *et al.*, 2019; Hesse, Owenier, *et al.*, 2021; Mantri *et al.*, 2021). Moreover, the epicardium and EPDCs regulate the proliferation of the compact myocardium through a non-cell autonomous mechanism that is still to be fully deciphered. In accordance with this latter finding, the depletion of key epicardial genes (e.g., *Wt1*, *Tbx18*, *Tcf21*) lead to severe defects not only in the epicardium and coronary blood vessels, but also results in severe ventricular myocardial hypoplasia leading to midgestational death (Kwee *et al.*, 1995; Yang *et al.*, 1995; Pérez-Pomares, Phelps, *et al.*, 2002; Lavine *et al.*, 2005; Acharya *et al.*, 2012). All these findings prompted us to study in more detail two key elements of the epicardial secretome, the extracellular matrix and the extracellular vesicle fraction, which we hypothesized to be relevant to the regulation of several aspects of cardiac biology.

Cardiac interstitial EPDCs persist until adulthood and have been reported to play an important role in cardiac response to pathological conditions (Pogontke *et al.*, 2019).

The adult epicardium is generally dormant in the healthy heart, but re-activates when a cardiac damage takes place, contributing to cardiac reparative responses to injury through the activation of embryonic transcriptional and signalling programs (Zhou *et al.*, 2011; van Wijk *et al.*, 2012; Bollini *et al.*, 2014; Farbehi *et al.*, 2019; Hesse, Owenier, *et al.*, 2021). For example, epicardial-derived CFs play a crucial role in the ventricular remodelling process after induction of cardiac injury (Moore-Morris *et al.*, 2014; Ruiz-Villalba *et al.*, 2015).

EMT has been claimed to be one of the main developmental mechanisms recapitulated in cardiac adult response to damage, but the real number of EPDCs generated *de novo* after cardiac injury is small (van Wijk *et al.*, 2012; Farbehi *et al.*, 2019), what suggests that the relevance of epicardial reactivation in cardiac reparative responses is rather mediated by its secretome. In detail, this hypothesis is based in the essential role known to be played by the epicardium and EPDC secretome during cardiac development (Lavine *et al.*, 2005, 2006; Lavine and Ornitz, 2008; Del Monte *et al.*, 2011; Zhou *et al.*, 2011). This signaling network is thought to be essentially paracrine in nature. For instance, both cardiac fibroblast growth factor (FGF) and Notch signalling participate EMT activation, EPDC migration and coronary vascular development (Lavine *et al.*, 2006; Del Monte *et al.*, 2011). WT1, master epicardial transcriptional regulator, is also involved in the progression of epicardial EMT and EPDC differentiation through the stimulation of the Wnt/ $\beta$ -catenin pathway and the control of cardiac retinoic acid signalling (Guadix *et al.*, 2011; von Gise *et al.*, 2011). These findings strongly rely on the analysis of *Wt1*-null mouse phenotype, including defective coronary vessel development and impaired cardiomyocyte proliferation (Guadix *et al.*, 2011; von Gise *et al.*, 2011). Together, these studies have consolidated the idea of epicardial-myocardial crosstalk as a necessary developmental mechanism guaranteeing the formation of a proper cardiac structure and efficient heart function.

As it can be inferred from the previous discussion, a systematic and detailed analysis of epicardial signalling mechanisms is still missing. In particular, very little information is available on the role played by extracellular vesicles (EVs) or extracellular matrix (ECM) molecules in these epicardial secretome-dependent mechanisms. Regarding epicardial-derived EVs, only one very recent report describes EVs secreted by primary epicardial cells and continuous (immortalized) epicardial cell line (del Campo *et*

*al.*, 2021). In this study, a murine epicardial cell line (Austin *et al.*, 2008) and primary cultures of human EPDCs isolated from right atrial appendages were used to isolate EVs by ultracentrifugation (UC). Results from this work, however, are likely to represent only part of the epicardial-EPDC secretome, since many epicardial cell lines only mesenchymalize after TGF $\beta$ 1 and  $\beta$ 2 treatment (Austin *et al.*, 2008; Ruiz-Villalba *et al.*, 2013). This is not the case of the EPIC epicardial cell line used in this thesis, whose standard phenotype is basically mesenchymal. Furthermore, del Campo and colleagues focussed on the microRNA profiling of epicardial-like EVs without considering their protein cargo, except for the standard CD63 immunogold labelling of epicardial cell line-derived EVs (del Campo *et al.*, 2021).

In what concerns the epicardial ECM during cardiac development, a crucial moment involves the activation of mesenchymal gene expression during epicardial EMT, which is necessary for ECM remodelling and cell migration. In the developing heart we find representatives of all classes of ECM proteins, including hyaluronan, proteoglycans, collagens, elastin, fibrillin, tenascin, fibronectins, and laminins. The importance of these components have been demonstrated by genetic linkage to cardiac malformations (Camenisch *et al.*, 2000; Costell *et al.*, 2002; Kern *et al.*, 2010). For instance, some cardiac defects are known to be regulated via Notch signalling pathway (Grego-Bessa *et al.*, 2007; Zhao *et al.*, 2014; D'Amato *et al.*, 2016), which affect the expression of ECM proteases, such as A disintegrin and metalloproteinase with thrombospondin motifs 1 (*Adamts1*), matrix metalloproteinase-2 (*Mmp2*) and hyaluronidase-2 (*Hyal2*) (del Monte-Nieto *et al.*, 2018). In addition to that, embryonic cardiac ECM from E18-E19 (Williams *et al.*, 2014) as well as matricellular components secreted by embryonic CFs (fibronectin, tenascin and hyaluran) (Ieda *et al.*, 2009) were previously demonstrated to induce cardiomyocyte proliferation (Ieda *et al.*, 2009). Nevertheless, almost all available studies on this topic have used a limited panel of antibodies for the immunohistochemical identification of extracellular molecules in the vicinity of epicardial cells (e.g. the subepicardial space).

In summary, the composition of the epicardial secretome and the regulatory mechanisms that regulate its dynamics are not clear yet. This lack of information is mostly related to technical issues, such as limitations in tracing the origin of the secretome and the high number of cells required for studying epicardial-derived components. To circumvent this limitation, we took advantage of the EPIC embryonic epicardial-derived

immortal cell, developed in our laboratory from E11.5 murine primary epicardial explants (Ruiz-Villalba *et al.*, 2013). This cell line retains the ability to differentiate into various cardiovascular cell types, especially those related to the cardiac interstitium (epicardial-derived cardiac fibroblasts and smooth muscle cells). Moreover, EPIC display the activation of a complex proteolytic program *in vitro* (including molecules such as *Adam15*, *17* and *19*, *Mmp11* and *14*, and *Timp1* and *3*), that has been hypothesized to result from the interaction of the characteristic proteolytic properties of various EPIC subpopulations. This unique characteristic make of EPIC an excellent model to study epicardial-derived cell secretome (Ruiz-Villalba *et al.*, 2013).

### 1.1. Extracellular vesicles isolated by ultracentrifugation are better preserved than by size exclusion chromatography

The use of the EPIC cell line allowed us to scale-up EPDC culture for continuous EV harvesting and isolation of significant amounts of epicardial-derived ECM. However, this approach requires a strong effort in the optimization of the protocols to obtain reproducible and reliable results that can be translated into the *in vivo* context. These technical aspects have been studied, most especially for the isolation of EVs (Royo *et al.*, 2016). Indeed, the International Society of Extracellular Vesicles (ISEV) has established guidelines that represent the current state-of-art in EV isolation and characterization, listing the minimal technical requirements to standardize these procedures (Théry *et al.*, 2018).

The critical analysis of our data reveals significant differences in stability, particle size distribution and protein quantity between EVs isolated using two standard methods: UC and size exclusion chromatography (SEC) (Fig. R1.1, R1.2.1 and R1.2.2). EVs isolated via UC (EVs-UC) conserved vesicle integrity and enriched in small and medium-sized EVs. To allow for a robust physical characterization, we first compared DLS and NTA measurements of EPI-EVs from UC and SEC isolations. Particle sizes revealed by DLS presented a higher variability than those measured by NTA. Thus we have concluded that NTA evaluation of EVs sizes is the more consistent one, as the sizes of EPIC-derived EVs were very similar among biological replicates. Moreover, we have concluded that NTA is capable of resolving and quantifying particles of different sizes, being more reliable for the analysis of polydisperse solutions than DLS (Filipe *et al.*, 2010). As compared with other EVs isolated from other EPDCs culture, our EPIC-EVs sizes were larger (del Campo *et al.*, 2021). However, the UC isolation methodology that Villa del Campo and colleagues employed has differences from ours (isolated by ultracentrifugation without 10,000 g centrifugation step), which could have influenced resulting EVs sizes (del Campo *et al.*, 2021).

An important step in the characterization of small EVs-enriched solutions is the detection of proteins related to their biogenesis. Positive markers of EVs subtypes are associated to their specific subcellular trafficking. Therefore, transmembrane or glycosylphosphatidylinositol (GPI)-anchored proteins associated to plasma membrane,



cytosolic proteins (proteins of ESCRT-I/II/III complexes such as TSG101) and related proteins such as ALIX; flotillins-1 and 2, or annexins, among others) are all of great relevance in EV characterization (Théry *et al.*, 2018). When considering ALIX cargo in EVs-SEC and EVs-UC, EVs-UC seem to be more enriched in this endosomal sorting complexes required for transport (ESCRT)-related protein. Regarding TSG101, EVs-UC show a stronger TSG101 expression, while in EVs-SEC this protein was undetectable. Thus, only from EVs-UC it was possible to recover EV samples expressing both TSG101 and ALIX, while ALIX-containing EVs were mostly collected after SEC isolation. These results, which are in accordance with our NTA analysis, indicate that UC isolation returns higher small/medium EVs enrichment as compared to SEC isolation methods.

Next, we proceeded with protein assessment in EVs from both enrichment methods (UC and SEC) (Théry *et al.*, 2018; Takov *et al.*, 2019; Tian *et al.*, 2019; Brennan *et al.*, 2020). In this regard, our EVs-SEC samples yield a higher protein concentration (1.6 times more) than EVs-UC samples. When normalized to the number of particles in the solution, EVs-SEC samples showed 1.5 times more particles than EVs-UC ones. This result is in conflict with a previous study in which EVs isolated via UC showed higher protein content than EVs isolated by SEC (Nordin *et al.*, 2015). However, and as reported before, SEC isolation may co-isolate components present in FBS and other secreted cellular components and contaminants at a higher enrichment rate than UC, which thus remains a highly recommended method for EV isolation (Takov *et al.*, 2019; Tian *et al.*, 2019; Brennan *et al.*, 2020).

In contrast to results derived from SEC isolation, UC is frequently regarded as an EV isolation method more prone to EV disruption, fusion or aggregation, especially when compared to protocols based on ultrafiltration (UF) followed by SEC isolation (Nordin *et al.*, 2015). A possible reason for some of the differential characteristics of the particulates and protein concentration observed between these two methods could relate to the physical force used during the ultrafiltration (UF) steps that precede SEC isolation (Konoshenko *et al.*, 2018). Furthermore, due to the interaction between vesicles and the UF membrane, particles may aggregate more frequently and block the membrane pores, leading to low EV enrichment (Sidhom *et al.*, 2020). On the other hand, it is important to consider that our EVs-SEC were frozen and stored at Imperial College London and then transported to Málaga. This storage could have affected the stability of our EV-SEC

samples. By comparing our data from EPIC EVs-UC with other epicardial-derived EVs, TEM imaging reveals particulate artifacts in these samples that are not present in our EVs-UC samples.

The final part of our analysis of EV isolation methods indicates that EPIC-EVs isolated by UC method display more small/medium-EVs size ranges (from 76 to 210 nm) and particles per million of EPIC as compared to the samples from the SEC isolation method.

In summary, EVs size and concentration analysis did not show highly significant differences between both isolation methods. Nevertheless, UC outperformed SEC in the isolation of EPIC-derived EVs with respect to the structural stability and EVs sample enrichment. This is relevant because equipments for ultracentrifugation are readily available in many laboratories, so that the cost for EVs isolation can be minimized by routinely avoiding SEC. Altogether, our results strongly suggest that the UC method is quantitatively and qualitatively advantageous for downstream analysis of EVs, as reported by previous studies (Takov *et al.*, 2019; Tian *et al.*, 2019; Brennan *et al.*, 2020).

## 1.2. Hypoxia did not affect the physical properties of epicardial-derived extracellular vesicles

Hypoxia has a relevant role in the biology of epicardial cells and EPDCs in both embryonic development (Ream *et al.*, 2008; Bock-Marquette *et al.*, 2009; Diman *et al.*, 2014) and adulthood (Hesse, Groterath, *et al.*, 2021; Hesse, Owenier, *et al.*, 2021). Furthermore, cell preconditioning to hypoxia is known to result in EVs that significantly improve cardiac performance after injury as compared to EVs isolated from cells cultured in normoxia. For instance, cardiac progenitor cell (CPC)-derived EVs isolated from cells submitted to hypoxia, as compared to those isolated from normoxic conditions, can induce angiogenesis and reduce the fibrotic response in infarcted rats (Gray *et al.*, 2015). Bone marrow mesenchymal stem cell (BM-MSC)-derived EVs isolated from preconditioned cells (0.5 or 1% O<sub>2</sub>) also exerted important therapeutic effects in infarcted mice and rats (Zhu *et al.*, 2018; Zhu *et al.*, 2018; Zhang *et al.*, 2019). For this reason, one of the main objectives of this thesis was to evaluate the proteomic content of EVs isolated from cells submitted to hypoxia (5%-O<sub>2</sub>).

In a first series of experiments, EPIC cultured at 5% O<sub>2</sub> (EVs-H5%) were considered. Hypoxia did not affect particle stability or protein yield, although a significant increase in medium-sized EVs (166 and 210 nm) as compared to EVs-derived from normoxic EPIC cultures (EVs-N) was observed (Figures 9 and 10). These results are similar to those reported for human renal tubular epithelial cells (1% O<sub>2</sub>) indicating an increase in EV size as compared to those isolated from cells cultured in normoxia (L. Zhang *et al.*, 2019). We also found that protein concentration in EVs cultured under hypoxia and normoxia was not significantly altered. EVs-H5%, however, present slightly lower protein concentration than EVs-N, whereas the protein quantity per particle was found to be similar between EVs-N and EVs-H5% (Fig. 11). Other studies could not record any difference in particle concentration from iPSCs-derived EVs of cultured under hypoxia (1% and 5% O<sub>2</sub>) when compared with their normoxic controls (Andrade *et al.*, 2021). Another important finding was that EVs-H5% showed a trend to increase the amount of ALIX protein, while TSG101 appears to be equally present in EVs-N and EVs-H5%. These results corroborated the EVs secretion pattern previously described for other cell types (Liu *et al.*, 2018; Kenneweg *et al.*, 2019; L. Zhang *et al.*, 2019; Andrade *et al.*, 2021). Taken together, all these data seem

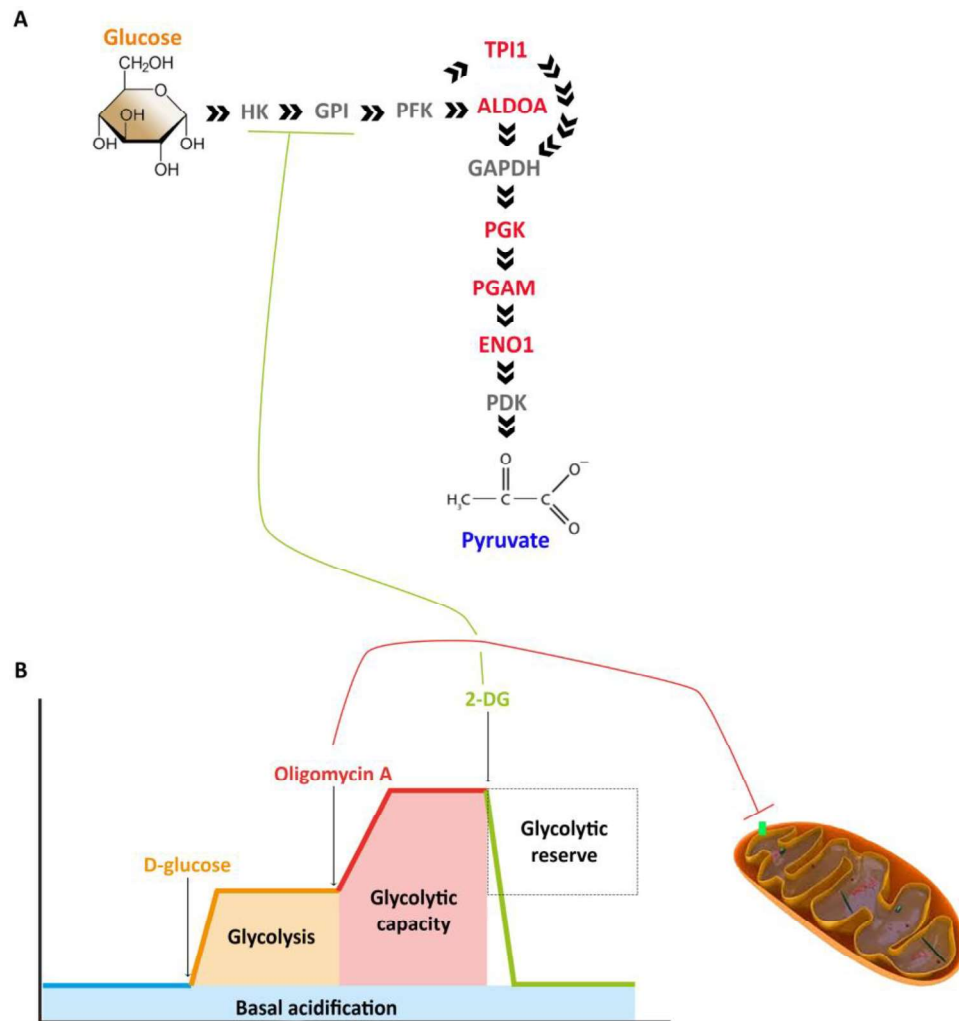
to indicate that EPIC cells could have a mechanism of resistance to hypoxia that prevents these cells from marked changes in the composition of their EV secretome. This hypothesis, however, needs further support and we thus did carry out a proteomic characterization of our EVs to determine potential changes in their cargo related to hypoxic preconditioning.

### 1.3. Extracellular vesicles isolated from epicardial cells submitted to hypoxia are enriched in proteins associated with glycolysis/gluconeogenesis

In order to scrutinize the proteomic profile of EVs-N and EVs-H5%, a multiplexing method (known as Tandem Mass Tagging or TMT), was applied. This method, based on an isobaric protein tagging strategy, allows for the simultaneous analysis of multiple samples in a single mass spectrometry run, and reduces technical variability in the results found in label-free proteomic studies (Thompson *et al.*, 2003). In this thesis, TMT2plex and TMT6plex were compared to select the most reproducible assay regarding protein identification and statistical power. Of these methods, TMT6plex analysis is known to result a higher number of identified proteins and minor mismatch occurrences as compared to TMT2plex (Fig. 12). This finding is supported by a previous report in which it was suggested that differences observed between samples derived from the tagging specificity in TMT2plex replicates and technical variability (Storey *et al.*, 2020). Thus, due to the higher statistical power and lower variability of TMT6plex as compared with TMT2plex, further analysis on EVs proteomics was carried out from TMT6plex dataset.

To identify differentially abundant proteins in EVs-N and EVs-H5%, we considered the proteins that presented abundance differences with p-values below 0.05. The analysis revealed that EVs-H5% show an increase in proteins associated to biological processes related to the activation of the glycolysis/gluconeogenesis signalling pathway (Fig. 14B), such a phosphoglycerate kinase 1 (PGK1), pyruvate kinase (PKM), phosphoglycerate mutase (PGAM) and triosephosphate isomerase (TPI1). Of them, PGK1 and PKM, which are the only ATP-generating enzymes in glycolysis, are among the most enriched proteins in EVs-H5% (Fig. 14B). PGK1 catalyses the reversible reaction of 1,3-diphosphoglycerate and ADP to 3-phosphoglycerate and ATP (Thomson *et al.*, 2019), while PKM converts phosphoenolpyruvate and ADP to pyruvate (Li *et al.*, 2016). Therefore, both enzymes play a key role in glycolytic metabolism (Fig. 32A). PGAM is also found in the enriched portion of proteins identified in EVs-H5%. This enzyme converts 3-phosphoglycerate into 2-phosphoglycerate; PGAM has two isoforms that share about 79% of their sequence, PGAM1 and PGAM2 (Mikawa *et al.*, 2020). This detail explains the ambiguous PGAM identification in our dataset (Fig. 14B). Finally, TPI1, responsible to convert dihydroxyacetone phosphate into glyceraldehyde-3-phosphate and necessary for

glycolysis completion, was also found in our analysis. Activation of TPI1 was shown to direct cells to glycolytic pathway, while its inhibition guides dihydroxyacetone phosphate into pentose phosphate pathway (PPP) (Lincet and Icard, 2015).



**Figure 32 – Glycolytic enzymes and glycolysis assay.** A) Schematic representation of enzymes involved in glycolysis. Of them, the ones that are present in EPIC-EVs are highlighted in red; B) Conceptual representation of the Seahorse assay. Measurement parameters in Glycolysis stress assay, from where basal acidification, glycolysis, glycolytic capacity and glycolytic reserve calculations were taken based on their graph area, as well as pathway inhibitors (Oligomycin A and 2-DG).

Most interestingly, all the proteins listed above are known to be transcriptionally activated by HIF-1 $\alpha$ , a key regulator of tissue responses to hypoxia (Hamaguchi *et al.*, 2008). In accordance to this finding, glycolytic transcriptional activation in the epicardium and subepicardium may relate with its embryonic status as a cardiac hypoxic niche (Kocabas *et al.*, 2012). In this work, Kocabas and colleagues isolated adult cardiac cells with the lowest amount of mitochondrial content and named them “glycolysis cardiac progenitor cells”. It turned out that these cells presented expression of proteins typically found in embryonic epicardial cells (GATA4, WT1, and Tbx18) and demonstrated to have higher HIF-1 $\alpha$  expression and higher cell viability under hypoxia than CFs. The authors concluded that these cells mostly rely on glycolysis to meet their energetic demands (Kocabas *et al.*, 2012).

Our study also identified an accumulation of monocarboxylate transporter (MCT4) in EVs-H5%. MCT4 is one of the four lactic acid transporters known, and it is localized in the cell membrane. The MCT family facilitates the transportation of short chain carbohydrates (pyruvate and lactate, for instance), thus sustaining the glycolytic pathway. It is interesting to note that *Mct4* upregulation is also mediated by HIF-1 $\alpha$  (Ullah *et al.*, 2006). Although not enriched in EVs-H5%, our proteomic study also identified the glycoprotein basigin (BSG) in EPIC-EVs. This protein is required for MCT4 trafficking and proper incorporation into the plasma membrane (Parks *et al.*, 2013).

Altogether, these results strongly argue in favour of epicardial-derived EV-based signalling as a significant mechanism for cell-to-cell communication. This mechanism could be used by epicardium and epicardial-derived cells to induce some sort of preconditioning in the target cells therefore modulating their glycolytic metabolism under hypoxia. This might be a relevant mechanism to modulate the cellular environment in response to an ischemic event in the adult (Pang *et al.*, 2018) and even during embryonic development (Yang *et al.*, 2021).

Besides EVs-H5% enrichment in glycolytic proteins, calcium-binding protein S100A6 was also found to be enriched in hypoxic-derived EVs. S100A6 overexpression was previously described to improve cardiac function and reduce the infarct area in a murine model of myocardial ischemia/reperfusion (Mofid *et al.*, 2017). Relevant to this discussion, polyadenylate-binding protein 1 (PABP1) is also found to be enriched in EVs-H5%. In accordance to our results, expression of PABP1 was described to be lower in adult



murine hearts as compared to hearts at E17.5 (Chorghade *et al.*, 2017). PABP1 expression was shown to be notably increased in a cardiac hypertrophy experimental mouse model (Chorghade *et al.*, 2017) and in hypoxic cultures of a glioma cell line (Baghbani *et al.*, 2013). Regarding proteins enriched EVs-N, we verified a poor grouping correlation among these proteins, resulting in their lack of significance.

In this thesis we have demonstrated that hypoxic stress conditioning of epicardial cells may alter the secretory profile of these cells, so that their secretome becomes enriched in glycolytic proteins as compared to EVs-N. This finding is similar to those reported by other studies in different biological contexts such as cancer (Wei *et al.*, 2016; Walbrecq, Margue, *et al.*, 2020; Hayasaka *et al.*, 2021) or liver fibrosis (Wan *et al.*, 2019).

#### 1.4. Epicardial-derived cells promote proliferation and a glycolytic metabolism through extracellular vesicles in both autocrine and paracrine manner

It is widely accepted that cells can use EVs to exert a physiological effect on both close and distant cells. This cellular behaviour is likely to result from the adaptation to significant changes in the surrounding milieu. Therefore, it is reasonable to hypothesize that physiological changes in a parental cell will also alter the molecular content of its secreted EVs (Poe and Knowlton, 2017). In this regard, studies are commonly carried out to investigate the specific function of paracrine signalling mechanisms involving EVs. Important to this discussion, it has been suggested that around 70% of ligands secreted by a human cell can be recognized by 60% of its own receptors. This finding argues in favour of the idea that autocrine signalling could be as widespread and biologically relevant as paracrine signalling (Ramilowski et al., 2015). In fact, epicardial-derived EVs were recently demonstrated to be uptaken by cardiomyocytes (CM) and to induce CM proliferation *in vitro* and in infarcted neonatal mice *in vivo*, as well as to increase  $\alpha$ -SMA expression in CFs in the context of an engineered human myocardium model (del Campo et al., 2021).

Our results show that EPIC-EVs were internalized by both EPIC and HUVEC cells (Figures 15C and 17, respectively). This finding confirms that the species of origin of EVs does not preclude their uptake by different cells. Previous reports have shown the interspecies crosstalk mediated by EVs is possible. Indeed, *in vitro*, murine EVs were shown to be uptaken in human mast cells, and functional mouse derived-exosomal mRNA was translated in human recipient cells (Valadi et al., 2007). *In vivo*, EVs from human cardiosphere derived cells (CDC) have ameliorated the hearts in pig I/R models by reducing its infarct size, the fibrotic mass, and the inflammatory response (De Couto et al., 2017; Gallet et al., 2017). Finally, human umbilical cord MSC-derived EVs have been reported to improve cardiac function and cardiomyocyte survival in a rat model of LAD surgery (Wang et al., 2018). However, our technical approach does not allow us to identify whether EVs are being uptaken individually or as small clusters because the diffraction limit of microscope objectives, which only reach a minimal resolution of 200 nm. Thus, smaller particles can be fluorescently detected, but these may either be smaller than 200 nm (Lai et al., 2015) or be a cluster of small EVs (Ter-Ovanesyan et al., 2017;

Théry et al., 2018). However, the co-localization of EVs in endosomes or lysosomes confirm EVs uptake by endocytosis is effective in our cultures (Fitzner et al., 2011; Joshi et al., 2020).

Although we showed that EPIC-EVs are internalized by other cells, EPIC-EVs did not show a significant enhancement of cell proliferation or glycolysis in any of the cell types used in our experiments (EPIC and HUVEC) after EPIC EV treatment (Figures 16A-B and 18A-B, respectively). As cell proliferation and glycolysis tend to be closely associated (M. Li et al., 2019; Dumas, García-Caballero and Carmeliet, 2020), these results can be explained by: (1) the presence of other molecules in EPIC-EVs that affect EPIC and HUVECs metabolism; (2) the starvation period being too short to induce meaningful effects on target cells metabolism; or (3) the relative quantity of glycolytic proteins from EVs-H5% in relation to the tested cells not being sufficient to induce a high glycolytic activities. Nevertheless, incubation of HUVECs with 50 µg/mL of EVs-H5% was the only condition that did not present a significant difference against HUVECs at optimal conditions. This observation could suggest that EVs-H5% may improve the proliferative capacity of endothelial cells.

Our results are in contrast to those from a study focused on carbonic anhydrase 9 cellular expression and loading in EVs; this molecule was found to be increased in renal cancer cell lines cultured under hypoxia, conferring a higher angiogenic potential to HUVECs than EVs from normoxic cultures (Horie *et al.*, 2017). Considering that, we decided to evaluate whether inducing a higher hypoxic condition to EPIC would result in a higher glycolytic role of EPIC-derived EVs. In order to do so, we evaluated the effect of EVs-H1% on EPIC and HUVECs proliferation and glycolysis. Interestingly, EVs-H1% significantly enhanced EPIC proliferative rate, although this increase was not reflected in their glycolytic response (Fig. 19A, C, E and G). The lack of autocrine response to hypoxic-derived EVs when glycolysis was imposed could result from an innately active glycolytic metabolism. In accordance with the Kocabas and colleagues work discussed above, epicardial-like cells presented lower mitochondrial content (Kocabas et al., 2012). If this finding is extrapolated to EPIC, it would be possible that these cells rely almost exclusively on glycolysis. In turn, this would mean that epicardial cells could be highly equipped to respond to special energetic demands, so that an excessive quantity on glycolytic proteins may not affect EPIC behaviour. Accordingly, an aerobic environment as that of normoxic

cell cultures, may increase EPIC reliance to mitochondrial oxidative phosphorylation and diminish their capacity to respond to a glycolytic shift. In contrast, and although the co-localization of EVs in endosomes or lysosomes confirm EVs uptake by endocytosis (Fitzner et al., 2011; Joshi et al., 2020), some dyed EVs seem to co-localize with the acidic lysotracker dye, a finding that could indicate that lysosomal degradation could be taken place.

Our results reveal a trend in the increase of HUVECs proliferative responses in the experimental treatments. EVs-H1% tend to enhance HUVEC glycolytic capacity as compared to EVs-H5% and EVs-N (Fig. 19B, D, F and H). This indicates that EVs-H1% might capacitate these cells to respond to a higher ATP demand. Taking this finding into account, we suggest that EVs-H1% promote greater glycolytic capacity to HUVECs when the switch to glycolytic metabolism is forced. These results are supported by a recent study from Yetkin-Arik and colleagues, describing differences between angiogenic tip and non-tip endothelial cells in terms of energetic demands required for their proliferation capacity (Yetkin-Arik *et al.*, 2019). In this study, the authors suggest that non-tip cells rely on mitochondrial respiration for proliferation, but that their basal energetic demand depends mainly on glycolysis. When glycolysis was induced, it was shown that differentiation to tip cells seemed to be stimulated. Such effect would then induce higher differentiation into tip-like cells, which are less proliferative than stalk cells.

Although no proteomic studies were assessed in this thesis for EVs-H1%, we hypothesize that lowering oxygen levels to 1% might increase the levels of aerobic glycolysis in EPIC, thus making them to modulate their EV secretome towards a pro-glycolytic one and strengthen its effect on endothelial cells in a paracrine manner. Similarly, it was recently shown that iPSCs-derived EVs from 1% O<sub>2</sub> cultures induced angiogenesis at higher rates than EVs obtained from 5% O<sub>2</sub> or normoxic cultures (Andrade et al., 2021). However, a deeper molecular characterization of EPIC-EVs is needed to identify other signalling molecules that might shed light on the interpretation of our data.

In summary, the first part of this PhD thesis demonstrates that conditioning EPDCs by restricting oxygen availability in culture affects the EV secretory profile of these cells, so that they secrete more medium-sized EVs enriched in glycolytic proteins. Moreover, increasing levels of hypoxia also results in changes in the ability of EVs to promote cell proliferation in their parental cells and glycolytic function, in endothelial cells, therefore

indicating that the effect of hypoxic-derived EVs is dependent on the receiving cell type. We believe that the potential ability of hypoxic derived EVs to induce proliferation in an autocrine manner could be relevant to understand cardiac developmental events, as EMT and cell migration, and identify a potential therapeutic role for EPDCs-derived EVs in cardiac injuries.

### 1.5. TMT6 proteomic analysis identifies potential markers for EPIC-derived extracellular vesicles

Nowadays, cardiac EVs are considered as biomarkers of cardiac diseases (Polizzotti *et al.*, 2015). However, it is extremely difficult to discern the cellular origin of the EVs subpopulation of interest, especially in the plasma of patients. This limits our understanding of EV specificity in certain therapeutic contexts. It would therefore be ideal to identify EVs derived from cardiac cells, more specifically those delivery by the epicardium and EPDCs. The low number of these cells in the heart could be a limiting factor in this approach that could be circumvented by the use of the pericardial fluid (PF), whose enrichment in cardiac EVs is higher than that of plasma. The close ontogenetic relationship existing between epicardial and pericardial cells suggests parallels between these two cell types. Furthermore, epicardial cells are potential EV secretors to the pericardial fluid, a phenomenon that could be enhanced by the positive net pressure that drives fluids from the epicardial surface capillaries to the pericardial cavity (Vogiatzidis *et al.*, 2015). For all these reasons, it is logical to suggest PF-derived EVs both as the basis of potential cardiac 'liquid biopsies' (Beltrami *et al.*, 2017) and a potential source of EV for the implementation of cardiac specific therapies.

Potential EPIC-EVs surface markers should be localized in the EVs membrane and present in both EVs-N and EVs-H5%. Thus, during the development of this thesis, we thought that our proteomic analysis could allow us to identify potential surface markers for EPDCs-derived EVs. In order to do so, non-significantly differential proteins abundances ( $p$ -value > 0.05) between EVs-N and EVs-H5% ones were identified and analysed. GO analysis confirmed that the most enriched cellular component in our protein sampling was "extracellular exosome" (Fig. 13B). This means that a fraction of proteins, similarly found in EVs-N and EVs-H5%, are involved in the complex intracellular endocytic pathway of membrane trafficking and sorting that culminates in exosome secretion (Peng *et al.*, 2020). Tetraspanins, such as CD9, CD63 and CD81, are among the most abundant proteins in EVs-N and EVs-H5% (Table A6, in Appendix), and widely considered to be transversally carried in small/medium EVs, and multivesicular body biogenesis-related proteins, such as ALIX and TSG101 (Théry *et al.*, 2018). In addition to these findings, 14 of the 24 most abundant proteins in both EV conditions are associated

to “membrane”-related cellular component GO annotation. Of the most abundant cell membrane proteins found in EPIC-EVs, integrin  $\beta 1$  (ITGB1) and  $\alpha 3$  (ITGA3) are included in the KEGG pathway GO annotation “ECM-receptor interactor”. Integrin  $\alpha 3/\beta 1$  is a specific receptor for laminin-5 (Fukushima *et al.*, 1998), an essential molecule inducing epithelial cell migration on laminin-based basement membrane (Olivero and Furcht, 1993). It has been recently hypothesized that interaction of integrin  $\alpha 3/\beta 1$  with laminin increase human mesenchymal stem cells (MSCs) migration in native bovine anisotropic ECM niche (Xing *et al.*, 2021).

Another significant group of proteins that appears in both EPIC-EVs samples are the Annexins, a family of  $\text{Ca}^{2+}$  binding proteins that interact with the plasma membrane at varied  $\text{Ca}^{2+}$  levels. We found that EPIC-EVs were enriched in Annexin-1 (ANXA1), known to inhibit neutrophil recruitment. This finding suggests a possible anti-inflammatory role for these vesicles, as it has been previously shown in epithelial-derived EVs containing Anxa1 (Leoni *et al.*, 2015). Moreover, Anxa1 also takes a cardioprotective role by limiting inflammatory response (Qin *et al.*, 2015; de Jong *et al.*, 2017), so that this molecule has been considered for therapeutical approaches in cardiac ischemic diseases (Qin *et al.*, 2019). Annexin-A2 (ANXA2) is another highly abundant annexin in EPIC-EVs. Previous *in situ* hybridization studies have shown *Anxa2* to be expressed in the epicardial lining, as well as in cell clusters within the developing myocardium of E14.5 mice (Diez-Roux *et al.*, 2011). Importantly, cytoplasmic Anxa2 is normally found as monomeric protein, but when associated with S100A10 (also present among the non-significantly different proteins of EVs-N and EVs-H5%) it takes a hetero-tetrameric conformation and is directed to membrane surfaces, participating in the recovery of vascular injuries (He *et al.*, 2008). Additionally, ANXA2/S100A10 complex trafficking to endothelial cells surface is stimulated by induced cell injury (He *et al.*, 2008). Interestingly, epicardial adipose tissue presented a pro-calcifying protein profile found to be dependent on the upregulation of annexin-A2 in patients with severe aortic stenosis (Mancio *et al.*, 2020). Besides ANXA1 and ANXA2 loading in EPIC-derived EVs, also annexin-A3 (ANXA3), A4 (ANXA4), A5 (ANXA5), A6 (ANXA6), A7 (ANXA7), A8 (ANXA8) and A11 (ANXA11) have been identified in both EPIC-EVs from normoxic and hypoxic conditions (Table A6, in Appendix). Due to its relatively high abundancy in EPIC-derived EVs, annexins such as ANXA1, ANXA2, ANXA5 and ANXA6 are possible candidates for identify EPIC-EVs, especially ANXA2 due its highest

abundancy among the identified annexins. The combination of these proteins with membrane ITGA3 and Itgb1 may aid in resolving epicardial-derived EVs identification. All these results need to be considered in a new series of experiments aiming at identifying a specific annexin signature for epicardial-derived EVs *in vivo*.



## 1.6. EPIC-derived extracellular matrix is enriched in basement membrane proteins

During embryonic development, cellular cross-signalling and interplay determine tissue formation and functional maturation. In particular, the generation of the cardiac extracellular matrix (ECM) is a pivotal event in histogenesis, as extracellular molecules provide the milieu in which multiple developmental processes will take place. Embryonic development modulation by the ECM is a dynamic process. Around E8, endocardial-dependent Notch signalling already plays a decisive role in cardiac trabeculation and ventricular chamber development. At this stage, large amounts of ECM (referred to as the “cardiac jelly”) occupy the space between the endocardium and the myocardium, and actively participates in cardiac valve formation –a process mediated by endocardial EMT–, and ventricular trabeculation (del Monte-Nieto *et al.*, 2018). Later on (between E9.5 and E11.5), the cardiac ECM that accumulates between the myocardium and the epicardium (known as subepicardium) also participates in epicardial EMT. This epicardial phenotypical transformation involves a decrease of epithelial markers and the loss of apico-basal polarity in epicardial cells as well as the activation of a proteolytic program in charge of degrading the basement membrane, thus fostering EPDCs migration and colonization of myocardial layers (Zito, 2012; Ruiz-Villalba *et al.*, 2015). ECM synthesis, deposition and degradation are mandatory phenomena for effective cardiac cell attachment, migration and differentiation during heart formation. Moreover, ECM is critical to the articulation of cardiac responses to pathological and non-pathological situations during the adulthood (Grego-Bessa *et al.*, 2007; del Monte-Nieto *et al.*, 2018). Accordingly, high degradation rates or excessive synthesis of ECM during cardiac development can result in severe heart congenital malformations as ventricular dysplasia or ventricular hypertrabeculation leading to ventricular non compaction (del Monte-Nieto *et al.*, 2018), similarly to cardiac phenotypes associated to deletion of epicardial-markers genes (Martínez-Estrada *et al.*, 2010; von Gise *et al.*, 2011; Acharya *et al.*, 2012).

As previously discussed, multiple evidences suggest that EPDCs participate in the development of this nascent cardiac interstitium. However, the specific cellular origin of cardiac ECM is still unclear since no effective tracing methods exist to determine the

specific cellular origin of ECM proteins found in the heart. We therefore undertook a strategy based in studying the ECM synthesized by a continuous cell line with a known origin. This cell line (EPIC) derives from the embryonic epicardium and allows for the molecular characterization of its secreted proteome, which is assumed to represent, at least in part, the ECM produced by native epicardial cells. To implement this analysis, we used an adaptation of a previously described method that is based in the decellularization of the matrix through the osmotic rupture of the cells (Harris et al., 2018). During the chemical decellularization process, two ECM fractions were obtained: one insoluble (EPIC IM) and other soluble (EPIC SM). As expected, both fractions showed an expected matrix-like aspect, with an irregular patterning of filaments that assemble into a mesh-like organization (Figures 20A and 21C-D), and it is enriched in both fibronectin and laminin (Fig. 21C-D), two of the main components in basement membrane matrices (Silva *et al.*, 2021).

Interestingly, both fractions revealed structural differences (Fig. 21C-D). EPIC IM keeps attached to the plastic surface after decellularization, but the EPIC SM does not, a finding that confirms its major soluble nature. In accordance to these results, EPIC SM contains intracellular components (Fig. 21B), probably resulting from the massive release of the cell contents after the osmotic shock induced by ammonium hydroxide, but also many soluble ECM components that are collected with intracellular components. This result was expected, mostly because common methods for native ECM isolation that include chemical disruption of the plasma membrane, mechanical disruption or a combination of both techniques, lead to variable decellularization efficiency. Thus, double checking on such efficiency is mandatory to ensure a good quality in ECM protein extraction and characterization (Gilpin and Yang, 2017).

In order to perform a proteomic characterization of both fractions, we recurred to shotgun proteomics of both EPIC IM and EPIC SM fractions. As expected, EPIC SM returned a higher heterogeneity of proteins than EPIC IM, as intracellular components are extracted together with soluble ECM proteins. Remarkably, both fractions share unique proteins associated to vasculogenic and wound healing potential (Figures 22 and 23). These results are in accordance to the established knowledge on the epicardial contribution to vascular development and stability in the developing heart, as well as with data on epicardial differentiation and EPDC migration (Kwee et al., 1995; Yang, Rayburn

and Hynes, 1995; Lavine et al., 2006; Vega-Hernández et al., 2011; von Gise et al., 2011). Furthermore, ECM, EMT and epithelial-related processes associate with some of the proteins identified that also support some well-known EPDC phenotypical traits. Without doubts, this is the most complete protein characterization of the ECM of epicardial origin available to date.

### 1.7. EPIC-derived extracellular matrix is enriched in cardiac ECM proteins

To evaluate the correspondence between EPIC-ECM and native cardiac ECM, proteomic analyses for both EPIC IM and EPIC SM were compared with the proteome of decellularized embryonic murine hearts at 17.5 days of development. As proof of specificity, the proteomic composition of Engelbreth-Holm-Swarm (EHS) sarcoma-derived ECM, known as Matrigel, one of the most used basement membrane-derived materials, was also included in this analysis.

In this thesis, EPIC-ECM secretory profile is shown to closely resemble insoluble fractions of mouse embryonic hearts, while its similarity to Matrigel is rather limited. Importantly, most of the shared proteins in EPIC-ECM and decellularized hearts are related to structural ECM proteins such as laminins, fibronectin and collagens. This observation may also emphasize the embryonic origin of both groups of samples. The extracellular proteins shared between EPIC SM and E17.5-derived ECM were grouped in a biological process (gene ontology, GO) related to developmental morphogenesis, from which GO definition goes by “the developmental process pertaining to the initial formation of an anatomical structure from unspecified parts”. In contrast, the uniquely identified extracellular proteins found in Matrigel are mostly enriched in enzymatic-related processes (regulated by peptidases, endopeptidases and hydrolases as well as to proteolytic regulation). The enrichment in such processes suggest that protease inhibitors are added prior to the commercialization of the matrix to ensure ECM viability to the end user, a common practice to improve the function of 3D *in vitro* cell substrates (Pagliarosi *et al.*, 2020). Regarding EPIC-ECM and Matrigel, the abundance in the extract of proteins related to ECM organization and cell adhesion suggests a strong resemblance between the two matrices.

Among the proteins typically found in basal membranes (laminins, type IV collagen, heparan sulfates, proteoglycans, among others) (Hohenester and Yurchenco, 2013), laminins were the most frequently identified proteins in the studied matrices. However, the abundance of the extracellular proteins varies in each sample. For instance, Matrigel was extremely enriched in laminins, followed by nidogen-1 (NID-1), and basement membrane-specific heparan sulfate proteoglycan core protein (HSPG2). This was to be expected because these proteins are typically found in many different basement membranes (Hohenester and Yurchenco, 2013). Accordingly, lower

abundances of these molecules were identified in EPIC IM and decellularized mouse embryonic hearts. Fibronectin (FN) was inferred to be less abundant in EPIC IM than in EPIC SM fraction. However, FN enrichment did not reach 1% in decellularized hearts and Matrigel. As expected from the inferred abundancies, EPIC SM showed the highest FN enrichment by western blot (Fig. 29). This is relevant due to the important role of FN in cardiac development and disease. Deletion of Fn1-related exons led to a severed vascular phenotype at E9.5 and E10.5 in murine embryonic hearts (Astrof *et al.*, 2007). In the chick embryonic heart, cardiomyocytes close to the epicardial layer aligned with fibronectin fibres around the sixth day of incubation (HH28), before capillary formation takes place at HH27 (Hamburger and Hamilton, 1951; Jallerat and Feinberg, 2020). In injured zebrafish hearts, the activated epicardium induces fibronectin expression in the injured site to which cardiomyocytes responds by increasing integrin  $\beta 3$  expression (ITGB3) (Wang *et al.*, 2013), a protein that was also identified in EPIC SM and IM fractions.

Our proteomic study also described the existence of proteins that, despite their low abundance in the EPIC-ECM fraction, could exert a potent effect in cardiac signalling pathways (Tables A7 and A8 in Appendix). As an example, agrin (AGRN), a protein that is present in the EPIC SM ECM fraction, was just recently shown to be cardioprotective when injected into murine neonatal hearts and pig models submitted to ischemic cardiac damage (Bassat *et al.*, 2017; Baehr *et al.*, 2020). It is thus not surprising that this matricellular protein was shown to be present in epicardial cells during development regulating ECM deposition and EMT in epicardial cells (Sun *et al.*, 2021). Interestingly, AGRN responds to matrix stiffness, increasing its expression when the matrix is softened (Wang *et al.*, 2020).

The three isoforms of Class-3 semaphorins, 3A, B and E (SEMA3A, SEMA3B, and SEMA3E, respectively), were found in EPIC IM. This class of semaphorins is the only secreted type of these molecules (Toledano *et al.*, 2019). Relevant to this discussion, SEMA3E is known to directly bind plexin-D1 (identified in both EPIC-ECM fractions) and described to be essential for proper cardiac trabeculation (Sandireddy *et al.*, 2019). In addition to these findings, collagen triple helix repeat-containing protein 1 (CTHRC1), recently shown to be a crucial protein during post-injury cardiac remodelling and secreted by reparative cardiac fibroblasts (Ruiz-Villalba *et al.*, 2020), was also found in EPIC IM and SM. Of note, this protein was also described to be expressed by SMCs and to

influence ECM and vascular remodelling (Leclair *et al.*, 2008). Another developmentally relevant molecule, TGF- $\beta$ 2, was found in EPIC IM, and TGF- $\beta$  receptor type-2 (TGFR-2) and type-1 (TGFR-1) are also present in EPIC SM. Latent TGF- $\beta$  forms are secreted and stored in the ECM, so that TGF- $\beta$ -dependent signalling is intricately regulated by ECM perturbations (Xu *et al.*, 2018). Also, TGF- $\beta$ 2 has been shown to be crucial during cardiac development, as disrupted TGF- $\beta$  signalling may compromise aortic valve formation, trabeculation, mitral valve disease and impair EMT regulation in cardiac cells (Bhattacharya *et al.*, 2021).

Finally, and in order to evaluate the real capacity of EPIC-ECM to support real cell growth, we performed an *in vitro* assay that allowed us to develop a functional comparison between Matrigel and EPIC-ECM fractions in HUVECs. Since human primary cell culture needs supplementary surface-coating to ensure spontaneous proliferation (Relou *et al.*, 1998), gelatine was used for all surface-coated conditions to allow for direct comparison between all conditions. Two time points were considered in our study (3 and 5 days) that was designed to capture the potential proliferative window of HUVECs after seeding. Intriguingly, EPIC IM and EPIC SM-coated maintained HUVECs proliferative capacity over the course of five days, while HUVECs seeded in only gelatine or Matrigel-coated wells reduced drastically their proliferative capacity from the third day of incubation onwards (Figures 30 and 31). As such, HUVEC proliferation in surfaces containing EPIC IM was significantly higher than in HUVECs seeded in Matrigel or Matrigel + EPIC IM after five days. These results are in accordance with our *in silico* data showing that an enrichment in certain ECM proteins associated to vasculogenesis and wound healing terms (Figures 22 and 23).

In summary, all these data confirm that EPIC-ECM might be useful to study the real contribution of epicardium and EPDCs to the nascent cardiac ECM. Furthermore, and based on all the listed evidences, we hypothesized that a functional integration of both EPIC-ECM fractions exists, so that EPIC IM acts as basement membrane, regulating the accumulation and organization of the FN-enriched EPIC SM fraction and generating instructive signals to the growing cells EPIC (Lu *et al.*, 2020). More research is needed to validate and unravel these ECM-linked potential signalling mechanism, that could be relevant to the understanding of EPDC biology in normal and pathological conditions.

### 1.8. Extracellular vesicles and extracellular matrix derived from epicardium and epicardial-derived cells could interact in the cardiac interstitium during cardiac development and in the adult response to damage

EVs-ECM interaction has been demonstrated during the last decade. EVs have shown their capacity to influence ECM modulation cell behaviour and ECM reorganization (Sung *et al.*, 2015; Huleihel *et al.*, 2016; French *et al.*, 2017). Matricellular proteins are suggested to be uptaken by endocytosis and re-secreted via EVs. This model was verified for FN-integrin complexes that promote cell motility by carrying ECM components through an autocrine signalling mechanism (Sung *et al.*, 2015). In this regard, Sung and colleagues also demonstrated that EVs can regulate cell migration speed and directionality. Moreover, integrin-ECM interaction (mediated by proteins such as laminin and fibronectin) have shown important functions for EV-cell docking and subsequent vesicle uptake (French *et al.*, 2017). In this thesis, EPIC-ECM proteins were also identified in EPIC-EVs, suggesting an epicardial ECM-EVs interplay in the heart, which ultimately may affect autocrine and paracrine EV functions. ANXA2, ANXA1, FN, high temperature requirement serine protease A1 (HTRA1), stromal cell-derived factor 1 (SDF-1, or CXCL12), EMILIN-1 and myosin-9 (MYH9, also known as non-muscle myosin II isoform A, NMIIA) were all proteins identified among EPIC-ECM and EPIC-derived EVs. Again, many of these proteins have been shown to be relevant to cardiac development. FN enrichment during cardiac formation is associated to its essential role in cardiac vascular morphogenesis and repair (Astrof *et al.*, 2007; Wang *et al.*, 2013; Jallerat and Feinberg, 2020). HTRA1 was also identified among the proteins found in EPIC-EVs and ECM (specifically in EPIC IM). HTRA1 seems to be an important protein for ECM homeostasis and turnover, as it degrades several matrix components including decorin, FN, aggrecan, Collagen  $\alpha 1(\text{II})$  and  $\alpha 1(\text{VI})$ , NID-1 (identified in EPIC IM) and NID-2 (Vierkotten *et al.*, 2011; Owida *et al.*, 2017) and induces A disintegrin and metalloproteinase with thrombospondin motifs 5 (ADAMTS5) protein expression (identified in EPIC IM) (Li *et al.*, 2019). As for CXCL12 (also known as SDF1), its presence in EPIC IM and EVs enrichment is in line with the multiple roles played this chemokine in mouse and zebrafish cardiac development (Cavallero *et al.*, 2015; Marín-Juez *et al.*, 2019). For example, in zebrafish, SDF-1 mediated collagen deposition, augmenting ECM formation (Patalano *et al.*, 2018). On the other hand, its expression in E11.5-E14 mouse embryos was implicated in the

maturation of the coronary plexus so that this molecule is thought to be required for arterial differentiation and assembly during coronary development (Cavallero *et al.*, 2015).

Another interesting protein found in EPIC secretome is EMILIN-1. This protein is known to inhibit SMC elastin deposition as well as its characteristic TGF- $\beta$  activity. Its inhibitory effect on TGF- $\beta$  is also responsible for the decrease of SMC proliferation (Rabajdová *et al.*, 2017). Dysregulation of EMILIN-1 expression in the heart was shown to result in congenital diseases such as bicuspid aortic valve in human hearts (Skeffington *et al.*, 2019), or latent aortic valve disease in aged murine hearts (Angel *et al.*, 2017). Although not much is known on the role of EMILIN-1 during cardiac development, this molecule has been described to be expressed in migrating chick embryo EPDCs (Hurle *et al.*, 1994).

MYH9 was another protein identified as extracellular protein in EPIC-ECM fractions, and is present in EPIC-EVs. However, this protein is mostly involved in cytoplasmic functions, where it interacts with actin filaments and generate contractile forces. Thus, non-muscle myosins roles like MYH9 are related to cell adhesion, motility and structure in response to ECM signalling cues (Liu *et al.*, 2014; Popa and Gutzman, 2018). In the developing heart, MYH9 is expressed in non-myocytes only (Pecci *et al.*, 2018). A possible reason for the GO annotation of this protein as “extracellular” could be related to its association to secreted cortical granules during fertilization (Vogt *et al.*, 2019). Nonetheless, as this protein is also found in EPIC-EVs, and thus forms part of the EPIC secretome, it is logical to regard it as an extracellular protein.

Finally, there is a set of proteins shared between EPIC-ECM and EPIC-EVs that are also shared with the decellularized embryonic hearts. These proteins are related to the ECM structure and composition (“extracellular matrix organization” and “extracellular structure organization” GO terms), in which laminins, fibronectin and collagens are among the proteins detected in all groups of samples. Annexin A2, Annexin A1, EMILIN-1 and thrombospondin-1 are also among the commonly found proteins. This group of proteins are related to “response to organic substance” biological process, which according to GO description relates to “any process that results in a change in state or activity of a cell or an organism (in terms of movement, secretion, enzyme production, gene expression, etc.) because of an organic substance stimulus”. We believe it is of



relevance that many of these proteins, which are present in the EPIC-derived ECM, are also to be found in EPIC-EVs. This finding is an additional support to the reported essential contribution of epicardium and epicardial-derived cells to cardiac development and adult heart biology.

## 2. Clinical implications

The results of this thesis have a significant clinical translational potential. On one hand, cellular therapies, specifically experimental stem cell therapies, are being superseded by the use of stem cell-derived EVs to avoid the caveat of increased tumorigenesis risk after cell infusion. For instance, EVs from cardiosphere-derived cells (CDC-EVs) were shown to mimic CDC cardioprotective effects by reducing infarction size in rats and mice, regardless of being from human origin (De Couto *et al.*, 2017; Maring *et al.*, 2019). Additionally, iPSC-derived EVs have also been reported to ameliorate cardiac function in a mouse model of chronic myocardial infarction (Adamiak *et al.*, 2018). Due to experimental results like these ones, translational studies involving EVs have grown exponentially, rising the promise of EV-based therapies for the repair/regeneration of the diseased heart (reviewed in Saludas *et al.*, 2021). Indeed, EVs have shown promising effects in preclinical settings of cardiac ischemic injury, especially those derived from stem cells and cardiac progenitor cells. Nevertheless, therapeutical applications of EVs have many limitations. One of these limitations is that these vesicles contain a myriad of bioactive molecules, and therefore trying to assign an effector role to one active compound alone may be misleading. Therefore, the optimal concentration of EVs to be delivered in the context of specific therapies is not at all clear. The development of customized, artificial EVs that allow for the fine control of the EVs cargo could be a useful tool in this context (Man *et al.*, 2020).

The cardiac regeneration field has traditionally exploited the abilities of ECM-based scaffolds and materials. Currently, acellular cardiac therapies based on ECM applications include the use of patch and hydrogel-based biomaterials. Implantation of synthetical collagen type I or alginate patches containing Matrigel and decellularized tissues, such as myocardium small intestinal submucosa, have been shown to improve cardiac function and revascularization in infarcted pigs and rodents (Rane and Christman, 2011). But, how is this effect articulated? It is well-known that a fine balance between ECM protein deposition and degradation is necessary to ensure tissue integrity. Studies on matrix stiffness have been shown to modulate cellular stemness and to have positive angiogenic and anti-fibrotic effects when applied to injured hearts (Baicu *et al.*, 2003; Mewhort *et al.*, 2017; McLaughlin *et al.*, 2019). For instance, ECM from postnatal day 1

(P1) mice induces higher cardiac regeneration than the matrix extracted from older embryos, most likely due to modest differences in ECM composition and stiffness between these samples (Notari *et al.*, 2018). In fact, mouse P1-derived cardiac ECM has been demonstrated to improve cardiac function, to reduce the ischemic fibrotic scar *in vivo*, and promote angiogenesis *in vitro* (Wang *et al.*, 2019). Remarkably, ECM-based patches are commonly applied at the epicardial surface for direct delivery of factors to promote tissue regeneration, while hydrogel-based ECM delivery is usually performed by intramyocardial injection (Baicu *et al.*, 2003).

In summary, it is evident that the full understanding of epicardial contribution to cardiac development and cardiac repair is still in need of extensive research on intercellular communication mechanisms in physiological and pathological contexts. The biological relevance of both EVs and ECM obviously exceed the basic functions of excreting cellular waste or providing material support to cells. This thesis contributes to the knowledge in the field by providing detailed information on epicardial-derived molecules carried via EVs as well as by proposing specific roles as biological modulators for epicardial-derived ECM proteins. These studies demonstrate the ability of epicardial-derived ECM and EVs to modulate cellular responses and highlight the importance of these mechanisms under normal conditions and its potential role as therapeutical agents in a pathological context.

# CONCLUSIONS

---



## Conclusions

---

In this doctoral thesis we have characterized two components of the epicardial-derived cells secretome: extracellular vesicles (EVs) and extracellular matrix (ECM). The specific conclusions from these studies are:

1. Ultracentrifugation allows to recover a major number of small and medium-size EVs than size exclusion chromatography. These EVs-UC show a higher integrity and purity.
2. Hypoxia (5% oxygen) induces an increase in the number of medium-size EVs delivered by EPIC, a cell line derived from E11.5 mouse embryonic epicardium.
3. TMT6plex represents a more reproducible method than TMT2plex for proteomics analysis of EVs.
4. Proteomic analysis of epicardial-derived EVs cargo is a potent approach to identify markers for tissue-specific EVs.
5. Hypoxic-derived EVs are enriched in glycolysis-related proteins.
6. EPIC-EVs are internalized by EPIC and HUVECs.
7. EVs-H5% do not affect EPIC nor HUVECs proliferative and glycolytic behaviours.
8. EVs-H1% induce proliferation in EPIC but does not change their glycolytic behaviour.
9. EVs-H1% increase glycolytic response in HUVECs, although it did not influence their proliferative capacity.
10. Isolated EPIC-ECM fractions (EPIC IM and EPIC SM) are composed by proteins related to wound healing, and cell adhesion.
11. EPIC-ECM presents proteins related to structural components found in Matrigel, including laminins. However, Matrigel and EPIC-ECM presents poor biological correlation.

12. EPIC-ECM presents similar composition to ECM from E17.5 embryonic hearts, corroborating the critical contribution of the epicardium and the EPDCs to the development of the heart.
13. EPIC-ECM is enriched in proteins related to vasculogenesis that extend HUVECs proliferative response up to five days.

## REFERENCES

---





- Acharya, A. *et al.* (2012) 'The bHLH transcription factor Tcf21 is required for lineage-specific EMT of cardiac fibroblast progenitors', *Development (Cambridge)*, 139(12), pp. 2139–2149. doi:10.1242/dev.079970.
- Adamiak, M. *et al.* (2018) 'Induced Pluripotent Stem Cell (iPSC)-derived extracellular vesicles are safer and more effective for cardiac repair than iPSCs', *Circulation Research*, 122(2), pp. 296–309. doi:10.1161/CIRCRESAHA.117.311769.
- Ali, S.R. *et al.* (2014) 'Developmental heterogeneity of cardiac fibroblasts does not predict pathological proliferation and activation', *Circulation Research*, 115(7), pp. 625–635. doi:10.1161/CIRCRESAHA.115.303794.
- Andrade, A.C. *et al.* (2021) 'Hypoxic conditions promote the angiogenic potential of human induced pluripotent stem cell-derived extracellular vesicles', *International Journal of Molecular Sciences*, 22(8). doi:10.3390/ijms22083890.
- Angel, P. *et al.* (2017) 'Proteomic alterations associated with biomechanical dysfunction are early processes in the Emilin1 deficient mouse model of aortic valve disease', *Physiology & Behavior*, 45(11), pp. 2548–2562. doi:10.1007/s10439-017-1899-0.Proteomic.
- Armulik, A., Genové, G. and Betsholtz, C. (2011) 'Pericytes: Developmental, Physiological, and Pathological Perspectives, Problems, and Promises', *Developmental Cell*, 21(2), pp. 193–215. doi:10.1016/j.devcel.2011.07.001.
- Asimaki, A., Kleber, A.G. and Saffitz, J.E. (2016) 'Pathogenesis of Arrhythmogenic Cardiomyopathy', *Can J Cardiol*, 31(11), pp. 1313–1324.
- Astrof, S., Crowley, D. and Hynes, R.O. (2007) 'Multiple cardiovascular defects caused by the absence of alternatively spliced segments of fibronectin', *Developmental Biology*, 311(1), pp. 11–24. doi:10.1016/j.ydbio.2007.07.005.
- Aujla, P.K. and Kassiri, Z. (2021) 'Diverse origins and activation of fibroblasts in cardiac fibrosis', *Cellular Signalling*, 78, p. 109869. doi:10.1016/j.cellsig.2020.109869.
- Austin, A.F. *et al.* (2008) 'Primary and immortalized mouse epicardial cells undergo differentiation in response to TGF $\beta$ ', *Developmental Dynamics*, 237(2), pp. 366–376. doi:10.1002/dvdy.21421.
- Azambuja, A.P. *et al.* (2010) 'Retinoic acid and VEGF delay smooth muscle relative to endothelial differentiation to coordinate inner and outer coronary vessel wall morphogenesis', *Circulation Research*, 107(2), pp. 204–216. doi:10.1161/CIRCRESAHA.109.214650.
- Baehr, A. *et al.* (2020) 'Agrin promotes coordinated therapeutic processes leading to improved cardiac repair in pigs', *Circulation*, 142(9), pp. 868–881. doi:10.1161/CIRCULATIONAHA.119.045116.
- Baghbani, F. *et al.* (2013) 'Identification of novel hypoxia response genes in Human Glioma cell line A172', *Iranian Journal of Basic Medical Sciences*, 16(5), pp. 675–682. doi:10.22038/ijbms.2013.779.
- Baicu, C.F. *et al.* (2003) 'Changes in extracellular collagen matrix alter myocardial systolic performance', *American Journal of Physiology - Heart and Circulatory Physiology*, 284(1 53-1), pp. 122–132. doi:10.1152/ajpheart.00233.2002.
- Bassat, E. *et al.* (2017) 'The extracellular matrix protein agrin promotes heart regeneration in mice', *Nature*, 547(7662), pp. 179–184. doi:10.1038/nature22978.

- Bax, N.A.M. *et al.* (2019) 'In vivo and in vitro Approaches Reveal Novel Insight Into the Ability of Epicardium-Derived Cells to Create Their Own Extracellular Environment', *Frontiers in Cardiovascular Medicine*, 6(June), pp. 1–14. doi:10.3389/fcvm.2019.00081.
- Beltrami, C. *et al.* (2017) 'Human Pericardial Fluid Contains Exosomes Enriched with Cardiovascular-Expressed MicroRNAs and Promotes Therapeutic Angiogenesis', *Molecular Therapy*, 25(3), pp. 679–693. doi:10.1016/j.yymthe.2016.12.022.
- Benton, G. *et al.* (2014) 'Matrigel: From discovery and ECM mimicry to assays and models for cancer research', *Advanced Drug Delivery Reviews*, 79, pp. 3–18. doi:10.1016/j.addr.2014.06.005.
- Bhattacharya, A. *et al.* (2021) 'Myocardial  $\text{tgf}\beta 2$  is required for atrioventricular cushion remodeling and myocardial development', *Journal of Cardiovascular Development and Disease*, 8(3), pp. 1–15. doi:10.3390/jcdd8030026.
- Bock-Marquette, I. *et al.* (2009) 'Thymosin  $\beta 4$  Mediated PKC Activation is Essential to Initiate the Embryonic Coronary Developmental Program and Epicardial Progenitor Cell Activation in Adult Mice in Vivo', *J Mol Cell Cardiol*, 46(5), pp. 728–738. doi:10.1016/j.yjmcc.2009.01.017.Thymosin.
- Bollini, S. *et al.* (2014) 'Re-activated adult epicardial progenitor cells are a heterogeneous population molecularly distinct from their embryonic counterparts', *Stem Cells and Development*, 23(15), pp. 1719–1730. doi:10.1089/scd.2014.0019.
- Bouchev, D., Drake, C., *et al.* (1996) 'Distribution of connective tissue proteins during development and neovascularization of the epicardium', *Cardiovascular Research*, Spec No, pp. 104–115.
- Bouchev, D., Argraves, W.S. and Little, C.D. (1996) 'Fibulin-1, vitronectin, and fibronectin expression during avian cardiac valve and septa development', *Anatomical Record*, 244(4), pp. 540–551. doi:10.1002/(SICI)1097-0185(199604)244:4<540::AID-AR12>3.0.CO;2-P.
- Brennan, K. *et al.* (2020) 'A comparison of methods for the isolation and separation of extracellular vesicles from protein and lipid particles in human serum', *Scientific Reports*, 10(1), pp. 1–13. doi:10.1038/s41598-020-57497-7.
- Burch, G.H. *et al.* (1995) 'Embryonic expression of tenascin-X suggests a role in limb, muscle, and heart development.', *Developmental dynamics: an official publication of the American Association of Anatomists*, 203(4), pp. 491–504. doi:10.1002/aja.1002030411.
- Camenisch, T.D. *et al.* (2000) 'Disruption of hyaluronan synthase-2 abrogates normal cardiac morphogenesis and hyaluronan-mediated transformation of epithelium to mesenchyme', *Journal of Clinical Investigation*, 106(3), pp. 349–360. doi:10.1172/JCI10272.
- del Campo, C.V. *et al.* (2021) 'Regenerative potential of epicardium-derived extracellular vesicles mediated by conserved miRNA transfer', *Cardiovascular Research*, 44(cvab054). doi:10.1093/cvr/cvab054.
- Cano, E. *et al.* (2016) 'Extracardiac septum transversum/proepicardial endothelial cells pattern embryonic coronary arterio-venous connections', *Proceedings of the National Academy of Sciences of the United States of America*, 113(3), pp. 656–661. doi:10.1073/pnas.1509834113.
- Cavallero, S. *et al.* (2015) 'CXCL12 Signaling is Essential for Maturation of the Ventricular Coronary Endothelial Plexus and Establishment of Functional Coronary Circulation', *Developmental Cell*, 33(4), pp. 469–477. doi:10.1016/j.devcel.2015.03.018.
- Chen, Q. *et al.* (2016) 'Endothelial cells are progenitors of cardiac pericytes and vascular smooth muscle cells', *Nature Communications*, 7. doi:10.1038/ncomms12422.

- Chen, T.H.P. *et al.* (2002) 'Epicardial induction of fetal cardiomyocyte proliferation via a retinoic acid-inducible trophic factor', *Developmental Biology*, 250(1), pp. 198–207. doi:10.1006/dbio.2002.0796.
- Chorghade, S. *et al.* (2017) 'Poly(A) tail length regulates PABPC1 expression to tune translation in the heart', *eLife*, 6, pp. 1–19. doi:10.7554/eLife.24139.
- Costell, M. *et al.* (2002) 'Hyperplastic conotruncal endocardial cushions and transposition of great arteries in perlecan-null mice', *Circulation Research*, 91(2), pp. 158–164. doi:10.1161/01.RES.0000026056.81424.DA.
- De Couto, G. *et al.* (2017) 'Exosomal MicroRNA Transfer into Macrophages Mediates Cellular Postconditioning', *Circulation*, 136(2), pp. 200–214. doi:10.1161/CIRCULATIONAHA.116.024590.
- D'Amato, G. *et al.* (2016) 'Sequential Notch activation regulates ventricular chamber development', *Nature Cell Biology*, 18(1), pp. 7–20. doi:10.1038/ncb3280.
- Daneman, R. *et al.* (2010) 'Pericytes are required for blood-brain barrier integrity during embryogenesis', *Nature*, 468(7323), pp. 562–566. doi:10.1038/nature09513.
- Diez-Roux, G. *et al.* (2011) 'A high-resolution anatomical atlas of the transcriptome in the mouse embryo', *PLoS Biology*, 9(1). doi:10.1371/journal.pbio.1000582.
- Diman, N.Y.S.G. *et al.* (2014) 'Tbx5 is required for avian and mammalian epicardial formation and coronary vasculogenesis', *Circulation Research*, 115(10), pp. 834–844. doi:10.1161/CIRCRESAHA.115.304379.
- Dubé, K.N. *et al.* (2017) 'Recapitulation of developmental mechanisms to revascularize the ischemic heart', *JCI insight*, 2(22), pp. 1–21. doi:10.1172/jci.insight.96800.
- Duncan, M.W., Aebersold, R. and Caprioli, R.M. (2010) 'The pros and cons of peptide-centric proteomics', *Nature Biotechnology*, 28(7), pp. 659–664. doi:10.1038/nbt0710-659.
- Fan, Z. and Guan, J. (2016) 'Antifibrotic therapies to control cardiac fibrosis', *Biomaterials Research*, 20(1), pp. 1–13. doi:10.1186/s40824-016-0060-8.
- Farbehi, N. *et al.* (2019) 'Single-cell expression profiling reveals dynamic flux of cardiac stromal, vascular and immune cells in health and injury', *eLife*, 8, pp. 1–39. doi:10.7554/eLife.43882.
- Feng, Y. *et al.* (2014) 'Ischemic preconditioning potentiates the protective effect of stem cells through secretion of exosomes by targeting Mecp2 via miR-22', *PLoS ONE*, 9(2), pp. 1–8. doi:10.1371/journal.pone.0088685.
- Filipe, V., Hawe, A. and Jiskoot, W. (2010) 'Critical evaluation of nanoparticle tracking analysis (NTA) by NanoSight for the measurement of nanoparticles and protein aggregates', *Pharmaceutical Research*, 27(5), pp. 796–810. doi:10.1007/s11095-010-0073-2.
- Fioret, B.A. *et al.* (2014) 'Endothelial cells contribute to generation of adult ventricular myocytes during cardiac homeostasis', *Cell Rep*, 8(1), pp. 229–241. doi:10.1016/j.celrep.2014.06.004.Endothelial.
- Frangogiannis, N.G. (2017) 'The extracellular matrix in myocardial injury, repair, and remodeling.', *The Journal of clinical investigation*, 127(5), pp. 1600–1612. doi:10.1172/JCI87491.
- Frangogiannis, N.G. and Kovacic, J.C. (2020) 'Extracellular Matrix in Ischemic Heart Disease, Part 4/4: JACC Focus Seminar', *Journal of the American College of Cardiology*, 75(17), pp. 2219–2235. doi:10.1016/j.jacc.2020.03.020.

- French, K.C., Antonyak, M.A. and Cerione, R.A. (2017) 'Extracellular vesicle docking at the cellular port: Extracellular vesicle binding and uptake', *Seminars in Cell and Developmental Biology*, 67, pp. 48–55. doi:10.1016/j.semcd.2017.01.002.
- Fu, X. *et al.* (2018) 'Specialized fibroblast differentiated states underlie scar formation in the infarcted mouse heart', *Journal of Clinical Investigation*, 128(5), pp. 2127–2143. doi:10.1172/JCI98215.
- Fukushima, Y. *et al.* (1998) 'Integrin  $\alpha 3\beta 1$ -mediated interaction with laminin-5 stimulates adhesion, migration and invasion of malignant glioma cells', *International Journal of Cancer*, 76(1), pp. 63–72. doi:10.1002/(SICI)1097-0215(19980330)76:1<63::AID-IJC11>3.0.CO;2-H.
- Gardiner, C. *et al.* (2013) 'Extracellular vesicle sizing and enumeration by nanoparticle tracking analysis', *Journal of Extracellular Vesicles*, 2(1), pp. 1–11. doi:10.3402/jev.v2i0.19671.
- Gilpin, A. and Yang, Y. (2017) 'Decellularization Strategies for Regenerative Medicine: From Processing Techniques to Applications', *BioMed Research International*, 2017. doi:10.1155/2017/9831534.
- von Gise, A. *et al.* (2011) 'WT1 regulates epicardial epithelial to mesenchymal transition through  $\beta$ -catenin and retinoic acid signaling pathways', *Developmental Biology*, 356(2), pp. 421–431. doi:10.1016/j.ydbio.2011.05.668.
- Gittenberger-de Groot, A.C. *et al.* (1998) 'Epicardium-derived cells contribute a novel population to the myocardial wall and the atrioventricular cushions', *Circulation Research*, 82(10), pp. 1043–1052. doi:10.1161/01.RES.82.10.1043.
- Gladka, M.M. *et al.* (2018) 'Single-Cell Sequencing of the Healthy and Diseased Heart Reveals Cytoskeleton-Associated Protein 4 as a New Modulator of Fibroblasts Activation', *Circulation*, 138(2), pp. 166–180. doi:10.1161/CIRCULATIONAHA.117.030742.
- González Gayte, I. *et al.* (2017) 'DEgenes Hunter - A Flexible R Pipeline for Automated RNA-seq Studies in Organisms without Reference Genome', *Genomics and Computational Biology*, 3(3), p. 31. doi:10.18547/gcb.2017.vol3.iss3.e31.
- Gourdie, R.G., Dimmeler, S. and Kohl, P. (2016) 'Novel therapeutic strategies targeting fibroblasts and fibrosis in heart disease', *Nat Rev Drug Discov*, 15(9), pp. 620–638. doi:10.1038/nrd.2016.89.Novel.
- Gray, W.D. *et al.* (2015) 'Identification of therapeutic covariant microRNA clusters in hypoxia-treated cardiac progenitor cell exosomes using systems biology', *Circulation Research*, 116(2), pp. 255–263. doi:10.1161/CIRCRESAHA.116.304360.
- Grego-Bessa, J. *et al.* (2007) 'Notch Signaling Is Essential for Ventricular Chamber Development', *Developmental Cell*, 12(3), pp. 415–429. doi:10.1016/j.devcel.2006.12.011.
- Guadix, J. *et al.* (2011) 'Wt1 controls retinoic acid signalling in embryonic epicardium through transcriptional activation of *Raldh2s*', *Development*, 138(6), pp. 1093–1097. doi:10.1242/dev.044594.
- Guadix, J.A. *et al.* (2006) 'In vivo and in vitro analysis of the vasculogenic potential of avian proepicardial and epicardial cells', *Developmental Dynamics*, 235(4), pp. 1014–1026. doi:10.1002/dvdy.20685.
- Hamaguchi, T. *et al.* (2008) 'Glycolysis module activated by hypoxia-inducible factor 1 $\alpha$  is related to the aggressive phenotype of hepatocellular carcinoma', *International Journal of Oncology*, 33, pp. 725–731. doi:10.3892/ijo.

- Hamburger, V. and Hamilton, H.L. (1951) 'A series of normal stages in the development of the chick embryo', *Journal of Morphology*, 88(1), pp. 49–92. doi:10.1002/jmor.1050880104.
- Harris, G.M., Raitman, I. and Schwarzbauer, J.E. (2018) 'Cell-derived decellularized extracellular matrices', *Methods in Cell Biology*, 143, pp. 97–114. doi:10.1016/bs.mcb.2017.08.007.
- Hay, E.D. (2005) 'The mesenchymal cell, its role in the embryo, and the remarkable signaling mechanisms that create it', *Developmental Dynamics*, 233(3), pp. 706–720. doi:10.1002/dvdy.20345.
- Hayasaka, R. *et al.* (2021) 'Metabolomic analysis of small extracellular vesicles derived from pancreatic cancer cells cultured under normoxia and hypoxia', *Metabolites*, 11(4). doi:10.3390/metabo11040215.
- He, K.L. *et al.* (2008) 'Endothelial cell annexin A2 regulates polyubiquitination and degradation of its binding partner S100A10/p11', *Journal of Biological Chemistry*, 283(28), pp. 19192–19200. doi:10.1074/jbc.M800100200.
- Hesse, J., Groterath, W., *et al.* (2021) 'Normoxic induction of HIF-1 $\alpha$  by adenosine-A2BR signaling in epicardial stromal cells formed after myocardial infarction', *FASEB Journal*, 35(5), pp. 1–12. doi:10.1096/fj.202002545R.
- Hesse, J., Owenier, C., *et al.* (2021) 'Single-cell transcriptomics defines heterogeneity of epicardial cells and fibroblasts within the infarcted murine heart', *eLife*, 10(Mi), pp. 1–21. doi:10.7554/elife.65921.
- Hohenester, E. and Yurchenco, P.D. (2013) 'Laminins in basement membrane assembly', *Cell Adh Migr*, 7(1), pp. 56–63.
- Horie, K. *et al.* (2017) 'Exosomes expressing carbonic anhydrase 9 promote angiogenesis', *Biochemical and Biophysical Research Communications*, 492(3), pp. 356–361. doi:10.1016/j.bbrc.2017.08.107.
- Hughey, C.C. *et al.* (2012) 'Mesenchymal stem cell transplantation for the infarcted heart: A role in minimizing abnormalities in cardiac-specific energy metabolism', *American Journal of Physiology - Endocrinology and Metabolism*, 302(2), pp. 163–172. doi:10.1152/ajpendo.00443.2011.
- Huleihel, L. *et al.* (2016) 'Matrix-bound nanovesicles within ECM bioscaffolds', *Science Advances*, 2(6). doi:10.1126/sciadv.1600502.
- Hurle, J.M. *et al.* (1994) 'Elastic extracellular matrix of the embryonic chick heart: an immunohistological study using laser confocal microscopy.', *Developmental dynamics : an official publication of the American Association of Anatomists*, 200(4), pp. 321–32. doi:10.1002/aja.1002000407.
- Ieda, M. *et al.* (2009) 'Cardiac Fibroblasts Regulate Myocardial Proliferation through  $\beta$ 1 Integrin Signaling', *Developmental Cell*, 16(2), pp. 233–244. doi:10.1016/j.devcel.2008.12.007.
- Isomi, M., Sadahiro, T. and Ieda, M. (2019) 'Progress and Challenge of Cardiac Regeneration to Treat Heart Failure', *Journal of Cardiology*, 73(2), pp. 97–101. doi:10.1016/j.jjcc.2018.10.002.
- Jaffe, E.A. *et al.* (1973) 'Culture of human endothelial cells derived from umbilical veins. Identification by morphologic and immunologic criteria', *Journal of Clinical Investigation*, 52(11), pp. 2745–2756. doi:10.1172/JCI107470.
- Jallerat, Q. and Feinberg, A.W. (2020) 'Extracellular Matrix Structure and Composition in the Early Four-Chambered Embryonic Heart', *Cells*, 9(2), pp. 1–14. doi:10.3390/cells9020285.

- de Jong, O.G. *et al.* (2012) 'Cellular stress conditions are reflected in the protein and RNA content of endothelial cell-derived exosomes', *Journal of Extracellular Vesicles*, 1(1). doi:10.3402/jev.v1i0.18396.
- de Jong, R. *et al.* (2017) 'The advantageous role of annexin A1 in cardiovascular disease', *Cell Adhesion and Migration*, 11(3), pp. 261–274. doi:10.1080/19336918.2016.1259059.
- Kálmán, F., Virágh, S. and Módis, L. (1995) 'Cell Surface glycoconjugates and the extracellular matrix of the developing mouse embryo epicardium', *Anatomy and Embryology*, 191(5), pp. 451–464.
- Kanisicak, O. *et al.* (2016) 'Genetic lineage tracing defines myofibroblast origin and function in the injured heart', *Nature Communications*, 7. doi:10.1038/ncomms12260.
- Kenneweg, F. *et al.* (2019) 'Long Noncoding RNA-Enriched Vesicles Secreted by Hypoxic Cardiomyocytes Drive Cardiac Fibrosis', *Molecular Therapy - Nucleic Acids*, 18, pp. 363–374. doi:10.1016/j.omtn.2019.09.003.
- Kern, C.B. *et al.* (2010) 'Reduced versican cleavage due to Adamts9 haploinsufficiency is associated with cardiac and aortic anomalies', *Matrix Biology*, 29(4), pp. 304–316. doi:10.1016/j.matbio.2010.01.005.
- Kim, N.N. *et al.* (1999) 'Regulation of cardiac fibroblast extracellular matrix production by bradykinin and nitric oxide.', *Journal of molecular and cellular cardiology*, 31(2), pp. 457–66. doi:10.1006/jmcc.1998.0887.
- Kirby, M.L., Gale, T.F. and Stewart, D.E. (1983) 'Neural crest cells contribute to normal aorticopulmonary septation', *Science*, 220(4601), pp. 1059–1061. doi:10.1126/science.6844926.
- Kocabas, F. *et al.* (2012) 'The hypoxic epicardial and subepicardial microenvironment', *Journal of Cardiovascular Translational Research*, 5(5), pp. 654–665. doi:10.1007/s12265-012-9366-7.
- Konoshenko, M.Y. *et al.* (2018) 'Isolation of Extracellular Vesicles: General Methodologies and Latest Trends', *BioMed Research International*, 2018. doi:10.1155/2018/8545347.
- Kreimer, S. *et al.* (2015) 'Mass-spectrometry-based molecular characterization of extracellular vesicles: Lipidomics and proteomics', *Journal of Proteome Research*, 14(6), pp. 2367–2384. doi:10.1021/pr501279t.
- Kwee, L. *et al.* (1995) 'Defective development of the embryonic and extraembryonic circulatory systems in vascular cell adhesion molecule (VCAM-1) deficient mice', *Development*, 121(2), pp. 489–503. doi:10.1242/dev.121.2.489.
- De la Pompa, J.L. and Epstein, J.A. (2012) 'Coordinating Tissue Interactions: Notch Signaling in Cardiac Development and Disease', *Developmental Cell*, 22(2), pp. 244–254. doi:10.1016/j.devcel.2012.01.014.
- Lajiness, J.D. and Conway, S.J. (2012) 'The dynamic role of cardiac fibroblasts in development and disease', *Journal of Cardiovascular Translational Research*, 5(6), pp. 739–748. doi:10.1007/s12265-012-9394-3.
- Lam, M.P.Y. *et al.* (2016) 'Cardiovascular proteomics in the era of big data: Experimental and computational advances', *Clinical Proteomics*, 13(1), pp. 1–14. doi:10.1186/s12014-016-9124-y.
- Lavine, K.J. *et al.* (2005) 'Endocardial and epicardial derived FGF signals regulate myocardial proliferation and differentiation *in vivo*', *Developmental Cell*, 8(1), pp. 85–95. doi:10.1016/j.devcel.2004.12.002.

- Lavine, K.J. *et al.* (2006) 'Fibroblast growth factor signals regulate a wave of Hedgehog activation that is essential for coronary vascular development', *Genes and Development*, 20(12), pp. 1651–1666. doi:10.1101/gad.1411406.
- Lavine, K.J. and Ornitz, D.M. (2008) 'Fibroblast growth factors and Hedgehogs: at the heart of the epicardial signaling center', *Trends in Genetics*, 24(1), pp. 33–40. doi:10.1016/j.tig.2007.10.007.
- Leask, A. (2015) 'Getting to the heart of the matter: New insights into cardiac fibrosis', *Circulation Research*, 116(7), pp. 1269–1276. doi:10.1161/CIRCRESAHA.116.305381.
- Leclair, R.J. *et al.* (2008) 'Intracellular localization of Cthrc1 characterizes differentiated smooth muscle', *Arteriosclerosis, Thrombosis, and Vascular Biology*, 28(7), pp. 1332–1338. doi:10.1161/ATVBAHA.108.166579.
- Leoni, G. *et al.* (2015) 'Annexin A1-containing extracellular vesicles and polymeric nanoparticles promote epithelial wound repair', *Journal of Clinical Investigation*, 125(3), pp. 1215–1227. doi:10.1172/JCI76693.
- Li, D. *et al.* (2019) 'HtrA1 upregulates the expression of ADAMTS-5 in HNPCs via the ERK/NF- $\kappa$ B/JNK signaling pathway', *American Journal of Translational Research*, 11(8), pp. 5114–5121.
- Li, X., Zheng, Y. and Lu, Z. (2016) 'PGK1 is a new member of the protein kinome', *Cell Cycle*, 15(14), pp. 1803–1804. doi:10.1080/15384101.2016.1179037.
- Lian, X. *et al.* (2012) 'Robust cardiomyocyte differentiation from human pluripotent stem cells via temporal modulation of canonical Wnt signaling', *Proceedings of the National Academy of Sciences of the United States of America*, 109(27). doi:10.1073/pnas.1200250109.
- Lincet, H. and Icard, P. (2015) 'How do glycolytic enzymes favour cancer cell proliferation by nonmetabolic functions?', *Oncogene*, 34(29), pp. 3751–3759. doi:10.1038/onc.2014.320.
- Litviňuková, M. *et al.* (2020) 'Cells of the adult human heart', *Nature*, 588(7838), pp. 466–472. doi:10.1038/s41586-020-2797-4.
- Liu, W.H. *et al.* (2018) 'Distinct anti-fibrotic effects of exosomes derived from endothelial colony-forming cells cultured under normoxia and hypoxia', *Medical Science Monitor*, 24, pp. 6187–6199. doi:10.12659/MSM.911306.
- Liu, Z., Ho, C.H. and Grinnell, F. (2014) 'The different roles of myosin IIA and myosin IIB in contraction of 3D collagen matrices by human fibroblasts', *Experimental Cell Research*, 326(2), pp. 295–306. doi:10.1016/j.yexcr.2014.04.013.
- Lobb, R.J. *et al.* (2015) 'Optimized exosome isolation protocol for cell culture supernatant and human plasma', *Journal of Extracellular Vesicles*, 4(1), pp. 1–11. doi:10.3402/jev.v4.27031.
- López, B., González, A. and Díez, J. (2010) 'Circulating biomarkers of collagen metabolism in cardiac diseases', *Circulation*, 121(14), pp. 1645–1654. doi:10.1161/CIRCULATIONAHA.109.912774.
- Lu, J. *et al.* (2020) 'Basement Membrane Regulates Fibronectin Organization Using Sliding Focal Adhesions Driven by a Contractile Winch', *Developmental Cell*, 52(5), pp. 631–646.e4. doi:10.1016/j.devcel.2020.01.007.
- Ludikhuizen, M.C. *et al.* (2021) 'Protocol to profile the bioenergetics of organoids using Seahorse', *STAR Protocols*, 2(1). doi:10.1016/j.xpro.2021.100386.
- Man, K. *et al.* (2020) 'Engineered extracellular vesicles: Tailored-made nanomaterials for medical applications', *Nanomaterials*, 10(9), pp. 1–30. doi:10.3390/nano10091838.



- Mancio, J. *et al.* (2020) *Epicardial adipose tissue volume and annexin A2/fetuin-A signalling are linked to coronary calcification in advanced coronary artery disease: Computed tomography and proteomic biomarkers from the EPICHEART study*, *Atherosclerosis*. Elsevier B.V. doi:10.1016/j.atherosclerosis.2019.11.015.
- Mantri, M. *et al.* (2021) 'Spatiotemporal single-cell RNA sequencing of developing chicken hearts identifies interplay between cellular differentiation and morphogenesis', *Nature Communications*, 12(1). doi:10.1038/s41467-021-21892-z.
- Marín-Juez, R. *et al.* (2019) 'Coronary Revascularization During Heart Regeneration Is Regulated by Epicardial and Endocardial Cues and Forms a Scaffold for Cardiomyocyte Repopulation', *Developmental Cell*, 51(4), pp. 503-515.e4. doi:10.1016/j.devcel.2019.10.019.
- Marín-Sedeño, E. *et al.* (2021) 'Understanding the Adult Mammalian Heart at Single-Cell RNA-Seq Resolution', *Frontiers in Cell and Developmental Biology*, 9(May). doi:10.3389/fcell.2021.645276.
- Maring, J.A. *et al.* (2019) 'Cardiac Progenitor Cell-Derived Extracellular Vesicles Reduce Infarct Size and Associate with Increased Cardiovascular Cell Proliferation', *Journal of Cardiovascular Translational Research*, 12(1), pp. 5–17. doi:10.1007/s12265-018-9842-9.
- Markwald, R.R., Fitzharris, T.P. and Manasek, F.J. (1977) 'Structural development of endocardial cushions', *American Journal of Anatomy*, 148(1), pp. 85–119. doi:10.1002/aja.1001480108.
- Martínez-Estrada, O.M. *et al.* (2010) 'Wt1 is required for cardiovascular progenitor cell formation through transcriptional control of Snail and E-cadherin', *Nature Genetics*, 42(1), pp. 89–93. doi:10.1038/ng.494.
- Martino, M.M. *et al.* (2014) 'Matrix Enhance Tissue Healing', 343(February), pp. 885–889.
- McLaughlin, S. *et al.* (2019) 'Injectable human recombinant collagen matrices limit adverse remodeling and improve cardiac function after myocardial infarction', *Nature Communications*, 10(1). doi:10.1038/s41467-019-12748-8.
- Mewhort, H.E.M. *et al.* (2017) 'Bioactive Extracellular Matrix Scaffold Promotes Adaptive Cardiac Remodeling and Repair', *JACC: Basic to Translational Science*, 2(4), pp. 450–464. doi:10.1016/j.jacbts.2017.05.005.
- Mikawa, T. *et al.* (2020) 'Phosphoglycerate Mutase Cooperates with Chk1 Kinase to Regulate Glycolysis', *iScience*, 23(7), p. 101306. doi:10.1016/j.isci.2020.101306.
- Mofid, A. *et al.* (2017) 'Cardiac overexpression of S100A6 attenuates cardiomyocyte apoptosis and reduces infarct size after myocardial ischemia-reperfusion', *Journal of the American Heart Association*, 6(2), pp. 1–15. doi:10.1161/JAHA.116.004738.
- del Monte-Nieto, G. *et al.* (2018) 'Control of cardiac jelly dynamics by NOTCH1 and NRG1 defines the building plan for trabeculation', *Nature*, 557(7705), pp. 439–445.
- Del Monte, G. *et al.* (2011) 'Differential notch signaling in the epicardium is required for cardiac inflow development and coronary vessel morphogenesis', *Circulation Research*, 108(7), pp. 824–836. doi:10.1161/CIRCRESAHA.110.229062.
- Moore-Morris, T. *et al.* (2014) 'Resident fibroblast lineages mediate pressure overload-induced cardiac fibrosis', *Journal of Clinical Investigation*, 124(7), pp. 2921–2934. doi:10.1172/JCI74783.
- Moore-Morris, T. *et al.* (2018) 'Infarct fibroblasts do not derive from bone marrow lineages', *Circulation Research*, 122(4), pp. 583–590. doi:10.1161/CIRCRESAHA.117.311490.
- Morabito, C.J. *et al.* (2001) 'Positive and negative regulation of epicardial-mesenchymal

- transformation during avian heart development', *Developmental Biology*, 234(1), pp. 204–215. doi:10.1006/dbio.2001.0254.
- Muller, L. *et al.* (2014) 'Isolation of biologically-active exosomes from human plasma', *Journal of Immunological Methods*, 411(Lm), pp. 55–65. doi:10.1016/j.jim.2014.06.007.
- Nakajima, Y. *et al.* (2000) 'Mechanisms involved in valvuloseptal endocardial cushion formation in early cardiogenesis: roles of transforming growth factor (TGF)-beta and bone morphogenetic protein (BMP)', *Anatomical Record*, 258(2), pp. 119–127.
- Van Niel, G., D'Angelo, G. and Raposo, G. (2018) 'Shedding light on the cell biology of extracellular vesicles', *Nature Reviews Molecular Cell Biology*, 19(4), pp. 213–228. doi:10.1038/nrm.2017.125.
- Nordin, J.Z. *et al.* (2015) 'Ultrafiltration with size-exclusion liquid chromatography for high yield isolation of extracellular vesicles preserving intact biophysical and functional properties', *Nanomedicine: Nanotechnology, Biology, and Medicine*, 11(4), pp. 879–883. doi:10.1016/j.nano.2015.01.003.
- Notari, M. *et al.* (2018) 'The local microenvironment limits the regenerative potential of the mouse neonatal heart', *Science Advances*, 4(5). doi:10.1126/sciadv.aao5553.
- Oatmen, K.E., Cull, E. and Spinale, F.G. (2020) 'Heart failure as interstitial cancer: emergence of a malignant fibroblast phenotype', *Nature Reviews Cardiology*, 17(8), pp. 523–531. doi:10.1038/s41569-019-0286-y.
- Olivero, D. and Furcht, L. (1993) 'Type IV Collagen, Laminin, and Fibronectin Promote the Adhesion and Migration of Rabbit Lens Epithelial Cells *in vitro*', *Invest Ophthalmol Vis Sci*, 34(10), pp. 2825–34.
- Ontoria-Oviedo, I. *et al.* (2018) 'Extracellular Vesicles Secreted by Hypoxic AC10 Cardiomyocytes Modulate Fibroblast Cell Motility', *Frontiers in Cardiovascular Medicine*, 5(152), pp. 1–8. doi:10.3389/fcvm.2018.00152.
- Owida, H.A. *et al.* (2017) 'Co-culture of chondrons and mesenchymal stromal cells reduces the loss of collagen VI and improves extracellular matrix production', *Histochemistry and Cell Biology*, 148(6), pp. 625–638. doi:10.1007/s00418-017-1602-4.
- Pagliarosi, O. *et al.* (2020) 'Building an Artificial Cardiac Microenvironment: A Focus on the Extracellular Matrix', *Frontiers in Cell and Developmental Biology*, 8(September), pp. 1–8. doi:10.3389/fcell.2020.559032.
- Palmquist-Gomes, P., Guadix, J.A. and Pérez-Pomares, J.M. (2018) 'Avian embryonic coronary arterio-venous patterning involves the contribution of different endothelial and endocardial cell populations', *Developmental Dynamics*, 247(5), pp. 686–698. doi:10.1002/dvdy.24610.
- Pang, B. *et al.* (2018) 'Systematic review and meta-analysis of the impact of hypoxia on infarcted myocardium: Better or worse?', *Cellular Physiology and Biochemistry*, 51(2), pp. 949–960. doi:10.1159/000495397.
- Parks, S.K., Chiche, J. and Pouyssegur, J. (2013) 'Disrupting proton dynamics and energy metabolism for cancer therapy', *Nature Reviews Cancer*, 13(9), pp. 611–623. doi:10.1038/nrc3579.
- Patalano, S. *et al.* (2018) 'CXCL12/CXCR4-Mediated Procollagen Secretion Is Coupled to Cullin-RING Ubiquitin Ligase Activation', *Scientific Reports*, 8(1), pp. 1–11. doi:10.1038/s41598-018-21506-7.
- Pecci, A. *et al.* (2018) 'MYH9: Structure, functions and role of non-muscle myosin IIA in human

- disease', *Gene*, 664(February), pp. 152–167. doi:10.1016/j.gene.2018.04.048.
- Peng, X. *et al.* (2020) 'Focus on the morphogenesis, fate and the role in tumor progression of multivesicular bodies', *Cell Communication and Signaling*, 18(1), pp. 1–15. doi:10.1186/s12964-020-00619-5.
- Pennisi, D.J. and Mikawa, T. (2005) 'Normal patterning of the coronary capillary plexus is dependent on the correct transmural gradient of FGF expression in the myocardium', *Developmental Biology*, 279(2), pp. 378–390. doi:10.1016/j.ydbio.2004.12.028.
- Perestrelo, A.R. *et al.* (2021) 'Multiscale Analysis of Extracellular Matrix Remodeling in the Failing Heart', *Circulation Research*, 128(1), pp. 24–38. doi:10.1161/CIRCRESAHA.120.317685.
- Pérez-Pomares, J.M. *et al.* (1998) 'The origin of the subepicardial mesenchyme in the avian embryo: An immunohistochemical and quail-chick chimera study', *Developmental Biology*, 200(1), pp. 57–68. doi:10.1006/dbio.1998.8949.
- Pérez-Pomares, J.M., Phelps, A., *et al.* (2002) 'Experimental studies on the spatiotemporal expression of WT1 and RALDH2 in the embryonic avian heart: A model for the regulation of myocardial and valvuloseptal development by epicardially derived cells (EPDCs)', *Developmental Biology*, 247(2), pp. 307–326. doi:10.1006/dbio.2002.0706.
- Pérez-Pomares, J.M., Carmona, R., *et al.* (2002) 'Origin of coronary endothelial cells from epicardial mesothelium in avian embryos', *International Journal of Developmental Biology*, 46(8), pp. 1005–1013. doi:10.1387/ijdb.12533024.
- Pinto, A.R. *et al.* (2016) 'Revisiting cardiac cellular composition', *Circulation Research*, 118(3), pp. 400–409. doi:10.1161/CIRCRESAHA.115.307778.
- Pogontke, C. *et al.* (2019) 'Development of the Myocardial Interstitium', *Anatomical Record*, 302(1), pp. 58–68. doi:10.1002/ar.23915.
- van der Pol, E. *et al.* (2014) 'Particle size distribution of exosomes and microvesicles determined by transmission electron microscopy, flow cytometry, nanoparticle tracking analysis, and resistive pulse sensing', *Journal of Thrombosis and Haemostasis*, 12(7), pp. 1182–1192. doi:10.1111/jth.12602.
- Polizzotti, B.D. *et al.* (2015) 'Neuregulin stimulation of cardiomyocyte regeneration in mice and human myocardium reveals a therapeutic window', *Science Translational Medicine*, 7(281). doi:10.1126/scitranslmed.aaa5171.
- Popa, I. and Gutzman, J.H. (2018) 'The extracellular matrix-myosin pathway in mechanotransduction: From molecule to tissue', *Emerging Topics in Life Sciences*, 2(5), pp. 727–737. doi:10.1042/ETLS20180043.
- Qin, C. *et al.* (2015) 'Cardioprotective potential of annexin-A1 mimetics in myocardial infarction', *Pharmacology and Therapeutics*, 148, pp. 47–65. doi:10.1016/j.pharmthera.2014.11.012.
- Qin, C.X. *et al.* (2019) 'Cardioprotective actions of the annexin-A1 N-terminal peptide, AC2-26, against myocardial infarction', *Frontiers in Pharmacology*, 10(APR), pp. 1–16. doi:10.3389/fphar.2019.00269.
- Quijada, P. *et al.* (2019) 'Pre-existing fibroblasts of epicardial origin are the primary source of pathological fibrosis in cardiac ischemia and aging', *Journal of Molecular and Cellular Cardiology*, 129(January), pp. 92–104. doi:10.1016/j.yjmcc.2019.01.015.
- Quijada, P. *et al.* (2021) 'Coordination of endothelial cell positioning and fate specification by the epicardium', *Nature Communications*, 12(1), pp. 1–18. doi:10.1038/s41467-021-24414-z.

- Quijada, P., Trembley, M.A. and Small, E.M. (2020) 'The Role of the Epicardium during Heart Development and Repair', *Circulation Research*, 126(3), pp. 377–394. doi:10.1161/CIRCRESAHA.119.315857.
- Rabajdová, M. *et al.* (2017) 'Detection of pathological changes in the aorta during thoracic aortic aneurysm progression on molecular level', *Disease Markers*, 2017. doi:10.1155/2017/9185934.
- Rane, A.A. and Christman, K.L. (2011) 'Biomaterials for the treatment of myocardial infarction: A 5-year update', *Journal of the American College of Cardiology*, 58(25), pp. 2615–2629. doi:10.1016/j.jacc.2011.11.001.
- Rappolee, D., Iyer, A. and Patel, Y. (1996) 'Hepatocyte growth factor and its receptor are expressed in cardiac myocytes during early cardiogenesis', *Circulation Research*, 78(6), pp. 1028–1036.
- Ream, M. *et al.* (2008) 'Early fetal hypoxia leads to growth restriction and myocardial thinning', *American Journal of Physiology - Regulatory Integrative and Comparative Physiology*, 295(2), pp. 583–595. doi:10.1152/ajpregu.00771.2007.
- Relou, I.A.M. *et al.* (1998) 'Effect of culture conditions on endothelial cell growth and responsiveness', *Tissue and Cell*, 30(5), pp. 525–530. doi:10.1016/S0040-8166(98)80032-3.
- Ribeiro-Rodrigues, T.M. *et al.* (2017) 'Exosomes secreted by cardiomyocytes subjected to ischaemia promote cardiac angiogenesis', *Cardiovascular Research*, 113(11), pp. 1338–1350. doi:10.1093/cvr/cvx118.
- Rog-Zielinska, E.A. *et al.* (2016) 'The Living scar - cardiac fibroblasts and the injured heart', *Trends in Molecular Medicine*, 22(2), pp. 99–114. doi:10.1016/j.molmed.2015.12.006.
- Royo, F. *et al.* (2016) 'Different EV enrichment methods suitable for clinical settings yield different subpopulations of urinary extracellular vesicles from human samples', *Journal of Extracellular Vesicles*, 5(1). doi:10.3402/jev.v5.29497.
- Ruiz-Villalba, A. *et al.* (2013) 'Characterization of Epicardial-Derived Cardiac Interstitial Cells: Differentiation and Mobilization of Heart Fibroblast Progenitors', *PLoS ONE*, 8(1), pp. 17–19. doi:10.1371/journal.pone.0053694.
- Ruiz-Villalba, A. *et al.* (2015) 'Interacting resident epicardium-derived fibroblasts and recruited bone marrow cells form myocardial infarction scar', *Journal of the American College of Cardiology*, 65(19), pp. 2057–2066. doi:10.1016/j.jacc.2015.03.520.
- Ruiz-Villalba, A. *et al.* (2020) 'Single-Cell RNA Sequencing Analysis Reveals a Crucial Role for CTHRC1 (Collagen Triple Helix Repeat Containing 1) Cardiac Fibroblasts After Myocardial Infarction', *Circulation*, 142(19), pp. 1831–1847. doi:10.1161/CIRCULATIONAHA.119.044557.
- Ruiz-Villalba, A., Frangogiannis, N. and Pérez-Pomares, J.M. (2018) 'Origin and diversity of cardiac fibroblasts: developmental substrates of adult cardiac fibrosis', in *The ESC Textbook of Cardiovascular Development*, pp. 105–116.
- Saban, K.L. *et al.* (2014) 'Epigenetics and social context: Implications for disparity in cardiovascular disease', *Aging and Disease*, 5(5), pp. 346–355. doi:10.14336/AD.2014.0500346.
- Salic, A. and Mitchison, T.J. (2008) 'A chemical method for fast and sensitive detection of DNA synthesis *in vivo*', *Proceedings of the National Academy of Sciences of the United States of America*, 105(7), pp. 2415–2420. doi:10.1073/pnas.0712168105.
- Saludas, L. *et al.* (2021) 'Extracellular vesicle-based therapeutics for heart repair', *Nanomaterials*, 11(3), pp. 1–30. doi:10.3390/nano11030570.

- Sampaio-Pinto, V. *et al.* (2018) 'Neonatal Apex Resection Triggers Cardiomyocyte Proliferation, Neovascularization and Functional Recovery Despite Local Fibrosis', *Stem Cell Reports*, 10(3), pp. 860–874. doi:10.1016/j.stemcr.2018.01.042.
- Sandireddy, R. *et al.* (2019) 'Semaphorin 3E/PlexinD1 signaling is required for cardiac ventricular compaction', *JCI Insight*, 4(16), pp. 1–16. doi:10.1172/jci.insight.125908.
- Schelbert, E.B. *et al.* (2014) 'Therapeutic targets in heart failure: Refocusing on the myocardial interstitium', *Journal of the American College of Cardiology*, 63(21), pp. 2188–2198. doi:10.1016/j.jacc.2014.01.068.
- Sidhom, K., Obi, P.O. and Saleem, A. (2020) 'A review of exosomal isolation methods: Is size exclusion chromatography the best option?', *International Journal of Molecular Sciences*, 21(18), pp. 1–19. doi:10.3390/ijms21186466.
- Silva, A.C. *et al.* (2021) 'Bearing My Heart: The Role of Extracellular Matrix on Cardiac Development, Homeostasis, and Injury Response', *Frontiers in Cell and Developmental Biology*, 8(January), pp. 1–18. doi:10.3389/fcell.2020.621644.
- Skeffington, K.L. *et al.* (2019) 'Bicuspid Aortic Valve Alters Aortic Protein Expression Profile in Neonatal Coarctation Patients', *Journal of Clinical Medicine*, 8(4), p. 517. doi:10.3390/jcm8040517.
- Skelly, D.A. *et al.* (2018) 'Single-Cell Transcriptional Profiling Reveals Cellular Diversity and Intercommunication in the Mouse Heart', *Cell Reports*, 22(3), pp. 600–610. doi:10.1016/j.celrep.2017.12.072.
- Smith, C.L. *et al.* (2011) 'Epicardial-derived cell epithelial-to-mesenchymal transition and fate specification require PDGF receptor signaling', *Circulation Research*, 108(12). doi:10.1161/CIRCRESAHA.110.235531.
- Song, W., Majka, S.M. and McGuire, P.G. (1999) 'Hepatocyte growth factor expression in the developing myocardium: evidence for a role in the regulation of the mesenchymal cell phenotype and urokinase expression', *Dev Dyn*, 214(1), pp. 92–100. doi:10.1002/(SICI)1097-0177(199901)214:1<92::AID-DVDY9>3.0.CO;2-X.
- Spinale, F.G. (2007) 'MMP: Influence on Cardiac Form and Function', *Physiological reviews*, 87, pp. 1285–1342. doi:10.1152/physrev.00012.2007.
- Spinale, F.G. *et al.* (2016) 'Crossing into the Next Frontier of Cardiac Extracellular Matrix Research', *Circulation Research*, 119(10), pp. 1040–1045. doi:10.1161/CIRCRESAHA.116.309916.
- Storey, A.J. *et al.* (2020) 'Accurate and Sensitive Quantitation of the Dynamic Heat Shock Proteome Using Tandem Mass Tags', *Journal of Proteome Research*, 19(3), pp. 1183–1195. doi:10.1021/acs.jproteome.9b00704.
- Stuckmann, I., Evans, S. and Lassar, A.B. (2003) 'Erythropoietin and retinoic acid, secreted from the epicardium, are required for cardiac myocyte proliferation', *Developmental Biology*, 255(2), pp. 334–349. doi:10.1016/S0012-1606(02)00078-7.
- Sun, X. *et al.* (2021) 'The extracellular matrix protein agrin is essential for epicardial epithelial-to-mesenchymal transition during heart development', *Development (Cambridge)*, 148(9). doi:10.1242/dev.197525.
- Sun, Y. *et al.* (2000) 'Cardiac remodeling by fibrous tissue after infarction in rats', *Journal of Laboratory and Clinical Medicine*, 135(4), pp. 316–323. doi:10.1067/mlc.2000.105971.
- Sung, B.H. *et al.* (2015) 'Directional cell movement through tissues is controlled by exosome

- secretion', *Nature Communications*, 6(May). doi:10.1038/ncomms8164.
- Takov, K., Yellon, D.M. and Davidson, S.M. (2019) 'Comparison of small extracellular vesicles isolated from plasma by ultracentrifugation or size-exclusion chromatography: yield, purity and functional potential', *Journal of Extracellular Vesicles*, 8(1), pp. 1–18. doi:10.1080/20013078.2018.1560809.
- Tallquist, M.D. and Molkenin, J.D. (2017) 'Redefining the identity of cardiac fibroblasts', *Nature Reviews Cardiology*, 14(8), pp. 484–491. doi:10.1038/nrcardio.2017.57.
- Thavapalachandran, S. *et al.* (2020) 'Platelet-derived growth factor-AB improves scar mechanics and vascularity after myocardial infarction', *Science Translational Medicine*, 12(524). doi:10.1126/scitranslmed.aay2140.
- Théry, C. (2011) *Exosome explosion*, *The Scientist*. Available at: <https://www.the-scientist.com/features/exosome-explosion-42253> (Accessed: 21 October 2021).
- Théry, C. *et al.* (2018) 'Minimal information for studies of extracellular vesicles 2018 (MISEV2018): a position statement of the International Society for Extracellular Vesicles and update of the MISEV2014 guidelines', *Journal of Extracellular Vesicles*, 7(1), p. 1535750. doi:10.1080/20013078.2018.1535750.
- Thompson, A. *et al.* (2003) 'Tandem mass tags: A novel quantification strategy for comparative analysis of complex protein mixtures by MS/MS', *Analytical Chemistry*, 75(8), pp. 1895–1904. doi:10.1021/ac0262560.
- Thomson, T.M., Balcells, C. and Cascante, M. (2019) 'Metabolic Plasticity and Epithelial-Mesenchymal Transition', *Journal of Clinical Medicine*, 8(7), p. 967. doi:10.3390/jcm8070967.
- Tian, Y. *et al.* (2019) 'Quality and efficiency assessment of six extracellular vesicle isolation methods by nano-flow cytometry', *Journal of Extracellular Vesicles*, 9(1). doi:10.1080/20013078.2019.1697028.
- Tidball, J.G. (1992) 'Identification and distribution of a novel, collagen-binding protein in the developing subepicardium and endomysium', *Journal of Biological Chemistry*, 267(29), pp. 21211–21219.
- Toledano, S. *et al.* (2019) 'Class-3 semaphorins and their receptors: Potent multifunctional modulators of tumor progression', *International Journal of Molecular Sciences*, 20(3). doi:10.3390/ijms20030556.
- Tomanek, R.J. *et al.* (1998) 'VEGF and bFGF stimulate myocardial vascularization in embryonic chick', *American journal of physiology*, 274(5 Pt 2), pp. 1620–1626.
- Tomanek, R.J. *et al.* (1999) 'Vascular endothelial growth factor expression coincides with coronary vasculogenesis and angiogenesis', *Developmental Dynamics*, 215(1), pp. 54–61. doi:10.1002/(SICI)1097-0177(199905)215:1<54::AID-DVDY6>3.0.CO;2-0.
- Tomanek, R.J. *et al.* (2001) 'Vascular Endothelial Growth Factor and Basic Fibroblast Growth Factor Differentially Modulate Early Postnatal Coronary Angiogenesis', *Circulation Research*, 88(11), pp. 1135–1141. doi:10.1161/hh1101.091191.
- Tomanek, R.J. *et al.* (2002) 'Role of VEGF family members and receptors in coronary vessel formation', *Developmental Dynamics*, 225(3), pp. 233–240. doi:10.1002/dvdy.10158.
- Tsuda, T. *et al.* (2001) 'Fibulin-2 expression marks transformed mesenchymal cells in developing cardiac valves, aortic arch vessels, and coronary vessels', *Developmental Dynamics*, 222(1), pp. 89–100. doi:10.1002/dvdy.1172.

- Tsuda, T., Majumder, K. and Linask, K. (1998) 'Differential expression of flectin in the extracellular matrix and left-right asymmetry in mouse embryonic heart during looping stages', *Developmental Genetics*, 23(3), pp. 203–214.
- Ullah, M.S., Davies, A.J. and Halestrap, A.P. (2006) 'The plasma membrane lactate transporter MCT4, but not MCT1, is up-regulated by hypoxia through a HIF-1 $\alpha$ -dependent mechanism', *Journal of Biological Chemistry*, 281(14), pp. 9030–9037. doi:10.1074/jbc.M511397200.
- Vega-Hernández, M. *et al.* (2011) 'FGF10/FGFR2b signaling is essential for cardiac fibroblast development and growth of the myocardium', *Development*, 138(15), pp. 3331–3340. doi:10.1242/dev.064410.
- Vierkotten, S., Muether, P.S. and Fauser, S. (2011) 'Overexpression of HTRA1 leads to ultrastructural changes in the elastic layer of Bruch's membrane via cleavage of extracellular matrix components', *PLoS ONE*, 6(8). doi:10.1371/journal.pone.0022959.
- Visconti, R.P. and Markwald, R.R. (2006) 'Recruitment of new cells into the postnatal heart: Potential modification of phenotype by periostin', *Annals of the New York Academy of Sciences*, 1080, pp. 19–33. doi:10.1196/annals.1380.003.
- Vogiatzidis, K. *et al.* (2015) 'Physiology of pericardial fluid production and drainage', *Frontiers in Physiology*, 6(MAR), pp. 1–6. doi:10.3389/fphys.2015.00062.
- Vogt, E.J. *et al.* (2019) 'Anchoring cortical granules in the cortex ensures trafficking to the plasma membrane for post-fertilization exocytosis', *Nature Communications*, 10(1), pp. 2–5. doi:10.1038/s41467-019-10171-7.
- Volz, K.S. *et al.* (2015) 'Pericytes are progenitors for coronary artery smooth muscle', *eLife*, 4, pp. 1–22. doi:10.7554/elife.10036.
- Walbrech, G., Margue, C., *et al.* (2020) 'Distinct cargos of small extracellular vesicles derived from hypoxic cells and their effect on cancer cells', *International Journal of Molecular Sciences*, 21(14), pp. 1–19. doi:10.3390/ijms21145071.
- Walbrech, G., Lecha, O., *et al.* (2020) 'Hypoxia-induced adaptations of miRNomes and proteomes in melanoma cells and their secreted extracellular vesicles', *Cancers*, 12(3), pp. 1–25. doi:10.3390/cancers12030692.
- Wan, L. *et al.* (2019) 'Exosomes from activated hepatic stellate cells contain GLUT1 and PKM2: a role for exosomes in metabolic switch of liver nonparenchymal cells', *FASEB Journal*, 33(7), pp. 8530–8542. doi:10.1096/fj.201802675R.
- Wang, J. *et al.* (2013) 'Fibronectin is deposited by injury-activated epicardial cells and is necessary for zebrafish heart regeneration', *Developmental Biology*, 382(2), pp. 427–435. doi:10.1016/j.ydbio.2013.08.012.
- Wang, X. *et al.* (2020) 'Microenvironment stiffness requires decellularized cardiac extracellular matrix to promote heart regeneration in the neonatal mouse heart', *Acta Biomaterialia*, 113, pp. 380–392. doi:10.1016/j.actbio.2020.06.032.
- Wang, Z. *et al.* (2019) 'Decellularized neonatal cardiac extracellular matrix prevents widespread ventricular remodeling in adult mammals after myocardial infarction', *Acta Biomaterialia*, 87, pp. 140–151. doi:10.1016/j.actbio.2019.01.062.
- Wei, X. *et al.* (2016) 'Surface phosphatidylserine is responsible for the internalization on microvesicles derived from hypoxia-induced human bone marrow mesenchymal stem cells into human endothelial cells', *PLoS ONE*, 11(1), pp. 1–16. doi:10.1371/journal.pone.0147360.

- Wessels, A. *et al.* (2012) 'Epicardially derived fibroblasts preferentially contribute to the parietal leaflets of the atrioventricular valves in the murine heart', *Developmental Biology*, 366(2), pp. 111–124. doi:10.1016/j.ydbio.2012.04.020.
- Wessels, A. and Pérez-Pomares, J.M. (2004) 'The Epicardium and Epicardially Derived Cells (EPDCs) as Cardiac Stem Cells', *Anatomical Record - Part A Discoveries in Molecular, Cellular, and Evolutionary Biology*, 276(1), pp. 43–57. doi:10.1002/ar.a.10129.
- Westermann, D. *et al.* (2006) 'Inhibition of p38 mitogen-activated protein kinase attenuates left ventricular dysfunction by mediating pro-inflammatory cardiac cytokine levels in a mouse model of diabetes mellitus', *Diabetologia*, 49(10), pp. 2507–2513. doi:10.1007/s00125-006-0385-2.
- van Wijk, B. *et al.* (2012) 'Cardiac Regeneration from Activated Epicardium', *PLoS ONE*, 7(9). doi:10.1371/journal.pone.0044692.
- Wilkins, E. *et al.* (2017) *European Cardiovascular Disease Statistics 2017*, European Heart Network. Available at: [www.ehnheart.org](http://www.ehnheart.org).
- Williams, C. *et al.* (2014) 'Young developmental age cardiac extracellular matrix promotes the expansion of neonatal cardiomyocytes in vitro', *Acta Biomaterialia*, 10(1), pp. 194–204. doi:10.1016/j.actbio.2013.08.037.
- Wu, Q. *et al.* (2020) 'Extracellular vesicles from human embryonic stem cell-derived cardiovascular progenitor cells promote cardiac infarct healing through reducing cardiomyocyte death and promoting angiogenesis', *Cell Death and Disease*, 11(5). doi:10.1038/s41419-020-2508-y.
- Wynn, T.A. and Ramalingam, T.R. (2012) 'Mechanisms of fibrosis: Therapeutic translation for fibrotic disease', *Nature Medicine*, 18(7), pp. 1028–1040. doi:10.1038/nm.2807.
- Xing, Q. *et al.* (2021) 'Basement membrane proteins modulate cell migration on bovine pericardium extracellular matrix scaffold', *Scientific Reports*, 11(1), pp. 1–10. doi:10.1038/s41598-021-84161-5.
- Xu, X. *et al.* (2018) 'Transforming growth factor- $\beta$  in stem cells and tissue homeostasis', *Bone Research*, 6(1). doi:10.1038/s41413-017-0005-4.
- Yamagishi, T. *et al.* (1999) 'Bone morphogenetic protein-2 acts synergistically with transforming growth factor-beta3 during endothelial-mesenchymal transformation in the developing chick heart', *J Cell Physiol*, 180(1), pp. 35–45. doi:10.1002/(SICI)1097-4652(199907)180:1<35::AID-JCP4>3.0.CO;2-R.
- Yang, J.T., Rayburn, H. and Hynes, R.O. (1995) 'Cell adhesion events mediated by  $\alpha$ 4 integrins are essential in placental and cardiac development', *Development*, 121(2), pp. 549–560. doi:10.1242/dev.121.2.549.
- Yang, W. *et al.* (2021) 'A Functional Variant Rs492554 Associated With Congenital Heart Defects Modulates SESN2 Expression Through POU2F1', *Frontiers in Cell and Developmental Biology*, 9(June). doi:10.3389/fcell.2021.668474.
- Yano, T. *et al.* (2005) 'Intracardiac fibroblasts, but not bone marrow derived cells, are the origin of myofibroblasts in myocardial infarct repair', *Cardiovascular Pathology*, 14(5), pp. 241–246. doi:10.1016/j.carpath.2005.05.004.
- Yetkin-Arik, B. *et al.* (2019) 'Endothelial tip cells in vitro are less glycolytic and have a more flexible response to metabolic stress than non-tip cells', *Scientific Reports*, 9(1), pp. 1–17. doi:10.1038/s41598-019-46503-2.



- Yoshioka, Y. *et al.* (2013) 'Comparative marker analysis of extracellular vesicles in different human cancer types', *Journal of Extracellular Vesicles*, 2(1), pp. 1–9. doi:10.3402/jev.v2i0.20424.
- Zhang, C.S. *et al.* (2019) 'Hypoxic preconditioning BMSCs-exosomes inhibit cardiomyocyte apoptosis after acute myocardial infarction by upregulating MicroRNA-24', *European Review for Medical and Pharmacological Sciences*, 23(15), pp. 6691–6699. doi:10.26355/eurrev\_201908\_18560.
- Zhang, J. *et al.* (2012) 'Extracellular matrix promotes highly efficient cardiac differentiation of human pluripotent stem cells: The matrix sandwich method', *Circulation Research*, 111(9), pp. 1125–1136. doi:10.1161/CIRCRESAHA.112.273144.
- Zhang, L. *et al.* (2019) 'Hypoxia preconditioned renal tubular epithelial cell-derived extracellular vesicles alleviate renal ischaemia-reperfusion injury mediated by the HIF-1 $\alpha$ /rab22 pathway and potentially affected by microRNAs', *International Journal of Biological Sciences*, 15(6), pp. 1161–1176. doi:10.7150/ijbs.32004.
- Zhao, C. *et al.* (2014) 'Numb family proteins are essential for cardiac morphogenesis and progenitor differentiation', *Development (Cambridge)*, 141(2), pp. 281–295. doi:10.1242/dev.093690.
- Zheng, W. *et al.* (2001) 'Mechanisms of coronary angiogenesis in response to stretch: role of VEGF and TGF-beta.', *American journal of physiology. Heart and circulatory physiology*, 280(2), pp. H909–H917.
- Zhou, B. *et al.* (2011) 'Adult mouse epicardium modulates myocardial injury by secreting paracrine factors', *Journal of Clinical Investigation*, 121(5), pp. 1894–1904. doi:10.1172/JCI45529.
- Zhou, P. *et al.* (2016) 'Decellularization and Recellularization of Rat Livers With Hepatocytes and Endothelial Progenitor Cells', *Artificial Organs*, 40(3), pp. E25–E38. doi:10.1111/aor.12645.
- Zhu, J. *et al.* (2018) 'Myocardial reparative functions of exosomes from mesenchymal stem cells are enhanced by hypoxia treatment of the cells via transferring microRNA-210 in an nSMase2-dependent way', *Artificial Cells, Nanomedicine and Biotechnology*, 46(8), pp. 1659–1670. doi:10.1080/21691401.2017.1388249.
- Zhu, L.P. *et al.* (2018) 'Hypoxia-elicited mesenchymal stem cell-derived exosomes facilitates cardiac repair through miR-125b-mediated prevention of cell death in myocardial infarction', *Theranostics*, 8(22), pp. 6163–6177. doi:10.7150/thno.28021.
- Zito, F. (2012) 'Role of extracellular matrix in regulating embryonic epithelial-mesenchymal transition', *Biomolecular Concepts*, 3(4), pp. 333–344. doi:10.1515/bmc-2011-0065.

# RESUMEN

---



# Resumen

---

## Introducción

### 1. Antecedentes

El corazón es un órgano complejo cuya función es crucial para la supervivencia del individuo. Dicho órgano está compuesto por un grupo muy heterogéneo de células que coordinan sus funciones específicas para garantizar la contracción e irrigación vascular. Paradójicamente, esta red de células se forma inicialmente a partir de una estructura tubular sencilla compuesta principalmente por dos tipos celulares: el endocardio y el miocardio. Durante fases más tardías del desarrollo, un tercer tipo celular, el epicardio, un conjunto de células epiteliales de origen extracardiaco, se incorpora a la superficie del corazón hasta envolver el miocardio. Posteriormente, estas células sufren un proceso de transición epitelio-mesénquima (TEM) por el cual migran hacia el interior de la pared del miocardio y dan lugar a diferentes tipos de células cardíacas más especializadas. Estas células derivadas del epicardio (CDEP) constituyen parte elemental de la histoarquitectura del corazón desde la ontogenia hasta la vida adulta. Además, tienen un papel esencial en el desarrollo del órgano a través de su secretoma.

#### 1.1. El epicardio embrionario como fuente de células del intersticio cardíaco

El corazón adulto está formado por un gran número de células heterogéneas en origen, diversidad y función biológica. Sin embargo, la mayor parte de las células del intersticio cardíaco adulto, el espacio existente entre las fibras musculares cardíacas, tienen su origen en el epicardio embrionario. Esta capa de células epiteliales se genera a partir de una estructura celular extracardiaca llamada proepicardio (PE), la cual está situada en el polo arterial del corazón (E9.5 en el ratón, HH16/17 en pollo y alrededor de la cuarta semana de gestación en humanos). En estadios inmediatamente posteriores, el PE alcanza la superficie del corazón, momento en el cual se adhiere y expande sobre su superficie, dando lugar al epicardio. Tras un proceso de TEM, las CDEP se diferencian a diferentes tipos celulares cardíacos. Por un lado, dan lugar a los primeros fibroblastos cardíacos (FC) que colonizan el intersticio cardíaco; y a los vasos coronarios, compuestos

por células endoteliales, que forman la región más interna del vaso, y células murales como pericitos o células musculares lisas, que constituyen su pared. Estas células murales estabilizan los vasos mediante interacciones físicas y moleculares con células endoteliales. Todos estos tipos celulares están involucrados en cambios fisiológicos tanto en homeostasis como en el contexto de enfermedades cardíacas, especialmente en las que cursan con fibrosis.

Nuestro grupo de investigación 'Desarrollo y enfermedades cardiovasculares' lleva más de 20 años trabajando en este tema y ha demostrado, entre otras cosas, el origen epicárdico de los FC que responden al daño isquémico en corazón adulto.

### **1.2. El epicardio como fuente de componentes cardíacos no celulares**

Durante el desarrollo, la acumulación progresiva de moléculas secretadas por diferentes tipos de células cardíacas constituye la MEC cardíaca. En fases tempranas (E8,5-10,5), el espacio entre cardiomiocitos es escaso y, consecuentemente, la MEC acumulada entre estas células también. En estadios posteriores (E11,5), la MEC se reduce al espacio extracelular existente entre los cardiomiocitos, el presente entre el miocardio y el epicárdico (matriz subepicárdica), y el que se encuentra entre el miocardio y el endocardio (matriz subendocárdica). En este estadio, los principales componentes de la MEC cardíaca son fibronectina y colágenos I, IV, V y VI, seguido de otras proteínas relevantes como lamininas y proteoglicanos, fibrilina-2, elastina, vitronectina, tenascina-X, flectina y fibulina-2, entre otras moléculas. Además, de las moléculas que ofrecen soporte estructural, otras como factores de crecimiento (FGF, VEGF, HGF, TGF $\beta$ , BMP, entre otros) también se encuentran acumulados en la MEC.

En condiciones patológicas, como el infarto cardíaco, la muerte de cardiomiocitos activa modificaciones extensas en la MEC, tanto localmente como en zonas más remotas al daño. Una de las causas principales incluye la activación de FC y una de las principales consecuencias es el cambio mecánico y estructural del corazón. En este caso, los FC migran hacia el área dañada y secretan grandes cantidades de colágeno para reponer la arquitectura del miocardio y evitar su colapso. Tal respuesta conduce a una acumulación de proteínas de la matriz y culmina, generalmente, en fibrosis. Por otro lado, otros agentes celulares también participan en este proceso, como son las células circulantes, células endoteliales o pericitos, lo cual motiva la degradación de la matriz mediante

secreción de proteinasas y participando en la remodelación continua de la MEC en el lugar del daño. De esta forma, la MEC cardiaca no es solamente necesaria para garantizar la integridad física del musculo cardiaco, sino también lo es para articular señales intercelulares que determinan la homeostasis cardíaca y la respuesta patológica del órgano al daño.

### **1.3. El secretoma de las CDEP en la comunicación intercelular del corazón**

En este contexto, las CDEP, pioneras en la invasión del miocardio, pueden ser consideradas como una de las mayores fuentes de componentes de la MEC cardiaca embrionaria, aunque su contribución no haya sido considerablemente caracterizada. En concreto, la MEC y otros componentes bioactivos, como las vesículas extracelulares (VEs) derivados de epicardio/CDEP, participan en una red compleja de señalización que afecta el estado celular y la estabilidad de la matriz, participando en el desarrollo natural del órgano y en condiciones fisiológicas del corazón adulto.

Las células epicárdicas secretan moléculas que, entre otros procesos, incitan la proliferación del miocardio. Aunque se ha descrito una serie de mecanismos moleculares específicos que regulan la actividad del epicardio, como la vía Wt1/ácido retinoico, no se conoce la composición completa del secretoma de las CDEP. Por este motivo, uno de los objetivos principales de esta tesis es la caracterización de las VEs derivadas de células epicardicas.

Las VEs son vesículas secretadas, virtualmente, por todas las células del organismo. Estas vesículas cargan componentes celulares, como ácidos nucleicos, proteínas y lípidos, presentes en sus células de origen que van a desarrollar activamente su función en células receptoras. Su caracterización y función son todavía ambiguos debido a diferentes factores, como son su heterogeneidad, la complejidad asociada a su biogénesis y los mecanismos de secreción, además de las enormes limitaciones técnicas en términos de reproducibilidad asociadas al trabajo con las VEs. En función a estas variables, las VEs se clasifican en exosomas, microvesiculas o cuerpos apoptóticos, siendo principalmente su biogénesis la que marca su tamaño y ayuda a su definición.

Las VEs más estudiadas son los exosomas (de 30 a 150 nm) y las microvesículas (de 50 a 200 nm). Esta similitud en tamaños dificulta la obtención de fracciones

purificadas de poblaciones específicas de VEs, por lo que en 2018 la Sociedad Internacional de Vesículas Extracelulares (*ISEV* de su nombre en inglés) se estableció una nomenclatura para mejor definir las poblaciones de VEs basada en sus tamaños, densidades y composición proteica. En dicha clasificación se especifica que las VEs menores 100 nm son considerados VEs de pequeño tamaño; las VEs de entre 100 y 200 nm se denominan VEs de medio tamaño; y las mayores de 200 nm se denominan VEs de gran tamaño. Además, se han establecido ciertos criterios para distinguirlas según el tipo de proteínas transmembranales o citosólicas que contienen, lo que permite que se pueda estimar el grado de enriquecimiento en un tipo de VE o en otro que se ha obtenido en una muestra concreta y el nivel de pureza de esta.

En cuanto a su biogénesis, la formación de exosomas es dependiente de la producción de endosomas denominados cuerpos multivesiculares (CMV). Las membranas de los CMV son internalizadas, formando las vesículas intraluminales (VILs) mediante un proceso dependiente o no del complejo endosomal necesario para el transporte (*ESCRT* de su nombre en inglés). Durante este proceso, ciertas moléculas son seleccionadas para integrar el contenido de los exosomas. Así, su mecanismo de formación y carga puede señalar su degradación lisosomal o bien su secreción hacia el ambiente extracelular. Por el contrario, las microvesículas se forman a partir de evaginaciones de la membrana plasmática. Se ha descrito que su origen está relacionado con el cambio de la composición de lípidos de la membrana y con los niveles de calcio intracelular, procesos que pueden conducir a la reorganización de la membrana plasmática y, consecuentemente, a la formación de microvesículas. En este sentido, las moléculas constituyentes de las paredes de las microvesículas parecen estar relacionadas con su afinidad para las balsas de lípidos que se localizan en las zonas de evaginación.

En los últimos años, el interés clínico por las VEs ha crecido exponencialmente, debido a su valor como biomarcador tanto pronóstico como diagnóstico de patologías concretas y al potencial terapéutico de su carga. Sin embargo, hoy en día resulta complicado asociar un posible beneficio a un componente del contenido vesicular concreto, debido a la heterogeneidad del cargo y a la dificultad de conocer con certeza el origen celular de las VEs de interés. En este sentido, sólo un estudio ha puesto de manifiesto la relevancia clínica de las VEs secretadas por el epicardio. Dicho estudio se ha

centrado en la caracterización de los miRNA que forman parte del cargo de dichas VEs, pero no en el resto de sus componentes.

Por otro lado, y tal y cómo se ha explicado anteriormente, la MEC es fundamental para la señalización celular y soporte del órgano, así como para incitar respuestas específicas a señales locales. Para posibilitar el estudio de la MEC cardiaca, es crucial establecer un método de descelularización y preparación de muestras que permita obtener el mínimo de proteínas intracelulares y mantener al máximo la composición inicial de las proteínas extracelulares. El problema es que cuando se aplican estos métodos al tejido cardiaco al completo, se pierde el trazado ontogénico y, por tanto, la posibilidad de conocer la contribución de poblaciones específicas a la composición de la MEC.

Esta tesis doctoral se ha enfocado en el estudio de una parte de este secretoma, todavía por explorar en la comunidad científica: (1) las vesículas extracelulares (VEs) y (2) la matriz extracelular (MEC). Debido a la limitación del número celular del tejido de interés, este trabajo se ha centrado en el estudio del secretoma de una línea celular derivada del epicardio embrionario, denominada EPIC, que se generó en nuestro laboratorio a partir de epicardio embrionario murino y que representa fielmente al tejido originario a partir del cual se creó.

#### **1.4. El papel del epicardio en enfermedades cardiovasculares**

Las enfermedades cardiovasculares son unas de las causas principales de muerte en países desarrollados. Aunque esté establecido de que el diagnóstico prematuro y su tratamiento son clave para aumentar la esperanza media de vida del individuo, el conocimiento limitado de determinados mecanismos fisiopatológicos dificulta el progreso en el desarrollo de terapias eficaces.

De forma general, las enfermedades cardiacas comienzan con una mala función o la muerte de cardiomiocitos. La primera respuesta natural a este proceso es la activación de células no musculares localizadas en el intersticio cardiaco, las cuales van a acabar transformando la arquitectura celular de la pared ventricular. En corazones adultos, la respuesta a la pérdida de una cantidad substancial de células conlleva una activación de mecanismos reparativos basados en la sustitución de tejido del parenquimatoso por un



tejido fibroso. Este fenómeno se denomina fibrosis y, aunque existan señales comunes en el proceso fibrótico de distintos órganos, se han descrito diferencias significativas entre ellos. En todo proceso fibrótico los FC son las células intersticiales con mayor responsabilidad, ya sea por su activación rápida en respuesta a daño agudo, primariamente local, masivo y rápido, como ocurre en cardiomiopatía isquémica o en infarto agudo de miocardio; o bien están crónicamente activados y continuamente secretando pequeñas cantidades de MEC durante un periodo prolongado en el tiempo, como en la cardiomiopatía dilatada.

Para solucionar el problema, muchos laboratorios emplean estrategias de generación de cardiomiocitos funcionales en el corazón infartado. Sin embargo, hay pocos laboratorios focalizados en el estudio de los mecanismos moleculares que regulan la biología de los FC y, por tanto, puedan repercutir en el tamaño de la fibrosis e intentar minimizarla. Esto hace que la identificación de mecanismos de señalización celular de tipos celulares cardiacos concretos sea crucial para el desarrollo de tratamientos farmacológicos específicos y personalizados.

En este contexto, el epicardio adulto tiene mucho interés para la comunidad científica ya que varios grupos han descrito su reactivación tras un infarto. Teniendo en cuenta su papel esencial en el desarrollo del órgano, dicha reactivación podría aportar tanto células intersticiales *de novo* como componentes extracelulares de señalización clave en el proceso de remodelado ventricular. Además, recientemente, se ha hipotetizado sobre su papel como fuente mayoritaria de la composición del líquido pericárdico, lo cuál sería clave a la hora de buscar biomarcadores que indiquen el estado del corazón en un contexto patológico. Esto supondría un punto de partida para el estudio de VEs derivadas de epicardio como biomarcadores en diferentes enfermedades cardiovasculares.

## 2. Hipótesis y objetivos

La hipótesis general en la que se basa esta tesis es que **la caracterización de secretoma de células derivadas del epicardio, especialmente en las fracciones de las VEs y la MEC, contribuirá a la comprensión de los mecanismos celulares y moleculares que regulan el proceso de desarrollo del corazón y que, por tanto, pueden estar implicados en respuestas cardiacas a estímulos patológicos.**

El objetivo principal de estas tesis es definir la composición y función de las VEs y la MEC derivadas del epicardio embrionario. Para su consecución, se han desarrollado experimentos de caracterización física de estos componentes del secretoma epicárdico; se ha estudiado su perfil molecular mediante proteómica; y se ha realizado un análisis funcional *in silico* de dichas proteínas, cuyos resultados han sido validados *in vitro* para determinar su papel en la interacción celular cardiaca, tanto a nivel autocrino como paracrino.

### 3. Resultados

#### 3.1. Capítulo I: caracterización y comparación de VEs derivadas de epicardio aisladas por dos métodos distintos: ultracentrifugación vs cromatografía de exclusión por tamaño

Para estudiar y caracterizar las VEs derivadas de epicardio se ha recurrido a dos de las técnicas de aislamiento más comunes: ultracentrifugación (UC) y cromatografía de exclusión por tamaño (SEC). Para determinar el mejor método de aislamiento, se han realizado diversas técnicas de caracterización y análisis de la población obtenida: dispersión dinámica de luz (*DLS* de su nombre en inglés), análisis de movimiento de nanopartículas (*NTA* de su nombre en inglés), microscopía electrónica de transmisión (MET), cuantificación de proteínas por métodos colorimétricos y western blot.

En primer lugar, las VEs aisladas por ambos métodos presentan una conformación cóncava, típicamente descrita en la literatura. Sin embargo, las VEs aisladas por SEC (VEs-SEC) presentan también deformaciones y agrupaciones de vesículas y de restos de membranas celulares que ponen en duda la conservación de la integridad de las membranas de las VEs aisladas por este método. A continuación, se estudió si la media de los tamaños de vesículas aisladas por ambos los métodos son distinta. Para tal propósito, se emplearon dos métodos: DLS y NTA. Los resultados del análisis de tamaño por DLS presentan diámetros más grandes que los presentados por NTA en VEs-SEC y VEs-UC, siendo esta diferencia significativa entre DLS y NTA de VEs-UC. En este sentido, se ha observado una mayor reproducibilidad en las réplicas medidas con NTA que en las que se midieron por DLS. Además, una de las ventajas del NTA en comparación con el DLS es que permite inferir la concentración de partículas en solución. En este caso, ambas muestras de VEs-SEC y VEs-UC presentan concentraciones similares de VEs, aunque la concentración de nanopartículas medidas en VEs-UC en el rango entre los 76 y los 210 nm es significativamente más alta que en VEs-SEC. Este resultado se refleja también en la cantidad de nanopartículas secretadas por millón de EPIC. Finalmente, VEs-SEC presentan una cantidad proteica mayor que las VEs-UC. Cuando inferimos la cantidad de proteína existente por partícula, VEs-SEC también presenta un valor estadísticamente más elevado que las VEs-UC.

Para comparar el grado de enriquecimiento de las VEs aisladas por ambos métodos, se realizaron análisis por western blot de proteínas asociadas a exosomas,

como son ALIX y TSG101. Las VEs-UC presentan una banda relativamente más intensa para ALIX que en SEC. En consonancia, TSG101 fue identificada en VEs-UC pero no en VEs-SEC.

Debido a los resultados de este estudio inicial, se decidió continuar con las VEs aisladas por UC para realizar la caracterización de proteómica y los análisis funcionales *in vitro* de interés para la consecución de esta tesis.

A continuación, se realizó los mismos procedimientos experimentales para caracterizar VEs derivados de EPIC incubados previamente con un 5% oxígeno (VEs-H5%) y de EPIC cultivados en normoxia (~20% oxígeno; VEs-N). Estos estudios confirmaron que los cambios de presión de oxígeno en las células parentales no modificaron las propiedades físicas de las VEs. Al calcular el tamaño medio de ambos tipos de VEs, verificamos que presentan tamaños similares entre si cuando medidos tanto con DLS como con NTA.

Finalmente, se analizó la cantidad de VEs aisladas a partir de ambas condiciones de cultivo, y se verificó que no difieren estadísticamente. Sin embargo, al distribuir las concentraciones de partículas por tamaño se verifica que EPIC incubadas a 5% oxígeno secretan significativamente más VEs del rango entre 166 y 210 nm de que en normoxia. Aún así, la cantidad de VEs estimada que sea secretada por cada millón de EPIC en ambas condiciones no representa un cambio significativo. Relativamente a la cantidad de proteína estimada, se verifica que VEs-N y VEs-H5% presentan una cantidad similar de proteínas, aunque se detectó una clara diferencia en la marca de ALIX y TSG101 entre ambas muestras. Ambas proteínas están presentes en VEs-H5%, mientras que en VEs-N se aprecia una reducción en la marca de ALIX y la ausencia de TSG101.

### **3.2. Capítulo II: caracterización proteómica y validación funcional del efecto de la hipoxia en vesículas extracelulares derivadas de epicardio**

El siguiente grupo de experimentos se orientaron a la identificación de diferencias en la composición proteómica de VEs-N frente a VEs-H5%. Para ello, se empleó una técnica proteómica de marcaje múltiple para disminuir la variabilidad técnica asociada al análisis proteómico independiente de muestras.

En primer lugar, se comparó la reproducibilidad y profundidad de lectura entre dos tipos de etiquetado masivo en tándem (*Tandem Mass Tag* (TMT) en inglés): TMT2plex y TMT6plex. De esta forma, se observó que la técnica TMT2plex no permitía identificar determinados péptidos entre todas las réplicas biológicas estudiadas en comparación con el TMT6plex. Por tanto, se continuó el estudio de los datos generados por el TMT6Plex.

A continuación, se procedió a la caracterización proteómica de ambos tipos de VEs. El primer análisis de las muestras se enfocó en determinar la diferencia en la abundancia de las proteínas identificadas en VEs-N vs. VEs-H5%. Mediante un análisis de enriquecimiento funcional, verificamos que la mayoría de las proteínas encontradas en ambas muestras están asociadas a términos de ontología genética (a partir de ahora “GO terms” por su nombre en inglés) como “vesículas extracelulares”, “membrana” y “citósol”. A partir de este análisis, se identificaron las 24 proteínas comunes en ambos tipos de VEs, 14 de las cuales se asociaron a membranas celulares. Entre ellas destacamos fibronectina, vimentina, lactaderina,  $\alpha$ -tubulina 2, *heat shock 70 kDa protein 8*, miosina-9, anexinas 2 y 5, enolase, Alix y *clathrin heavy chain 1*, las cuales han sido descritas como importantes en el desarrollo cardiovascular según bibliografía.

### 3.2.1. La hipoxia afecta al contenido de las vesículas extracelulares derivadas del epicardio

El siguiente análisis identificó las proteínas significativamente diferenciales entre ambos tipos de VEs. Las VEs-H5% contienen una mayor acumulación de proteínas relacionados con el proceso de glicólisis, entre ellos, triosefosfato isomerase 1 (TPI1), transportador de monocarboxilato 4 (MCT4), fosfoglicerato mutase 1 (PGAM) y fosfoglicerato quinase 1 (PGK1). En contra, las proteínas significativamente representadas en las VEs-N fueron *complement component receptor 1-like protein*, *major vault protein*, *clathrin light chain B*, trombospondina-1, proteína 60S ribosomal L14, *immunoglobulin superfamily containing leucine-rich repeat protein*, glicoproteína asociada a membrana lisosomal 2 y *ferritin light chain 1 and 2*. Estos resultados, junto con la bibliografía consultada sobre el tema, sugieren que las VEs obtenidas en hipoxia podrían contener un potencial glucolítico y, por tanto, podrían

afectar significativamente a la capacidad proliferativa de células receptoras, al igual que a su metabolismo, de forma autocrina y paracrina.

Para confirmar esta hipótesis de trabajo, se realizó un ensayo de proliferación basado en la incorporación de Edu tanto en EPIC como en células endoteliales de cordón umbilical humano (*HUVECs* de su nombre en inglés). Para ello, incubamos las EPIC y las *HUVECs* con VEs-N y VEs-H5% a 20 y 50  $\mu\text{g}/\text{mL}$ . Previamente, se confirmó la internalización de VEs derivados de EPIC en EPIC y *HUVECs* usando microscopia TIRF. De esta forma, se verificó que VEs derivados de EPIC no inducen proliferación ni de manera autocrina ni paracrina.

A continuación, se utilizó un ensayo metabólico que permite la medición de la actividad glucolítica de EPIC y *HUVECs* incubadas con VEs-N y VEs-H5%, a concentraciones de 20 y 50  $\mu\text{g}/\text{mL}$ .

No se observaron diferencias significativas ni en EPIC ni en *HUVECs* incubados con VEs derivados de EPIC. Sin embargo, se observó una tendencia al alza en células cultivadas con VEs-H5%, lo que sugería que la hipoxia podría estar afectando al cargo de las VEs. Para confirmar esta hipótesis, se aumentó el nivel de hipoxia en cultivos EPIC hasta el 1% de oxígeno antes de aislar las VEs. En concordancia a los resultados previos, la incubación de 50  $\mu\text{g}/\text{mL}$  de VEs-H1% con EPIC generó un aumento significativo en proliferación al comparar con condiciones basales (0% FBS) y con EPIC incubados con VEs-N. Por otro lado, el aumento en el nivel de proliferación también fue observado en *HUVECs* incubadas con 50  $\mu\text{g}/\text{mL}$  de VEs-H1%. Además, esta condición tampoco presenta una diferencia significativa relativamente al control positivo (medio de cultivo completo para *HUVECs*, medio EGM).

En relación al metabolismo glucolítico de EPIC incubados con VEs-H1%, se verificó que el flujo de protones de EPIC incubados con 20  $\mu\text{g}/\text{mL}$  de VEs-H1% es más alto que en 50  $\mu\text{g}/\text{mL}$  VEs-H1%, 0% FBS y 10% FBS al largo del experimento. En *HUVECs*, por otro lado, el flujo de protones es más elevado cuando incubados con 50  $\mu\text{g}/\text{mL}$  de VEs-H1% que las restantes condiciones. Además, se verifica que su capacidad glucolítica es significativamente más elevada cuando incubados con 50  $\mu\text{g}/\text{mL}$  VEs-H1% que VEs-H5% a la misma concentración.

### 3.3. Capítulo III: caracterización de matriz extracelular derivada de EPIC

Otro de los objetivos específicos de esta tesis es el estudio y la caracterización de la matriz extracelular (MEC) derivado del epicardio. Para poder caracterizar los componentes de MEC de las EPIC recurrimos a un método clásico de descelularización química basada en cambios osmóticos del medio inducidos por hidróxido de amonio. Al proceder a descelularización con hidróxido de amonio, obtenemos dos fracciones de MEC: el EPIC IM, que corresponde a la fracción insoluble, y el EPIC SM, correspondiente a la fracción soluble.

Como primer análisis, ambas fracciones se caracterizaron mediante estudios de inmunocitoquímica. En concreto, se utilizaron anticuerpos para detección de fibronectina y laminina  $\alpha 1$  en EPIC IM, SM y células EPIC, donde confirmamos su secreción por células EPIC, retención en superficies de cristal en EPIC IM y en solución EPIC SM. Debido a su naturaleza, la fracción EPIC IM quedó retenida en la superficie de cristal, lo cual permitió su visualización por microscopía electrónica de barrido (SEM) para un estudio exploratorio de su topografía en comparación con las muestras celularizadas. Este estudio verificó la estructura matricial de la fracción EPIC IM. En contra, la naturaleza soluble de la fracción EPIC SM no permitió su observación microscópica, dando una idea de las diferencias entre ambas fracciones.

Para profundizar más aún en esta observación, se procedió a la caracterización detallada de los componentes de ambas fracciones mediante un estudio proteómico *label-free*. En primer lugar, se observó una gran diversidad de proteínas intracelulares retenida en EPIC SM en comparación con EPIC IM. De estas, 85 proteínas de un total de 352 proteínas encontradas en la fracción EPIC IM son extracelulares mientras en EPIC SM corresponde a 153 proteínas sobre un total de 1702, en lo cual 53 se encuentran en ambas fracciones. A continuación, se realizó un análisis de enriquecimiento funcional de proteínas exclusivas en EPIC IM y proteínas exclusivas de EPIC SM. Ambas fracciones se encuentran enriquecidas en proteínas asociadas a funciones biológicas relacionadas con organización y estructura de MEC. Además, se observó un enriquecimiento en proteínas asociadas a *GO terms* relacionados con angiogénesis en la fracción EPIC IM, lo que sugiere un potencial específico para esta fracción de la MEC derivada de epicardio.

### 3.3.1. La matriz extracelular derivada de epicardio muestra más similitudes con la matriz cardiaca que con otras matrices comerciales

Como se ha comentado, tanto EPIC IM como SM están compuestas por proteínas anotadas a *GO terms* relacionadas con funciones extracelulares asociadas a la organización y estructura del MEC. Para contextualizar los resultados en función al origen celular de la MEC, se realizó una comparación con la MEC de corazones E17,5 de celularizados. MEC de corazones embrionarios comparten 33 proteínas extracelulares con EPIC IM y SM, 42 proteínas extracelulares con EPIC SM y 4 con EPIC IM, de un total de 1531 proteínas. Treinta y nueve proteínas extracelulares se identificaron en MEC de corazones de E17,5 que también presentan un enriquecimiento funcional significativo en proteínas relacionadas con la organización y estructura del MEC.

Posteriorment, se hizo un estudio de enriquecimiento funcional en STRING para detectar las anotaciones de procesos biológicos más significativos entre los grupos de proteínas según las muestras de partida. En primer lugar, las proteínas compartidas por EPIC IM, SM y MEC de corazones embrionarios se asociaron a procesos biológicos relacionados con las organización y estructura de la MEC. Cuando se emplean las proteínas compartidas entre la MEC de corazones embrionarios y la fracción EPIC SM, o bien las que comparte con la fracción EPIC IM se observan correlaciones de muy poco valor estadístico, indicando pocas diferencias funcionales entre la EPIC MEC y el corazón embrionario.

Para confirmar esto, se incluyó en el estudio proteómico al Matrigel comercial como referente de matrices extracelulares disponible en el mercado. Matrigel comparte 21 proteínas extracelulares con EPIC IM y SM, 7 proteínas con EPIC IM y 20 con EPIC SM, de un total de 309 proteínas. Del total de 89 proteínas extracelulares de Matrigel, 41 proteínas no fueron identificadas en ninguna de las 2 fracciones de EPIC. En relación a la correlación entre las proteínas compartidas entre EPIC IM, SM y Matrigel se encontraron de nuevo similitudes en procesos relacionados con organización del MEC y regulación de estructura y localización celular. Debido a la escasez, poca diversidad y baja correlación funcional en las proteínas extracelulares compartidas entre Matrigel y EPIC IM, la significancia encontrada con *GO terms* es baja. Matrigel comparte un mayor número de



proteínas con EPIC-SM que con EPIC-IM, pero de nuevo se verifica también una baja correlación entre términos ontológicos de procesos biológicos.

Finalmente, se identifican 17 proteínas extracelulares en común cuando se comparan todas las matrices estudiadas en esta tesis (EPIC IM, SM, Matrigel y MEC de corazones embrionarios). Al realizar un análisis *in silico* de estas proteínas, se verificó que los procesos biológicos más significativos son relativos a estructura, adhesión y diferenciación celular. Como perfiles proteómicos únicos, se observó que en Matrigel, las proteínas con mayor abundancia relativa son las lamininas, específicamente LAMA1 (33,09% de abundancia), LAMB1 (22,30%) y LAMC1 (19,43%). NDG1 (14,55% de abundancia) y HSPG2 (1,62%) también se encuentran de entre las cinco proteínas extracelulares más abundantes en Matrigel. Relativo a EPIC SM, después de FN (40,43% de abundancia), las proteínas extracelulares más abundantes son MYH9 (19,76%), HSP90B1 (2,92%), ANXA2 (2,55%) y HSPA5 (1,94%) del total de proteínas en solución. En EPIC IM es HTRA1 (15,21% de abundancia) que presenta mayor abundancia, seguido de CXCL12 (5,26%), FN (3,36%), EMILIN-1 (3,01%) y LAMA1 (2,76%). En corazones embrionarios es FN la proteína extracelular más abundante, aunque con abundancia relativa muy baja (0,82%), seguido de HSPG2 (0,61%), HSPA5 (0,28%), COL1A2 (0,27%) y MYH9 (0,23%) en relación al total de proteínas en solución.

A continuación, se validaron estos datos mediante western blot para las proteínas más abundantes: fibronectina y laminina. La fracción EPIC SM fue la más enriquecida en fibronectina.

Una vez realizados los estudios previamente descritos, se realizaron una serie de experimentos para validar el carácter matricial de ambas fracciones de la MEC derivada de epicardio. Para ello, se realizaron estudios de proliferación en HUVECs, en comparación con Matrigel, el *gold* estándar del mercado en estudios de este tipo. En este ensayo, se validó el potencial angiogénico de la fracción EPIC IM mediante un incremento en la capacidad proliferativa en HUVECs, 3 y 5 días después de incubar estas células con EPIC IM, EPIC SM, EPIC IM + EPIC SM, Matrigel, Matrigel + EPIC IM o 1% gelatina. Después de 3 días en incubación, HUVECs incubadas con EPIC SM o con Matrigel presentaron niveles de proliferación celular significativamente más bajos que en 1% gelatina. A los cinco días de incubación, HUVECs incubados con Matrigel o Matrigel + EPIC IM,

presentaron niveles de proliferación más bajos que HUVECs incubados con EPIC IM. Al considerar conjuntamente los tiempos de incubación usados, HUVECs sembrados sobre EPIC IM o EPIC SM mantienen su capacidad desde el tercero hasta el quinto día de incubación. En contra, Matrigel, Matrigel con EPIC IM o 1% gelatina bajaron los niveles de proliferación de HUVECs después de los 3 días de incubación.

## Discusión

Esta tesis doctoral se enfoca en la caracterización de una parte específica del secretoma de células EPIC: las vesículas extracelulares (VEs) y la matriz extracelular (MEC). En el primer capítulo, comparamos dos métodos de aislamiento de VEs extensamente revisados en la literatura, UC y SEC, para determinar cuál es el más adecuado. Tras un análisis de la morfología de las VEs, de la eficiencia de recuperación basado en el número de células parentales y en estudios de enriquecimiento y heterogeneidad poblacional de VEs basados en tamaño de partícula y composición de su membrana, se demuestra que el uso de la UC es el más adecuado. Esto coincide con los resultados publicados por otros grupos de investigación, donde demuestran que el uso de UC es el método más adecuado para la caracterización más genérica de VEs.

Una vez decidido el uso de este método, se procede al estudio del efecto de la hipoxia en células parentales de origen epicárdico sobre las VEs. A nivel de propiedades físico-morfológicas, no encontramos diferencias significativas, aunque si se detecta un enriquecimiento en VEs de medio tamaño. Este hecho puede explicar el cambio descrito a posteriori (capítulo II) a nivel de composición proteica de las VEs, el cual está enriquecido en proteínas relacionadas con el metabolismo glucolítico en VEs-H5%. En dicho capítulo se realiza la caracterización proteómica de VEs aisladas de ambos tipos de vesículas. Para ello, se procede a un experimento de TMT6plex, que reduce significativamente la variabilidad técnica del análisis. A partir de este análisis, se sugiere un patrón común en las VEs derivadas de epicardio aisladas en ambas condiciones, el cuál podría ser considerado como un set de potenciales marcadores de VEs con este origen. Aunque se requieren experimentos que validen esta hipótesis, esto ayudaría al uso de las VEs derivadas de epicardio como biomarcadores asociados a diferentes enfermedades cardiovasculares a identificar tanto en plasma como en otras biopsias líquidas más enriquecidas en este tipo de VEs, como el líquido pericárdico.

El análisis contrario revela que las VEs-H5% están enriquecidas en proteínas relacionadas con el metabolismo glucolítico en respuesta a hipoxia por parte de las células parentales. Este hecho resalta el posible papel de las VEs como mediadores en la señalización intercelular que ha sido descrito en otros contextos biológicos en literatura. En otros sistemas, células parentales sometidas a un estímulo determinado son capaces

de modificar el cargo de sus VEs, los cuales son capaces de afectar el metabolismo de células receptoras una vez que éstas los integran. La validación de esta hipótesis sería muy relevante para el campo, ya que permitiría estudiar el papel de la hipoxia sobre la biología del epicardio tanto en el desarrollo cardiovascular como en respuesta a estímulos patológicos.

Para evaluar esta hipótesis, se plantearon dos aproximaciones distintas (proliferación y estudio metabólico *in vitro*) con dos tipos celulares diferentes (EPIC y HUVECs) para evaluar este posible mecanismo de señalización intercelular cardiaca desde un punto de vista tanto autocrino como paracrino. A pesar de que se demuestra que las VEs derivadas de epicardio son integradas por parte de ambos tipos celulares, ninguna de las dos condiciones de VEs estudiados es capaz de inducir proliferación en EPIC ni en HUVECs. Además, no se observaron cambios en el comportamiento glucídico de ninguno de los tipos celulares estudiados. Con relación a posibles cambios en el metabolismo celular, cambios en el comportamiento glucolítico de ambos tipos celulares no fueron demostrados. Esto podrá ocurrir por la presencia de otras moléculas en el contenido de estos VEs, que podrían influir en la respuesta metabólica de las células receptoras, o bien por una cantidad insuficiente de VEs como para lograr una respuesta metabólica en estas células.

Para evaluar esto, decidimos aumentar el nivel de estrés hipóxico en las células parentales bajando la difusión de oxígeno en cultivos para 1%. En esta ocasión, el cargo de las VEs-1H% inducen el aumento significativo la capacidad proliferativa de EPIC. En relación a cambios potenciales del metabolismo glucolítico, las VEs-H1% no han inducido cambios en la respuesta glucolítica de EPIC. En HUVECs, VEs-H1% inducen una capacidad glucolítica más alta que con VEs-H5%. En concreto, este tipo de VEs inducen una respuesta más eficaz cuando demandas más altas de ATP es necesaria en HUVECs. Así, en este capítulo demostramos como al aumentar el nivel de hipoxia en células del epicardio se una mayor actividad glucolítica que pueden afectar a otros tipos celulares adyacentes.

Finalmente, en el último capítulo de resultados de esta tesis, se estudió otra fracción del secretoma de las EPIC, la MEC. Para su estudio, se procede a una

descelularización química, que generó dos fracciones de MEC: EPIC IM y EPIC SM. Mediante métodos de imagen con alta resolución, se verificó que la fracción EPIC IM conservaba cierta estructura arquitectónica tras el tratamiento de descclularización. Por otro lado, y combinando métodos de marcación por fluorescencia y microscopia, se confirmó que las muestras de EPIC IM presentaban redes de fibronectina y laminina, proteínas clave en la MEC de corazones embrionarios, mientras en EPIC SM estas proteínas se encuentran dispersas en la masa resultante del aislamiento.

A continuación, se realiza un estudio proteómico basado en la tecnología de *label free proteomics* de ambas fracciones. A las proteínas identificadas, se les aplicó un filtro de selección de proteínas extracelulares y se verificó una mayor presencia de proteínas extracelulares en EPIC SM que en EPIC IM. En ambas fracciones se encontró un enriquecimiento en proteínas que regulan la estructura y organización de la matriz, además de procesos biológicos relacionados con funciones epiteliales y mesenquimales. Entre ellos, destacan *GO terms* relacionados con angiogénesis en términos de abundancia proteica de ambas fracciones, en especial la EPIC IM.

Por otro lado, y dado el origen celular de la MEC estudiada, se decide comparar esta matriz con la matriz derivada de corazones embrionarios con EPIC MEC sometidos al mismo proceso de descclularización que las EPIC. Mediante este estudio, se verificó que contienen grupos de proteínas en común entre sí, enseñando una correlación entre el MEC derivado de EPIC con el MEC cardiaco embrionario (79 proteínas extracelulares en 118 proteínas extracelulares de MEC embrionario y 181 proteínas extracelulares de EPIC MEC).

Para evaluar el potencial de la MEC derivada de las EPIC con otras matrices ben establecidas en el mercado, se analizó la composición proteica de Matrigel en comparación con ambas fracciones de la EPIC MEC. Se comprobó que EPIC presenta un grupo de proteínas, también presente en Matrigel, que podrá mimetizar el soporte físico característico de esta matriz. Al analizar la diversidad proteica y las proteínas extracelulares más abundantes en todas las fracciones estudiadas MEC verificamos que EPIC IM y Matrigel son las matrices que presentan mayor diversidad de proteínas extracelulares. En Matrigel, casi 75% de la composición extracelular es compuesta por lamininas. En EPIC IM la proteína más abundante es la protease HTRA1, importante en la regulación dinámica del MEC. EPIC SM y MEC de corazones embrionarios presentan la

menor diversidad en proteínas extracelulares. En EPIC SM, enseñamos una fuerte presencia de fibronectina, esencial para el desarrollo vascular y en la reparación de tejidos cardíacos. En el MEC de corazones embrionarios, por otro lado, las proteínas identificadas presentan abundancias menores de 1% en el total proteínas.

De esta forma, y teniendo en cuenta la capacidad vasculogénica de EPIC MEC proveniente del análisis ontogénico anteriormente mencionado, se realizan ensayos de proliferación de HUVECs cultivados en superficies tratadas con EPIC IM, SM y Matrigel. Mediante este ensayo, se demuestra el potencial angiogénico de la fracción EPIC MEC en las HUVECs en comparación con otros soportes empelados, incluyendo el Matrigel. Estos resultados indican claramente la contribución de las células derivadas del epicardio a la matriz extracelular cardíaca en desarrollo.

A modo de resumen, esta tesis doctoral es el primer estudio sistemático del perfil secretor de las células derivadas del epicardio. Dicho secretoma muestra cierta capacidad proliferativa, metabólica y remodeladora del ambiente cardíaco durante el desarrollo. Siendo el epicardio y los CDEP unos de los agentes celulares determinantes en la respuesta al daño cardíaco, estos resultados son clave para entender la señalización modulada por estas células tanto en el desarrollo cardíaco como en el adulto, así como explorar su potencial terapéutico.

## Conclusiones

En esta tesis doctoral se ha caracterizado la composición proteica de parte del secretoma de una línea celular derivada de epicardio: las vesículas extracelulares (VEs) y la matriz extracelular (MEC). Además, hemos estudiado su impacto en la biología de este tipo celular.

Las conclusiones de este trabajo son:

1. Las vesículas extracelulares derivadas de epicardio aisladas mediante ultracentrifugación presentan una mayor integridad y un enriquecimiento en subpoblaciones de tamaño pequeño y mediano, en comparación con las vesículas aisladas por cromatografía de exclusión por tamaños.
2. Las células de la línea celular EPIC (derivada del epicardio de ratón en el estadio 11,5 del desarrollo), secretan una mayor cantidad de VEs de tamaño mediano cuando se cultivan en hipoxia (5% de oxígeno) que cuando se cultivan en normoxia (21% de oxígeno).
3. Los resultados obtenidos en el análisis proteómico con la tecnología TMT6plex es más reproducible para el análisis proteómico de VEs que con la tecnología TMT2plex.
4. El análisis proteómico de VEs derivadas de EPIC es un método robusto para identificar marcadores específicos de VEs derivados del epicardio.
5. Las VEs derivadas de EPIC cultivadas en hipoxia (5% oxígeno) contienen una mayor abundancia de proteínas relacionadas con el metabolismo glicolítico.
6. Las VEs derivadas de las EPIC son internalizadas por EPIC y HUVECs.
7. Las VEs obtenidas de EPIC cultivadas en hipoxia (5% oxígeno) no afectan ni a la proliferación ni al metabolismo glicolítico de las células EPIC o HUVEC.
8. Las VEs aisladas de EPIC cultivadas en condiciones de 1% de oxígeno inducen proliferación en EPIC de forma autocrina, pero no induce cambios en su respuesta glicolítica.
9. Las VEs aisladas de EPIC cultivadas en 1% de oxígeno aumentan la capacidad de las HUVECs responder en a una demanda energética de forma paracrina, aunque no influyen en su proliferación.

10. La matriz extracelular producida por las EPIC está enriquecida en proteínas relacionadas con la cicatrización y adherencia celular.
11. La matriz extracelular producida por las EPIC difiere significativamente de la composición de la matriz extracelular comercial conocida como Matrigel.
12. La matriz extracelular producida por las EPIC presenta una composición similar a la analizada en muestras de corazones embrionarios de E17,5.
13. La matriz extracelular producida por las EPIC está enriquecida en proteínas relacionadas con vasculogénesis. Además, incrementa la capacidad proliferativa de HUVECs cuando éstas se cultivan sobre dicha matriz tras 3 y 5 días en cultivo.





## Appendix: Tables and published paper

Table A1 – Unique proteins identified in TMT2plex\_1 (7 proteins), TMT2plex\_2 (7 proteins) and TMT2plex\_3 (14 proteins) assays.

TMT2plex_1		TMT2plex_2		TMT2plex_3	
UniProt ID	Protein Name	UniProt ID	Protein Name	UniProt ID	Protein Name
P68372	TUBB4B	Q7TPR4	ACTN1	Q9QXY6	EHD3
P02535-1	Isoform 1 of KRT10	P57780	ACTN4	P68510	YWHAH
Q8VED5	KRT79	Q8VEJ9	VPS4A	P46467	VPS4B
P01900	H2-D1	Q80X90	FLNB	P27601	GNA13
Q3UV17	KRT76	P58774	TPM2	Q6PHN9	RAB35
Q91ZX7	LRP1	P80318	CCT3	P97384	ANXA11
P08730-1	Isoform 1 of KRT13	G5E829	ATP2B1	P97333	NRP1
				Q8C863	ITCH
				P54754	EPHB3
				Q6ZPF4-1	Isoform 1 of FMNL3
				P13595	NCAM1
				Q6P9J9	ANO6
				Q64008	RAB34
				Q60790	RASA3

Table A2 – Unique proteins identified in, at least, two TMT2plex resulting lists (29 proteins) and in TMT6plex resulting list (130 proteins).

Unique proteins from TMT2plex		Unique proteins from TMT6plex			
UniProt ID	Protein Name	Uniprot ID	Protein Name	Uniprot ID	Protein Name
O35646	CAPN6	E9Q7X6-1	Isoform 1 of HEG1	P70296	PEBP1
O54962	BANF1	G5E829	ATP2B1	P70389	IGFALS
O89086	RBM3	O08529	CAPN2	P80313	CCT7
P01029	C4B	O08553	DPYSL2	P80318	CCT3
P14152	MDH1	O08807	PRDX4	P84078	ARF1
P26638	SARS	O70251	EEF1B2	P84228	H3C14
P28665	MUG1	O88792	F11R	P97300	NPTN
P39061-1	Isoform 2 of COL18A1	P00688	AMY2A5	P97333	NRP1
P47738	ALDH2	P02535-1	Isoform 1 of KRT10	P97351	RPS3A1
P47955	RPLP1	P08556	NRAS	P97384	ANXA11
P61089	UBE2N	P08730-1	Isoform 1 of KRT13	P97820	MAP4K4
P61205	ARF3	P09528	FTH1	P99027	RPLP2
P63028	TPT1	P10810	CD14	Q01730	RSU1
P68033	ACTC1	P11688	ITGA5	Q02248	CTNNB1
P84084	ARF5	P11983	TCP1	Q3THW5	H2AZ2
P84244	H3F3A	P13595	NCAM1	Q3UV17	KRT76
Q07076	ANXA7	P14148	RPL7	Q4VAA7	SNX33
Q61702	ITIH1	P14869	RPLP0	Q60598	CTTN
Q8BKX1	BAIAP2	P15626	GSTM2	Q61316	HSPA4
Q8BU31	RAP2C	P15864	H1F2	Q61468	MSLN
Q8C166	CPNE1	P16125	LDHB	Q61879	MYH10
Q8R105-1	Isoform 1 of VPS37C	P16254	SRP14	Q62465	VAT1
Q8R143	PTTG1IP	P16301	LCAT	Q6GU68	ISLR
Q9JHH6	CPB2	P16460	ASS1	Q6IRU2	TPM4
Q9JM76	ARPC3	P19096	FASN	Q6P9J9	ANO6
Q9QYB1	CLIC4	P20352	F3	Q6PHN9	RAB35
Q9R087	GPC6	P25444	RPS2	Q6URW6-1	Isoform 1 of MYH14
Q9WTR5	CDH13	P25911-1	Isoform 1 of LYN	Q6ZPF4-1	Isoform 1 of FMNL3
Q9Z2P8	VAMP5	P26040	EZR	Q6ZWN5	RPS9
		P26043	RDX	Q76MZ3	PPP2R1A
		P27048	SNRPB	Q7TMB8-1	Isoform 1 of CYFIP1
		P27659	RPL3	Q7TPR4	ACTN1
		P29391	FTL1	Q810U5-1	Isoform 1 of CCDC50
		P29533-1	Isoform 1 of VCAM1	Q8BGK6-1	Isoform 1 of SLC7A6
		P31786	DBI	Q8BMK4	CKAP4
		P34022	RANBP1	Q8C863	ITCH
		P35969	FLT1	Q8CFI0	NEDD4L
		P45376	AKR1B3	Q8K1B8	FERMT3

P45591	CFL2	Q8R2Q8	BST2
P46467	VPS4B	Q8VCM7	FGG
P47757-4	Isoform 3 of CAPZB	Q8VED5	KRT79
P47911	RPL6	Q8VEJ9	VPS4A
P51863	ATP6V0D1	Q91ZX7	LRP1
P54754	EPHB3	Q921W0	CHMP1A
P57780	ACTN4	Q99K41	EMILIN-1
P57787	SLC16A3	Q99K85	PSAT1
P58774	TPM2	Q99LX0	PARK7
P61028	RAB8B	Q9CPU0	GLO1
P61079	UBE2D3	Q9CPW4	ARPC5
P61358	RPL27	Q9CQ10	CHMP3
P61979	HNRNPK	Q9CQD4	CHMP1B2
P62071	RRAS2	Q9CQV8-1	Isoform long of YWHAB
P62082	RPS7	Q9CWJ9	ATIC
P62137	PPP1CA	Q9CXY6	ILF2
P62281	RPS11	Q9CYL5	GLIPR2
P62702	RPS4X	Q9CZX8	RPS19
P62827	RAN	Q9DAS9	GNG12
P62835	RAP1A	Q9DB77	UQCRC2
P62852	RPS25	Q9DC51	GNAI3
P62900	RPL31	Q9ES46	PARVB
P62908	RPS3	Q9ET01	PYGL
P63037	DNAJA1	Q9JIW9	RALB
P63268	ACTG2	Q9JKZ2	SLC5A3
P68372	TUBB4B	Q9Z0P4-1	ISOFORM 1 OF PALM
P68510	YWHAH	Q9Z1X4	ILF3

Table A3 – Proteins identified in TMT2plex\_1 assay (321 proteins).

TMT2plex_1					
UniProt ID	Protein Name	UniProt ID	Protein Name	UniProt ID	Protein Name
P11276	FN	P68254-1	Isoform 1 of YWHAQ	P61226	RAP2B
Q05793	HSPG2	P35564	CANX	Q8R001	MAPRE2
Q68FD5	CLTC	P51150	RAB7	Q9R045	ANGPTL2
Q8VDD5	MYH9	Q61703	ITIH2	P02088	HBB-B1
P63017	HSPA8	P97298	SERPINF1	P53994	RAB2A
Q8VDN2	ATP1A1	P62331	ARF6	Q9D8E6	RPL4
P11087-1	IST1	Q8R366	IGSF8	Q9WTS6-1	Isoform A1B1 of TENM3
Q9WU78	PDCD6IP	Q01768	NME2	P50446	KRT6A
P60710	ACTB	B2RXS4	PLXNB2	Q8R422	CD109
P21956-1	Isoform 1 of COL1A1	P63094	GNAS	P59999	ARPC4
P07356	ANXA2	P01902	H2-K1	Q62433	NDRG1
P52480	PKM	P18572-1	Isoform 1 of BSG	Q9CZM2	RPL15
P26041	MSN	O35639	ANXA3	P08228	SOD1
P10126	EEF1A1	O88342	WDR1	Q9D8N0	EEF1G
P20152	VIM	Q61553	FSCN1	Q91V41	RAB14
P17182	ENO1	Q9D8B3	CHMP4B	O35566	CD151
P26039	TLN1	P41731	CD63	Q8BY89-1	Isoform 1 of SLC44A2
P68368	TUBA4A	P19324	SERPINH1	Q9CQ80	VPS25
P29341	PABPC1	Q78HU3	MVB12A	P80315	CCT4
P63038-1	Isoform 1 of HSPD1	Q9Z1Q5	CLIC1	Q61735-1	Isoform 1 of CD47
P68369	TUBA1A	Q04857	COL6A1	P02535-1	Isoform 1 of KRT10
P11499	HSP90AB1	Q6GQT1	A2M	P80317	CCT6A
P68033	ACTC1	Q09143	SLC7A1	Q9Z1R3	APOM
P48036	ANXA5	A2AQ07	TUBB1	P43406	ITGAV
P35441	THBS1	Q9QYJ0	DNAJA2	P84096	RHOG
P10107	ANXA1	P14211	CALR	O35682	MYADM
P16858	GAPDH	P58022	LOXL2	P02104	HBB-Y
Q99JI6	RAP1B	Q9DC53	CPNE8	Q60931	VDAC3
Q8BTM8	FLNA	P58771-2	Isoform 2 of TPM1	Q60634-1	Isoform 1 of FLOT2
Q9WV91	PTGFRN	P08207	S100A10	Q02257	JUP
P09055	ITGB1	P07724	ALB	O70589-1	Isoform 1 of CASK
Q8C0E3	TRIM47	O08848	RO60	Q8R1F1	NIBAN2
P18760	CFL1	O35640	ANXA8	P62242	RPS8
P08113	HSP90B1	Q3THE2	MYL12B	P13745	GSTA1
Q61990	PCBP2	P63001	RAC1	Q9DCT8	CRIP2
P58252	EEF2	Q8K2Q7-1	Isoform 1 of BROX	Q9QZC7-1	Isoform 1 of PLEKHB2
Q62470	ITGA3	Q9DBJ1	PGAM1	Q9QXP6	MKRN1
P01027-1	ISOFORM LONG OF C3	Q9D1C8	VPS28	P43274	H1F4
P07901	HSP90AA1	Q64523	H2AC20	Q8VED5	KRT79

P13020-1	ISOFORM 1 OF GSN	Q99PT1	ARHGDI A	Q8R550-1	Isoform 1 of SH3KBP1
P11370	FV4	P61982	YWHAG	Q91ZR2	SNX18
Q9WVE8	PACSIN2	Q02013	AQP1	Q9JM76	ARPC3
P99024	TUBB5	Q8VEM8	SLC25A3	Q9DCN2	CYB5R3
P97429	ANXA4	P01942	HBA	P18242	CTSD
P63101	YWHAZ	P49817	CAV1	Q9WTR5	CDH13
Q62419	SH3GL1	Q61704	ITIH3	Q9WVL3	SLC12A7
Q9Z0K8	VNN1	P51885	LUM	P30412	PPIC
Q61398	PCOLCE	P10649	GSTM1	P12815	PDCD6
P05064	ALDOA	Q64433	HSPE1	Q61838	PZP
P62874	GNB1	Q03145	EPHA2	Q8BU31	RAP2C
Q60932-1	Isoform PL-VDAC1 of VDAC1	P80314	CCT2	P01900	H2-D1
Q61187	TSG101	Q9JIZ9	PLSCR3	P97370	ATP1B3
P35762	CD81	Q60930	VDAC2	P62301	RPS13
Q01149	COL1A2	O08688	CAPN5	Q61171	PRDX2
P10852	SLC3A2	Q99P72-2	Isoform A of RTN4	Q8K0E8	FGB
P62880	GNB2	Q8R105-1	Isoform 1 of VPS37C	P04186	CFB
P14824	ANXA6	P30999-1	Isoform 1 of CTNND1	P32261	SERPINC1
P56480	ATP5B	P59108	CPNE2	Q922R8	PDIA6
Q8BH64	EHD2	P15379-14	Isoform 1 of CD44	P28667	MARCKSL1
P08249	MDH2	P05202	GOT2	O54962	BANF1
P68372	TUBB4B	Q9R118	HTRA1	Q61207	PSAP
P20029	HSPA5	P10639	TXN1	P14152	MDH1
Q9QZF2	GPC1	P61027	RAB10	Q8C166	CPNE1
Q9WVK4	EHD1	O08585	CLTA	P06745	GPI1
P62204	CALM	P63242	EIF5A	P35980	RPL18
Q9WTI7-1	Isoform 1 of MYO1C	O35874	SLC1A4	P61089	UBE2N
Q99JR5	TINAGL1	P35700	PRDX1	P26638	SARS
Q64727	VCL	P40237	CD82	P14069	S100A6
P23249	MOV10	O54890	ITGB3	P84244	H3F3A
P51881	SLC25A5	Q9R0G6	COMP	Q9Z2P8	VAMP5
P09411	PGK1	O88783	F5	O89086	RBM3
P48962	SLC25A4	P50543	S100A11	Q80SZ7	GNG5
P08752	GNAI2	Q64337	SQSTM1	Q6IRU5	CLTB
P62259	YWHA E	Q02788	COL6A2	P38647	HSPA9
P62806	H4C8	P63321	RALA	P35456	PLAUR
P17742	PPIA	Q9DCK3	TSPAN4	Q3UV17	KRT76
P62962	PFN1	Q9EQP2	EHD4	Q9CVB6	ARPC2
Q9QUI0	RHOA	Q08879	FBLN1	Q8BT07-1	Isoform 1 of CEP55
Q9EQK5	MVP	Q01853	VCP	P11438	LAMP1
P09103	P4HB	Q9CX00	IST1	E9Q414	APOB

Q9D379	EPHX1	Q9JIM1-1	Isoform 1 of SLC29A1	Q8C0Z1	FAM234A
P06151	LDHA	P63089	PTN	P01029	C4B
P61205	ARF3	P51655	GPC4	P47753	CAPZA1
P17751	TPI1	Q99L47	ST13	O88947	F10
P62984	UBA52	P60843	EIF4A1	E9PV24	FGA
Q64525	H2BC18	P05622	PDGFRB	Q91ZX7	LRP1
Q64475	H2BC3	Q8R3G9	TSPAN8	O55222	ILK
P62821	RAB1A	F8VPU2	FARP1	P39061-1	Isoform 2 of COL18A1
Q9JKF1	IQGAP1	P47955	RPLP1	Q02053	UBA1
P16045	LGALS1	Q9R0P5	DSTN	Q8R143	PTTG1IP
Q03265	ATP5A1	P07091	S100A4	P50247	GM4737
P14094	ATP1B1	A6X935-1	Isoform 1 of OF ITIH4	O35316	SLC6A6
Q91VH2	SNX9	Q6ZQ38	CAND1	Q91YQ5	RPN1
P26645	MARCKS	Q69ZN7-1	Isoform 1 of MYOF	P20918	PLG
P19221	F2	Q9JLQ0	CD2AP	P24369	PPIB
P40240	CD9	O54724	CAVIN1	P17047	LAMP2
Q61696	HSPA1A	Q3TH73-1	Isoform 1 of TTYH2	Q99LU0	CHMP1B
Q8R0J7	VPS37B	P17809	SLC2A1	P08730-1	Isoform 1 of KRT13
Q60605	MYL6	P67778	PHB	P50608	FMOD
P27773	PDIA3	Q6KAU4	MVB12B	Q61702	ITIH1
Q61598	GDI2	P16110	LGALS3	P28665	MUG1
P84084	ARF5	Q922M3	KCTD10	Q9JHH6	CPB2
P21550	ENO3	P63028	TPT1	P47738	ALDH2
Q9WVA4	TAGLN2	P40224-1	Isoform alpha of CXCL12	P61161	ACTR2
O08992	SDCBP	Q9R087	GPC6	Q8BKX1	BAIAP2
P60766-2	Isoform 2 of CDC42	P49962	SRP9		
P60335	PCBP1	Q9CZU6	CS		
P46638	RAB11B	Q8CFE6	SLC38A2		

Table A4 – Proteins identified in TMT2plex\_2 assay (324 proteins).

TMT2plex_2					
UniProt ID	Protein Name	UniProt ID	Protein Name	UniProt ID	Protein Name
P11276	FN	P35564	CANX	P63028	TPT1
Q05793	HSPG2	P51150	RAB7	P40224-1	Isoform alpha of CXCL12
Q68FD5	CLTC	Q61703	ITIH2	Q80X90	FLNB
Q8VDD5	MYH9	P97298	SERPINF1	Q9R087	GPC6
P63017	HSPA8	P62331	ARF6	P49962	SRP9
Q8VDN2	ATP1A1	Q8R366	IGSF8	Q9CZU6	CS
P11087-1	Isoform 1 of COL1A1	Q01768	NME2	Q8CFE6	SLC38A2
Q9WU78	PDCD6IP	B2RXS4	PLXNB2	P61226	RAP2B
P60710	ACTB	P63094	GNAS	P26231	CTNNA1
P21956-1	Isoform 1 of MFGE8	P01902	H2-K1	Q8R001	MAPRE2
P07356	ANXA2	P18572-1	Isoform 1 of BSG	P02088	HBB-B1
P52480	PKM	O35639	ANXA3	P53994	RAB2A
P26041	MSN	O88342	WDR1	Q9D8E6	RPL4
P10126	EEF1A1	Q61553	FSCN1	Q9WTS6-1	Isoform A1B1 of TENM3
P20152	VIM	Q9D8B3	CHMP4B	P50446	KRT6A
P17182	ENO1	P41731	CD63	P59999	ARPC4
P26039	TLN1	P19324	SERPINH1	Q62433	NDRG1
P68368	TUBA4A	Q78HU3	MVB12A	Q9CZM2	RPL15
P29341	PABPC1	Q9Z1Q5	CLIC1	P08228	SOD1
P63038-1	Isoform 1 of HSPD1	Q04857	COL6A1	Q9QX15	CLCA3A1
P68369	TUBA1A	Q6GQT1	A2M	Q9D8N0	EEF1G
P11499	HSP90AB1	P21278	GNA11	Q91V41	RAB14
P68033	ACTC1	Q09143	SLC7A1	O35566	CD151
P48036	ANXA5	A2AQ07	TUBB1	Q8BY89-1	Isoform 1 of SLC44A2
P35441	THBS1	Q7TPR4	ACTN1	P70168	KPNB1
P10107	ANXA1	Q9QYJ0	DNAJA2	P80315	CCT4
P16858	GAPDH	P14211	CALR	P80317	CCT6A
Q99JI6	RAP1B	P58022	LOXL2	P58774	TPM2
Q8BTM8	FLNA	Q9DC53	CPNE8	Q9Z1R3	APOM
Q9WV91	PTGFRN	P58771-2	Isoform 2 of TPM1	P43406	ITGAV
P09055	ITGB1	P08207	S100A10	P84096	RHOG
Q8C0E3	TRIM47	P07724	ALB	O35682	MYADM
P18760	CFL1	P57780	ACTN4	P02104	HBB-Y
P08113	HSP90B1	O70318	EPB41L2	Q60931	VDAC3
Q61990	PCBP2	O08848	RO60	Q02257	JUP
P58252	EEF2	O35640	ANXA8	O70589-1	Isoform 1 of CASK
Q62470	ITGA3	Q3THE2	MYL12B	Q8R1F1	NIBAN2
P01027-1	Isoform long of C3	P63001	RAC1	P62242	RPS8



P07901	HSP90AA1	Q8K2Q7-1	Isoform 1 of BROX	P13745	GSTA1
P13020-1	Isoform 1 of GSN	P35278	RAB5C	Q9DCT8	CRIP2
P11370	FV4	Q9DBJ1	PGAM1	Q9QXP6	MKRN1
Q9WVE8	PAC SIN2	Q9D1C8	VPS28	P43274	H1F4
P99024	TUBB5	Q64523	H2AC20	Q8R550-1	Isoform 1 of SH3KBP1
P97429	ANXA4	Q99PT1	ARHGDI A	Q07076	ANXA7
P63101	YWHAZ	P61982	YWHAG	Q9JM76	ARPC3
Q62419	SH3GL1	Q02013	AQP1	Q9DCN2	CYB5R3
Q9Z0K8	VNN1	Q8VEM8	SLC25A3	P28656	NAP1L1
Q61398	PCOLCE	P01942	HBA	P18242	CTSD
P05064	ALDOA	P49817	CAV1	Q9WVL3	SLC12A7
P62874	GNB1	P15532	NME1	P30412	PPIC
Q60932-1	Isoform PL-VDAC1 of VDAC1	Q61704	ITIH3	P12815	PDCD6
Q61187	TSG101	P51885	LUM	Q61838	PZP
P35762	CD81	P10649	GSTM1	P97370	ATP1B3
Q01149	COL1A2	Q64433	HSPE1	P62301	RPS13
P10852	SLC3A2	Q03145	EPHA2	Q61171	PRDX2
P62880	GNB2	P80314	CCT2	Q9QYB1	CLIC4
P14824	ANXA6	Q9JIZ9	PLSCR3	Q8K0E8	FGB
P56480	ATP5B	Q60930	VDAC2	P04186	CFB
Q8BH64	EHD2	O08688	CAPN5	P80318	CCT3
P08249	MDH2	Q99P72-2	Isoform A of RTN4	P32261	SERPINC1
P20029	HSPA5	Q8R105-1	Isoform 1 of VPS37C	Q9CQ65	MTAP
Q9QZF2	GPC1	P40124	CAP1	Q922R8	PDIA6
Q9WVK4	EHD1	P30999-1	Isoform 1 of CTNND1	P28667	MARCKSL1
P62204	CALM	P59108	CPNE2	O54962	BANF1
Q9WTI7-1	Isoform 1 of MYO1C	P15379-14	Isoform 1 of CD44	Q61207	PSAP
Q99JR5	TINAGL1	P05202	GOT2	P14152	MDH1
Q64727	VCL	Q9R118	HTRA1	Q8C166	CPNE1
P23249	MOV10	P10639	TXN1	P06745	GPI1
P51881	SLC25A5	P61027	RAB10	P35980	RPL18
P09411	PGK1	O08585	CLTA	P26638	SARS
P48962	SLC25A4	P63242	EIF5A	Q99JY9	ACTR3
P08752	GNAI2	O35874	SLC1A4	P14069	S100A6
P62259	YWHAE	P35700	PRDX1	P84244	H3F3A
P62806	H4C8	P40237	CD82	Q9Z2P8	VAMP5
P17742	PPIA	Q9R0G6	COMP	O89086	RBM3
P62962	PFN1	Q62351	TFRC	Q80SZ7	GNG5
Q9QUI0	RHOA	P50543	S100A11	Q6IRU5	CLTB
Q9EQK5	MVP	Q64337	SQSTM1	P38647	HSPA9
P09103	P4HB	Q02788	COL6A2	P53986	SLC16A1

Q9D379	EPHX1	P63321	RALA	P35456	PLAUR
P06151	LDHA	Q9DCK3	TSPAN4	Q9CVB6	ARPC2
P61205	ARF3	Q9EQP2	EHD4	Q8BT07-1	Isoform 1 of CEP55
P17751	TPI1	Q08879	FBLN1	P11438	LAMP1
Q62159	RHOC	P21279	GNAQ	E9Q414	APOB
P62984	UBA52	Q9CX00	IST1	Q8COZ1	FAM234A
Q64525	H2BC18	Q9JIM1-1	Isoform 1 of SLC29A1	P01029	C4B
Q64475	H2BC3	P63089	PTN	P14206	RPSA
P62821	RAB1A	P51655	GPC4	Q811D0	DLG1
Q9JKF1	IQGAP1	Q99L47	ST13	E9PV24	FGA
P16045	LGALS1	P60843	EIF4A1	P39061-1	Isoform 2 of COL18A1
Q03265	ATP5A1	P05622	PDGFRB	Q02053	UBA1
P14094	ATP1B1	Q8R3G9	TSPAN8	Q8R143	PTTG1IP
Q91VH2	SNX9	F8VPU2	FARP1	P50247	GM4737
P26645	MARCKS	P47955	RPLP1	O35316	SLC6A6
P19221	F2	Q8VEJ9	VPS4A	Q91YQ5	RPN1
P40240	CD9	P07091	S100A4	O70401	TSPAN6
P10404	MLV-related proviral Env polyprotein	A6X935-1	Isoform 1 of ITIH4	O35646	CAPN6
Q8R0J7	VPS37B	Q6ZQ38	CAND1	P20918	PLG
Q60605	MYL6	Q69ZN7-1	Isoform 1 of MYOF	P24369	PPIB
P27773	PDIA3	Q9JLQ0	CD2AP	P17047	LAMP2
Q61598	GDI2	O54724	CAVIN1	Q99LU0	CHMP1B
P21550	ENO3	Q3TH73-1	Isoform 1 of TTYH2	P50608	FMOD
Q9WVA4	TAGLN2	P17809	SLC2A1	Q61702	ITIH1
O08992	SDCBP	P67778	PHB	P62270	RPS18
P60766-2	Isoform 2 of CDC42	Q6KAU4	MVB12B	P28665	MUG1
P60335	PCBP1	P16110	LGALS3	Q9JHH6	CPB2
P46638	RAB11B	P47754	CAPZA2	G5E829	ATP2B1
P68254-1	Isoform 1 of YWHAQ	Q922M3	KCTD10	Q8BKX1	BAIAP2

Table A5 – Proteins identified in TMT2plex\_3 assay (330 proteins).

TMT2plex_2					
UniProt ID	Protein Name	UniProt ID	Protein Name	UniProt ID	Protein Name
P11276	FN	P51150	RAB7	Q9CZU6	CS
Q05793	HSPG2	Q61703	ITIH2	Q8CFE6	SLC38A2
Q68FD5	CLTC	P97298	SERPINF1	P61226	RAP2B
Q8VDD5	MYH9	P62331	ARF6	P26231	CTNNA1
P63017	HSPA8	Q8R366	IGSF8	Q8R001	MAPRE2
Q8VDN2	ATP1A1	Q01768	NME2	Q9R045	ANGPTL2
P11087-1	Isoform 1 of COL1A1	B2RXS4	PLXNB2	Q6PHN9	RAB35
Q9WU78	PDCD6IP	P63094	GNAS	P02088	HBB-B1
P60710	ACTB	P01902	H2-K1	P53994	RAB2A
P21956-1	Isoform 1 of MFGE8	P18572-1	Isoform 1 of BSG	Q9D8E6	RPL4
P07356	ANXA2	O35639	ANXA3	Q9WTS6-1	Isoform A1B1 of TENM3
P52480	PKM	O88342	WDR1	P50446	KRT6A
P26041	MSN	Q61553	FSCN1	Q8R422	CD109
P10126	EEF1A1	Q9D8B3	CHMP4B	P59999	ARPC4
P20152	VIM	P41731	CD63	Q62433	NDRG1
P17182	ENO1	Q78HU3	MVB12A	Q9CZM2	RPL15
P26039	TLN1	Q9Z1Q5	CLIC1	P08228	SOD1
P68368	TUBA4A	Q04857	COL6A1	Q9QX15	CLCA3A1
P29341	PABPC1	Q6GQT1	A2M	Q9D8N0	EEF1G
P63038-1	Isoform 1 of HSPD1	P21278	GNA11	Q91V41	RAB14
P68369	TUBA1A	Q09143	SLC7A1	O35566	CD151
P11499	HSP90AB1	A2AQ07	TUBB1	Q8BY89-1	Isoform 1 of SLC44A2
P68033	ACTC1	Q9QYJ0	DNAJA2	P70168	KPNB1
P48036	ANXA5	Q9DC53	CPNE8	Q9CQ80	VPS25
P35441	THBS1	P58771-2	Isoform 1 of TPM1	P80315	CCT4
P10107	ANXA1	P08207	S100A10	Q61735-1	Isoform 1 of CD47
P16858	GAPDH	P07724	ALB	Q9Z1R3	APOM
Q99JI6	RAP1B	O70318	EPB41L2	P43406	ITGAV
Q8BTM8	FLNA	O08848	RO60	P84096	RHOG
Q9WV91	PTGFRN	O35640	ANXA8	O35682	MYADM
P09055	ITGB1	Q3THE2	MYL12B	P02104	HBB-Y
Q8C0E3	TRIM47	P63001	RAC1	Q60634-1	Isoform 1 of FLOT2
P18760	CFL1	Q8K2Q7-1	Isoform 1 of BROX	Q02257	JUP
P08113	HSP90B1	P35278	RAB5C	Q8R1F1	NIBAN2
Q61990	PCBP2	Q9DBJ1	PGAM1	P62242	RPS8
P58252	EEF2	Q9D1C8	VPS28	P13745	GSTA1
Q62470	ITGA3	Q64523	H2AC20	Q9DCT8	CRIP2
P01027-1	Isoform long of C3	Q99PT1	ARHGDI A	Q9QZC7-1	Isoform 1 of PLEKHB2
P07901	HSP90AA1	P61982	YWHAG	Q9QXP6	MKRN1

P13020-1	Isoform 1 of GSN	Q02013	AQP1	P97384	ANXA11
P11370	FV4	Q8VEM8	SLC25A3	P43274	H1F4
Q9WVE8	PACSIN2	Q9QXY6	EHD3	P97333	NRP1
P99024	TUBB5	P01942	HBA	Q8R550-1	Isoform 1 of SH3KBP1
P97429	ANXA4	P49817	CAV1	Q91ZR2	SNX18
P63101	YWHAZ	P15532	NME1	Q8C863	ITCH
Q62419	SH3GL1	Q61704	ITIH3	Q07076	ANXA7
Q9Z0K8	VNN1	P51885	LUM	Q9JM76	ARPC3
Q61398	PCOLCE	P10649	GSTM1	P28656	NAP1L1
P05064	ALDOA	Q64433	HSPE1	P18242	CTSD
P62874	GNB1	P68510	YWHAH	Q9WTR5	CDH13
Q60932-1	Isoform PL-VDAC1 of VDAC1	Q03145	EPHA2	Q9WVL3	SLC12A7
Q61187	TSG101	P80314	CCT2	P54754	EPHB3
P35762	CD81	Q9JIZ9	PLSCR3	P30412	PPIC
Q01149	COL1A2	Q60930	VDAC2	Q6ZPF4-1	Isoform 1 of FMNL3
P10852	SLC3A2	O08688	CAPN5	P12815	PDCD6
P62880	GNB2	Q99P72-2	Isoform A of RTN4	Q61838	PZP
P14824	ANXA6	Q8R105-1	Isoform 1 of VPS37C	P13595	NCAM1
P56480	ATP5B	P40124	CAP1	Q8BU31	RAP2C
Q8BH64	EHD2	P30999-1	Isoform 1 of CTNND1	P97370	ATP1B3
P08249	MDH2	P59108	CPNE2	P62301	RPS13
P20029	HSPA5	P46467	VPS4B	Q61171	PRDX2
Q9QZF2	GPC1	P15379-14	Isoform 1 of CD44	Q6P9J9	ANO6
Q9WVK4	EHD1	Q9R118	HTRA1	Q9QYB1	CLIC4
P62204	CALM	P10639	TXN1	Q8K0E8	FGB
Q9WTI7-1	Isoform 1 of MYO1C	P61027	RAB10	P04186	CFB
Q99JR5	TINAGL1	O08585	CLTA	Q9CQ65	MTAP
Q64727	VCL	P63242	EIF5A	P28667	MARCKSL1
P23249	MOV10	O35874	SLC1A4	O54962	BANF1
P51881	SLC25A5	P35700	PRDX1	P14152	MDH1
P09411	PGK1	P40237	CD82	Q8C166	CPNE1
P48962	SLC25A4	O54890	ITGB3	P06745	GPI1
P08752	GNAI2	Q9R0G6	COMP	P61089	UBE2N
P62259	YWHAE	O88783	F5	P26638	SARS
P62806	H4C8	Q62351	TFRC	Q64008	RAB34
P17742	PPIA	P50543	S100A11	Q99JY9	ACTR3
P62962	PFN1	Q64337	SQSTM1	P14069	S100A6
Q9QUI0	RHOA	Q02788	COL6A2	P84244	H3F3A
Q9EQK5	MVP	P63321	RALA	Q9Z2P8	VAMP5
P09103	P4HB	Q9DCK3	TSPAN4	O89086	RBM3
Q9D379	EPHX1	Q9EQP2	EHD4	Q80SZ7	GNG5
P06151	LDHA	Q08879	FBLN1	P53986	SLC16A1
P61205	ARF3	Q01853	VCP	P35456	PLAUR
P17751	TPI1	P21279	GNAQ	Q9CVB6	ARPC2

Q62159	RHOC	Q9CX00	IST1	Q8BT07-1	Isoform 1 of CEP55
P62984	UBA52	Q9JIM1-1	SLC29A1	P11438	LAMP1
Q64525	H2BC18	P63089	PTN	E9Q414	APOB
Q64475	H2BC3	P27601	GNA13	Q8C0Z1	FAM234A
P62821	RAB1A	P51655	GPC4	P01029	C4B
Q9JKF1	IQGAP1	Q99L47	ST13	P14206	RPSA
P16045	LGALS1	P60843	EIF4A1	P47753	CAPZA1
Q03265	ATP5A1	P05622	PDGFRB	Q811D0	DLG1
P14094	ATP1B1	Q8R3G9	TSPAN8	O88947	F10
Q91VH2	SNX9	F8VPU2	FARP1	O55222	ILK
P26645	MARCKS	P47955	RPLP1	P39061-1	Isoform 2 of COL18A1
P19221	F2	Q9R0P5	DSTN	Q02053	UBA1
P40240	CD9	P07091	S100A4	Q8R143	PTTG1IP
Q61696	HSPA1A	A6X935-1	Isoform 1 of ITIH4	P50247	GM4737
P10404		Q6ZQ38	CAND1	O35316	SLC6A6
Q8R0J7	VPS37B	Q69ZN7-1	Isoform 1 of MYOF	O70401	TSPAN6
Q60605	MYL6	Q9JLQ0	CD2AP	O35646	CAPN6
P27773	PDIA3	O54724	CAVIN1	P20918	PLG
Q61598	GDI2	Q3TH73-1	Isoform 1 of TTYH2	P17047	LAMP2
P84084	ARF5	P17809	SLC2A1	Q99LU0	CHMP1B
Q9WVA4	TAGLN2	Q6KAU4	MVB12B	P62270	RPS18
O08992	SDCBP	P16110	LGALS3	P28665	MUG1
P60766-2	Isoform 2 of CDC42	P47754	CAPZA2	Q9JHH6	CPB2
P60335	PCBP1	Q922M3	KCTD10	Q60790	RASA3
P46638	RAB11B	P40224-1	Isoform alpha of CXCL12	P47738	ALDH2
P68254-1	Isoform 1 of YWHAQ	Q9R087	GPC6	P61161	ACTR2
P35564	CANX	P49962	SRP9	Q8BKX1	BAIAP2

Table A6 – Proteins identified in TMT6plex assay and respective normalized abundancies organized from higher to lower in value in EVs-N and EVs-H5% (459 proteins).

TMT6plex					
Ordered proteins in EVs-N			Ordered proteins in EVs-H5%		
Majority Protein Uniprot IDs	Protein Names	Average Normalized intensities	Majority Protein Uniprot IDs	Protein Names	Average Normalized intensities
P11276	FN1	21.95	P11276	FN1	21.43
P63017	HSPA8	20.80	P63017	HSPA8	21.23
Q68FD5	CLTC	20.60	Q68FD5	CLTC	20.89
P21956	MFGE8	20.43	P21956	MFGE8	20.54
P63260;P60710	ACTG1;ACTB	20.30	P63260;P60710	ACTG1;ACTB	20.46
P07356	ANXA2	20.02	Q9WU78	PDCD6IP	20.19
Q9WU78	PDCD6IP	19.97	P07356	ANXA2	20.02
Q05793	HSPG2	19.86	P29341	PABPC1	19.70
P11087	COL1A1	19.52	P17182	ENO1	19.61
P17182	ENO1	19.50	P63101	YWHAZ	19.52
P63101	YWHAZ	19.48	P11370	FV4	19.50
P29341	PABPC1	19.48	P10126;P62631	EEF1A1;EEF1A2	19.36
P11370	FV4	19.21	P05213	TUBA1B	19.27
P20152	VIM	19.15	P17742	PPIA	19.25
Q8VDD5	MYH9	19.13	P62984;P62983;POCG49;POCG50	UBA52;RPS27A;	19.15
P05213	TUBA1B	19.12	P48036	ANXA5	19.08
P10126;P62631	EEF1A1;EEF1A2	19.12	P26041	MSN	19.06
P17742	PPIA	19.11	Q8VDD5	MYH9	19.05
P62984;P62983;POCG49;POCG50	UBA52;RPS27A;	19.07	P62806	H4C1	19.05
Q8VDN2	ATP1A1	19.04	Q8VDN2	ATP1A1	19.02
P62806	H4C1	18.90	P52480	PKM	18.97
P48036	ANXA5	18.89	Q05793	HSPG2	18.90
P26041	MSN	18.89	P20152	VIM	18.77
P52480	PKM	18.79	P11499	HSP90AB1	18.70
P11499	HSP90AB1	18.75	Q99JI6;P62835	RAP1B;RAP1A	18.67
Q8CGP2;Q8CGP1;Q64475;P10853;Q9D2U9;Q8CGP0;Q64524;P70696	HIST1H2BP;H2BC12;	18.51	P18760	CFL1	18.65
Q9WVE8	PACSIN2	18.51	P16045	LGALS1	18.62
Q64433	HSPE1	18.48	P41731	CD63	18.55
P18760	CFL1	18.44	Q8CGP2;Q8CGP1;Q64475;P10853;Q9D2U9;Q8CGP0;Q64524;P70696	HIST1H2BP;H2BC12;	18.55

P16045	LGALS1	18.43	Q9WVE8	PACSIN2	18.53
P10852	SLC3A2	18.39	P16858	GAPDH	18.43
Q99J16;P62835	RAP1B;RAP1A	18.36	P05064	ALDOA	18.33
P41731	CD63	18.35	P10107	ANXA1	18.31
P16858	GAPDH	18.32	Q9WV91	PTGFRN	18.25
PODP28;PODP27;PODP26	CALM3;CALM2;CALM1	18.32	P40240	CD9	18.24
P10107	ANXA1	18.30	P14824	ANXA6	18.20
P14824	ANXA6	18.26	P06151	LDHA	18.19
P05064	ALDOA	18.18	P10852	SLC3A2	18.16
P35441	THBS1	18.16	P26039	TLN1	18.15
P06151	LDHA	18.15	Q61990	PCBP2	18.14
P40240	CD9	18.12	Q9JLZ6	HIC2	18.13
Q9JLZ6	HIC2	17.96	PODP28;PODP27;PODP26	CALM3;CALM2;CALM1	18.11
Q9WV91	PTGFRN	17.93	P11087	COL1A1	18.09
Q62470	ITGA3	17.89	P99024;Q9CW F2;Q7TMM9	TUBB5;TUBB2 B;	18.02
P99024;Q9CW F2;Q7TMM9	TUBB5;TUBB2 B;	17.84	Q62470	ITGA3	18.01
P26039	TLN1	17.84	P35762	CD81	17.94
Q9DC53	CPNE8	17.83	Q61187	TSG101	17.91
Q61990	PCBP2	17.77	Q62419	SH3GL1	17.90
Q62419	SH3GL1	17.71	Q9DC53	CPNE8	17.90
P09055	ITGB1	17.67	P09055	ITGB1	17.85
Q61398	PCOLCE	17.66	P62874	GNB1	17.81
P51881	SLC25A5	17.66	E9PVA8	GCN1	17.81
P09103	P4HB	17.63	Q8BTM8	FLNA	17.76
Q61187	TSG101	17.60	P62821;Q9D1 G1	RAB1A;RAB1B	17.71
P62821;Q9D1 G1	RAB1A;RAB1B	17.60	P68033;P6813 4	ACTC1;ACTA1	17.70
E9PVA8	GCN1	17.59	Q64433	HSPE1	17.70
P35290	RAB24	17.57	P35290	RAB24	17.64
P68033;P6813 4	ACTC1;ACTA1	17.55	Q8COE3	TRIM47	17.57
P84228	HIST1H3B	17.54	P63094;Q6ROH 7	GNAS;	17.55
P62874	GNB1	17.53	P84228	HIST1H3B	17.52
P35762	CD81	17.53	P58252	EEF2	17.51
Q8BTM8	FLNA	17.49	O08585	CLTA	17.50
P08113	HSP90B1	17.49	P14069	S100A6	17.50
Q9Z0K8	VNN1	17.40	P84078;P6120 5;Q8BSL7;P840 84	ARF1;ARF3;	17.49
Q9D379	EPHX1	17.39	P17751	TPI1	17.46
P14094	ATP1B1	17.39	Q9WVK4	EHD1	17.38
P63038	HSPD1	17.37	P14094	ATP1B1	17.32
Q60930	VDAC2	17.36	P51881	SLC25A5	17.30
P14069	S100A6	17.32	P10400	POL	17.27

P63094;Q6ROH 7	GNAS;	17.26	P35441	THBS1	17.24
Q8C0E3	TRIM47	17.26	Q9D379	EPHX1	17.19
P58252	EEF2	17.25	O08992	SDCBP	17.17
P35564	CANX	17.23	Q60930	VDAC2	17.15
P17751	TPI1	17.22	P09103	P4HB	17.15
O08585	CLTA	17.20	P62259	YWHAE	17.13
Q60932	VDAC1	17.19	P63001;P6076 4;Q05144	RAC1;RAC3;	17.11
P08249	MDH2	17.17	P08113	HSP90B1	17.10
P84078;P6120 5;Q8BSL7;P840 84	ARF1;ARF3;	17.17	Q9JLQ0	CD2AP	17.10
P01942	HBA	17.15	P07091	S100A4	17.09
P17047	LAMP2	17.14	P17047	LAMP2	17.06
P62259	YWHAE	17.10	Q09143	SLC7A1	17.05
Q9WVK4	EHD1	17.09	Q9QUI0	RHOA	17.04
Q09143	SLC7A1	17.05	Q922P8	TMEM132A	17.04
P08207	S100A10	17.04	P08207	S100A10	17.04
P97429	ANXA4	17.02	P97429	ANXA4	17.03
Q9JLQ0	CD2AP	16.98	P10649;Q80W 21	GSTM1;GSTM7	16.92
P10400	POL	16.95	Q8BH64	EHD2	16.90
P07091	S100A4	16.92	P35564	CANX	16.89
P56480	ATP5F1B	16.90	P23249	MOV10	16.88
P26645	MARCKS	16.90	P51150	RAB7A	16.87
P51655	GPC4	16.88	Q01768	NME2	16.87
P10649;Q80W 21	GSTM1;GSTM7	16.86	P01942	HBA	16.83
P35700	PRDX1	16.86	P08752	GNAI2	16.82
Q99JR5	TINAGL1	16.86	P63038	HSPD1	16.81
P63001;P6076 4;Q05144	RAC1;RAC3;	16.83	Q9Z0K8	VNN1	16.79
Q01768	NME2	16.82	P26645	MARCKS	16.79
P51150	RAB7A	16.81	P35700	PRDX1	16.79
Q922P8	TMEM132A	16.80	Q9WTI7	MYO1C	16.77
O08992	SDCBP	16.80	P52196	TST	16.77
Q9QUI0	RHOA	16.80	P09411	PGK1	16.76
P57780	ACTN4	16.77	Q61398	PCOLCE	16.76
Q01149	COL1A2	16.72	B2RXS4	PLXNB2	16.75
P23249	MOV10	16.72	Q9D8B3	CHMP4B	16.73
P18572	BSG	16.71	Q60932	VDAC1	16.73
P52196	TST	16.69	P57780	ACTN4	16.72
Q9WTI7	MYO1C	16.69	P34884	MIF	16.68
B2RXS4	PLXNB2	16.65	P51655	GPC4	16.68
Q8VEM8	SLC25A3	16.64	P18572	BSG	16.66
O35639	ANXA3	16.60	P08249	MDH2	16.64
Q60605	MYL6	16.60	O35639	ANXA3	16.62
P08752	GNAI2	16.58	Q99L47	ST13	16.61
P34884	MIF	16.58	P17809	SLC2A1	16.55



Q9D8B3	CHMP4B	16.56	Q60605	MYL6	16.49
Q8BH64	EHD2	16.55	Q91VH2	SNX9	16.46
P17809	SLC2A1	16.51	Q8R0J7	VPS37B	16.45
P09411	PGK1	16.48	Q9EQK5	MVP	16.41
P27773	PDIA3	16.47	Q61553	FSCN1	16.39
Q61553	FSCN1	16.42	Q61598	GDI2	16.36
Q99L47	ST13	16.41	P56480	ATP5F1B	16.35
Q9EQK5	MVP	16.35	Q9QZH3	PPIE	16.34
Q61598	GDI2	16.27	F8VPU2	FARP1	16.32
Q8R0J7	VPS37B	16.26	Q3THW5;POCO S6	H2AFV;H2AZ1	16.23
P48962	SLC25A4	16.18	P15379	CD44	16.22
P15379	CD44	16.16	Q9DBJ1	PGAM1	16.17
P20029	HSPA5	16.14	Q8R0K2	TRIM31	16.13
Q3THW5;POCO S6	H2AFV;H2AZ1	16.13	Q9DCK3	TSPAN4	16.12
P97370	ATP1B3	16.10	Q9WVA4	TAGLN2	16.09
Q91VH2	SNX9	16.09	Q64727	VCL	16.08
Q9DBJ1	PGAM1	16.09	P27773	PDIA3	16.08
F8VPU2	FARP1	16.07	Q8VEM8	SLC25A3	16.07
Q9QZF2	GPC1	16.04	Q62465	VAT1	16.05
Q9QZH3	PPIE	16.03	O88342	WDR1	16.02
Q64337	SQSTM1	16.02	P60843;P1063 0	EIF4A1;EIF4A2	15.99
Q64727	VCL	16.02	Q64337	SQSTM1	15.99
P59999	ARPC4	16.00	Q8R550	SH3KBP1	15.97
Q8R0K2	TRIM31	15.98	Q9QZF2	GPC1	15.97
P01902	H2-K1	15.98	P97370	ATP1B3	15.97
P46638;P6249 2	RAB11B;RAB11 A	15.96	P50247	AHCY	15.93
O88342	WDR1	15.95	P46638;P6249 2	RAB11B;RAB11 A	15.92
Q9WVA4	TAGLN2	15.93	Q9D1C8	VPS28	15.92
Q03145	EPHA2	15.92	Q03145	EPHA2	15.91
P60843;P1063 0	EIF4A1;EIF4A2	15.92	P62702	RPS4X	15.88
Q8CFE6	SLC38A2	15.91	Q8CFE6	SLC38A2	15.87
O08848	RO60	15.89	P60766	CDC42	15.85
Q62465	VAT1	15.88	P48962	SLC25A4	15.83
Q03265	ATP5F1A	15.86	P59999	ARPC4	15.80
P50247	AHCY	15.86	O08848	RO60	15.80
P43274;P4327 7;P15864;Q07 133;P43275;P4 3276	H1-4;H1-3;H1- 2;	15.83	Q9JIM1	SLC29A1	15.78
Q9D1C8	VPS28	15.80	P43274;P4327 7;P15864;Q07 133;P43275;P4 3276	H1-4;H1-3;H1- 2;	15.77
Q9JIM1	SLC29A1	15.79	P01902	H2-K1	15.76

Q6ZWN5	RPS9	15.78	Q9JIW9;P6332 1	RALB;RALA	15.76
P07901	HSP90AA1	15.78	Q9R118	HTRA1	15.74
P62702	RPS4X	15.77	P20029	HSPA5	15.74
O70456	SFN	15.77	P07901	HSP90AA1	15.70
P49817	CAV1	15.72	P10648;P1374 5;P30115	GSTA2;GSTA1;	15.70
Q99PT1	ARHGDI A	15.71	Q78HU3	MVB12A	15.70
Q9JIW9;P6332 1	RALB;RALA	15.70	Q99PT1	ARHGDI A	15.68
P29533	VCAM1	15.69	P25911;P0810 3;P39688;Q04 736;P05480	LYN;HCK;	15.68
Q9DCK3	TSPAN4	15.62	Q99MV1	TDRD1	15.68
Q99MV1	TDRD1	15.61	P50543	S100A11	15.68
Q8R550	SH3KBP1	15.60	O70456	SFN	15.67
Q9R118	HTRA1	15.59	P16110	LGALS3	15.67
P60766	CDC42	15.59	P46467	VPS4B	15.64
P10648;P1374 5;P30115	GSTA2;GSTA1;	15.58	Q9CX00	IST1	15.63
P50543	S100A11	15.57	P60335	PCBP1	15.59
Q78HU3	MVB12A	15.56	O35566	CD151	15.57
P60335	PCBP1	15.54	Q6ZWN5	RPS9	15.57
O35566	CD151	15.53	Q9Z1Q5	CLIC1	15.54
Q9CX00	IST1	15.52	Q99JR5	TINAGL1	15.51
P25911;P0810 3;P39688;Q04 736;P05480	LYN;HCK;	15.50	P29533	VCAM1	15.51
P59108	CPNE2	15.48	P59108	CPNE2	15.48
P14211	CALR	15.47	P63242;Q8BGY 2	EIF5A;EIF5A2	15.38
O35874	SLC1A4	15.42	Q01149	COL1A2	15.33
Q9Z1Q5	CLIC1	15.42	Q03265	ATP5F1A	15.32
P46467	VPS4B	15.40	P49817	CAV1	15.31
P16110	LGALS3	15.37	Q6KAU4	MVB12B	15.30
P63242;Q8BGY 2	EIF5A;EIF5A2	15.34	Q61838	PZP	15.26
Q8R366	IGSF8	15.29	Q8R366	IGSF8	15.21
Q02013	AQP1	15.12	O35874	SLC1A4	15.18
Q99P72	RTN4	15.10	P62331	ARF6	15.15
P09528	FTH1	15.10	P31650	SLC6A11	15.15
P62270	RPS18	15.08	Q04857	COL6A1	15.13
E9Q8D0	DNAJC21	15.08	Q99P72	RTN4	15.09
Q6KAU4	MVB12B	15.08	Q61468	MSLN	15.00
P58022	LOXL2	15.07	Q8R3G9	TSPAN8	14.99
Q61838	PZP	15.06	P16254	SRP14	14.97
Q9JLT2	TREH	15.05	Q9JLT2	TREH	14.97
Q8R3G9	TSPAN8	15.04	P62242	RPS8	14.96
P31650	SLC6A11	15.03	P61294;P3527 9;Q8BHDO	RAB6B;RAB6A;	14.96
P58771	TPM1	15.02	P40124	CAP1	14.96

P61294;P3527 9;Q8BHD0	RAB6B;RAB6A;	15.00	P10639	TXN	14.94
P10639	TXN	14.96	P31786	DBI	14.94
Q9D8N0	EEF1G	14.96	P09528	FTH1	14.94
P62331	ARF6	14.93	Q9Z1W8	ATP12A	14.93
Q6ZQ38	CAND1	14.91	O54890	ITGB3	14.91
P31786	DBI	14.91	Q9EQP2	EHD4	14.90
P62242	RPS8	14.89	P68368	TUBA4A	14.90
Q9Z1W8	ATP12A	14.89	Q02013	AQP1	14.90
P16254	SRP14	14.89	E9Q8D0	DNAJC21	14.87
P49962	SRP9	14.86	Q3TH73	TTYH2	14.86
Q3THE2;Q9CQ 19	MYL12B;MYL9	14.82	P05622	PDGFRB	14.85
Q8CA71	SHISA4	14.82	P14211	CALR	14.84
P80318	CCT3	14.80	Q02788	COL6A2	14.84
P05622	PDGFRB	14.78	Q9ES97	RTN3	14.83
P99027	RPLP2	14.78	P62270	RPS18	14.81
O35640	ANXA8	14.77	Q9QZC7	PLEKHB2	14.79
P40124	CAP1	14.75	P58771	TPM1	14.78
Q61468	MSLN	14.74	Q8CA71	SHISA4	14.78
Q9QZC7	PLEKHB2	14.74	E9PV24	FGA	14.77
Q9DCN2	CYB5R3	14.70	P80318	CCT3	14.76
Q9EQP2	EHD4	14.66	Q6ZQ38	CAND1	14.74
Q3TH73	TTYH2	14.64	Q3THE2;Q9CQ 19	MYL12B;MYL9	14.74
Q91ZX7	LRP1	14.63	P49962	SRP9	14.70
P28656	NAP1L1	14.62	Q9D8N0	EEF1G	14.70
P68368	TUBA4A	14.62	O35640	ANXA8	14.69
P62852	RPS25	14.61	P28656	NAP1L1	14.67
Q04857	COL6A1	14.59	O88947	F10	14.65
O54890	ITGB3	14.58	Q91ZX7	LRP1	14.65
Q61207	PSAP	14.56	P61226;Q8BU3 1;Q80ZJ1	RAP2B;RAP2C;	14.64
Q9CR57	RPL14	14.55	P62880	GNB2	14.61
E9PV24	FGA	14.51	P99027	RPLP2	14.58
P38647	HSPA9	14.51	P62852	RPS25	14.56
Q9ES97	RTN3	14.51	P40237	CD82	14.56
Q9CZU6	CS	14.49	P68369;P0521 4	TUBA1A;TUBA 3A	14.53
P43406	ITGAV	14.48	Q8R1F1	NIBAN2	14.49
Q6URW6	MYH14	14.48	P61089	UBE2N	14.49
P67778	PHB	14.47	Q9QYJ0	DNAJA2	14.46
P68369;P0521 4	TUBA1A;TUBA 3A	14.46	Q9DCN2	CYB5R3	14.46
G5E829	ATP2B1	14.44	Q9CR57	RPL14	14.43
P61226;Q8BU3 1;Q80ZJ1	RAP2B;RAP2C;	14.43	P43406	ITGAV	14.43
P40237	CD82	14.42	Q6URW6	MYH14	14.43
Q80SZ7	GNG5	14.41	G5E829	ATP2B1	14.40
Q01853	VCP	14.40	Q80SZ7	GNG5	14.37

Q8R1F1	NIBAN2	14.38	P62137;P6308 7;P62141	PPP1CA;PPP1C C	14.36
P61089	UBE2N	14.38	Q02053	UBA1	14.33
P25444	RPS2	14.36	Q9CQW9;Q99J 93	IFITM3;IFITM2	14.31
P62137;P6308 7;P62141	PPP1CA;PPP1C C	14.34	Q9JIZ9	PLSCR3	14.31
P62880	GNB2	14.33	Q9QUM0	ITGA2B	14.31
P35278;Q9CQ D1;P61021	RAB5C;RAB5A;	14.32	P35278;Q9CQ D1;P61021	RAB5C;RAB5A;	14.28
Q9CQW9;Q99J 93	IFITM3;IFITM2	14.27	Q8R001;Q6PE R3	MAPRE2;MAPR E3	14.27
Q9CQV8	YWHAB	14.26	P25444	RPS2	14.27
Q02788	COL6A2	14.24	Q9R0P5	DSTN	14.27
O88792	F11R	14.23	Q61207	PSAP	14.25
Q62351	TFRC	14.23	O88792	F11R	14.21
Q02053	UBA1	14.23	P63325	RPS10	14.21
O88947	F10	14.20	Q9CQV8	YWHAB	14.17
P63325	RPS10	14.19	Q62351	TFRC	14.16
Q9QYJ0	DNAJA2	14.17	Q6ZPF4;A2APV 2	FMNL3;FMNL2	14.13
P80314	CCT2	14.17	O55222	ILK	14.13
P53986	SLC16A1	14.15	Q9DCT8	CRIP2	14.12
Q9DCT8	CRIP2	14.15	P53986	SLC16A1	14.11
P35456	PLAUR	14.14	Q9CZU6	CS	14.09
P47955	RPLP1	14.12	Q01853	VCP	14.09
Q9R0P5	DSTN	14.11	P40224	CXCL12	14.08
Q9WTX8	MAD1L1	14.11	P35456	PLAUR	14.07
P11983	TCP1	14.10	P47955	RPLP1	14.06
Q9JIZ9	PLSCR3	14.07	P11983	TCP1	14.05
Q9Z127;Q8BG K6	SLC7A5;SLC7A 6	14.06	Q921E2;P3528 5	RAB31;RAB22A	14.05
Q9JKF1	IQGAP1	14.05	P28667	MARCKSL1	14.04
P28667	MARCKSL1	14.01	P38647	HSPA9	14.04
P62827	RAN	13.98	P58022	LOXL2	14.02
Q8CJ26	NRADD	13.97	P67778	PHB	14.01
P63089	PTN	13.96	P97298	SERPINF1	13.97
Q6P9J9	ANO6	13.94	Q60790	RASA3	13.97
Q8R001;Q6PE R3	MAPRE2;MAPR E3	13.92	Q9JKF1	IQGAP1	13.95
Q9CZE3	RAB32	13.92	Q6P9J9	ANO6	13.94
Q9QUM0	ITGA2B	13.92	Q9WTX8	MAD1L1	13.94
Q60931	VDAC3	13.91	Q8CJ26	NRADD	13.94
P40224	CXCL12	13.91	P80314	CCT2	13.93
P61027	RAB10	13.90	P62827	RAN	13.92
P70296	PEBP1	13.89	Q91YN9	BAG2	13.90
Q921E2;P3528 5	RAB31;RAB22A	13.85	Q8BWT5;Q3U H60	DIP2A;DIP2B	13.90
Q6ZPF4;A2APV 2	FMNL3;FMNL2	13.85	O70401	TSPAN6	13.89
P08228	SOD1	13.85	Q9CR26	VTA1	13.85

O70401	TSPAN6	13.84	P70296	PEBP1	13.81
Q6IRU5	CLTB	13.81	Q9DB34	CHMP2A	13.80
Q91YN9	BAG2	13.79	P63089	PTN	13.79
Q9CR26	VTA1	13.75	Q9CYL5	GLIPR2	13.78
Q8R422	CD109	13.75	Q8K2Q7	BROX	13.78
Q9D8E6	RPL4	13.74	P63037	DNAJA1	13.76
P70168	KPNB1	13.72	Q6IRU5	CLTB	13.74
P15532	NME1	13.70	P32037	SLC2A3	13.73
O55222	ILK	13.70	Q9CZE3	RAB32	13.73
P14869	RPLP0	13.69	O70318;Q9WV 92	EPB41L2;EPB4 1L3	13.72
B1B212	H60B	13.69	B1B212	H60B	13.71
Q64695	PROCR	13.66	Q9JKP5;Q8C18 1	MBNL1;MBNL2	13.69
Q61735	CD47	13.64	Q8R422	CD109	13.67
Q9JKP5;Q8C18 1	MBNL1;MBNL2	13.61	P61027	RAB10	13.66
P61161	ACTR2	13.61	P15532	NME1	13.65
Q9CYL5	GLIPR2	13.60	P14869	RPLP0	13.63
Q8BWT5;Q3U H60	DIP2A;DIP2B	13.59	Q9D8E6	RPL4	13.62
P63037	DNAJA1	13.59	Q9Z127;Q8BG K6	SLC7A5;SLC7A 6	13.61
Q60790	RASA3	13.59	Q61735	CD47	13.61
Q9Z0P4	PALM	13.59	P26231;Q6130 1	CTNNA1;CTNN A2	13.60
Q9R045	ANGPTL2	13.56	Q9JKZ2	SLC5A3	13.59
P26231;Q6130 1	CTNNA1;CTNN A2	13.55	Q9Z0P4	PALM	13.57
O70318;Q9WV 92	EPB41L2;EPB4 1L3	13.54	P47754	CAPZA2	13.57
Q8K2Q7	BROX	13.54	P08228	SOD1	13.55
Q9DB34	CHMP2A	13.52	P70168	KPNB1	13.54
P21279	GNAQ	13.51	Q9JM76	ARPC3	13.51
Q8BY89	SLC44A2	13.50	Q60931	VDAC3	13.50
P47754	CAPZA2	13.50	P61161	ACTR2	13.50
P47757	CAPZB	13.50	Q8BY89	SLC44A2	13.47
P62908	RPS3	13.50	P20352	F3	13.46
Q61411;P3288 3;P08556	HRAS;KRAS;NR AS	13.48	Q61411;P3288 3;P08556	HRAS;KRAS;NR AS	13.46
Q9JKZ2	SLC5A3	13.47	Q99K41	EMILIN1	13.46
Q9R0Y5	AK1	13.45	P21279	GNAQ	13.45
P68510	YWHAH	13.44	P47757	CAPZB	13.45
Q9JM76	ARPC3	13.42	Q64695	PROCR	13.43
P97298	SERPINF1	13.40	Q9R045	ANGPTL2	13.43
P32037	SLC2A3	13.40	P62908	RPS3	13.39
Q9DB77	UQCRC2	13.37	Q99JY9	ACTR3	13.29
P53994;P5927 9	RAB2A;RAB2B	13.34	P53994;P5927 9	RAB2A;RAB2B	13.25
Q99K41	EMILIN1	13.34	Q9R0Y5	AK1	13.25
P20352	F3	13.33	P62900	RPL31	13.25

Q9CXP8	GNG10	13.32	Q9QZ06	TOLLIP	13.24
P62900	RPL31	13.31	Q9CQ10	CHMP3	13.21
Q9QZ06	TOLLIP	13.27	P13595	NCAM1	13.18
Q99LX0	PARK7	13.24	P68510	YWHAH	13.17
Q9CWJ9	ATIC	13.23	Q99LX0	PARK7	13.16
Q99JY9	ACTR3	13.12	Q9CXP8	GNG10	13.16
Q810U5	CCDC50	13.07	Q9CWJ9	ATIC	13.12
P62301	RPS13	13.06	Q9CQD4;Q99L U0	CHMP1B2;CH MP1B1	13.12
Q9CQ10	CHMP3	13.04	Q810U5	CCDC50	13.10
Q9CZN7	SHMT2	13.02	Q62159	RHOC	13.08
P27659	RPL3	13.00	P16125	LDHB	13.00
P80313	CCT7	12.99	Q8R143	PTTG1IP	13.00
O08807	PRDX4	12.94	Q9DB77	UQCRC2	12.99
P13595	NCAM1	12.93	P62301	RPS13	12.99
P14148	RPL7	12.93	O89086	RBM3	12.94
Q9CQD4;Q99L U0	CHMP1B2;CH MP1B1	12.91	P26883	FKBP1A	12.89
Q62159	RHOC	12.90	Q6PHN9	RAB35	12.88
P26883	FKBP1A	12.89	P14148	RPL7	12.87
Q6PHN9	RAB35	12.89	Q8K1B8	FERMT3	12.86
Q9Z1R3	APOM	12.88	P27659	RPL3	12.83
P61982	YWHAG	12.84	Q8BH43;Q8R5 H6	WASF2;WASF1	12.82
P11438	LAMP1	12.82	P97384	ANXA11	12.79
P99028	UQCRH	12.81	O08807	PRDX4	12.78
Q9DCDO	PGD	12.80	Q01730	RSU1	12.78
P19324	SERPINH1	12.79	O70589	CASK	12.76
P16125	LDHB	12.78	P80313	CCT7	12.75
Q8K1B8	FERMT3	12.77	Q99JT2;Q9Z2 W1;Q99KH8	STK26;STK25;	12.74
Q8R143	PTTG1IP	12.70	Q921W0	CHMP1A	12.73
Q8BH43;Q8R5 H6	WASF2;WASF1	12.68	P11438	LAMP1	12.72
Q01730	RSU1	12.66	Q9Z1R3	APOM	12.65
Q921W0	CHMP1A	12.65	P61982	YWHAG	12.62
O89086	RBM3	12.64	P99028	UQCRH	12.60
O70589	CASK	12.63	P55258	RAB8A	12.58
Q6GU68	ISLR	12.62	Q9CZN7	SHMT2	12.58
P11688	ITGA5	12.62	P11688	ITGA5	12.55
Q6ZWY9;Q645 25;Q64478;P1 0854	H2BC4;HIST2H 2BB;	12.61	P19096	FASN	12.54
Q69ZN7	MYOF	12.61	Q99JW4	LIMS1	12.52
P51863	ATP6VOD1	12.60	P62838;P6107 9;Q6ZWY6	UBE2D2;UBE2 D3;	12.52
P97384	ANXA11	12.56	Q9QUM9	PSMA6	12.51
Q9CVB6	ARPC2	12.55	Q61316	HSPA4	12.51
Q9QUM9	PSMA6	12.53	P16460	ASS1	12.51
Q61316	HSPA4	12.48	Q9CVB6	ARPC2	12.49

P14206	RPSA	12.47	Q9D2Q3	PAAT	12.49
Q9R087	GPC6	12.47	P14206	RPSA	12.47
P15116	CDH2	12.46	Q6GU68	ISLR	12.46
Q811D0	DLG1	12.41	Q9R087	GPC6	12.45
P62962	PFN1	12.40	Q6ZWY9;Q64525;Q64478;P10854	H2BC4;HIST2H2BB;	12.45
Q922Q8	LRRC59	12.39	Q8BGX0	TRIM23	12.45
P19096	FASN	12.38	P62962	PFN1	12.44
P62838;P61079;Q6ZWY6	UBE2D2;UBE2D3;	12.38	P19324	SERPINH1	12.44
P62082	RPS7	12.36	Q69ZN7	MYOF	12.43
P16460	ASS1	12.36	P06745	GPI	12.42
Q02248	CTNNB1	12.33	Q9DCD0	PGD	12.42
Q9D2Q3	PAAT	12.31	P51863	ATP6V0D1	12.41
Q9WTR5	CDH13	12.31	P15116	CDH2	12.41
P11152	LPL	12.30	Q9WTR5	CDH13	12.40
Q99JW4	LIMS1	12.30	P62082	RPS7	12.33
P62281	RPS11	12.30	O35682	MYADM	12.32
P62071	RRAS2	12.28	P97333	NRP1	12.32
P97333	NRP1	12.28	Q811D0	DLG1	12.26
Q07797	LGALS3BP	12.25	Q02248	CTNNB1	12.22
P47911	RPL6	12.21	P11152	LPL	12.16
Q99JT2;Q9Z2W1;Q99KH8	STK26;STK25;	12.21	P70389	IGFALS	12.16
P18242	CTSD	12.19	Q922Q8	LRRC59	12.12
P55258	RAB8A	12.17	Q64008	RAB34	12.08
P57776	EEF1D	12.17	P57776	EEF1D	12.07
P68254	YWHAQ	12.05	P18242	CTSD	12.06
P06745	GPI	12.04	Q07797	LGALS3BP	12.05
P50608	FMOD	12.04	Q6P5F7	TTYH3	12.04
P68372;Q9D6F9	TUBB4B;TUBB4A	12.04	P35980	RPL18	12.03
P35980	RPL18	11.99	Q9DC51;B2RS H2	GNAI3;GNAI1	12.02
Q8BGX0	TRIM23	11.98	Q8C863	ITCH	12.01
Q6P5F7	TTYH3	11.92	Q8C166	CPNE1	11.98
P70389	IGFALS	11.89	P62281	RPS11	11.97
Q9DC51;B2RS H2	GNAI3;GNAI1	11.89	Q9ES46	PARVB	11.95
Q8C166	CPNE1	11.87	P68372;Q9D6F9	TUBB4B;TUBB4A	11.86
P12970	RPL7A	11.83	P68254	YWHAQ	11.81
Q64008	RAB34	11.82	Q9CPW4	ARPC5	11.81
Q9CPW4	ARPC5	11.79	P62071	RRAS2	11.80
Q60598	CTTN	11.78	P12970	RPL7A	11.79
Q91ZR2	SNX18	11.78	Q91ZR2	SNX18	11.78
Q3UV17	KRT76	11.77	P47911	RPL6	11.78
Q9Z1X4	ILF3	11.74	Q9Z1X4	ILF3	11.77
Q8C863	ITCH	11.73	Q9QXP6	MKRN1	11.77

Q9CZ13	UQCRC1	11.72	Q60598	CTTN	11.75
Q8R105	VPS37C	11.66	P50608	FMOD	11.74
Q99K51	PLS3	11.66	P12815	PDCD6	11.67
Q9D2M8;Q9CZ Y3	UBE2V2;UBE2 V1	11.65	Q8R105	VPS37C	11.65
P12815	PDCD6	11.63	Q99K51	PLS3	11.62
Q921Y0;Q8BPP 0	MOB1A;MOB1 B	11.63	Q62433	NDRG1	11.59
P14152	MDH1	11.62	Q921Y0;Q8BPP 0	MOB1A;MOB1 B	11.57
Q9Z2X1;O3573 7	HNRNPF;HNRN PH1	11.61	Q9Z2X1;O3573 7	HNRNPF;HNRN PH1	11.48
Q9QXP6	MKRN1	11.51	P84244;P0230 1	H3-3A;H3F3C	11.48
P63024;P6304 4	VAMP3;VAMP 2	11.49	P84096	RHOG	11.47
O08529	CAPN2	11.46	Q3UV17	KRT76	11.45
P97300	NPTN	11.42	Q9D2M8;Q9CZ Y3	UBE2V2;UBE2 V1	11.45
Q6X893	SLC44A1	11.41	O08529	CAPN2	11.41
P45376	AKR1B1	11.35	P68433	H3C1	11.37
P84244;P0230 1	H3-3A;H3F3C	11.32	Q9R1Q6	TMEM176B	11.36
P68433	H3C1	11.30	Q6X893	SLC44A1	11.30
Q9JIG7	CCDC22	11.28	P30999	CTNND1	11.29
Q9Z0T9	ITGB6	11.28	P63024;P6304 4	VAMP3;VAMP 2	11.27
Q62433	NDRG1	11.27	P14152	MDH1	11.25
Q7TPR4	ACTN1	11.24	Q9Z0T9	ITGB6	11.24
Q7TMB8	CYFIP1	11.14	Q9JIG7	CCDC22	11.20
Q9R1Q6	TMEM176B	11.13	Q8VEJ9	VPS4A	11.15
Q61696;P1787 9	HSPA1A;HSPA1 B	11.13	P26043	RDX	11.14
P30999	CTNND1	11.10	P45376	AKR1B1	11.13
Q9CQ80	VPS25	11.08	Q7TMB8	CYFIP1	11.09
Q8VE98	CD276	11.08	Q7TPR4	ACTN1	11.06
P35282	RAB21	11.07	Q61696;P1787 9	HSPA1A;HSPA1 B	11.03
P84096	RHOG	11.06	P57787	SLC16A3	11.02
P26043	RDX	11.03	P97300	NPTN	10.94
Q8BMK4	CKAP4	11.02	Q9CZ13	UQCRC1	10.91
P50516	ATP6V1A	11.01	Q8VE98	CD276	10.89
P80316	CCT5	11.01	Q923D2	BLVRB	10.88
Q9ES46	PARVB	11.00	Q9JHU4	DYNC1H1	10.88
P57787	SLC16A3	10.89	Q64735	CR1L	10.87
Q9CQQ7	ATP5PB	10.85	P50516	ATP6V1A	10.86
P30677;P2127 8	GNA14;GNA11	10.71	P35282	RAB21	10.85
P61358	RPL27	10.67	Q9CQ80	VPS25	10.82
Q923D2	BLVRB	10.65	P99029	PRDX5	10.79
Q64735	CR1L	10.64	P61358	RPL27	10.69



P11440	CDK1	10.64	Q9D7S9	CHMP5	10.64
Q9D7S9	CHMP5	10.62	P11440	CDK1	10.54
Q8VEJ9	VPS4A	10.55	O08553	DPYSL2	10.53
P49945;P2939 1	FTL2;FTL1	10.52	P80316	CCT5	10.49
Q9JHU4	DYNC1H1	10.51	P30677;P2127 8	GNA14;GNA11	10.45
P16627	HSPA1L	10.45	Q8BMK4	CKAP4	10.44
O35682	MYADM	10.44	Q9CQQ7	ATP5PB	10.43
Q8CFI0	NEDD4L	10.28	P16627	HSPA1L	10.41
O08553	DPYSL2	10.22	Q9EQH3	VPS35	10.17
P99029	PRDX5	10.14	Q91V92	ACLY	10.11
Q91V92	ACLY	10.07	Q8CFI0	NEDD4L	9.96
Q9EQH3	VPS35	9.99	P49945;P2939 1	FTL2;FTL1	9.91
Q91VR2	ATP5F1C	9.91	P63323	RPS12	9.79
P63323	RPS12	9.88	Q07076	ANXA7	9.65
Q07076	ANXA7	9.79	Q91VR2	ATP5F1C	9.15
O35379	ABCC1	8.97	O35379	ABCC1	9.00
Q75N73	SLC39A14	8.72	O88746	TOM1	8.91
Q9WTS6	TENM3	8.70	Q9JHZ2	ANKH	8.75
Q9JHZ2	ANKH	8.24	Q9WTS6	TENM3	7.77
O88746	TOM1	7.60	Q75N73	SLC39A14	7.23
P28571	SLC6A9	7.41	P28571	SLC6A9	7.03
Q9QX15	CLCA3A1	6.11	Q9QX15	CLCA3A1	6.92

Table A7 - Unique proteins identified in. at least. two lists of extracellular filtered proteins in EPIC SM (100 proteins) and EPIC IM (32 proteins)

Unique proteins from EPIC SM				Unique proteins from EPIC IM	
UniProt ID	Protein Name	UniProt ID	Protein Name	UniProt ID	Protein Name
A2ASQ1-1	Isoform 1 of AGRN	Q00780	COL8A1	A2A5I3	R3HDML
D3YXK1	SAMD1	Q02788	COL6A2	A6X935-1	Isoform 1 of ITIH4
E9Q414	APOB	Q04857	COL6A1	O09118	NTN1
O08638-1	Isoform 1 of MYH11	Q07797	LGALS3BP	P01027-1	Isoform long C3
O08912	GALNT1	Q3U962	COL5A2	P07724	ALB
O08992	SDCBP	Q3V1T4	P3H1	P09535-2	Isoform 2 of IGF2
O35516	NOTCH2	Q5SS80-1	Isoform 1 of DHRS13	P10493	NID1
O35604	NPC1	Q60847	COL12A1	P11214	PLAT
O35658	C1QBP	Q60854	SERPINB6A	P14069	S100A6
O35887	CALU	Q61147	CP	P18406	CCN1
O88207	COL5A1	Q61207	PSAP	P19137	LAMA1
O88531	PPT1	Q61245-1	Isoform long of COL11A1	P24383	WNT7A
O89051	ITM2B	Q61592	GAS6	P27090	TGFB2
P02463	COL4A1	Q61699	HSPH1	P29268	CCN2
P07091	S100A4	Q62086	PON2	P31240	PDGFB
P07214	SPARC	Q62087	PON3	P40224-2	Isoform beta of CXCL12
P08121	COL3A1	Q62165	DAG1	P43028	GDF6
P08122	COL4A2	Q64437	ADH7	P63089	PTN
P08207	S100A10	Q6GU68	ISLR	P70275	SEMA3E
P09528	FTH1	Q80ZW2	THEM6	P97298	SERPINF1
P10605	CTSB	Q8C7K6	PCYOX1L	P97857	ADAMTS1
P10810	CD14	Q8C7V8-1	Isoform 1 of CCDC134	Q3UQ28	PXDN
P14211	CALR	Q8CC88	VWA8	Q3USZ8	DIPK2A
P16045	LGALS1	Q8CIE6	COPA	Q62177	SEMA3B
P18242	CTSD	Q8K4Z3	NAXE	Q66PY1-1	Isoform 1 of SCUBE3
P21460	CST3	Q8R422	CD109	Q6GQT1	A2M
P21803-1	Isoform long of FGFR2	Q8VDL4	ADPGK	Q6R0H7	GNAS
P23188	FURIN	Q91VU0	FAM3C	Q80T21	ADAMTSL4
P25446	FAS	Q91ZA3	PCCA	Q8K0E8	FGB
P25785	TIMP2	Q920A5	SCPEP1	Q91V88-4	Isoform 4 of NPNT
P28481-1	Isoform 2 of COL2A1	Q99104	MYO5A	Q9JK53	PRELP
P28653	BGN	Q99JR5	TINAGL1	Q9Z0J7	GDF15
P28654	DCN	Q99M71	EPDR1		
P29391	FTL1	Q99MN1	KARS		
P30681	HMGB2	Q9CPT4	MYDGF		
P31230	AIMP1	Q9CXI5	MANF		
P32261	SERPINC1	Q9CYA0	CRELD2		

P39061-1	Isoform 2 of COL18A1	Q9CYD3	CRTAP
P40124	CAP1	Q9CZD3	GARS
P40224-1	Isoform alpha of CXCL12	Q9D0L4-1	Isoform 1 of ADCK1
P40240	CD9	Q9DCZ4	APOO
P41731	CD63	Q9EQ06	HSD17B11
P42703-1	Isoform 1 of LIFR	Q9ET22	DPP7
P51655	GPC4	Q9JHR7	IDE
P51859	HDGF	Q9JKR6	HYOU1
P55302	LRPAP1	Q9QXP7	C1QTNF1
P63094	GNAS	Q9QZF2	GPC1
P63158	HMGB1	Q9WTR5	CDH13
P81117	NUCB2	Q9Z204	HNRNPC
P97352	S100A13	Q9Z2W0	DNPEP

Table A8 – Proteins in common in. at least. two lists of EPIC IM and EPIC SM (53 proteins).

Proteins in common between EPIC SM and EPIC IM			
UniProt ID	Protein Name	UniProt ID	Protein Name
O08573	LGALS9	Q01149	COL1A2
O88569	HNRNPA2B1	Q05793	HSPG2
P01029	C4B	Q08879	FBLN1
P01887	B2M	Q61001	LAMA5
P01902	H2-K1	Q61292	LAMB2
P02468	LAMC1	Q61398	PCOLCE
P02469	LAMB1	Q61703	ITIH2
P06745	GPI1	Q62351	TFRC
P07356	ANXA2	Q8CG19-1	Isoform long of LTBP1
P08113	HSP90B1	Q8R2G6	CCDC80
P10107	ANXA1	Q8VDD5	MYH9
P10649	GSTM1	Q924C6	LOXL4
P11087-1	Isoform 1 of COL1A1	Q99K41	EMILIN1
P11152	LPL	Q9CYL5	GLIPR2
P11276	FN1	Q9D1D6	CTHRC1
P11499	HSP90AB1	Q9D6X6	PRSS23
P16110	LGALS3	Q9R118	HTRA1
P13020-1	Isoform 1 of GSN	Q9WU78	PDCD6IP
P17742	PPIA	Q9WVJ9	EFEMP2
P18760	CFL1	P39876	TIMP3
P19788	MGP	P48759	PTX3
P20029	HSPA5	P55065	PLTP
P21956-1	Isoform 1 of MFGE8	P62960	YBX1
P27773	PDIA3	P62962	PFN1
P28301	LOX	P82198	TGFBI
P35441	THBS1	P97792-1	Isoform 1 of CXADR
P37889	FBLN2		

Table A9 – Proteins in common between E17.5 murine hearts and EPIC IM (4 proteins) and EPIC SM (42 proteins) and proteins in common between all conditions (33 proteins)

Proteins in common between EPIC IM and E17.5 murine hearts		Proteins in common between EPIC SM and E17.5 murine hearts		Proteins in common between EPIC IM, EPIC SM and E17.5 murine hearts	
UniProt ID	Protein Name	UniProt ID	Protein Name	UniProt ID	Protein Name
P07724	ALB	A2ASQ1-1	Isoform 1 of AGRN	O08573	LGALS9
P10493	NID1	E9Q414	APOB	O88569	HNRNPA2B1
Q3UQ28	PXDN	O08638-1	Isoform 1 of MYH11	P02468	LAMC1
Q8K0E8	FGB	O35604	NPC1	P02469	LAMB1
		O35658	C1QBP	P06745	GPI1
		O35887	CALU	P07356	ANXA2
		P02463	COL4A1	P08113	HSP90B1
		P08122	COL4A2	P10107	ANXA1
		P14211	CALR	P11087-1	Isoform 1 of COL1A1
		P28653	BGN	P11152	LPL
		P28654	DCN	P11276	FN1
		P29391	FTL1	P11499	HSP90AB1
		P30681	HMGB2	P13020-1	Isoform 1 of GSN
		P31230	AIMP1	P17742	PPIA
		P39061-1	Isoform 2 of COL18A1	P18760	CFL1
		P40124	CAP1	P20029	HSPA5
		P51655	GPC4	P21956-1	Isoform 1 of MFGE8
		P63094	GNAS	P27773	PDIA3
		P63158	HMGB1	P28301	LOX
		Q02788	COL6A2	P35441	THBS1
		Q04857	COL6A1	P37889	FBLN2
		Q3V1T4	P3H1	P62962	PFN1
		Q5SS80-1	Isoform 1 of DHRS13	P97792-1	Isoform 1 of CXADR
		Q60847	COL12A1	Q01149	COL1A2
		Q61207	PSAP	Q05793	HSPG2
		Q62087	PON3	Q61001	LAMA5
		Q62165	DAG1	Q61292	LAMB2
		Q6GU68	ISLR	Q61703	ITIH2
		Q8CC88	VWA8	Q62351	TFRC
		Q8CIE6	COPA	Q8CG19-1	Isoform long of LTBP1
		Q8K4Z3	NAXE	Q8VDD5	MYH9
		Q8VDL4	ADPGK	Q99K41	EMILIN1
		Q91ZA3	PCCA	Q9CYL5	GLIPR2
		Q99MN1	KARS		
		Q9CYD3	CRTAP		
		Q9CZD3	GARS		
		Q9D0L4-1	Isoform 1 of ADCK1		
		Q9DCZ4	APOO		

Q9JKR6	HYOU1
Q9QZF2	GPC1
Q9WTR5	CDH13
Q9Z2W0	DNPEP

Table A10 - Unique proteins identified in. at least. two lists of extracellular filtered proteins in EPIC SM and EPIC IM (20 proteins) and unique proteins found in E17.5 murine hearts (40 proteins)

Unique proteins from EPIC SM and IM		Unique proteins from E17.5 hearts	
UniProt ID	Protein Name	UniProt ID	Protein Name
P01029	C4B	A2AAJ9-1	Isoform 1 of OBSCN
P01887	B2M	E9PV24	FGA
P01902	H2-K1	O08999	LTBP2
P10649	GSTM1	O35206	COL15A1
P16110	LGALS3	O88322	NID2
P19788	MGP	P02772	AFP
P39876	TIMP3	P09535	IGF2
P48759	PTX3	P28843	DPP4
P55065	PLTP	P51885	LUM
P62960	YBX1	P54320	ELN
P82198	TGFBI	P97927	LAMA4
Q08879	FBLN1	Q60675	LAMA2
Q61398	PCOLCE	Q61282	ACAN
Q8R2G6	CCDC80	Q61554	FBN1
Q924C6	LOXL4	Q61555	FBN2
Q9D1D6	CTHRC1	Q62009	POSTN
Q9D6X6	PRSS23	Q62059-1	Isoform V0 of VCAN
Q9R118	HTRA1	Q640N1-1	Isoform 1 of AEBP1
Q9WU78	PDCD6IP	Q6DYE8	ENPP3
Q9WVJ9	EFEMP2	Q80X19-1	Isoform 1 of COL14A1
		Q80YX1	TNC
		Q8BH61	F13A1
		Q8C6K9-1	Isoform 1 of COL6A6
		Q8CFZ4	GPC3
		Q8K482	EMILIN2
		Q8K4G1	LTBP4
		Q8R2Y2-1	Isoform 1 of MCAM
		Q8VCM7	FGG
		Q921I1	TRF
		Q99MQ4	ASPN
		Q9CXY6	ILF2
		Q9QUP5	HAPLN1
		Q9QZS0	COL4A3
		Q9QZZ6	DPT
		Q9R069	BCAM
		Q9R087	GPC6
		Q9WVH9	FBLN5
		Q9Z1R2	BAG6
		Q9Z1T2	THBS4

Table A11 – Unique proteins identified in. at least. two lists of extracellular filtered proteins in EPIC SM and EPIC IM (32 proteins) and unique proteins found in Matrigel (41 proteins)

Unique proteins from EPIC SM and IM		Unique proteins from Matrigel	
UniProt ID	Protein Name	UniProt ID	Protein Name
O08573	LGALS9	E9PV24	FGA
P01029	CALU	O08677-1	Isoform HMW of KNG1
P01887	COL4A1	O35206	COL15A1
P01902	SPARC	O70456	SFN
P06745	COL4A2	O88322	NID2
P10107	CALR	P01864-1	Isoform membrane bound of Ig gamma-2A chain C region secreted form
P10649	CTSD	P01867-1	Isoform 1 of IGH-3
P11087-1	BGN	P01872-1	Isoform 1 of IGHM
P11152	LPL	P06909	CFH
P18760	CFL1	P07758	SERPINA1A
P19788	LRPAP1	P07759	SERPINA3K
P21956-1	HMGB1	P08228	SOD1
P28301	P3H1	P10639	TXN1
P35441	COL12A1	P20918	PLG
P37889	CP	P21614	GC
P39876	PSAP	P22599	SERPINA1B
P48759	TINAGL1	P28665	MUG1
P55065	CRTAP	P28798	GRN
P82198	HYOU1	P29699	AHSG
P97792-1	HNRNPC	P29788	VTN
Q01149	COL1A2	P46412	GPX3
Q61398	PCOLCE	P58022	LOXL2
Q61703	ITIH2	P70663	SPARCL1
Q62351	TFRC	Q00623	APOA1
Q8CG19-1	Isoform long of LTBP1	Q00897	SERPINA1D
Q8R2G6	CCDC80	Q00898	SERPINA1E
Q924C6	LOXL4	Q06890	CLU
Q99K41	EMILIN1	Q08879-2	Isoform 1 of FBLN1
Q9D1D6	CTHRC1	Q60675	LAMA2
Q9D6X6	PRSS23	Q61646	HP
Q9R118	HTRA1	Q61702	ITIH1
Q9WVJ9	EFEMP2	Q61838	PZP
		Q8BH61	F13A1
		Q8CJ69	BMPER
		Q8R2Z5	VWA1
		Q8VCM7	FGG
		Q91WP6	SERPINA3N
		Q91X72	HPX
		Q92111	TRF
		Q9D106	PGA5
		Q9ESB3	HRG



Table A12 – Extracellular proteins in common between Matrigel and EPIC IM (7 proteins). EPIC SM (20 proteins) proteins in common between all conditions (21 proteins)

Proteins in common between EPIC IM and Matrigel		Proteins in common between EPIC SM and Matrigel		Proteins in common between EPIC IM, EPIC SM and Matrigel	
UniProt ID	Protein Name	UniProt ID	Protein Name	UniProt ID	Protein Name
A6X935-1	Isoform 1 of ITIH4	A2ASQ1-1	Isoform 1 of AGRN	O88569	HNRNPA2B1
P01027-1	Isoform long of C3	O35887	CALU	P02468	LAMC1
P07724	ALB	P02463	COL4A1	P02469	LAMB1
P10493	NID1	P07214	SPARC	P07356	ANXA2
P19137	LAMA1	P08122	COL4A2	P08113	HSP90B1
Q3UQ28	PXDN	P14211	CALR	P11276	FN1
Q8K0E8	FGB	P18242	CTSD	P11499	HSP90AB1
		P28653	BGN	P13020-1	Isoform 1 of GSN
		P29391	FTL1	P16110	LGALS3
		P39061-1	Isoform 2 of COL18A1	P17742	PPIA
		P55302	LRPAP1	P20029	HSPA5
		P63158	HMGB1	P27773	PDIA3
		Q3V1T4	P3H1	P62960	YBX1
		Q60847	COL12A1	P62962	PFN1
		Q61147	CP	Q05793	HSPG2
		Q61207	PSAP	Q08879	FBLN1
		Q99JR5	TINAGL1	Q61001	LAMA5
		Q9CYD3	CRTAP	Q61292	LAMB2
		Q9JKR6	HYOU1	Q8VDD5	MYH9
		Q9Z204	HNRNPC	Q9CYL5	GLIPR2
				Q9WU78	PDCD6IP

Table A13 – Extracellular proteins in common between EPIC-derived ECM. E17.5 decellularized hearts and Matrigel (17 proteins)

**Proteins in common between EPIC-derived ECM. E17.5 decellularized hearts and Matrigel**

UniProt ID	Protein Name
O88569	HNRNPA2B1
P02468	LAMC1
P02469	LAMB1
P07356	ANXA2
P08113	HSP90B1
P11276	FN1
P11499	HSP90AB1
P13020-1	Isoform 1 of GSN
P17742	PPIA
P20029	HSPA5
P27773	PDIA3
P62962	PFN1
Q05793	HSPG2
Q61001	LAMA5
Q61292	LAMB2
Q8VDD5	MYH9
Q9CYL5	GLIPR2



Review

# Extracellular Vesicle-Based Therapeutics for Heart Repair

Laura Saludas<sup>1,2</sup>, Cláudia C. Oliveira<sup>3,4</sup> , Carmen Roncal<sup>2,5,6</sup> , Adrián Ruiz-Villalba<sup>3,4</sup> , Felipe Prósper<sup>2,7,8,9</sup> , Elisa Garbayo<sup>1,2,\*</sup> and María J. Blanco-Prieto<sup>1,2,\*</sup>

- <sup>1</sup> Department of Pharmaceutical Technology and Chemistry, Faculty of Pharmacy and Nutrition, University of Navarra, 31008 Pamplona, Spain; lsaludas@alumni.unav.es
- <sup>2</sup> Instituto de Investigación Sanitaria de Navarra (IdiSNA), 31008 Pamplona, Spain; croncalm@unav.es (C.R.); fprosper@unav.es (F.P.)
- <sup>3</sup> Department of Animal Biology, Institute of Biomedicine of Málaga (IBIMA), Faculty of Science, University of Málaga, 29010 Málaga, Spain; claudia.ol.556@gmail.com (C.C.O.); adrian.ruizvillalba@gmail.com (A.R.-V.)
- <sup>4</sup> Andalusian Centre for Nanomedicine and Biotechnology (BIONAND), 29590 Málaga, Spain
- <sup>5</sup> Laboratory of Atherothrombosis, Program of Cardiovascular Diseases, CIMA, University of Navarra, 31008 Pamplona, Spain
- <sup>6</sup> Centro de Investigación Biomédica en Red (CIBERCV), Carlos III Institute of Health, 28029 Madrid, Spain
- <sup>7</sup> Program of Regenerative Medicine, CIMA, University of Navarra, 31008 Pamplona, Spain
- <sup>8</sup> Cell Therapy Area and Haematology Department, Clínica Universidad de Navarra, 31008 Pamplona, Spain
- <sup>9</sup> Centro de Investigación Biomédica en Red (CIBERONC), Carlos III Institute of Health, 28029 Madrid, Spain
- \* Correspondence: egarbayo@unav.es (E.G.); mjblanco@unav.es (M.J.B.-P.); Tel.: +34-948-425-600 (ext. 806312) (E.G.); +34-948-425-600 (ext. 806519) (M.J.B.-P.)

**Abstract:** Extracellular vesicles (EVs) are constituted by a group of heterogeneous membrane vesicles secreted by most cell types that play a crucial role in cell–cell communication. In recent years, EVs have been postulated as a relevant novel therapeutic option for cardiovascular diseases, including myocardial infarction (MI), partially outperforming cell therapy. EVs may present several desirable features, such as no tumorigenicity, low immunogenic potential, high stability, and fine cardiac reparative efficacy. Furthermore, the natural origin of EVs makes them exceptional vehicles for drug delivery. EVs may overcome many of the limitations associated with current drug delivery systems (DDS), as they can travel long distances in body fluids, cross biological barriers, and deliver their cargo to recipient cells, among others. Here, we provide an overview of the most recent discoveries regarding the therapeutic potential of EVs for addressing cardiac damage after MI. In addition, we review the use of bioengineered EVs for targeted cardiac delivery and present some recent advances for exploiting EVs as DDS. Finally, we also discuss some of the most crucial aspects that should be addressed before a widespread translation to the clinical arena.

**Keywords:** cardiovascular diseases; myocardial infarction; cardiac repair; extracellular vesicles; exosomes; drug delivery; cargo loading; targeting



**Citation:** Saludas, L.; Oliveira, C.C.; Roncal, C.; Ruiz-Villalba, A.; Prósper, F.; Garbayo, E.; Blanco-Prieto, M.J. Extracellular Vesicle-Based Therapeutics for Heart Repair. *Nanomaterials* **2021**, *11*, 570. <https://doi.org/10.3390/nano11030570>

Academic Editor: Gianluca Ciardelli

Received: 30 December 2020

Accepted: 20 February 2021

Published: 25 February 2021

**Publisher's Note:** MDPI stays neutral with regard to jurisdictional claims in published maps and institutional affiliations.



**Copyright:** © 2021 by the authors. Licensee MDPI, Basel, Switzerland. This article is an open access article distributed under the terms and conditions of the Creative Commons Attribution (CC BY) license (<https://creativecommons.org/licenses/by/4.0/>).

## 1. Introduction

Cardiovascular diseases (CVDs) include a wide diversity of pathologies of the heart and blood vessels such as coronary artery disease, rheumatic heart disease, cerebrovascular disease, ischemic heart disease, and heart failure [1]. Among them, myocardial infarction (MI) and stroke remain the highest cause of mortality globally [2]. Furthermore, they are included in the top-ten ranked diseases associated with age, sex, and territories in the last study of the Global Burden of Disease, which included 369 diseases and injuries, and 204 countries and territories [3]. Despite major advances in pharmacology and device surgery, CVDs remain a significant public health challenge. Their prognosis is poor, especially for MI. The majority of patients who survive their first MI have a high chance of recurrent MI or other complications [4]. The origin of these complications derives from the absence of a regenerative capacity in adult mammal hearts. After damage, a fibrotic